

THE WORTH OF DATA IN PREDICTING AQUITARD
CONTINUITY IN HYDROGEOLOGICAL DESIGN

By

BRUCE RENNIE JAMES

B.A.Sc., University of Waterloo, 1986

A THESIS SUBMITTED IN PARTIAL FULFILLMENT OF
THE REQUIREMENTS FOR THE DEGREE OF
DOCTOR OF PHILOSOPHY

in

THE FACULTY OF GRADUATE STUDIES
(Department of Geological Sciences)

We accept this thesis as conforming
to the required standard

THE UNIVERSITY OF BRITISH COLUMBIA

April 1992

© Bruce Rennie James, 1992

In presenting this thesis in partial fulfilment of the requirements for an advanced degree at the University of British Columbia, I agree that the Library shall make it freely available for reference and study. I further agree that permission for extensive copying of this thesis for scholarly purposes may be granted by the head of my department or by his or her representatives. It is understood that copying or publication of this thesis for financial gain shall not be allowed without my written permission.

Department of Geological Sciences

The University of British Columbia
Vancouver, Canada

Date April 21, 1992

ABSTRACT

A Bayesian decision framework is developed for addressing data worth questions for hydrogeological design in heterogeneous geological environments. This framework is developed specifically for aiding hydrogeologists, dealing with groundwater contamination, in the design of exploration programs searching for aquitard discontinuities. It can be used to evaluate, and compare, the cost effectiveness of (a) patterns of precise point measurements (e.g. boreholes), which are often expensive, and (b) areal geophysical surveys which are imprecise, but usually less expensive.

The framework consists of two basic modules: a geostatistical indicator algorithm for simulating aquitard heterogeneity and a numerical model for simulating contaminant transport. Bayesian decision analysis ties these two modules together. The Bayesian nature of the framework also provides a methodology for combining a conceptual understanding of the local geology with quantitative information. Indicator geostatistics allows the handling of hydrogeological parameters which behave in space as non-Gaussian random variables.

The estimated worth of a measurement was found to be particularly sensitive to economic parameters. It was less sensitive to hydrogeological and geostatistical parameters.

The framework was applied in a retrospective fashion to the design of a remediation program for soil contaminated by radioactive waste disposal at the Savannah River Site, in South Carolina. The cost effectiveness of different patterns of point measurements was studied. This study included determining the number and spacing of the most cost effective pattern. Contour maps were produced of the net worth of a single, point measurement. These contour maps can be used to design sequential sampling programs involving single or multiple measurements. Good potential was also shown for determining the cost

effectiveness of an areal geophysical survey. The net worth of patterns of precise, point measurements was compared to that of an imprecise, areal seismic survey.

These results indicate that the framework can be very valuable in determining if additional exploration is cost effective and in designing efficient exploration programs. Results also show that ignoring a conceptual understanding of geology can lead to erroneous data worth analysis.

The framework could be modified to handle other data worth questions in hydrogeology or other disciplines, such as mining, or petroleum reservoir engineering.

TABLE OF CONTENTS

	Page
ABSTRACT	ii
LIST OF TABLES	vii
LIST OF FIGURES	viii
ACKNOWLEDGEMENTS	xi
CHAPTER 1: INTRODUCTION	1
1.1 HYDROGEOLOGICAL DESIGN AND GEOLOGICAL HETEROGENEITY	2
1.2 PREVIOUS WORK	3
1.3 APPROACH AND CONTRIBUTION OF THESIS	6
CHAPTER 2: AN OVERVIEW OF BAYESIAN DECISION ANALYSIS	10
2.1 INTRODUCTION	10
2.2 PRIOR ANALYSIS	10
2.3 POSTERIOR ANALYSIS	15
2.4 DATA WORTH THROUGH PREPOSTERIOR ANALYSIS	19
2.4.1 EXPECTED VALUE OF PERFECT INFORMATION (EVPI)	20
2.4.2 EXPECTED VALUE OF SAMPLE INFORMATION (EVSI)	22
2.4.2.1 Method 1: The EVSI from the Expected Increase in the Maximum Objective Function	22
2.4.2.2 Method 2: The EVSI from Expected Reduction in Minimum Expected Regret	24
2.4.2.3 Method 3: Expected Posterior Worth of a Measurement	26
2.5 APPLICATION AND EXTENSION OF THE METHODS	29
2.6 NOTATION	29
CHAPTER 3: GEOLOGICAL PREDICTION OF AQUITARD CONTINUITY	33
3.1 INTRODUCTION	33
3.2 THE EFFECT OF DEPOSITIONAL ENVIRONMENT ON THE GEOMETRIC CHARACTERISTICS OF CLAY LAYERS.	33
3.2.1 BRAIDED STREAM	33
3.2.2 MEANDERING STREAM	34
3.2.3 DELTAIC	35
3.2.4 ESTUARINE	36
3.2.5 SUBMARINE FAN	37
3.2.6 MARINE	37
3.2.7 GLACIAL	37
3.3 QUANTITATIVE DESCRIPTION OF SHALE HETEROGENEITY	39
3.4 THE IMPORTANCE OF GEOLOGY IN PREDICTING AQUITARD CONTINUITY	40
CHAPTER 4: SEQUENTIAL INDICATOR SIMULATIONS OF AQUITARDS	45
4.1 INTRODUCTION	45
4.2 BASIC GEOSTATISTICAL CONCEPTS	45
4.3 INDICATOR KRIGING (IK)	50
4.3.1 INDICATOR RANDOM VARIABLE	50
4.3.2 TYPES OF DATA	52
4.3.3 SIMPLE INDICATOR KRIGING (SIK) WITH HARD DATA	53
4.3.4 ORDINARY INDICATOR KRIGING (OIK) WITH HARD DATA	54
4.3.5 COMPARISON OF OIK AND SIK	55
4.3.6 EXTENSION OF SIMPLE INDICATOR KRIGING TO HANDLE TYPE (a) SOFT DATA	57
4.4 SEQUENTIAL INDICATOR SIMULATION ALGORITHM (SIS)	58
4.5 INFERENCE OF GEOSTATISTICAL PARAMETERS	61
4.5.1 NON-BAYESIAN INFERENCE	61

4.5.1.1 Inference of the Mean and Variance	61
4.5.1.2 Inference of Cov(h)	65
4.5.2 BAYESIAN INFERENCE	68
4.5.3 SUMMARY OF INFERENCE OF GEOSTATISTICAL PARAMETERS	76
4.6 LIMITATIONS OF SIS ALGORITHM	77
4.6.1 GEOSTATISTICAL ASSUMPTIONS	78
4.6.2 FINITE SIZE OF AQUITARD REALIZATIONS	79
4.6.3 VOLUME VARIANCE RELATIONSHIP	79
4.6.4 TYPES OF UNCERTAINTY HANDLED	80
4.6.5 NUMBER OF CONDITIONING DATA	81
4.7 ALTERNATIVE SIMULATION ALGORITHMS	81
4.8 GEOSTATISTICAL NATURE OF CLAY LAYERS	83
4.9 NOTATION	83
CHAPTER 5: CONTAMINANT TRANSPORT	86
5.1 INTRODUCTION	86
5.2 TRANSPORT PROCESSES	86
5.2.1 ADVECTION	87
5.2.1 HYDRODYNAMIC DISPERSION	88
5.2.3 IMPORTANCE OF ADVECTION	90
5.3 MODELING OF CONTAMINANT TRANSPORT	90
5.3.1 2-D MODELING OF SOLUTE TRANSPORT	91
5.3.2 3-D MODELING OF SOLUTE TRANSPORT	94
5.4 NOTATION	95
CHAPTER 6: OUTLINE OF FRAMEWORK	96
6.1 INTRODUCTION	96
6.2 MEASURING AQUITARD DISCONTINUITIES	96
6.3 EVALUATING THE WORTH OF HARD, POINT MEASUREMENTS	99
6.3.1 EXAMPLE DESIGN	99
6.3.2 TWO METHODS OF GENERATING REALIZATIONS FOR THE FRAMEWORK	101
6.3.2.1 Realizations Generated During Both Prior and Preposterior Analysis (Abandoned Approach)	102
6.3.2.1.1 The Prior Analysis	102
6.3.2.1.2 Preposterior Analysis	102
6.3.2.2 Realizations Generated During the Preposterior Analysis (Method Used in Thesis)	107
6.4 SENSITIVITY OF ESTIMATED WORTH OF SINGLE HARD MEASUREMENT TO NUMERICAL ARTIFACTS	110
6.4.1 THE NUMBER OF REALIZATIONS GENERATED PER SAMPLE OUTCOME	111
6.4.2 STARTING SEED USED IN RANDOM NUMBER GENERATOR	112
6.4.3 NUMBER OF FIRST AQUITARD BLOCK GENERATED	112
6.4.4 NUMBER OF BLOCKS INTO WHICH AQUITARD IS DISCRETIZED	113
6.4.5 COMBINED AFFECT ON RELIABILITY OF DATA WORTH	113
6.5 PREPOSTERIOR ANALYSIS OF A SOFT, AREAL SURVEY	114
6.6 MODIFICATION TO FRAMEWORK TO HANDLE DATA WORTH PROBLEMS IN OTHER DISCIPLINES	116
6.7 SUMMARY OF CHAPTER 6	118
6.8 NOTATION	118
CHAPTER 7: GENERIC DESIGN CASE: A SENSITIVITY ANALYSIS OF DATA WORTH	123
7.1 INTRODUCTION	123
7.2 TWO CONTAMINATION SCENARIOS	124
7.2.1 SCENARIO NUMBER 1	124
7.2.2 CONTAMINATION SCENARIO 2:	127

7.3. SENSITIVITY TO ECONOMIC PARAMETERS	127
7.3.1 KNOWN COST OF CONTAINMENT (SCENARIO 1)	128
7.3.2 COST OF FAILURE (SCENARIO 1)	130
7.3.3 DISCOUNT RATE (SCENARIO 1)	131
7.4 SENSITIVITY TO HYDROGEOLOGICAL PARAMETERS	131
7.4.1 VERTICAL HYDRAULIC CONDUCTIVITY OF AQUITARD (SCENARIO 2)	132
7.4.2 HORIZONTAL HYDRAULIC CONDUCTIVITY OF LOWER AQUIFER (SCENARIO 2)	132
7.4.3 CONSTANT HEAD BOUNDARY CONDITION, h_4 , IN LOWER AQUIFER (SCENARIO 2)	133
7.5 SENSITIVITY TO GEOSTATISTICAL PARAMETERS	135
7.5.1 PRIOR ESTIMATE OF MEAN OF $I(x)$ (SCENARIO 1)	135
7.5.2 CORRELATION LENGTH of $I(x)$ (SCENARIO 2)	136
7.5.3 CONFIDENCE IN THE PRIOR ESTIMATE OF MEAN (SCENARIO 1)	137
7.6 SENSITIVITY TO EXISTING HARD DATUM	139
7.7 SUMMARY OF CHAPTER 7	140
7.8 NOTATION	141
CHAPTER 8: SAVANNAH RIVER SITE CASE HISTORY	150
8.1 INTRODUCTION	150
8.1.1 PHYSIOGRAPHY AND GEOLOGY	151
8.1.2 HYDROGEOLOGY	153
8.2 SET UP OF BASE CASE	155
8.2.1 ALTERNATIVE CLOSURE DESIGNS	155
8.2.2 MODELING OF CONTAMINANT TRANSPORT NEAR H-AREA SEEPAGE BASINS	157
8.2.3 GREEN CLAY DATA BASE	161
8.2.4 INFERENCE OF GEOSTATISTICAL PARAMETERS	164
8.2.4.1 Inference of Correlation Length	164
8.2.4.2 Inference of Mean and Variance	165
8.3 PRIOR ANALYSIS	167
8.4 PREPOSTERIOR ANALYSIS OF HARD DATA	168
8.4.1 SINGLE HARD MEASUREMENT	168
8.4.2 SENSITIVITY OF NET WORTH OF HARD SINGLE HARD MEASUREMENT TAKEN AT POINT B TO PARAMETERS SET UP IN BASE CASE	170
8.4.2.1 Numerical Artifacts	171
8.4.2.2 Economic Parameters	173
8.4.2.3 Geostatistical Parameters	175
8.4.3 NET WORTH OF SINGLE, HARD MEASUREMENT TAKEN AT DIFFERENT LOCATIONS	177
8.4.4 PATTERNS OF MULTIPLE, HARD MEASUREMENTS	179
8.5 PREPOSTERIOR ANALYSIS OF SOFT, AREAL SURVEY	182
8.6 SUMMARY OF CHAPTER 8	186
8.7 NOTATION	188
CHAPTER 9: SUMMARY AND CONCLUSIONS	202
REFERENCES	206
APPENDIX 1: GREEN CLAY DATA BASE	213

LIST OF TABLES

	Page
Table 6-1: Economic parameters used in example design.....	101
Table 6-2: Numerical parameters used in example design.....	101
Table 6-3: The values of parameters used in the prior analysis and the expected value of parameters used in the preposterior analysis.....	106
Table 7-1: Costs and benefits for the containment and no containment alternatives.....	126
Table 7-2: Hydrogeological parameters used in Scenario 1	126
Table 7-3: Numerical parameters used in Scenario 1	127
Table 8-1: Summary of cost and benefits associated with the no action and waste removal alternatives	158
Table 8-2: Hydraulic parameters of hydrostratigraphic units used in the base case	161
Table 8-3: Summary of geostatistical parameters used in base case.....	167
Table 8-4: Aquitard discretizations used in evaluating net worth of hard measurement taken at point B	172

LIST OF FIGURES

	Page
Figure 2-1: Cross section through example landfill.	12
Figure 2-2: Decision tree used in the prior analysis of the example landfill.	15
Figure 2-3: Decision tree used in posterior analysis of example landfill	19
Figure 2-4: Expected regret calculations for the landfill example.	21
Figure 2-5: Decision tree of preposterior analysis of example borehole using method 1.	25
Figure 2-6: Decision tree used in preposterior analysis of example borehole using method 2.	26
Figure 3-1: Cumulative probability distribution of shale length in different depositional environments	41
Figure 3-2: Prediction of shale continuity in the Ivishak Formation without geological information	42
Figure 3-3: Prediction of shale continuity in the Ivishak Formation with geological information	42
Figure 4-1: Plot of the exponential, spherical and Gaussian covariance functions, for $\sigma_z^2 = 1$, $\lambda = 10$ m and $a = 10$ m.	49
Figure 4-2: Plot of $i^*(x)$ on 1-d line by both OIK and SIK.	56
Figure 4-3: Variance of $i^*(x)$ from SIK and OIK.	57
Figure 4-4: One dimensional stratigraphic section divided into blocks	59
Figure 4-5: An example of nh hard data which are declustered	63
Figure 4-6: $F^*I(0)$ versus different cell size d.	64
Figure 5-1: Boundary conditions on two-dimensional flow field	91
Figure 5-2: Sample finite element grid for two dimensional vertical cross section.	93
Figure 6-1: Boundary conditions, hydrogeological and geostatistical parameters used in the example design	100
Figure 6-2: Finite element mesh used in example design with eight times vertical exaggeration	101
Figure 6-3: Decision tree used in prior analysis and its simplified version to right	102
Figure 6-4: Preposterior analysis of example design when realizations are generated in both the prior and the preposterior analysis.	105
Figure 6-5: The preposterior analysis for example design for case where realizations are generated during preposterior analysis only.	109
Figure 6-6: Sensitivity of the worth and median failure time to number of realizations per sample outcome	111
Figure 6-7: Sensitivity of the worth to the starting seed used in the random number generator	112
Figure 6-8: Sensitivity of the worth to first aquitard block in starting path	113
Figure 6-9: Sensitivity of W to the number of blocks that the aquitard is discretized into.	113
Figure 7-1: Plan view of contaminated aquifer system	125
Figure 7-2: Cross section through contaminated aquifer system	125
Figure 7-3: Sensitivity of W to the known cost of containment	129
Figure 7-4: The expected prior objective function of the two alternatives and the expected expected objective function of the posterior best design alternative versus known cost of containment	129
Figure 7-5: The effect of sampling a window on the objective functions of the different alternatives	129
Figure 7-6: The effect of sampling no window on the objective functions of the different alternatives	130
Figure 7-7: W versus cost of failure	130
Figure 7-8: The expected prior objective function of the two alternatives and the expected expected objective function of the posterior best design alternative versus cost of failure	131
Figure 7-9: W versus discount rate.	131

Figure 7-10: The expected prior objective function of the two alternatives and the expected expected objective function of the posterior best design alternative versus discount rate	131
Figure 7-11: The sensitivity of W and prior probability of failure to aquitard hydraulic conductivity for Scenario 2	132
Figure 7-12: The sensitivity of W and prior probability of failure to the transmissivity of the lower aquifer.....	133
Figure 7-13: The sensitivity of W to the constant head boundary condition in lower aquifer	134
Figure 7-14: Sensitivity of W to the prior estimate of the mean.....	135
Figure 7-15: Effect of sampling no window on the prior and posterior objective function of the containment and no containment alternatives	135
Figure 7-16: Effect of sampling a window on the prior and posterior objective functions of the containment and no containment alternatives	135
Figure 7-17: Probability of sampling a window versus the mean chance of a window	136
Figure 7-18: Sensitivity of W and prior probability of failure to correlation length	137
Figure 7-19: Sensitivity of W to the prior confidence in the estimates of the geostatistical parameters	137
Figure 7-20: The updated mean versus ne	138
Figure 7-21: Effect of sampling a window on the objective functions	139
Figure 7-22: Effect of an existing hard datum on the worth of single borehole taken along an east-west line through the datum.....	140
Figure 8-1: Location map of the Savannah River Site	150
Figure 8-2: H-Area seepage basins in the General Separations Area.....	151
Figure 8-3: Geologic cross section through the General Separations Area	153
Figure 8-4: Area where flow and transport are modeled around the H-Area seepage basins.....	158
Figure 8-5: Contours of hydraulic head in Barnwell Formation and paths of particles of contamination near the H Area seepage basins.....	162
Figure 8-6: Locations of global hard data.....	163
Figure 8-7: Locations of global soft data.....	163
Figure 8-8: Local hard and soft data used to condition aquitard realizations.....	163
Figure 8-9: Decision tree used in prior analysis, where Cost of failure = \$70 million	168
Figure 8-10: Location of hard measurement taken at point B	169
Figure 8-11: Decision tree used in preposterior analysis of hard measurement taken at point B, for cost of failure = \$70 million	170
Figure 8-12: Sensitivity of net worth to aquitard block discretization.....	172
Figure 8-13: Sensitivity of net worth to the discount rate	174
Figure 8-14: Sensitivity of net worth to cost of failure	174
Figure 8-15: Sensitivity of net worth to known cost of lay cap alternative.....	175
Figure 8-16: Sensitivity of net worth to known cost of no clay cap alternative	175
Figure 8-17: Sensitivity of net worth to geological estimate of mean	176
Figure 8-18: Sensitivity of net worth to correlation length.....	176
Figure 8-19: Sensitivity of net worth to confidence in prior estimate of mean	177
Figure 8-20: Contour map of net worth of a single, hard measurement taken at different locations for cost of failure = \$45 million	177
Figure 8-21: Contour map of net worth of a single, hard measurement taken at different locations for cost of failure = \$70 million	179
Figure 8-22: Pattern of hard measurement taken on a 29 m spacing	179
Figure 8-23: Pattern of hard measurement taken on a 145 m spacing	180
Figure 8-24: Pattern of hard measurement taken on a 290 m spacing	180
Figure 8-25: Net worth of multiple hard measurements taken at spacings of 29, 145, and 290 m versus number of measurements taken, for cost of failure = \$70 million	181
Figure 8-26: Net worth of multiple hard measurements taken at spacings of 29 145 and 290 m versus number of measurements taken, for cost of failure=\$45 million	181
Figure 8-27: Contour plot of total worth for single, hard, point measurements taken throughout the region of study, for cost of failure=\$45 million.	183

Figure 8-28: Decision tree used in preposterior analysis of soft geophysical survey	184
Figure 8-29: Net worth of the geophysical survey vs the probability of sampling a window that will cause failure, given that a window that will cause failure exists	186
Figure 8-30: Net worth of the seismic survey compared to net worth of patterns of hard, point measurements taken on a 290 m spacing	186

ACKNOWLEDGEMENTS

First and foremost, I would like to thank Al Freeze, my advisor, for giving me the opportunity to study under him. He has given me many things: a role model to follow and an understanding of what good research is really about, to just name a few. Secondly, I would like to thank Les Smith. He helped me on many occasions with technical problems relating to my thesis. I barged into his office dozens of times over the last five years with, "Have you got a sec?" Never once do I remember him saying no. It is a unique opportunity to be able to work under two scientists who are both world class researchers and first rate people.

One of the nicest aspects of my graduate studies was the rest of the groundwater gang. I would like to thank Brian Berkowitz, Joann Bessler, Elizabeth Hill, Karen Jardine, Dina Lopez, Tony Sperling, Dan Walker, and Chistoph Wels for many technical discussions, for feedback on practice talks that I have given, and for providing a really enjoyable working environment. One outstanding individual who I am particularly in debt to is Tom Clemo. He not only helped me solve a couple of very critical problems that I was faced with in my research, but was continuous a source of feedback. He is one of the best people that I have ever met. I would also like to thank Bryon Cranston for getting me into hockey, Keith Everard for baking lots of muffins, and Peiwen Ke for teaching me about China. The hardest thing about leaving Vancouver is missing all of the people who I have met and worked with.

Many thanks are also given to the Natural Sciences and Engineering Research Council of Canada who funded my research through scholarships and research operating grants. Finally, I would like to thank Dale Stephenson of Westinghouse Savannah River Co. and Glenn Duffield of the Geraghty & Miller Modeling Group. They provided invaluable aid in helping me complete the Savannah River Site case history, an important component of my thesis.

CHAPTER 1: INTRODUCTION

High costs are the major challenge presently facing the remediation of groundwater/soil contamination. In 1990, the U.S. EPA estimated that there were 951 Superfund sites, 27 000 potential Superfund sites, as well as up to 100 000 other potential major sources of groundwater/soil contamination in the U.S. alone (National Research Council, 1990). These numbers do not include the many sites on US military installations. The cost of cleaning up individual major contamination sites is commonly in the \$10's of millions, but can range up to the billions of dollars. The total cost of cleaning up all of these sites could exceed a trillion dollars. Such high costs are unacceptable to society, particularly when there are other more pressing social and environmental problems, such as economic competitiveness and air pollution, facing us. Therefore, it is critical to remediate these contamination sites in a cost effective fashion.

A crucial key to cost effective remediation is making good design decisions for remediation programs. However, making good decisions on designs is not a simple task since there can be much uncertainty in the quality of any particular design. Making good design decisions requires two important questions be answered:

- (1) Given uncertain conditions, how does one choose a good design?
- (2) Is it cost effective to collect more information so that one can improve a design?

Massmann and Freeze (1987a and b), Massmann, et al. (1991), Sperling (1991), and Sperling et al. (in press) address the former question. The objective of this thesis is to address the second question. This objective is reached by developing a Bayesian decision framework for addressing data worth questions in realistic hydrogeological design problems that deal with groundwater contamination. The framework can be valuable in reducing costs because it provides the site engineer with a tool not only for spending site exploration dollars more efficiently, but for deciding when enough information has been collected and a

final remediation design decision can be chosen. This latter point is very important as it reduces the time necessary to make design decisions. The framework is specifically applicable to the hydrogeological design of new waste disposal sites or remediation programs for existing sites of groundwater contamination.

The framework must be able to handle geological heterogeneity for it to be useful in realistic design.

1.1 HYDROGEOLOGICAL DESIGN AND GEOLOGICAL HETEROGENEITY

The design of new waste disposal sites, or remediation programs for sites of existing groundwater contamination, involves selecting the best design from a set of possible design alternatives. For example, in the design of a new landfill, one must consider whether an expensive synthetic liner is required to contain leachate, or whether no liner is needed. Selecting the best design is often an expensive balancing act. On one side, the range of costs of constructing new landfill sites, or remediating existing contamination, is large. For example, the cost of proposed design alternatives for closing down four seepage basins at the Savannah River Site, South Carolina ranged from only \$3.3 million to over \$100 million (Killian et al., 1987). An overly conservative design can be a huge waste of resources.

On the other side, a poorly designed remediation program that does not halt contamination, or a poorly designed waste disposal site that leaks leachate and contaminates local groundwater supplies, can result in large remediation costs and irreparable damage. The best design minimizes the combined cost of carrying out the design as well as any subsequent costs if the design performance fails to meet expectations. Choosing a poor design can be expensive.

Uncertainty caused by geological heterogeneity can make the choice of the best design alternative difficult. The performance of any alternative may depend upon where and how fast leaking contaminants

will be transported. Often, the major factor controlling contaminant transport is geological heterogeneity, that is the variability of hydrogeological parameters such as the hydraulic conductivity, dispersivity, or bed thickness. The true states of these parameters are uncertain since the porous medium is hidden below the surface, and is often highly variable. Therefore, there is a wide range of possible states for the three dimensional distribution, and a wide range of possible performances of the various design alternatives.

The choice of design can be facilitated by reducing the uncertainty in geological heterogeneity by gathering additional information through a sampling program. However, gathering data can be expensive. Will the expense of additional data collection be cost effective in allowing a better design decision to be made? And if so, what is the best sampling program to obtain this information? Decisions are needed as to the number and types of measurements to be taken, and their locations.

Present exploration programs are generally based solely on the professional judgment of the site engineer or geologist. However, the complexity of the heterogeneity of hydrogeological parameters can be overwhelming. On one hand, many cases exist where insufficient exploration resulted in expensive, poor designs. For these cases, more information might have prevented the poor design. On the other hand, the adversarial and regulatory environment that exists at many Superfund sites in the U.S.A. has sometimes led to too many data being collected and delay in action. This has resulted in a waste of resources that could have been better spent cleaning up other contamination sites.

It is clear that in many cases the worth of data is not analyzed properly. Consequently, there is need for a tool which can help hydrogeologists/engineers evaluate the worth of data in hydrogeological design.

1.2 PREVIOUS WORK

Evaluating the worth of data is not a new question. Over the last 50 years, much work has been done in

designing sampling programs in geology. However, "with few exceptions, the research to date on sample network design has focused on the goal of improved estimation of spatial averages over a predefined area of interest." (Barnes, 1989. p.12). Some selected references are Slichter (1955), Drew (1979), Delhomme (1983), and Bogardi et al. (1985). While this type of work makes valuable contributions to the design of sampling networks, there is no consideration of the monetary worth of a sampling program. Excluding monetary worth misses the fundamental point of a sampling program in hydrogeological design: the question of whether it is worth paying for a sampling in the first place.

The work which has put a monetary worth on sampling programs has been based on Bayesian decision theory. (Bayesian decision theory will be discussed in Chapter 2.) Davis and Dvoranchick (1971), Davis et al. (1972), Dawdy (1979), Davis et al. (1979), and Attanasi (1979) utilized Bayesian decision theory to evaluate the worth of hydrological data. Ben-Zvi et al. (1988) evaluated the worth of a borehole in a simple groundwater contamination problem. Maddock (1973), in one of the pioneering works, extended Bayesian decision analysis to the management of a farm, utilizing an analytical groundwater flow model. Management decisions involved many factors including pumping rates for irrigation and types of crops to be planted. However, hydrogeological parameters were assumed to be homogeneous. Such an approach can be used in some hydrogeological design problems. Often, however, geological heterogeneity must be dealt with to effectively carry out design, particularly when dealing with groundwater contamination.

Gates and Kisiel (1974) did a very interesting study that evaluated the worth of measurements of hydraulic conductivity, storativity, hydraulic head and recharge/discharge rates using a computer model that predicted hydraulic head in the Tucson Basin in Arizona. The parameters were heterogeneous; however, the worth of data was quantified in terms of a cost associated with the precision of the predicted heads, rather than a design decision.

None of the previous work that puts a monetary value on a sampling program has utilized geostatistics, or the concept of regional variables. Utilizing geostatistics is important because it is the most powerful tool

available today for handling geological heterogeneity. Many hydrogeological parameters that govern groundwater flow and contaminant transport behave as regional variables (de Marsily, 1984, and Rouhani, 1985). A regional variable is correlated in space. Geostatistics utilizes the spatial correlation to constrain the variability of possible states of the three dimensional distribution of hydrogeological parameters. Thus, by using the spatial correlation, an improved estimate of geological heterogeneity can be achieved and the performance of a design alternative can be estimated more closely. Nevertheless, these estimates can still involve great uncertainty. Massman and Freeze (1987a and b), Massman et al. (1991), Sperling (1991), and Sperling et al. (in press) used geostatistical methods to address the problems of hydrogeological design under conditions of uncertainty, but they did not address the issue of data worth.

Cahn (1987) developed strategies for sampling programs utilizing geostatistical concepts. However, she did not evaluate the worth of a measurement before it was taken. Rouhani (1985) linked the worth of a measurement of hydraulic head to the economic value related to the precision of the predicted hydraulic head, but he did not link the worth to a design decision.

More recently, Marin et al. (1989) and Medina (1989) outlined a Bayesian risk methodology for the permitting of waste disposal sites under conditions of uncertainty. Permitting was based upon whether the contaminant concentration would reach a critical level at some compliance point. Uncertainty in the contaminant concentration was estimated using Monte-Carlo simulations. In their work, they discuss how the worth of a measurement is quantified in terms of the increased precision of the estimated concentration. However the worth is not linked to an engineering design decision, nor do they actually carry out an analysis of the worth of data.

Freeze et al. (1988) and Freeze et al. (in press) produced a general outline of a Bayesian stochastic framework for addressing the data worth question in hydrogeological design involving correlated random variables. However, they did not put their ideas into practice.

1.3 APPROACH AND CONTRIBUTION OF THESIS

Many hydrogeological parameters affect contaminant transport. As a first step, the framework will deal with only one hydrogeological parameter: aquitard continuity. This parameter has been chosen for three reasons. Firstly, aquitard continuity is one of the major parameters controlling contaminant transport. In aquifer systems of non-zero vertical gradients, aquitard discontinuities are often the most significant factor controlling flow behavior and the spread of contaminants (Haldorsen and Chang, 1986; Fogg, 1986; and Duffield et al. 1989). This factor is particularly important when there is a great difference between the hydraulic conductivity of the aquifers and the aquitard of interest. Variations of other hydraulic parameters, such as porosity, hydraulic conductivity, or storativity, within a hydrogeological unit are of lesser importance. This contention is supported by Fogg (1986), Desbarats (1987) and Haldorsen and Chang (1986) who report that the most significant factor controlling the flow pattern is often the transition between sand and shale units rather than variations within a particular unit. Newson and Wilson (1988) report that even abandoned wells have provided important paths for contamination to spread vertically through aquifer/aquitard systems.

Secondly, it is a common problem. Aquitard discontinuities have enhanced the spread of contamination, or have been a significant problem at numerous contamination sites (Roux and Altoff, 1980; Jackson et al., 1985; Duffield et al., 1989; and Kennedy, et al., 1990).

Finally, aquitard continuity affects the transport that is most critical: the vertical spreading of contamination to clean aquifers. Previous experience has shown that the clean up of a contaminated aquifer is often economically impossible. Therefore, the horizontal spreading of contamination in an aquifer that is already contaminated is not as important as the vertical spreading of contamination to a clean aquifer. To the best of the author's knowledge, no other work has been done on evaluating the

effect of uncertainty of aquitard continuity on the prediction of contaminant transport.

The framework consists of two basic modules. The first is an indicator geostatistical simulation algorithm for handling aquitard heterogeneity. It accounts for the spatial correlation between measurements. Indicator geostatistics allows the handling of (a) hard, point measurements (which are precise, but are probably few and expensive), (b) soft, point measurements (which are imprecise, but are probably cheaper and more numerous), and (c) hydrogeological parameters which behave in space as non Gaussian random variables. Bed thickness determined from complete borehole logs represent an example of hard data. Bed thickness determined from incomplete borehole logs could represent soft data. Geophysical measurements could also represent soft data. The incorporation of soft data is important because there is often a lack of hard data.

The second module is a numerical model (finite element or finite difference) for simulating contaminant transport. Bayesian decision analysis ties the two modules together. The Bayesian nature of the framework provides a methodology for combining a conceptual understanding of the local geology with quantitative information. Including a conceptual understanding of geology is vital in many cases. For example, whether an aquitard is formed in a meandering stream environment or in a deep marine environment has immense implications as to how far an aquitard can be extrapolated from a measurement point. A case study illustrates that ignoring a conceptual understanding of geology can lead to erroneous data worth predictions, resulting in a poor design decision.

The framework can evaluate and compare the cost effectiveness of sampling programs consisting of (a) point, hard measurements, or (b) soft, geophysical surveys covering a large area. The framework will determine the best sampling strategy from a series of proposed ones. The best sampling strategy is not guaranteed to be the optimal pattern because the optimal pattern is the best of all possible sampling strategies, not just the best of a finite set of proposed ones.

This thesis will concentrate on unconsolidated aquifer/aquitard systems formed in clastic depositional environments. It assumes that the discontinuities in an aquitard are a result of depositional processes and post depositional erosional processes only. Discontinuities caused by tectonic or other processes, such as faulting, are not considered.

In summary, the major contribution of this thesis is the development of a Bayesian decision framework for evaluating the worth of data in hydrogeological design in heterogeneous geological environments. It can be used for tackling one of the most significant problems in environmental contamination: reducing the high costs associated with it. The framework provides a tool for allowing decision makers to not only expend site exploration dollars more efficiently, but to determine when enough information has been collected. This latter point is particularly important as it reduces the time necessary to make design decisions.

The second major contribution is the holistic approach used to develop the framework. This approach is accomplished by two factors. The first, and primary factor, is the Bayesian nature of the framework. This is the key to the integration of all the factors affecting a design and the expression of data worth in monetary terms, the major driving force of any exploration program. The second factor is the incorporation of many different types of information, including soft data, hard data, and a conceptual understanding of the local geology. Including as many sources of information as possible is critical because there are often few reliable hard data.

In addition, to the best of the author's knowledge, the framework is unique in its tackling of aquitard continuity, often the critical uncertainty confronting decision makers involved in groundwater contamination. Also, the framework is not just conceptual in nature, but has been demonstrated with a real field case.

Finally, the framework is applicable to other exploration programs in hydrogeology and other fields. The

methodology is sufficiently general that it can be easily modified to handle other hydrogeological parameters such as hydraulic conductivity, or to similar problems in other disciplines, particularly mining and petroleum engineering.

Chapters 2 to 5 present the different components of the framework. Chapter 6 describes how the different components are tied into the framework. Chapter 7 presents a sensitivity study of data worth using generic design examples, while Chapter 8 demonstrates the framework using a case history. The case history is the closure of four seepage basins at the Savannah River Site in South Carolina.

CHAPTER 2: AN OVERVIEW OF BAYESIAN DECISION ANALYSIS

2.1 INTRODUCTION

Bayesian decision analysis is a powerful method of mathematically selecting the best design from a number of alternatives under uncertainty. It is powerful because it combines both engineering judgement and measured data in the decision process. It also provides a method for evaluating the worth of obtaining further information, which is one of the principal questions asked in design under uncertain conditions: Is it cost effective to get more information so that uncertainty will be reduced, allowing a better decision to be made? Or would it be more cost effective to go with the currently available data, and use a more-conservative design approach. In hydrological design, the number of uncertain events affecting different design alternatives can be overwhelming.

This chapter will introduce the basic concepts of Bayesian decision theory using a simple design problem. The incorporation of the methodology into the framework described in this thesis will be discussed in later chapters.

The three major components of Bayesian decision analysis are the prior, posterior, and preposterior analyses. The prior analysis is used to choose the best design alternative from a series of available ones, based on current information. A posterior analysis is used to choose the best design alternative once new information becomes available. A preposterior analysis is used to determine whether collecting new information is cost effective.

2.2 PRIOR ANALYSIS

The prior analysis selects the best design alternative, A_D , from a set of "I" possible alternatives, A_i , based on present information. For this discussion, there will be J possible events, E_j , that affect the performance of the design alternatives. Only one event can be true, E_T , but it is unknown.

The methodology will be illustrated with the design of a simple landfill (Fig. 2-1). The landfill is to be constructed on an unconfined surficial aquifer. Beneath the surficial aquifer is a thick clay aquitard, which in turn is underlain by a confined aquifer of economic importance for water supply. A downward vertical gradient exists across the aquitard. The lower aquifer is bounded from below by impermeable bedrock. In this thesis, a landfill failure is defined as any event in which contamination of the lower aquifer occurs. If failure occurs, then the owner of the landfill will have to pay for an expensive cleanup.

It is assumed that failure will only occur if a permeable discontinuity, or window, exists in the aquitard. The aquitard is a marine clay formed during a marine transgression over the lower sandy aquifer. Its deposition was followed by a marine regression during which fluvial sands were deposited, forming the upper aquifer. Marine clay is generally continuous over distances on the order of kilometers. However, during this regression, there existed a large fluvial channel which could have eroded through the clay layer, creating a window. The approximate location of this fluvial channel is assumed known, but it is not known whether the channel has created a discontinuity in the form of a window through the aquitard.

The landfill is to be designed to minimize the combined cost of landfill construction and cleanup if failure occurs. For simplicity, only two alternative designs are considered here:

- 1) A_L , install a synthetic liner, or
- 2) A_{NL} , install no liner.

It is assumed that the synthetic liner will leak to some degree in the future. Therefore, its benefit will be in reducing the amount of leachate escaping, rather than completely containing it.

The two events affecting the performance of the design alternatives are

- 1) E_W , a window is present in the aquitard at the fluvial channel, and
- 2) E_{NW} , no window is present in the aquitard at the fluvial channel.

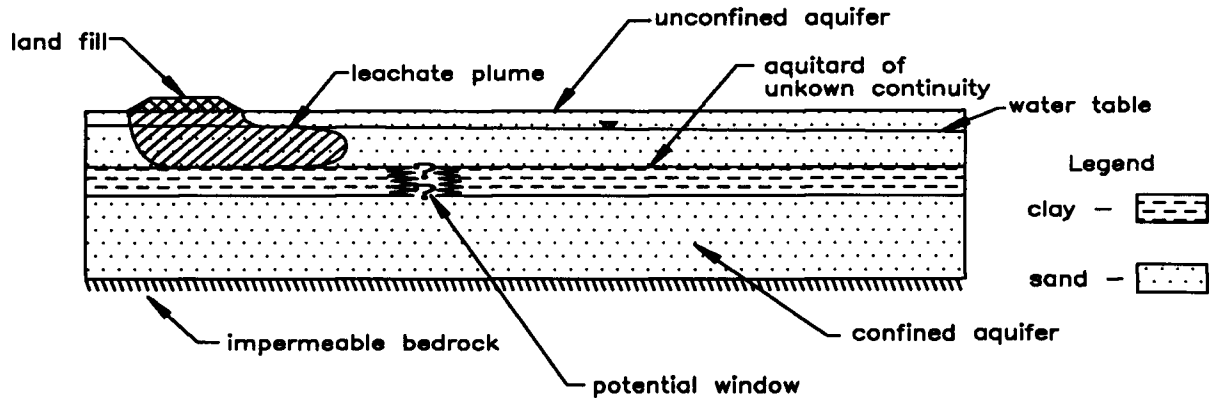


Figure 2-1: Cross section through example site.

If no window is present, E_{NW} , then failure cannot occur and there is no need for a synthetic liner. However, if a window does exist, then a liner will substantially reduce the amount of contamination and associated cleanup costs.

An expected maximum utility criterion will be used here to select the best design alternative. It takes into account the probability of different events occurring. It is based on an economic objective function which is defined as the net present value of the expected stream of future benefits, costs, and risks, taken over an engineering time horizon. The best alternative, or the design alternative, A_D , is the one with the maximum expected value of the objective function. The objective function, Z , (Crouch and Wilson, 1982) takes the form:

$$Z = \sum_{t=0}^T \frac{1}{(1+i)^t} [B(t) - C(t) - R(t)] \quad (2.1)$$

where:

i = discount rate (decimal fraction)

t = time (years)

T = time horizon (years)

$B(t)$ = benefits in year t (\$)

$C(t)$ = costs in year t (\$)

$R(t)$ = risks in year t (\$)

$B(t)$ represents known benefits. For the landfill, these would include the annual income from disposing of waste. $C(t)$ represents known costs, such as the cost of building and operating the landfill, and the costs of future monitoring to check for leachate plumes leaking from the landfill. $R(t)$ is defined as the expected cost of failure. It is calculated by:

$$R(t) = P_f(t)C_f(t)U(C_f) \quad (2.2)$$

where:

$P_f(t)$ = probability of failure in year t (decimal fraction)

$C_f(t)$ = cost of failure in year t (\$)

$U(C_f)$ = utility function (decimal fraction ≥ 1)

The cost of failure, C_f , represents all costs that could occur as a result of failure. These could include cleanup costs of any contamination as well as legal or other costs. The utility function, $U(C_f)$, accounts for risk-averse tendencies of some decision makers. Conservative decision makers, leery of failure, will set $U(C_f) > 1$ to increase the weighting of the risk. Risk neutral decision makers will use an expected value approach, that is, one for which $U(C_f) = 1$. Refer to any introductory textbook on decision analysis such as Benjamin and Cornell (1970) for more details on utility theory and how to choose values for $U(C_f)$. An expected value approach will be followed here. Therefore, equation (2.1) becomes:

$$Z = \sum_{t=0}^T \frac{1}{(1+i)^t} [B(t) - C(t) - P_f(t)C_f(t)] \quad (2.3)$$

In the simple landfill example to be presented now, the probability of a window at the fluvial channel is arbitrarily assumed to be 0.2. Therefore:

$$P(E_W) = 0.2 \quad (2.4)$$

$$P(E_{NW}) = 0.8 \quad (2.5)$$

For simplicity, all benefits, known costs, and costs of failure will be assumed to occur immediately; therefore, the time term in equation (2.3) drops out and (2.3) becomes:

$$Z = B - C - P_f C_f \quad (2.6)$$

It is further assumed that B for both alternatives will be \$1 000 000 and C will be \$500 000 and \$200 000 for A_L and A_{NL} , respectively. C_f will be \$1 000 000 for A_{NL} . C_f for A_L will be only \$200 000 because of the reduced volume of leachate.

The prior analysis can be visualized using a decision tree (Fig. 2-2). The square at the left of the tree marks a decision between different alternatives. Each branch from the square represents a possible design alternative. At the end of each branch is a circle with another series of branches emanating from it. Each branch of this second set represents a possible event, which is beyond the control of the decision maker. Each event affects the objective function of the alternative. Here there are only two possible events: E_{NW} and E_W . The probability of each event is marked below the event's branch.

The objective function, Z, for each alternative, given that a particular event occurs, is shown at the right of the decision tree. The objective functions for the different combinations of alternatives and events are

1) for a liner and a window

$$\begin{aligned} Z(A_L, E_W) &= \$1\,000\,000 - \$500\,000 - \$200\,000 & (2.7) \\ &= \$300\,000 \end{aligned}$$

2) for a liner and no window

$$\begin{aligned} Z(A_L, E_{NW}) &= \$1\,000\,000 - \$500\,000 & (2.8) \\ &= \$500\,000 \end{aligned}$$

3) for no liner and a window

$$\begin{aligned} Z(A_{NL}, E_W) &= \$1\,000\,000 - \$200\,000 - \$1\,000\,000 & (2.9) \\ &= -\$200\,000 \end{aligned}$$

4) for no liner and no window

$$\begin{aligned} Z(A_{NL}, E_{NW}) &= \$1\,000\,000 - \$200\,000 & (2.10) \\ &= \$800\,000 \end{aligned}$$

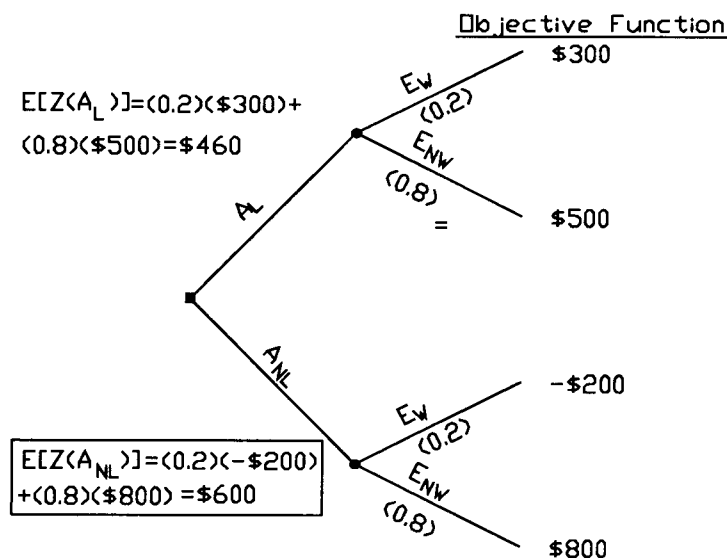


Figure 2-2: Decision tree used in the prior analysis of the example landfill.

The expected value of the objective function for each alternative, $E[Z(A_j)]$, is marked beside it. $E[Z(A_{NL})]$ is \$600 000 ($= 0.2 \times (-\$200\,000) + 0.8 \times \$800\,000$). $E[Z(A_L)]$ is only \$460 000 ($= 0.2 \times \$300\,000 + 0.8 \times \$500\,000$). Therefore, the no-liner design, A_{NL} is the best design because it has the maximum expected objective function. The maximum expected objective function has been enclosed in a box. This convention will be followed throughout this thesis.

2.3 POSTERIOR ANALYSIS

The posterior analysis incorporates new information into the decision process. The new information is used to reduce the uncertainty by updating the prior probabilities, $P(E_i)$, of the different events, E_i , occurring.

Traditionally, Bayes' equation is used to update the probabilities. Once the prior probabilities have been updated, the steps of the prior analysis are repeated to choose the best posterior design alternative.

Bayes' equation updates $P(E_i)$, given that a sample S_j has been taken, by:

$$P(E_i|S_j) = \frac{P(S_j|E_i)P(E_i)}{P(S_j)} \quad (2.11)$$

where,

- $P(E_i|S_j)$ is the posterior probability of E_i , given that sample S_j has been taken,
- $P(S_j|E_i)$ is the probability of sampling S_j , given that E_i exists,
- $P(E_i)$ is the prior probability of event E_i , and
- $P(S_j)$ is the probability of sampling S_j .

$P(S_j|E_i)$ is also referred to as the likelihood function of sampling S_j . $P(S_j)$ is calculated from the total probability of all of the different ways of sampling S_j :

$$P(S_j) = \sum_{i=1}^I P(S_j|E_i)P(E_i) \quad (2.12)$$

One of the powers of Bayes' equation is that the quality of the sample is automatically included in the updating by the likelihood function. The likelihood function can, for example, take into account the precision of the sampling device. Bayes' equation also allows the inclusion of subjective information through the prior term. The prior probability can be based on previous measurements and/or intuition.

Returning to the earlier landfill example, a single borehole is to be drilled at the probable location of the fluvial channel to determine if a window exists in the aquitard. It is arbitrarily assumed that if the window exists there is a 70% chance that it will be found with the measurement technology selected. It is also assumed that the borehole will not give a false outcome; therefore, if a window is sampled then it exists with certainty. Obviously, if no window exists, then there is no chance of finding one. Therefore, the likelihood functions for the borehole are

$$P(S_W|E_W) = 0.7 \quad (2.13)$$

$$P(S_{NW}|E_W) = 1. - P(S_W|E_W) \quad (2.14)$$

$$= 1. - 0.7$$

$$= 0.3$$

$$P(S_W|E_{NW}) = 0. \quad (2.15)$$

$$P(S_{NW}|E_{NW}) = 1.0 \quad (2.16)$$

For the case where a window is sampled, S_W , the updated probability of a window existing is determined from Bayes' equation by

$$P(E_W|S_W) = \frac{P(S_W|E_W)P(E_W)}{P(S_W)} \quad (2.17)$$

The probability of sampling a window, $P(S_W)$ is calculated using equation (2.12):

$$\begin{aligned}
 P(S_W) &= P(S_W|E_W)P(E_W) + P(S_W|E_{NW})P(E_{NW}) \\
 &= (0.7)(0.2) + (0)(0.8) \\
 &= 0.14
 \end{aligned} \tag{2.18}$$

Therefore, from equations (2.4), (2.13), and (2.18):

$$\begin{aligned}
 P(E_W|S_W) &= \frac{(0.7)(0.2)}{(0.14)} \\
 &= 1.0
 \end{aligned} \tag{2.19}$$

$P(E_{NW}|S_W)$ can also be calculated using Bayes' equation, but since there are only two events it can be more easily calculated by:

$$\begin{aligned}
 P(E_{NW}|S_W) &= 1.0 - P(E_W|S_W) \\
 &= 1.0 - 1.0 \\
 &= 0.
 \end{aligned} \tag{2.20}$$

For the case of S_{NW}

$$P(E_W|S_{NW}) = \frac{P(S_{NW}|E_W)P(E_W)}{P(S_{NW})} \tag{2.21}$$

where:

$$\begin{aligned}
 P(S_{NW}) &= 1.0 - P(S_W) \\
 &= 1.0 - 0.14 \\
 &= 0.86
 \end{aligned} \tag{2.22}$$

Therefore, from equations (2.22), (2.14) and (2.4):

$$\begin{aligned}
 P(E_W|S_{NW}) &= \frac{(0.3)(0.2)}{(0.86)} \\
 &= 0.07
 \end{aligned}
 \tag{2.23}$$

Note, that S_{NW} has reduced the probability of a window from its prior value of 0.2 to 0.07. The updated probability of no window, given S_{NW} , $P(E_{NW}|S_{NW})$, is

$$\begin{aligned}
 P(E_{NW}|S_{NW}) &= 1 - P(E_W|S_{NW}) \\
 &= 1 - 0.07 \\
 &= 0.93
 \end{aligned}
 \tag{2.24}$$

For the landfill example, let us assume that no window was found at the fluvial channel by the borehole. The updated probabilities from equations (2.23) and (2.24) are marked on the decision tree shown in Figure 2-3. The same steps used in the prior analysis are then used to select the posterior best alternative. The posterior expected objective function for A_L is \$490 000, but the expected objective function for A_{NL} is now \$752 000, or \$152 000 higher than calculated during the prior analysis. A_{NL} is still the best design. In fact, now that additional information is available, it is better than originally thought during the prior analysis.

2.4 DATA WORTH THROUGH PREPOSTERIOR ANALYSIS

The preposterior analysis can be separated into two components: the expected value of perfect information (EVPI) and the expected value of sample information (EVSI). The EVPI is an estimate of the value of having perfect information so that uncertainty is reduced to zero and a perfect design decision can be made. The EVSI is an estimate of the expected value of a normal, imperfect, sampling program which will not reduce uncertainty to zero and there will still be uncertainty in any design decision.

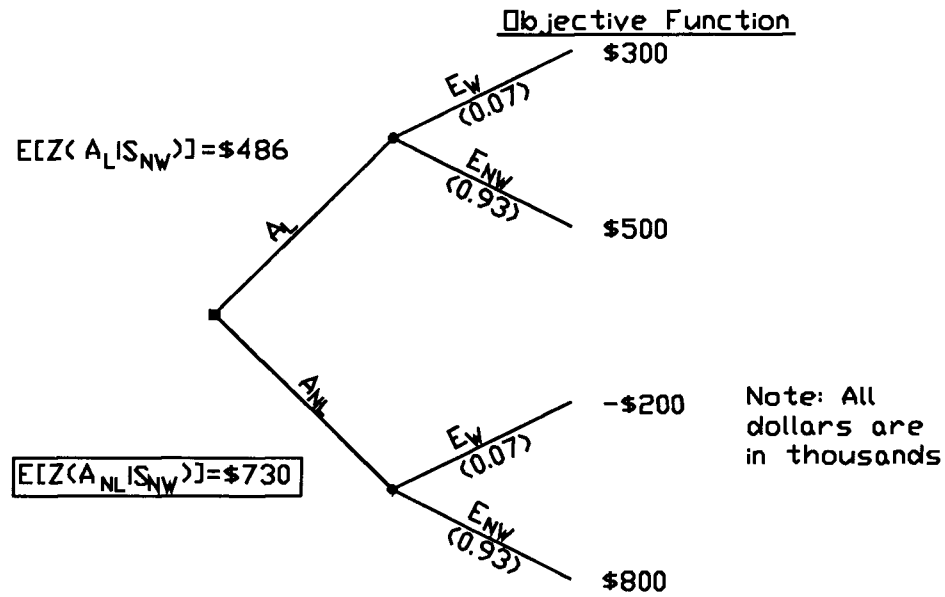


Figure 2-3: Decision tree used in posterior analysis of example landfill

2.4.1 EXPECTED VALUE OF PERFECT INFORMATION (EVPI)

The EVPI can be explained using the concept of regret. The regret associated with a decision represents the monetary loss incurred by not making the best decision. It is defined as the difference between the value of the objective functions $Z(A_T)$ and $Z(A_D)$, where A_T represents the true best design alternative and A_D represents the chosen design alternative. Both are evaluated at the true event, E_T . The regret associated with A_D , $\text{Reg}(A_D, E_T)$, is calculated by:

$$\text{Reg}(A_D, E_T) = Z(A_T, E_T) - Z(A_D, E_T) \quad (2.25)$$

where,

- $Z(A_T, E_T)$ is the objective function for A_T evaluated at E_T , and
- $Z(A_D, E_T)$ is the objective function for A_D evaluated at E_T .

Note, that the regret can be calculated for any alternative, A_j , not just A_D .

Unfortunately, E_T is never known. Therefore, we must calculate an expected regret, $E[\text{Reg}(A_D)]$, over all the possible events, E_i :

$$E[\text{Reg}(A_D)] = \sum_{i=1}^I [Z(A_T, E_i) - Z(A_D, E_i)]P(E_i) \quad (2.26)$$

The expected regret gives the expected monetary loss when A_D is not A_T . In other words, it is the maximum improvement that could be expected in A_D , if E_T was known. The $E[\text{Reg}(A_D)]$ represents the EVPI. Since no exploration program will yield perfect information, the EVPI is an estimate of the maximum worth of any normal exploration program. An exploration program should not be carried out if its costs exceed the EVPI.

An example calculation of the expected regret for the prior design of a liner is presented in Figure 2-4. The regret associated with each design/event pair is shown at the right hand side of Figure 2-4. If E_T is a window, then from Figure 2-2 and equations (2.7) and (2.9), $Z(A_L, E_W) = \$300\,000$ and $Z(A_{NL}, E_W) = -\$200\,000$. Hence, the prior A_D of the no liner alternative really would have been poor. The true best alternative would really have been a liner. The regret in choosing A_{NL} in the prior analysis would be:

$$\begin{aligned} \text{Reg}(A_{NL}, E_W) &= Z(A_T, E_W) - Z(A_{NL}, E_W) \\ &= Z(A_L, E_W) - Z(A_{NL}, E_W) \\ &= \$300\,000 - (-\$200\,000) \\ &= \$500\,000 \end{aligned} \quad (2.27)$$

However, if E_T is no window, then from Figure 2-2 and equations (2.8) and (2.10) $Z(A_L, E_{NW}) = \$500\,000$ and $Z(A_{NL}, E_{NW}) = \$800\,000$. Under this outcome, the prior A_D of no-liner would still be the best. Hence the regret would be zero.

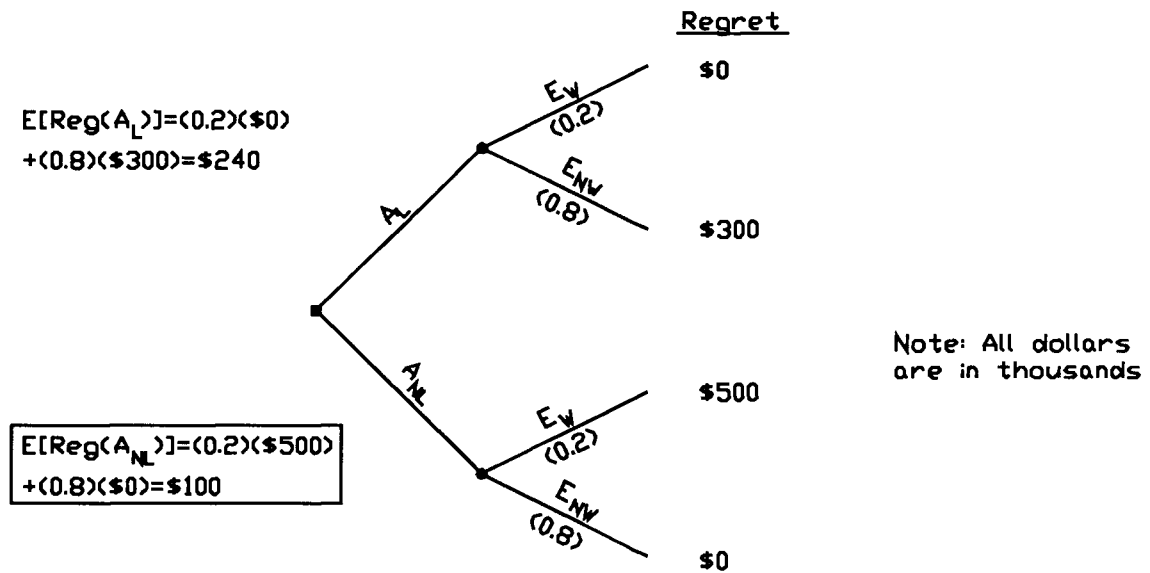


Figure 2-4: Expected regret calculations for the landfill example.

The expected regret of the prior best design alternative of no-liner is

$$\begin{aligned}
 E[\text{Reg}(A_{NL})] &= \text{Reg}(A_{NL}, E_{NW})P(E_{NW}) + \text{Reg}(A_{NL}, E_W)P(E_W) \\
 &= (\$0)(0.8) + (\$500\,000)(0.2) \\
 &= \$100\,000
 \end{aligned}
 \tag{2.28}$$

therefore,

$$\text{EVPI} = \$100\,000
 \tag{2.29}$$

It would not be worth carrying out any exploratory work that cost more than \$100 000.

Expected regret can also be used in the prior analysis to choose the best alternative. A_D has the lowest expected regret. For example, $E[\text{Reg}(A_L)] = \$240\,000$ while $E[\text{Reg}(A_{NL})] = \$100\,000$ (Fig. 2-4). The alternative with the minimum expected regret is the alternative with the highest expected objective function.

2.4.2 EXPECTED VALUE OF SAMPLE INFORMATION (EVSI)

There are two standard approaches for calculating the EVSI. The first is based on the increase in the maximum expected objective function. The second is based on the reduction in the minimum expected regret. These are well established in the literature (refer to Benjamin and Cornell, 1970; Davis and Dvoranchik (1971); or Davis, Kisiel, and Duckstein (1972)). A third approach is developed by rearranging the equations used in the first method to isolate the individual contributions of the different sample outcomes to the EVSI. It is utilized in this thesis to visualize how different factors affect the data worth process. The three methods will first be outlined in more detail below.

2.4.2.1 Method 1: The EVSI from the Expected Increase in the Maximum Objective Function

In this method, the worth of data, W_1 , is calculated from the expected increase of the expected objective function of the posterior best design alternative, A_D' , over the expected objective function of the prior best design alternative, A_D . W_1 is calculated by:

$$W_1 = E[E(Z(A_D'))] - E(Z(A_D)) \quad (2.30)$$

where,

- $Z(A_D)$ is the objective function of A_D ,
- $E(Z(A_D))$ is the expected value of $Z(A_D)$, and
- $E[E(Z(A_D'))]$ is the expected value of $E(Z(A_D'))$.

For the discrete case of I events, E_i , and J sample outcomes, S_j , equation (2.30) becomes:

$$W_1 = \sum_{j=1}^J \left[\sum_{i=1}^I Z(A_{Dj}', E_i) P(E_i | S_j) \right] P(S_j) - \sum_{i=1}^I Z(A_D, E_i) P(E_i) \quad (2.31)$$

where,

- A_{Dj}' is the best design alternative given S_j ,
- $Z(A_D, E_i)$ is the objective function A_D evaluated for event E_i ,
- $P(E_i | S_j)$ is the posterior probability of event, E_i , given that sample S_j has been taken,
- $P(E_i)$ is the prior probability that event E_i will occur, and
- $P(S_j)$ is the probability of sampling S_j .

An example preposterior analysis using method 1 is carried out below. The worth of the example borehole carried out in the posterior analysis (Section 2.3) will be evaluated. In a preposterior analysis, the outcome of the borehole is not known. A decision tree used in the preposterior analysis is shown in Figure 2-5. It consists of two parts. The first part, associated with the decision not to drill the borehole, is identical to the prior analysis. The second part, associated with the decision to drill the borehole represents the preposterior analysis.

The preposterior analysis can be thought to consist of two stages. Stage 1 is a series of branches for each possible sample outcome. In this example, there are two: sampling either a window, S_W , or no window, S_{NW} . The probability that a particular outcome will be sampled is marked in brackets beside each branch. Recall that these were calculated in (2.18) and (2.22).

Stage 2 consists of a series of pseudo-posterior analyses. A pseudo-posterior analysis is associated with each sample outcome. The probabilities used in each pseudo-posterior analysis are updated according to the sample outcome. For the case of S_{NW} , $P(E_W | S_{NW})$ and $P(E_{NW} | S_{NW})$ have already been calculated in equations (2.23) and (2.24). The expected objective functions are $E[Z(A_{NL} | S_{NW})] = \$730\,000$, and $E[Z(A_L | S_{NW})] = \$486\,000$. Therefore, A_D' would be A_{NL} .

For the case of S_W , $P(E_W|S_W)$ and $P(E_{NW}|S_W)$ have already been calculated in equations (2.19) and (2.20).

$E[Z(A_{NL}|S_W)] = -\$200\,000$, and $E[Z(A_L|S_W)] = \$300\,000$. Therefore, A_D' would now be A_L .

The worth of the borehole from equation (2.30) is

$$\begin{aligned} W_1 &= E[E(Z(A_D'))] - E(Z(A_D)) \\ &= \$670\,000 - \$600\,000 \\ &= \$70\,000 \end{aligned} \tag{2.32}$$

Therefore, the borehole is worth \$70 000. It would not be worth drilling the borehole, if it is going to cost more than \$70 000.

2.4.2.2 Method 2: The EVSI from Expected Reduction in Minimum Expected Regret

Method 2 calculates the worth of data, W_2 , from the expected reduction in the $E[\text{Reg}(A_D)]$ from the $E[\text{Reg}(A_D)]$. W_2 is calculated by

$$W_2 = E(\text{Reg}(A_D)) - E[E(\text{Reg}(A_D'))] \tag{2.33}$$

where,

- $\text{Reg}(A_D)$ is the regret of A_D ,
- $E(\text{Reg}(A_D))$ is the expected regret of A_D , and
- $E[E(\text{Reg}(A_D'))]$ is the expected expected regret of A_D' .

For the discrete case, (2.33) becomes

$$\begin{aligned} W_2 &= \sum_{i=1}^I [Z(A_T, E_i) - Z(A_D, E_i)]P(E_i) - \\ &\quad \sum_{j=1}^J \sum_{i=1}^I \{ [Z(A_{Tj}', E_i) - Z(A_{Dj}', E_i)]P(E_i|S_j) \} P(S_j) \end{aligned} \tag{2.34}$$

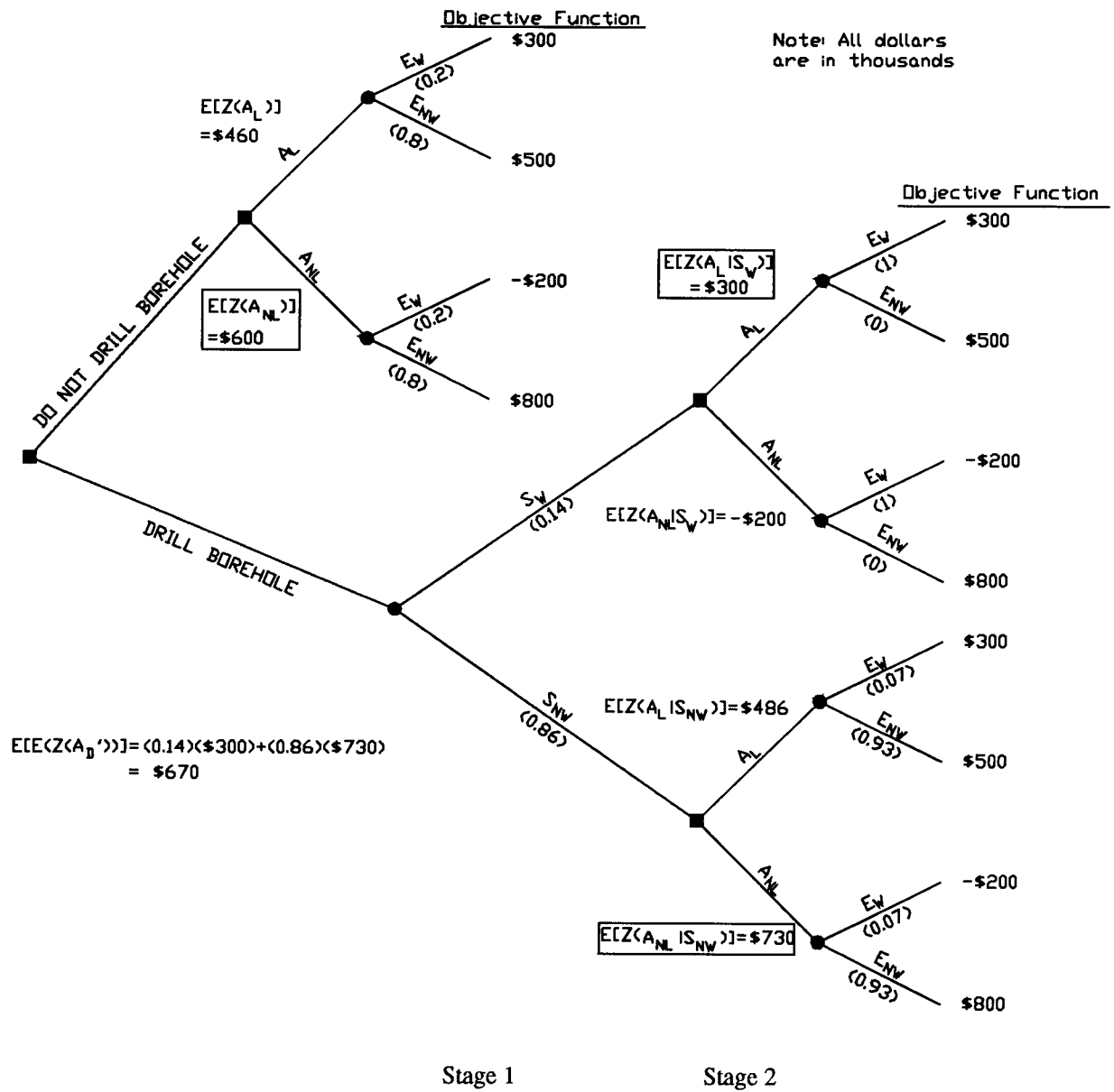


Figure 2-5: Decision tree of preposterior analysis of example borehole using method 1.

where

- $Z(A_{Tj'}, E_i)$ is the objective function of the posterior true best alternative evaluated for event, E_i ,

given sample, S_j , and

- $Z(A_T, E_i)$ is the objective function of the prior true best alternative evaluated for the event, E_i .

A decision tree used in the preposterior analysis is shown in Figure 2-6. The regret for each combination of E_j and A_j is marked to the right of the branch representing E_j . The calculation of these values was discussed in Section 2.3. In the case of S_{NW} , the expected regret for A_D' (no liner) is \$34 900. In the case of S_W , the expected regret for A_D' (a liner) is \$0. Therefore, the $E[E(\text{Reg}(A_D'))] = \$30\,000$.

Therefore, from equation (2.33) W_2 is

$$\begin{aligned} W_2 &= E(\text{Reg}(A_D)) - E[E(\text{Reg}(A_D'))] \\ &= \$100\,000 - \$30\,000 \\ &= \$70\,000 \end{aligned} \tag{2.35}$$

Therefore, the worth of the borehole is again \$70 000.

2.4.2.3 Method 3: Expected Posterior Worth of a Measurement

Method 3 is developed by rearranging Method 1 to show contributions of the different sample outcomes to the EVSI. The basic philosophy of the method is to put the EVSI, or worth, of the measurement in terms of the posterior worth of sample outcomes. Or in other words, what is the real worth of a measurement that samples a window (or no window) after it has been taken.

Recall from Method 1 that the worth of taking a measurement for the discrete case, is calculated by

$$W_1 = \sum_{j=1}^J \sum_{i=1}^I Z(A_{Dj}', E_i) P(E_i | S_j) P(S_j) - \sum_{i=1}^I Z(A_D, E_i) P(E_i) \tag{2.36}$$

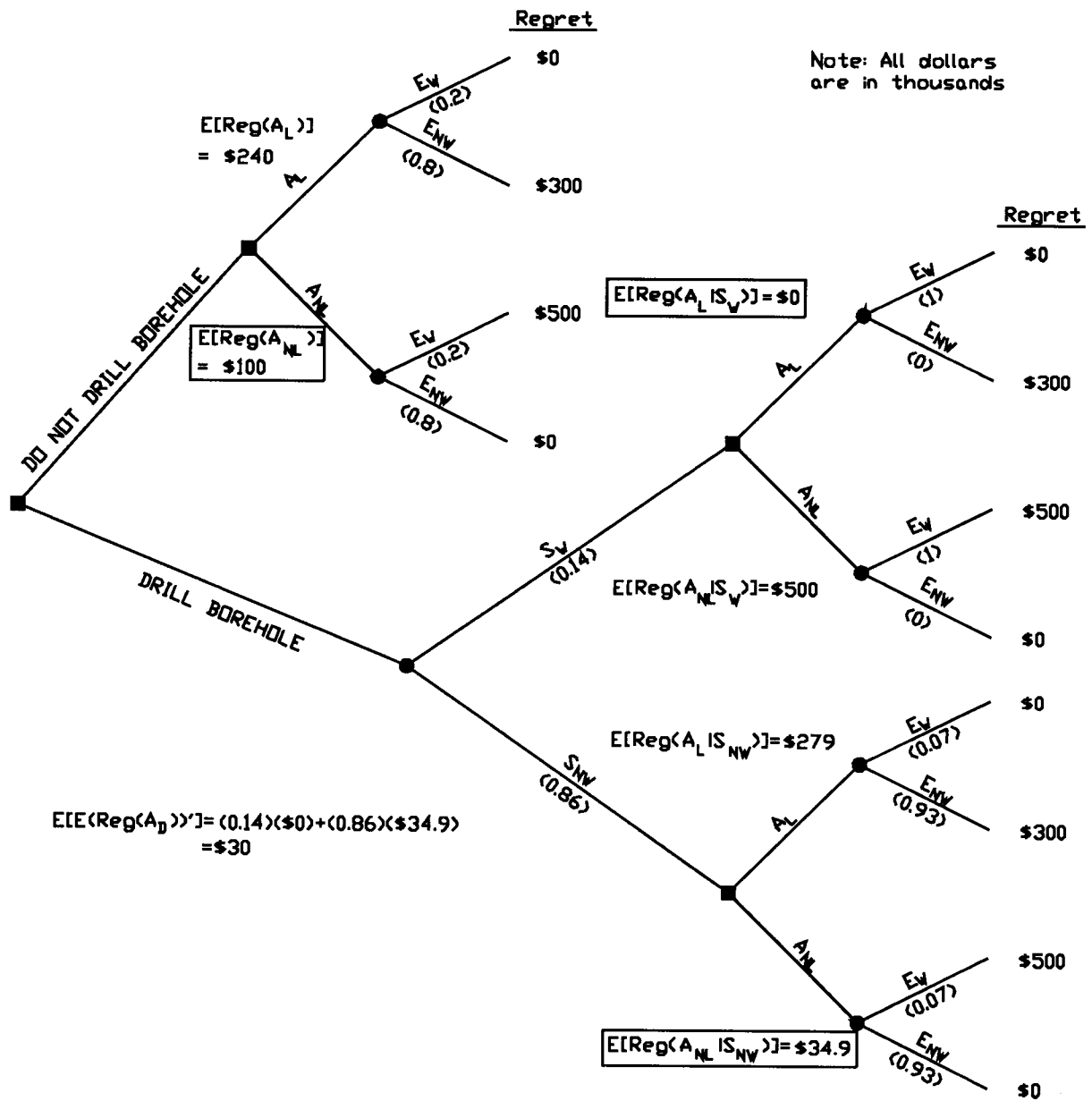


Figure 2-6: Decision tree used in preposterior analysis of example borehole using method 2.

For a given particular event, E_i , the sum of all possible sample outcomes, S_j , is one; hence,

$$\sum_{j=1}^J P(S_j | E_i) = 1 \quad (2.37)$$

Therefore, equation (2.36) can be rewritten as

$$W_1 = \sum_{j=1}^J \sum_{i=1}^I Z(A_{Dj}', E_i) P(E_i | S_j) P(S_j) - \sum_{i=1}^I \sum_{j=1}^J Z(A_D, E_i) P(S_j | E_i) P(E_i) \quad (2.38)$$

Substituting Bayes' equation,

$$P(E_i | S_j) = \frac{P(S_j | E_i) P(E_i)}{P(S_j)} \quad (2.39)$$

into equation (2.38) yields:

$$W_1 = \sum_{j=1}^J \sum_{i=1}^I Z(A_{Dj}', E_i) P(E_i | S_j) P(S_j) - \sum_{i=1}^I \sum_{j=1}^J Z(A_D, E_i) P(E_i | S_j) P(S_j) \quad (2.40)$$

Reversing the summation terms on the second term of the right hand side yields:

$$W_1 = \sum_{j=1}^J \sum_{i=1}^I Z(A_{Dj}', E_i) P(E_i | S_j) P(S_j) - \sum_{j=1}^J \sum_{i=1}^I Z(A_D, E_i) P(E_i | S_j) P(S_j) \quad (2.41)$$

The above equation can be rearranged to give:

$$W_3 = \sum_{j=1}^J \left[\sum_{i=1}^I Z(A_{Dj}', E_i) P(E_i | S_j) - \sum_{i=1}^I Z(A_D, E_i) P(E_i | S_j) \right] P(S_j) \quad (2.42)$$

where W_1 has been replaced by W_3 to denote that the EVSI is now being calculated by Method 3. For the continuous case, W_3 can be calculated by:

$$W_3 = E[E(Z(A_D' | S)) - E(Z(A_D | S))] \quad (2.43)$$

where $E(Z(A_D|S))$ is the expected value of the prior best design alternative, but evaluated with additional sample information S . The contributions of the different sample outcomes have now been isolated. One can use this method to examine the posterior worth of a measurement. For example, if the sample outcome was S_W , its worth would be

$$W(S_W) = E(Z(A_D'|S_W)) - E(Z(A_D|S_W)) \quad (2.44)$$

which represents the difference between the expected value of the new posterior best design alternative, A_D' , and the new estimate of the expected value of the old prior best design alternative, A_D . In other words, it represents the difference between the new best alternative and what the A_D is really worth. If the outcome of a measurement does not change A_D to a different one, then the outcome has no value.

A preposterior analysis using method 3 can be illustrated with the decision tree used in method 1 (Fig. 2-5). Recall that for S_{NW} , $E(Z(A_{NL}|S_{NW})) = \$730\,000$ and $E(Z(A_L|S_{NW})) = \$486\,000$. Therefore, S_{NW} has only reconfirmed that the prior best alternative of no-liner is still the best and sampling no window is worth nothing.

In the case of S_W , the best alternative is now to have a liner ($E(Z(A_L|S_W)) = \$300\,000$). The expected objective function of the prior no-liner decision was found to be really only $-\$200\,000$, rather than its previous value of $\$600\,000$ calculated in the prior analysis. Therefore, S_W has resulted in an improvement of $\$500\,000$ ($\$300\,000 - -\$200\,000$) in the design decision.

The worth of taking a sample from equation (2.42) is

$$\begin{aligned} W_3 &= (\$500\,000)(0.14) + (\$0)(0.86) \\ &= \$70\,000 \end{aligned} \quad (2.45)$$

which is the same as calculated by methods 1 and 2.

In general, the worth of data will be expressed in terms of Method 1 because it is commonly used in the literature. Method 3 will only be used for some demonstration examples. It is felt that Method 3 is a more intuitive approach which simplifies the understanding of how different factors affect the estimated worth of a measurement.

2.5 APPLICATION AND EXTENSION OF THE METHODS

The methods presented in Section 2.4 for discrete events will be applied to more complex cases involving spatial correlation and multiple realizations to determine probabilities. The presentation of these ideas must await the presentation of the geological arguments (Chapter 3), sequential indicator simulation (Chapter 4) and contaminant transport concepts (Chapter 5).

2.6 NOTATION

A_D	prior best design alternative
A_L	liner alternative
A_{NL}	no liner alternative
A_T	true best design alternative
$B(t)$	known benefits in year t
$C(t)$	known costs in year t
E_j	j^{th} possible event
E_{NW}	event of no window in aquitard
E_T	true event
E_W	event of a window in aquitard

i	discount rate
$P_f(t)$	probability of failure in year t
$R(t)$	risk in year t
$\text{Reg}(A_j)$	regret of design alternative A_j
S_j	j^{th} sample outcome
S_{NW}	sample outcome is no window
S_{W}	sample outcome is a window
t	time
T	engineering time horizon
$U(C_f)$	utility function
W_1	worth of data by the expected increase in the maximum objective function
W_2	worth of data by the expected reduction in minimum regret
W_3	worth of data by the expected posterior worth of a measurement
Z	objective function

CHAPTER 3: GEOLOGICAL PREDICTION OF AQUITARD CONTINUITY

3.1 INTRODUCTION

The purpose of Chapter 3 is to explain why a conceptual understanding of local geology can be important in predicting aquitard continuity.

There is a strong relationship between patterns of heterogeneity of clastic rocks and the depositional environment that formed them (Le Blanc, 1977a and b; Weber, 1982; and Weber, 1986). A brief overview is presented below of a number of depositional environments and the geometric characteristics of clay layers deposited in them. Refer to Ravenne et al. (1989), Sneider et al. (1978), Jardine et al. (1977), and Le Blanc (1977a and b) for a more detailed overview of patterns of heterogeneity formed in different depositional environments. A review of previous work in quantifying shale/clay layer heterogeneity is then presented. Finally, the importance of a conceptual understanding of the local geology in predicting aquitard continuity is emphasized.

In general, the relationship between depositional environment and patterns of geological heterogeneity is poorly understood for two reasons. Firstly, the patterns of heterogeneity can be very complex. And secondly, the available data base on the three dimensional geometry of clastic rock stratigraphy is small.

3.2 THE EFFECT OF DEPOSITIONAL ENVIRONMENT ON THE GEOMETRIC CHARACTERISTICS OF CLAY LAYERS.

3.2.1 BRAIDED STREAM

Braided streams occur in high energy environments where there is an abundant supply of coarse grained sediments (Walker, 1983). They also have easily erodible banks which allows the stream to laterally migrate. The Brahmaputra, for example laterally migrates up to 900 m per year (Selby, 1985). The result is that fine grained material generally washes through the system and any clay deposits formed are often eroded by the constantly changing river. Patches of shale are rare, elongate in shape and are often less than a meter in size (Potter et al. 1980). Leopold and Wolman (1957), cited by Wadman et al. (1979) found in a study of 17 braided and straight channel deposits that the average length to width ratio of shale layers was three.

3.2.2 MEANDERING STREAM

Meandering rivers form under lower energy environments than braided streams and generally carry smaller volumes of sediments, which are fine grained. The meander belt is generally 15 to 20 times the width of the channel (Le Blanc, 1977a). The Mississippi River meander belt is up to 15 to 20 miles wide. Shale in meandering streams predominantly occurs as accretionary flood plain deposits, as plugs in abandoned stream channels, or as clay drapes.

Clay plugs are formed from clay being deposited in abandoned channels. The amount of clay deposited depends upon the rate at which the channel was abandoned. Rapidly abandoned channels are predominantly filled with clay, while slowly abandoned channels are composed of sand and silt as well. The size of the plugs are limited to the size of the stream channel (Richardson et al., 1978). The plugs are generally resistant to erosion by the meandering stream.

Flood plain deposits are formed during flood periods when the river overflows its banks. The flood plain deposits are areally extensive, but are subjected to erosion by the meandering river. Consequently, flood plain shales are preserved in elongated isolated bodies that range in size from 400 to 1600 m wide and 1600 to 3200 m long. Studies of ancient flood plain deposits indicate that shales make up from five to

15% of the flood plain on an areal basis (Richardson et al., 1978). Potter et al. (1980) report that flood plain shales can extend up to tens of km parallel to shoreline and can be up to ten or more meters thick. Some flood plain deposits in back-swamps and flood basins are not on the meander belt, and will not be eroded by the migrating river (Le Blanc, 1977a).

Drapes are formed when clay is deposited on point bars at the ebb of a flood when the stream velocity is almost zero (Le Blanc, 1977a). Drapes are generally small in size compared to either flood plain or abandoned channel clays with their size ranging from that of local depressions to entire point bars. Clay drapes generally range from one mm to more than 30 to 60 mm in thickness and are more common in the upper half of the point bar sequence (Le Blanc, 1977a).

3.2.3 DELTAIC

There are many types of deltas depending upon the energy of the environment, sediment source and supply. For simplicity, the discussion here will be limited to the two extreme types of deltas. These are (a) high energy sand deltas and (b) low energy mud deltas. High energy sand deltas are characterized by a few active meandering, distributary channels. Low energy mud deltas are characterized by many bifurcating distributary channels which tend to be straight, and not meander as much. There are a vast number of different types of deltas in between the two extremes.

All deltas can be divided into a number of subenvironments consisting of distributary channels, delta flood plains, the delta front and the prodelta. Delta flood plains commonly contain dozens of abandoned distributary channels and have only a few active channels (Le Blanc, 1977a). Just as in the meandering stream environment, the abandoned channels are filled with sediments. Quickly abandoned channels are predominantly filled with clay while slowly abandoned channels are filled with more silt and sand. Delta flood plain deposits are formed in the same manner as meandering river flood plain deposits.

The size of a distributary channel, and hence its associated deposits is dependent upon several factors including: the delta size, type of bed material being eroded, and the position of the channel in the delta. For example distributary channels in the Mississippi near the sea are typically less than 200 m wide and 10 m deep, while the upstream channels are up to 1000 m wide and 60 m deep (Sneider et al., 1978).

In high energy sand deltas, fines are winnowed away from the delta front deposits. Consequently, only very discontinuous shale layers are deposited. Shale layers are more common at the bottom of distributary mouth bars. In low energy deltas, shale layers have a much greater continuity. In distributary mouth bars, 2 cm thick clay beds extend over hundreds of meters, particularly in the lower half of the bar deposits (Sneider et al., 1978). The prodelta shales can be very continuous, having dimensions similar to that of marine shales (Richardson et al., 1978). Shallow deltaic clays can be greatly affected by bioturbation, gas production, and growth faults. Bioturbation is important because it can greatly increase the hydraulic conductivity of a clay.

3.2.4 ESTUARINE

Estuaries occur where a river mouth is affected by tidal action. Tidal channels meander between mudflats and channel bars of mud and sand. The difference between deltas and estuaries is that deltas have a large amount of sediments being deposited in the river mouth. In estuaries, tidal currents and river discharge keep the river channels open (Selby, 1985). However, similar depositional features are associated with both estuaries and deltas. For example, barrier bars, lagoons and coastal swamps can be found in both types of environments.

The nature of the clay deposits is dependent upon the forces affecting them. For example, in estuaries with low wave energy, mud banks can occur with areal dimensions which are up to 100's to 1000's of meters squared. In estuaries with high wave energy, clay mostly occurs in small to medium sized patches

which are a few meters thick. In tidally dominated estuaries, drapes can occur on point bars and on sheets parallel to the channel (Potter et al, 1980). Estuarine clays can be greatly affected by bioturbation.

3.2.5 SUBMARINE FAN

The classical depositional process of the submarine fan is the turbidity current. Submarine fans predominantly occur on delta fronts, continental shelves and deeper ocean basins. Turbidite layers tend to be laterally extensive covering hundreds of meters and with little variation in thickness (Walker, 1983).

Shales are predominantly deposited in the lower portion of submarine fans and can cover large areal extents. However, shales of smaller size can be deposited in the proximal portions of the fan. Hazue et al. (1988), in a study of a submarine fan found that the average length of non-correlative shales was approximately 500 m in distal portions of the fan and 200 m in proximal portions. Shale layers often occur in thin layers interbedded with sandstone and silt. Shales layers can be eroded in cases of increased sediments supply because fan channels may cut down into lower fan sediments (Walker, 1983), incising the clay layers.

3.2.6 MARINE

Deep marine shales have large areal extents with thin (0.3 m) shale layers commonly covering two to five square kilometers. Thicker shales are commonly continuous for a hundred km (Richardson et al., 1978). Shallow marine clays are very susceptible to bioturbation.

3.2.7 GLACIAL

There are two main types of deposits associated with glaciation: tills which are deposited directly by the ice, and sediments deposited by meltwater. Deposits of glaciolacustrine clay form some of the most extensive shallow aquitards in North America (Freeze and Cherry, 1979). Clay deposited by meltwater streams will be similar in character to those deposited by fluvial processes and therefore will not be discussed here.

Tills are generally composed of clay sized particles and are hydrologically important because they often form aquitards. The hydraulic conductivity of dense, fine grained unfractured glacial till, typically ranges from 10^{-10} to 10^{-12} m/s.

Glacial tills form a major portion of near-surface aquitards in Canada and the northern U.S.A. because the last period of glaciation covered most of northern North America only 8 000 to 14 000 years ago (Press and Siever, 1974). Not enough geologic time has occurred for other surface deposits to form.

Till can be formed by both alpine and continental glaciation. However, till deposits from alpine glaciation will not be discussed here because they comprise a small percentage of the till relative to those formed in continental glaciation in North America. Only the two most significant types will be discussed: supraglacial and subglacial till. Supraglacial till is carried on top of the glacier. Subglacial, or basal, till is laid down at the bottom of the glacier.

The subglacial till forms a ground moraine that can be several meters thick. Massive basal till is the most widespread Pleistocene facies on land (Reading, 1983). Supraglacial till forms an ablation moraine. It forms on the sloping snout of the glacier and is left behind as the glacier recedes.

Sheets of ablation and basal till can be continuous over extensive areas. For example, in Southern Ontario till sheets are continuous over tens of kilometers. Till units are generally thicker near the source rock and thinner towards the outer margins of the glacier. However, the thickness of till sheets is also

controlled by the relief. The till is thicker in hollows and thinner or absent in topographic highs. The erodibility of the substrata is a major factor in controlling till thickness. Even though extensive deposits of massive till occur, they often contain isolated bodies of coarse, stratified sediments deposited by englacial and subglacial streams. In general, the stratigraphy of glacial deposits tends to be very complex.

The composition of till can be heavily dependent upon its source. For example, glaciers that cross over old lakes pick up fine grained lacustrine sediments and leave a clayey till. In general, when the source rocks are sedimentary, till is predominantly clay sized. When the source rocks are granite, or other crystalline rocks, till is more sandy or silty. Tills formed from crystalline source rocks are less likely to form aquitards.

3.3 QUANTITATIVE DESCRIPTION OF SHALE HETEROGENEITY

Most of the work in quantifying the relationship between shale/clay layer heterogeneity and depositional environments is recent and is restricted to the field of petroleum geology. Zeito (1965), noted the dimensions of shales in different types of environments. Weber (1982) extended this work. He presented the cumulative probability distribution of the lengths of shale layers formed in marine, delta barrier, delta fringe, delta plain, distributary channel, and coarse point bars environments (Fig. 3-1). Haldorsen (1989) and Hazeu et al. (1988) present similar cumulative probability distributions for shale layers formed in submarine fans. Geehan et al. (1986) also presents similar curves for shales formed in flood plains, abandoned channels, and as drapes on point bars.

Haldorsen and Lake (1984, p. 449) note that "No universal validity is claimed for the findings of Zeito, but there appears to be significant confidence in some of the data." The important point to note is that there is a distinct difference between the different cumulative distributions.

However, there is uncertainty in the exact probability distribution for a particular environment for two reasons. The first is the cumulative probability distributions are estimated from a limited number of measurements. The second reason, as pointed out by Haldorsen (1989), is that the dimensions measured in outcrop of shale layers, as reported by Weber (1982), are not the true length of the shale, but a cross section through the shale layer at some unknown angle.

Little work has been done in quantifying the spatial distribution and correlation of shale/clay layers formed in different sedimentary environments. Zeito (1965) found in a study of outcrops that the centers of shale layers were randomly distributed.

Inconclusive work has been done on relating the length of a shale layer to its thickness. Delhomme and Giannesini (1979), cited by Haldorsen and Chang (1986), concluded that in the deltaic system that they studied, the thickness of shale layers was only related to local topography that prevailed at the time of deposition and was independent of shale length. However, Wu et al. (1973) found an approximate relationship between the thickness of different layers and their lengths in Mississippi alluvial deposits. Kossack (1989), in the most comprehensive study, reported that there were only six publications with enough layer length and thickness data to permit analysis. His results are inconclusive.

Some work has been done on quantifying the geostatistical nature of clay/shale layers. However, this work will be presented in Chapter 4, after geostatistical concepts have been introduced.

3.4 THE IMPORTANCE OF GEOLOGY IN PREDICTING AQUITARD CONTINUITY

A conceptual understanding of the local geology can be the most critical factor in predicting aquitard continuity in clastic depositional environments. This will be particularly true when there is a shortage of measurements of the aquitard, which will be the norm in most hydrogeological design situations. This is

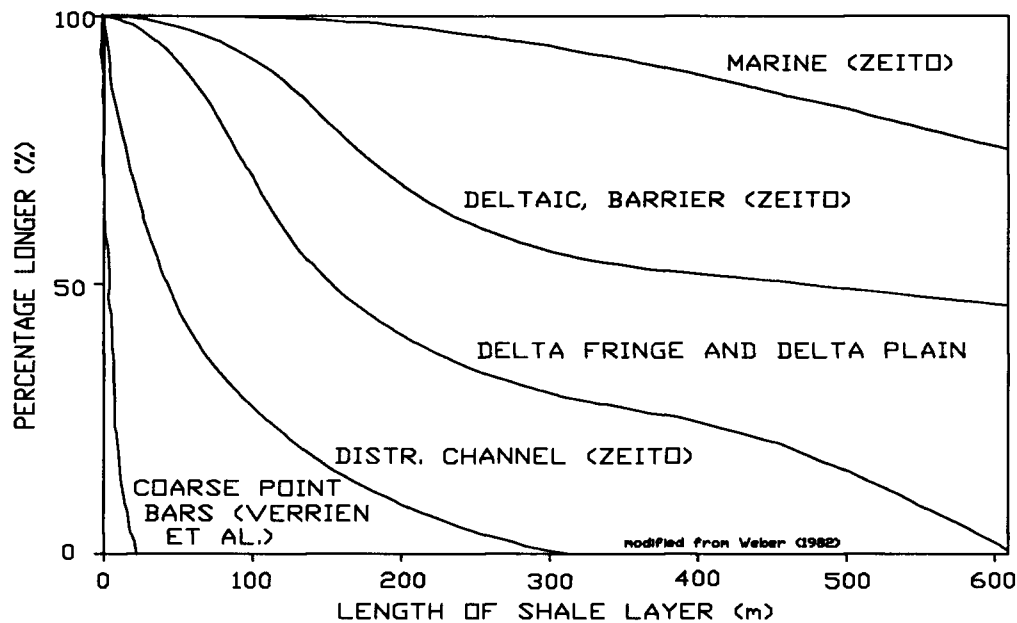


Figure 3-1: Cumulative probability distribution of shale length in different depositional environments. (modified from Weber (1982))

clearly demonstrated in an interesting study of shale continuity in the Ivishak petroleum reservoir at Prudhoe Bay by Geehan et al. (1986). The Ivishak Formation is a combination of sandstones, conglomerates, and shales deposited in a largely progradational, fluvial/deltaic complex. The continuity of shales in one chronostratigraphic horizon was studied. The thickness of intersected shales was first contoured without any geological input (Fig. 3-2). This results in a maximum continuity case. (Note, for example the three data points at X, Y, and Z.)

However, a very different picture is obtained once the data are contoured to geologically conform to the genetic type of shale (Fig. 3-3). The reason for this change can be seen by examining the shale at X, Y, and Z. The shale at these points was assumed to be continuous in Figure 3-2. However, the shale at points X, Y, and Z represent drape, abandoned channel, and flood plain facies respectively and therefore

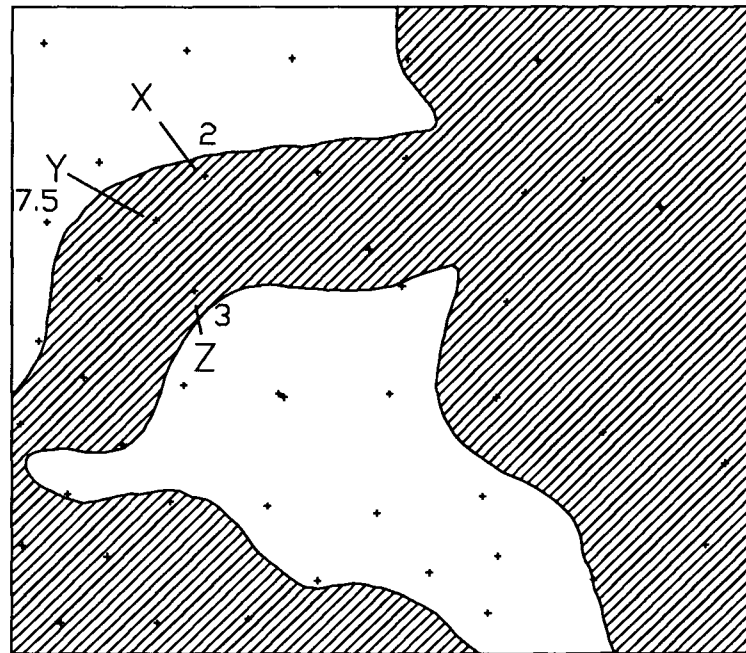
cannot be one continuous unit. The flood plain shale will have a large lateral continuity, but the abandoned channel and drape shales will have a lateral continuity on the order of 10's of meters. Hence, even though the three shale units are present in three adjacent wells, are chronostratigraphically equivalent, and are of the same approximate thickness, they do not correlate. Consequently, the addition of geological information has fundamentally altered the picture of shale continuity.

The importance of using geological information is shown by the strong relationship which exists between patterns of clay heterogeneity and depositional environment. Even if the relationship is not well quantified, it could be vital to include because the range of characteristics is immense. For example, a clay layer formed in a braided stream environment would be expected to have a continuity on the order of meters while a clay layer formed in a deep marine environment would be expected to have a continuity on the order of kilometers. Therefore, simply knowing the depositional environment that formed an aquitard can provide crucial information in predicting aquitard continuity.

Geological information will be most useful when it can be combined with existing quantitative information. The Bayesian methodology for carrying out this combination is developed in Chapter 4 and is carried out for the Savannah River Site case history in Chapter 8.

However, it must be noted that combining geological understanding with quantitative data can be limited at present. Not enough work has been done in establishing the necessary quantitative relationships between environment of deposition and patterns of shale/clay layer heterogeneity. But, these relationships will become better established in the future as more research is carried out.

0 1 MILE 1 SHALE THICKNESSES ARE IN FEET



modified from Geehan et al. (1986)

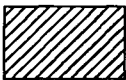


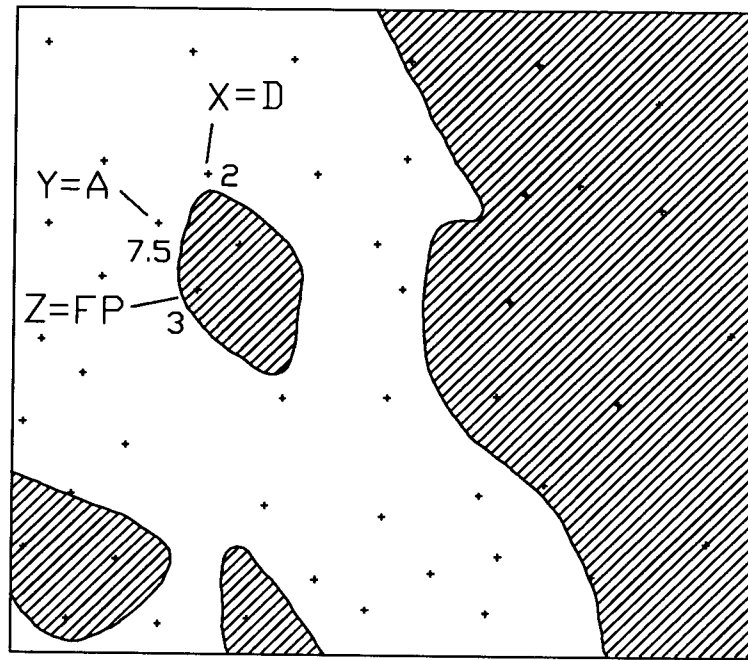
-  - "CONTINUOUS" SHALE: NO GEOLOGIC BIAS
-  - ZERO THICKNESS CONTOUR
-  - DATUM POINT

Figure 3-2: Prediction of shale continuity in the Ivishak Formation without geological information. (modified from Geehan et al. (1986))

0 1 MILE 1 SHALE THICKNESS IS IN FEET



modified from Geehan et al. (1986)




-  - CONTINUOUS FLOOD PLAIN SHALE
-  - ZERO THICKNESS CONTOUR
-  - DATUM POINT

Figure 3-3: Prediction of shale continuity in the Ivishak Formation with geological information. (modified from Geehan et al. (1986))

CHAPTER 4: SEQUENTIAL INDICATOR SIMULATIONS OF AQUITARDS

4.1 INTRODUCTION

This chapter describes how aquitards are numerically generated using the sequential indicator simulation (SIS) algorithm. The SIS algorithm is powerful because it not only accounts for the spatial correlation of a random variable of interest, but provides a means of incorporating measurements that have a wide range of reliability. Incorporating measurements with a wide range of reliability is vital in hydrogeological design because precise (hard) data is usually scarce and expensive while cheaper, imprecise measurements are often more readily available.

Some general geostatistical concepts will be presented in Section 4.2. This will be followed by a discussion of indicator kriging, the mathematical basis of SIS (Section 4.3), and how the SIS algorithm works (Section 4.4). Section 4.5 will present non-Bayesian and Bayesian methods of inference of the geostatistical parameters used by the SIS algorithm. The Bayesian method will be used as much as possible in this thesis; however, the non-Bayesian method will also be used in some cases for practical reasons. Bayesian inference is the key to incorporating geological understanding into the SIS algorithm. Limitations of the SIS algorithm are then discussed in Section 4.6. Finally, alternative simulation algorithms will be covered (Section 4.7) and the geostatistical nature of clay layers will be reviewed (Section 4.8).

4.2 BASIC GEOSTATISTICAL CONCEPTS

Only the basic geostatistical concepts that are necessary for understanding this thesis will be covered here. For a more detailed presentation refer to de Marsily (1984), Clark (1979), or Journel and

Huijbregts (1978). Geostatistics is analogous to classical statistics. A realization, or data set, z (denoted by a lower case letter) is used to infer statistical parameters governing a random variable, Z , (denoted by a capital letter) from which z was drawn. However, in geostatistics the random variable is a regional variable, $Z(x)$, with spatial correlation. From now on, unless otherwise stated, all random variables are assumed to be regionalized variables.

Only statistical parameters based on the first two moments of $Z(x)$ are of interest here: the mean, μ_Z , the variance, σ_Z^2 , and the covariance function, $Cov(h)$. In all practical situations, there will never be enough available data to estimate parameters based on higher order moments. The covariance function quantifies the spatial correlation of $Z(x)$. It is similar in nature to the variogram, a term more familiar to many practitioners of geostatistics. The variogram will be discussed in more detail later in this section. However, this thesis will utilize the covariance function rather than the variogram.

The covariance between Z at two points x_1 and x_2 is defined by:

$$Cov(Z(x_1), Z(x_2)) = E[(Z(x_1) - \mu_{Z(x_1)})(Z(x_2) - \mu_{Z(x_2)})] \quad (4.1)$$

where x_1 and x_2 represent locations in two dimensional space and E denotes the expected value. The covariance between two coincident points is the variance:

$$\begin{aligned} Cov(Z(x_1), Z(x_1)) &= E[(Z(x_1) - \mu_{Z(x_1)})(Z(x_1) - \mu_{Z(x_1)})] \\ &= Var(Z(x_1)) \end{aligned} \quad (4.2)$$

Geostatistics is based on two fundamental assumptions: ergodicity and stationarity. Ergodicity says that the actual realization, z , has the same statistical properties, or probability density function, as the ensemble of possible realizations generated by the random process $Z(x)$. This is analogous to the

assumption in classical statistics that the sample is representative of the population from which it was drawn. The assumption of ergodicity is necessary for the inference of the geostatistical parameters governing $Z(x)$ to be made because it allows one to trade spatial averages for ensemble averages.

The assumption of stationarity greatly simplifies the statistical properties of $Z(x)$ allowing tractable estimations of $Z(x)$ to be made. $Z(x)$ is stationary if, for a finite number of points n and any separation distance h , the joint distribution of $Z(x_1), Z(x_2), \dots, Z(X_n)$ is the same as the joint distribution of $Z(x_1 + h), Z(x_2 + h), \dots, Z(X_n + h)$ (Meyers, 1989). This means that all of the moments of $Z(x)$ are independent of spatial location, x . This assumption is too strong to be useful in practical situations; therefore, a weaker assumption of second order stationarity is often made. In second order stationarity, only the first two moments are stationary. Therefore, the mean and the covariance of $Z(x)$ are independent of x . Second order stationarity will be assumed in this thesis.

If the spatial correlation is isotropic, then the covariance of $Z(x)$ at two points is only dependent upon the separation distance, h , and not on the direction of the separation. Equation (4.1) then becomes:

$$\text{Cov}(Z(x), Z(x - h)) = E[(Z(x) - \mu_Z)(Z(x - h) - \mu_Z)] \quad (4.3)$$

Therefore, for simplicity $\text{Cov}(Z(x), Z(x - h))$ will be referred to as $\text{Cov}(h)$. $\text{Cov}(h)$ is usually assumed to follow a well defined analytical function, such as the exponential, spherical or Gaussian functions.

The exponential covariance function has the form:

$$\text{Cov}(h) = \sigma_Z^2 \exp(-h/\lambda) \quad (4.4)$$

while the Gaussian covariance function has the form:

$$\text{Cov}(h) = \sigma_Z^2 \exp(-(h/\lambda)^2) \quad (4.5)$$

where σ_Z^2 is the variance of $Z(x)$ and λ is the correlation length. The correlation length is a measure of the strength of the spatial correlation. It represents the distance at which the covariance function drops to a value of $\text{Cov}(0) \cdot e^{-1}$. The spherical model has the form

$$\begin{aligned} \text{Cov}(h) &= \sigma_Z^2 \left(1 - \frac{3h}{2a} + \frac{h^3}{a^3}\right) & h < a \\ &= 0 & h > a \end{aligned} \quad (4.6)$$

where a is the range. The range is another common term used to express the strength of the spatial correlation. It differs from the correlation length in that it represents the separation distance, h , at which the correlation becomes zero. Therefore, an exponential or Gaussian covariance function with $\lambda=10$ m has a stronger correlation than a spherical covariance function with $a = 10$ m. Example spherical, Gaussian and exponential covariance functions with λ and $a=10$ m are shown in Figure 4-1.

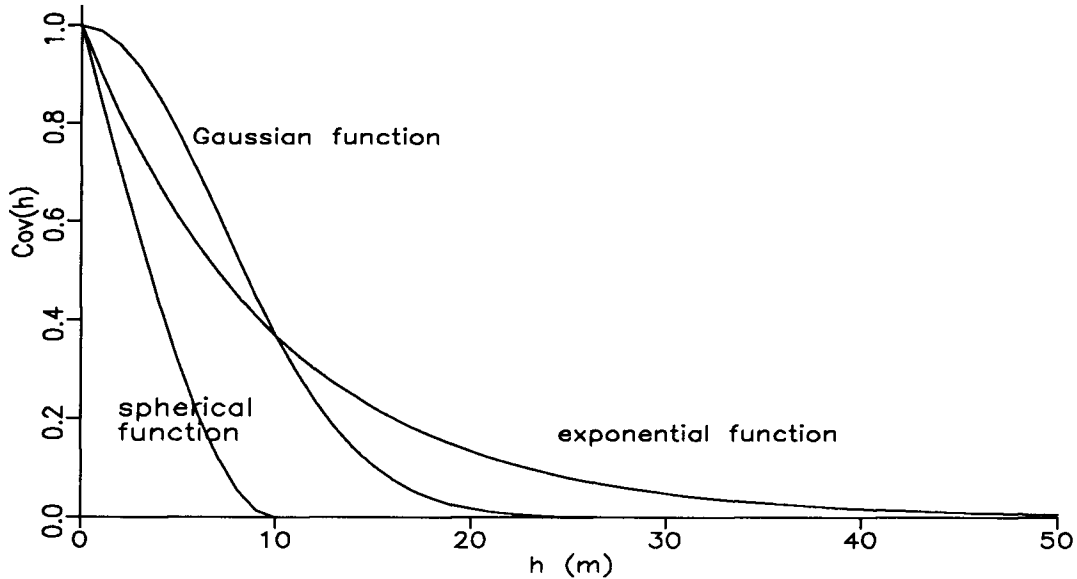


Figure 4-1: Plot of the exponential, spherical and Gaussian covariance functions, for $\sigma_Z^2 = 1$, $\lambda = 10$ m and $a = 10$ m.

The assumption of isotropy of $Cov(h)$ may be poor in many real geological situations because correlation is often dependent upon direction. For example, the spatial correlation in an aquitard is generally higher parallel to bedding than perpendicular to bedding. Unless stated otherwise, it will be assumed that the spatial correlation of an aquitard is isotropic in the horizontal plane.

A weaker form of stationarity than second order stationarity is the intrinsic hypothesis. It assumes that the variance of the first increment is finite and weakly stationary. This concept is utilized with the variogram, $\gamma(h)$, which is defined by:

$$\gamma(h) = 0.5 E[(Z(x+h) - Z(x))^2] \quad (4.7)$$

Consequently, $\gamma(h)$ is only dependent upon the squared differences of $Z(x)$ and not on μ_Z . Under conditions of second order stationarity, the $Cov(h)$ and $\gamma(h)$ are related by:

$$Cov(h) = Cov(0) - \gamma(h) \quad (4.8)$$

An important concept in geostatistics is the volume-variance relationship. The variance and covariance of Z depend upon the volume, or scale, of the measurement of $Z(x)$. The covariance functions shown in Fig 4-1 are for the point scale. As the volume increases, σ_z^2 and $Cov(h)$ will decrease, until the extreme where the volume represents the entire domain of interest and both σ_z^2 and $Cov(h)$ are zero.

Normally the volume variance relationship poses problems in estimating the geostatistical parameters of $Z(x)$. The volume variance relationship will be ignored in this thesis for reasons that are explained in Section 4.5.

4.3 INDICATOR KRIGING (IK)

This section will introduce indicator kriging (IK). It begins with a discussion of indicator random variables, the different types of data, and the estimation of geostatistical parameters. The problem of estimating the occurrence of the aquitard at a point x , will then be discussed. There are several geostatistical methods for tackling this problem, depending upon the strictness of the statistical assumptions made. Only two methods will be covered here: simple and ordinary indicator kriging. For a more detailed description of indicator geostatistics, refer to Journel (1989), Alabert (1987), or Journel (1983).

4.3.1 INDICATOR RANDOM VARIABLE

In IK, it is not the specific value of a random variable Z that is of interest, but whether Z falls into a particular class or not. The indicator random variable $I(x)$ is defined as:

$$\begin{aligned} i(x,z) &= 1 \text{ if } z(x) \leq z_c \\ &= 0 \text{ if } z(x) > z_c \end{aligned} \quad (4.9)$$

where z_c is some critical cutoff. $I(x)$ has a mean μ_I and variance σ_I^2 . The mean represents the expected value of $I(x)$ at a point x . Therefore,

$$\begin{aligned} \mu_I = E[I(x)] &= P(z(x) \leq z_c)(1) + P(z(x) > z_c)(0) \\ &= P(z(x) \leq z_c) \end{aligned} \quad (4.10)$$

In other words, μ_I represents the expected probability that $z(x)$ at some point x is less than the critical value z_c . Since it has only two possible states (0 or 1) it is a binary, random variable with variance, σ_I^2 , equal to:

$$\sigma_I^2 = \mu_I(1 - \mu_I) \quad (4.11)$$

Hence, the exponential covariance function will have the form:

$$\text{Cov}(h) = \mu_I(1 - \mu_I)e^{-h/\lambda} \quad (4.12)$$

The concept of the indicator random variable fits exactly with our interest in aquitard continuity. Is the aquitard present or not? If $Z(x)$ represents the thickness of the aquitard at point x then:

$$\begin{aligned} i(x,z) &= 1 \text{ if } z(x) = 0 \quad (\text{i.e. aquitard is not present}) \\ &= 0 \text{ if } z(x) > 0 \quad (\text{i.e. aquitard is present}) \end{aligned} \quad (4.13)$$

where the inequality in equation (4.9) has been changed to an equality since negative thicknesses are impossible.

In the above case, there are only two classes; however, there can be any number of classes in indicator kriging. Hence, it is possible to handle a variety of different types of heterogeneities, such as a sand, silt, clay sequence. The only drawback is that computational requirements dramatically increase with the number of class intervals handled.

4.3.2 TYPES OF DATA

There are two main classes of data in indicator kriging: hard and soft data. Hard data represent measurements which have a negligible uncertainty. For hard data, the presence, or absence, of the aquitard will be known with certainty and $I(x)$ will have a value of either 1 or 0. An example of a hard

measurement would be a borehole which was cored in its entirety, with a distinct aquitard that could be easily recognized. In this thesis, a hard random variable is referred to as $I(x)$ and a hard datum as $i(x)$.

Soft data represent measurements which have uncertainty. Geophysical surveys, or a borehole that was incompletely cored could represent soft measurements. In this thesis a soft random variable is referred to as $I_s(x)$ and a soft datum as $i_s(x)$. Alabert (1987) defined three types of soft data: types (a), (b), and (c). For a more detailed description, refer to Alabert (1987).

Type (a) soft data represents a single valued measurement $z_s(x)$ which is only an estimate of the true value $z(x)$. Therefore, a type (a) soft measurement will have a value of either $i_s(x)=0$ or $i_s(x)=1$.

However, it is of questionable reliability. The reliability of type (a) data is quantified by two probabilities $p_1(x)$ and $p_2(x)$ defined as

$$p_1(x) = P(Z_s(x) = 0 | Z(x) = 0) \text{ or } P(I_s(x) = 1 | I(x) = 1)$$

$$p_2(x) = P(Z_s(x) = 0 | Z(x) > 0) \text{ or } P(I_s(x) = 1 | I(x) = 0)$$

$p_1(x)$ is the probability that a window will be sampled given that one exists. This represents the confidence that the soft measurement is correct. $p_2(x)$ is the probability that a window will be sampled, given that one does not exist. This represents the chance of the measurement being incorrect. The error in the soft data is assumed to be independent of spatial location; therefore, $p_1(x)$ and $p_2(x)$ will simply be referred to as p_1 and p_2 . Alabert (1987) discusses how these probabilities can be estimated using calibration samples. Calibration samples are samples which have been sampled by both "hard" and "soft" techniques. They allow the soft data to be directly compared to the hard data.

Type (b) soft data represents an interval ($Z_{\min}(x)$, $Z_{\max}(x)$) over which the true value is known to be bound. In type (c) soft data, the true value of $Z(x)$ is assumed to follow a probability distribution. Only type (a) soft data will be used in this thesis; therefore, types (b) and (c) will not be discussed further.

4.3.3 SIMPLE INDICATOR KRIGING (SIK) WITH HARD DATA

In SIK, $I(x_o)$ is estimated at point x_o by the following linear combination of the n_h hard data points:

$$i(x_o)^* = \mu_I + \sum_{j=1}^{n_h} a_j(i(x_j) - \mu_I) \quad (4.14)$$

where $i(x_o)^*$ is the estimate of $I(x_o)$. It is an unbiased estimator. The weights, a_j , $j=1, \dots, n$, in equation (4.14) are calculated by solving the following system of equations:

$$\sum_{j=1}^{n_h} a_j C_{jk} = C_{ok}, \quad k=1, \dots, n \quad (4.15)$$

where C_{jk} is a covariance coefficient, representing $\text{Cov}(I(x_j), I(x_k))$. C_{ok} represents the covariance between data point x_k and the estimation point x_o . The development of the system of equations (4.15) is given in Journel (1989) and will not be repeated here. They are developed as an optimization problem by minimizing the variance, $\text{Var}(i(x_o)^* - i(x_o)_T)$, between $i(x_o)^*$ and the true value, $i(x_o)_T$:

$$\text{Var}(i(x_o)^* - i(x_o)_T) = \sum_{j=0}^{n_h} \sum_{k=0}^{n_h} (-a_j)(-a_k)C_{jk} \quad (4.16)$$

where $a_0 = -1$ and $C_{jk} = \text{Cov}(I(x_j), I(x_k))$.

After some simplification of equation (4.16) $\text{Var}(i(x_o)^* - i(x_o)_T)$ can be calculated by:

$$\text{Var}(i(x_o)^* - i(x_o)_T) = \sigma_I^2 - \sum_{j=1}^n a_j C_{0j} \quad (4.17)$$

From equations (4.14) and (4.15) $i(x_o)^*$, is dependent upon knowledge of μ_I and $\text{Cov}(h)$. SIK also requires second order stationarity. If no data points exist, then $i(x_o)^* = \mu_I$.

4.3.4 ORDINARY INDICATOR KRIGING (OIK) WITH HARD DATA

In OIK, $I(x_o)$, is estimated by the following linear combination of the n_h data points:

$$i(x_o)^* = \sum_{j=1}^{n_h} a_j i(x_j) \quad (4.18)$$

The weights a_j $j=1, \dots, n_h$, are calculated by solving the following system of equations:

$$\sum_{j=1}^{n_h} a_j C_{jk} + \eta = C_{ok}, \quad k=1, \dots, n \quad (4.19)$$

$$\sum_{j=1}^{n_h} a_j = 1 \quad (4.20)$$

where η is a Lagrange multiplier. These equations are derived similarly to the SIK equations by calculating the weights a_j such that the variance of the estimate, $\text{Var}(i(x_o)^* - i(x_o)_T)$, is a minimum, with the constraint that the estimate is unbiased. For a more detailed development of the OIK equations, refer to Journel (1989) or Journel and Huijbregts (1978).

The statistical assumptions necessary to apply OIK are more relaxed than those needed to apply SIK.

As noted in the above three equations, only the covariance function is assumed known. In addition, OIK does not require second order stationarity. OIK can be carried out under the intrinsic hypothesis using the variogram.

4.3.5 COMPARISON OF OIK AND SIK

The difference between estimates based on SIK and OIK are illustrated in Figure 4-2. The probability of a hole existing at fifteen points ($x_1, x_2, x_3 \dots x_{15}$) spaced ten meters apart along a one dimensional line has been estimated by both SIK and OIK. Two hard measurements exist: $i(x_3)=1$ and $i(x_8)=0$. For SIK, it has been assumed that μ_I is equal to the sample average, $m_I=0.5$. Therefore,

$$\begin{aligned}\sigma_I^2 &= (0.5)(1 - 0.5) \\ &= 0.25\end{aligned}\tag{4.21}$$

An exponential covariance function with $\lambda_I = 5$ m has been assumed for both OIK and SIK. Therefore,

$$\text{Cov}(h) = 0.25e^{-5/h}\tag{4.22}$$

Note that both OIK and SIK give the same estimates. This is because μ_I was assumed to be equal to m_I .

Note that at the measurement points, the measured datum is reproduced. However, as estimation locations get further from the measured data points, $i^*(x)$ approaches μ_I in the case of SIK and m_I in the case of OIK.

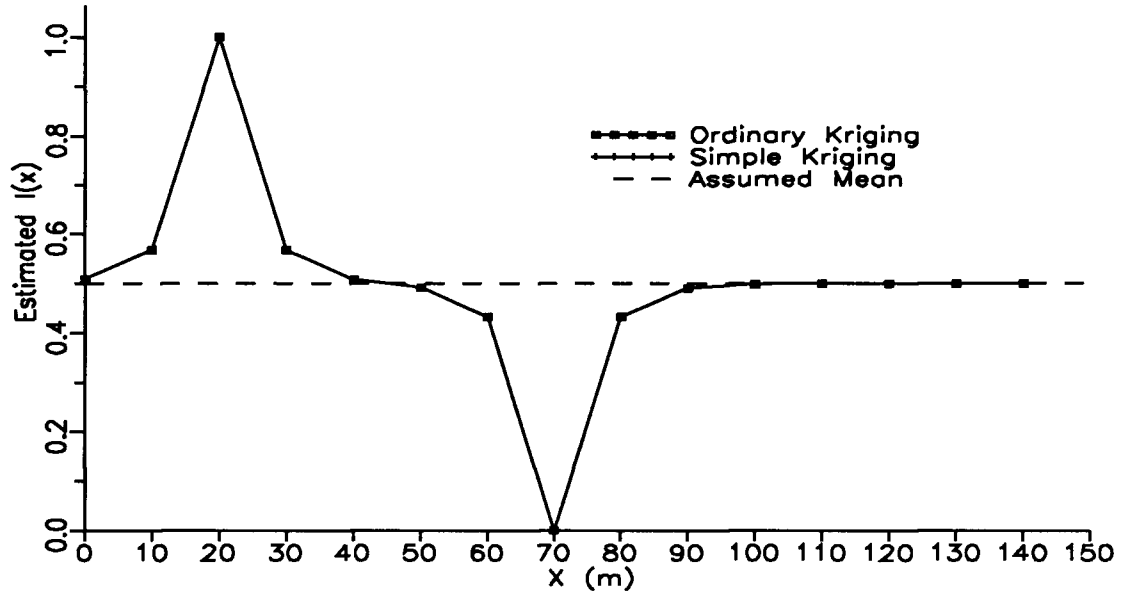


Figure 4-2: Plot of $i^*(x)$ on 1-d line by both OIK and SIK.

The variance of the estimates, $\text{Var}(i(x_o)^* - i(x_o)_T)$, by both SIK and OIK are zero at the data points (Fig. 4-3). However, at estimation points away from data points, the variance of estimates by SIK are lower than those by OIK. There is more certainty in $i^*(x)$ by SIK because of the more rigid statistical assumptions necessary to carry out SIK. Recall that in SIK, μ_1 is assumed known while in OIK it is not. Knowing μ_1 provides an extra constraint on $i^*(x)$, reducing the variance or increasing the certainty.

4.3.6 EXTENSION OF SIMPLE INDICATOR KRIGING TO HANDLE TYPE (a) SOFT DATA

There are now n_s soft data available in addition to the n_h hard data. The indicator value, $i^*(x_o)$ at some point x_o is estimated by co-kriging the soft and hard data through the following system of equations:

$$i^*(x_o) = \mu_1 + \sum_{j=1}^{n_h} a_j(i(x_j) - \mu_1) + \sum_{k=1}^{n_s} b_k(i_s(x_k) - \mu_{1_s}) \quad (4.23)$$

where,

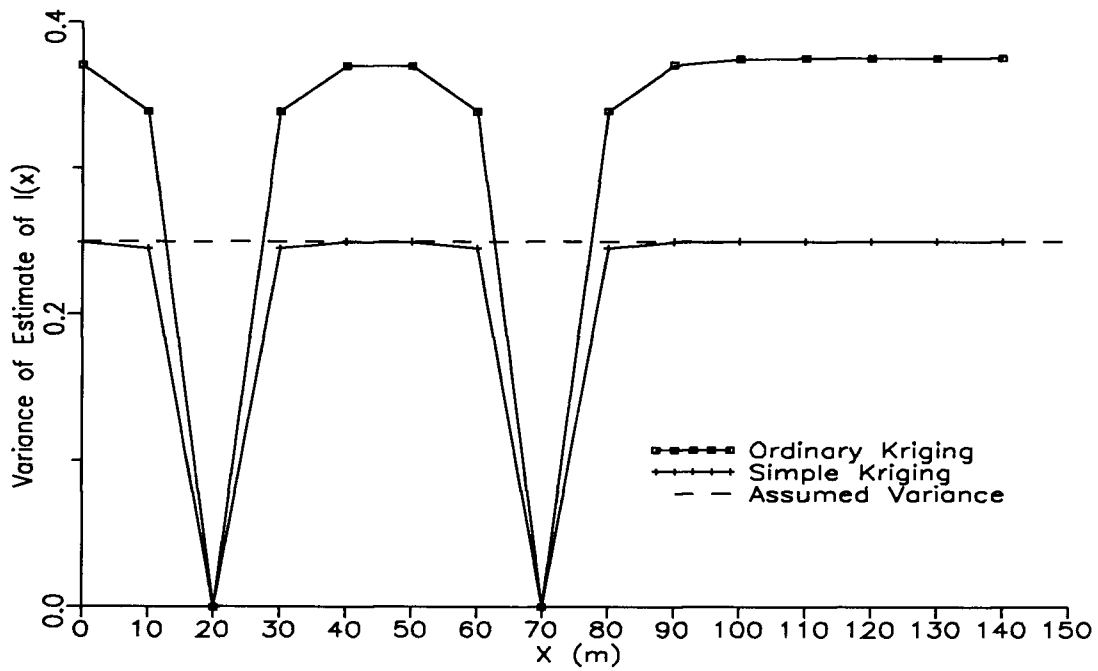


Figure 4-3: Variance of $i^*(x)$ from SIK and OIK.

- μ_I is the average of the hard data, and
- μ_{I_s} is the average of the soft data.

The co-kriging weights are calculated by solving the following system of equations:

$$\begin{aligned} \sum_{j=1}^{n_h} a_j \text{Cov}_I(x_l - x_j) + \sum_{k=1}^{n_s} b_k \text{Cov}_{II_s}(x_l - x_k) &= \text{Cov}_I(x_l - x_o) \quad l=1, \dots, n_h \\ \sum_{j=1}^{n_h} a_j \text{Cov}_{II_s}(x_m - x_j) + \sum_{k=1}^{n_s} b_k \text{Cov}_{I_s}(x_m - x_k) &= \text{Cov}_I(x_o - x_m) \quad m=1, \dots, n_s \end{aligned} \quad (4.24)$$

where

- $\text{Cov}_I(x_l - x_j)$ represents the covariance between two hard datum, one at point x_l and the other at point x_j .

- $\text{Cov}_{\Pi_s}(x_l-x_k)$ represents the covariance between a soft datum at point x_l and a hard datum at point x_k , or vice versa.
- $\text{Cov}_{I_s}(x_m-x_k)$ represents the covariance between two soft data, one at point x_m and the other point at x_k .

The covariances, $\text{Cov}_{\Pi_s}(x_l-x_k)$ and $\text{Cov}_{I_s}(x_m-x_k)$ are calculated from $\text{Cov}_I(x_l-x_j)$ using the probabilities p_1 , and p_2 . These calculations are discussed in Section 4.5. For a more detailed development of equation (4.24), refer to Alabert (1987). A number of different sources of soft data could be incorporated into the above system of equations. However, the probabilities p_1 and p_2 would have to be known for each source of information.

The indicator kriging technique used here for soft data is a Taylor-series type linear approximation of Bayes' equation (Alabert, 1987). For the case of one soft datum and no hard data, it is equivalent to Bayesian updating. However, for greater than one soft datum, soft data points are not reproduced exactly. Consequently, the conditioning of a soft datum may not be as strong as it should be. All hard data points will be reproduced exactly.

4.4 SEQUENTIAL INDICATOR SIMULATION ALGORITHM (SIS)

The SIS algorithm is a simple method of numerically generating patterns of the indicator random variable in one, two or three dimensions. Only one and two dimensional patterns will be generated here. A one dimensional pattern will represent a two dimensional vertical cross section through an aquitard. A two dimensional pattern will represent a map view of an aquitard, for use in three dimensional hydrogeological representations.

The methodology will be illustrated with the generation of a one dimensional pattern of an aquitard.

The stratigraphic horizon representing the possible aquitard is first divided into a series of equal sized blocks (Fig 4-4) . The selection of the block size will be discussed in Chapter 6.

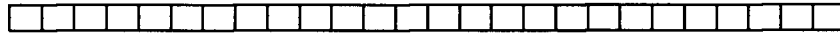


Figure 4-4: One dimensional stratigraphic section divided into blocks

The SIS algorithm is then carried out in the following steps:

Step 1: A random generation path is chosen through all of the blocks. This has been done in this thesis using the following congruential generator (Bratley et al., 1987):

$$B_j = (5 \times B_{j-1} + 1) \bmod 2^n \quad (4.25)$$

where B_j is the j^{th} block along the path. Any block can be the starting point of the path. Each integer between 1 and 2^n will be generated once. Therefore, n is chosen to be as small as possible, while maintaining 2^n greater than the total number of blocks. Integers greater than the number of blocks are discarded. A random path ensures that generated realizations have a maximum degree of disorder.

Step 2: An estimate, $i(B_j)^*$ is kriged at block j , the first block in the path along the aquitard.

Step 3: A random number, p , is generated between 0 and 1 using a uniform random number generator.

Step 4: The random number, p , is transformed into an indicator value by the following criteria:

if $p > i(B_j)^*$, then $i(B_j) = 0$ and the block represents aquitard, or

if $p \leq i(B_j)^*$, then $i(B_j) = 1$ and the block represent a window.

Step 5: The indicator value, $i(B_j)$, is then added to the data set where it is used to condition the generation of the next block in the path.

Step 6: Return to step 2 until aquitard or a discontinuity has been generated at all aquitard blocks.

In step two, either SIK or OIK can be used; however, the framework developed in this thesis utilizes SIK. While SIK is more restrictive to apply than OIK because it requires an estimate of μ_i and $\text{Cov}(h)$, using both parameters is a distinct advantage. Utilizing the mean in addition to the covariance function allows greater power in manipulating the characteristics of the numerically generated aquitards. Through Bayesian updating, the mean can incorporate one's conceptual understanding of the geology. Hence, the generated aquitards can be forced to conform more with one's understanding of the geology in SIK than in OIK.

Using SIK can be of fundamental importance, particularly with sparse data sets. This will be illustrated with the following example. As discussed in section 4.3.2, kriged estimates range between the sample average, or mean, and the measured data values. If no holes are measured, which is likely in the advent of a sparse data set, the indicator value at all data points will be zero and the average indicator value will be zero. Hence, in OIK there will be a zero chance of a discontinuity everywhere. This is clearly unacceptable because an aquitard formed in any depositional environment, will always have a chance of having a discontinuity. In SIK, μ_i can be assumed to have a value greater than zero, forcing a finite chance of a discontinuity.

As data sets increase in size, the difference between SIK and OIK decreases.

4.5 INFERENCE OF GEOSTATISTICAL PARAMETERS

The geostatistical parameters can be estimated using either Bayesian updating or non-Bayesian approaches. In the non-Bayesian approach, only sampled data are used to estimate the parameters. In Bayesian updating, one's conceptual understanding of geology can be included in the inference. However, as will be explained below, the Bayesian approach can only be practically used for estimating the mean. The correlation length will have to be estimated using non-Bayesian methods. Both of the methods of inference will now be discussed below.

4.5.1 NON-BAYESIAN INFERENCE

4.5.1.1 Inference of the Mean and Variance

The mean, μ_I , is the expected value of $I(x)$. Therefore,

$$\begin{aligned}\mu_I &= E[I(x)] \\ &= (1)P(Z(x)=0) + (0)P(Z(x)>0)\end{aligned}\tag{4.26}$$

since for $Z(x)=0$, $I(x)=1$ and for $Z(x)>0$, $I(x)=0$. The above relationship then simplifies to

$$\begin{aligned}\mu_I &= P(Z(x)=0) \\ &= F(0)\end{aligned}\tag{4.27}$$

where $F(0)$ is the cumulative probability distribution of $Z(x)$. Therefore, $F(0)$ is used as an estimator of the mean. Hence,

$$m_I = F^*(0) \quad (4.28)$$

where $F^*(0)$ is an estimate of $F(0)$ and m_I is an estimate of μ_I . As a convention that will be used throughout this thesis, unless otherwise stated an asterisk will be used to denote an estimate of a parameter or a random variable. An estimate of $F(0)$ by hard and soft data will be referred to by $F_I^*(0)$ and $F_{Is}^*(0)$, respectively. $F_I^*(0)$ is calculated from n_h hard data by:

$$F_I^*(0) = \sum_{j=1}^{n_h} a_j i(x_j) \quad (4.29)$$

where a_j is a weight for $i(x_j)$.

If the data were independent random variables, then $a_j = 1/n_h$. However, the data are spatially correlated and is generally clustered about areas of special interest. These factors must be accounted for if m_I is to be unbiased. One way of accounting for these two factors is cell declustering, which is a simple nonprobabilistic technique (Journel, 1983). Cell declustering will calculate non equal weights a_j in the above equation. Cell declustering is a very useful technique because knowledge of the correlation length is not needed. There are other possible methods of estimating $F(0)$ from spatially correlated data. For example, μ_I could be estimated over a block representing the entire domain of interest using ordinary kriging. Cell declustering has been chosen here because of its simplicity.

Consider the case of n_h hard data located in some area D (Fig. 4-5) Declustering is carried out in the following steps:

- (1) Area D is overlaid with a regular grid of n_d cells of size d .
- (2) The number of data n_j is counted in each cell d_j .
- (3) Each datum in cell d_j is weighted by n_j and then summed.
- (4) The sum of data for each cell is then weighted equally.
- (5) $F^*_I(0)$ is then calculated by:

$$F^*_I(0) = \frac{1}{n_d} \sum_{j=1}^{n_d} \sum_{k=1}^{n_j} \frac{1}{n_j} i(x_{k_j}) \quad (4.30)$$

where n_d is the number of cells that contain data points and n_j is the number of data points in cell j .

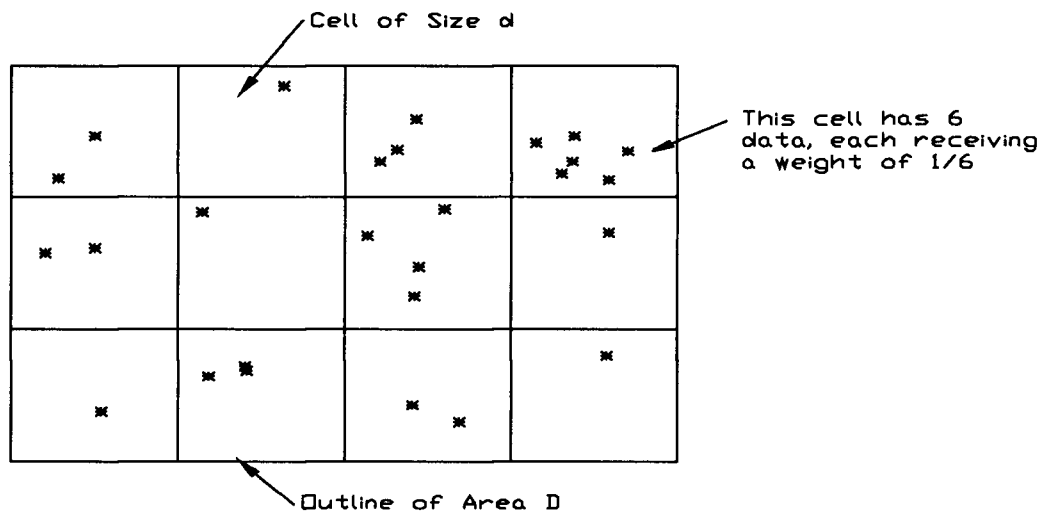


Figure 4-5: An example of n_h hard data which are declustered (modified from Journel, 1983).

A number of different cell sizes d should be tried. The d providing the lowest $F^*_I(0)$ should be used (Fig. 4-6). For very small d and very large d , $F^*_I(0)$ simply represents an equal weighting of all data.

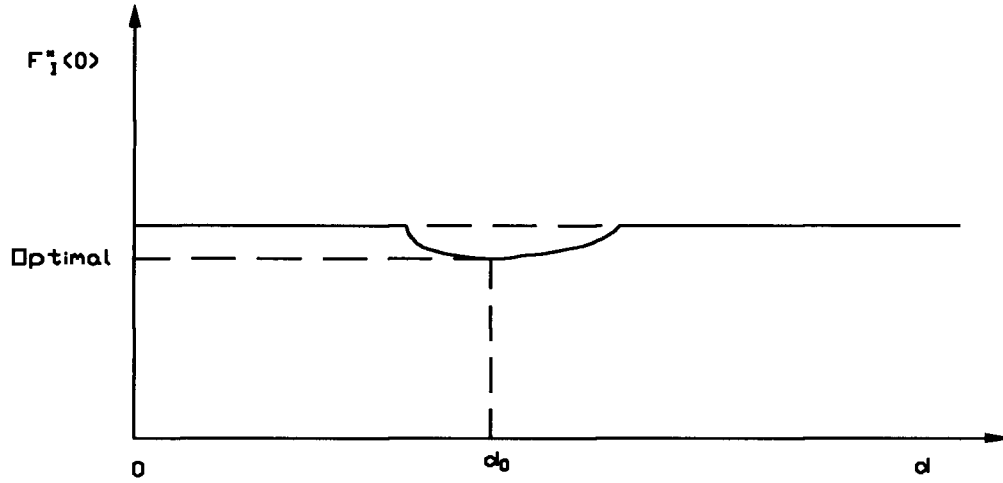


Figure 4-6: $F^*_{I_1}(0)$ versus different cell size d (modified from Journal, 1983)

$F^*_{I_s}(0)$ can be calculated in a similar manner from n_s soft data. However, the lack of reliability of the soft data will bias $F^*_{I_s}(0)$ relative to $F^*(0)$. The reliability is accounted for by the following relation:

$$\begin{aligned}
 F_{I_s}(0) &= P(Z_s(x) = 0) = E[I_s(x)] \\
 &= E_I[E[I_s(x)|I(x)]] \\
 &= E[I_s(x)|I(x)]P(I(x)=1) + E[I_s(x)|I(x)]P(I(x)=0) \\
 &= p_1 P(I(x)=1) + p_2 (1 - P(I(x)=1)) \\
 &= p_1 F(0) + p_2(1 - F(0))
 \end{aligned} \tag{4.31}$$

Therefore, the unbiased estimate of $F^*(0)$, based on soft data, is

$$F^*(0) = \frac{F^*_{I_s}(0) - p_2}{p_1 - p_2} \tag{4.32}$$

$F^*(0)$ can be calculated from a combination of hard and soft data by:

$$F^*(0) = \omega F_I^*(0) + (1 - \omega) \frac{F_{I_s}^*(0) - p_2}{p_1 - p_2} \quad (4.33)$$

The relative weight, ω , represents the relative number of hard and soft data and the quality of the soft data. Alabert (1987) suggests that when the number of soft data is large, and p_1 and p_2 are correctly estimated, $\omega = n_s/(n_d + n_s)$. If the estimates of p_1 and p_2 are unreliable, or the number of soft data is small, then ω should be increased.

4.5.1.2 Inference of Cov(h)

Recall that the covariance function, defined by:

$$\text{Cov}(I(x), I(x - h)) = E[(I(x) - \mu_I)(I(x - h) - \mu_I)] \quad (4.34)$$

is dependent upon μ_I . Under conditions of second order stationarity and ergodicity, the covariance function can be estimated from the variogram, which is estimated without knowledge of μ_I , using equation (4.7). However, Isaaks and Srivastava (1987), quoted by Alabert (1987) report that it is better to estimate a covariance function directly from data, rather than deriving it indirectly from a variogram.

Therefore, μ_I will have to be estimated first by some method which accounts for the spatial correlation when it is not known, such as cell declustering. The estimate of Cov(h) from hard data alone will be referred to as $\text{Cov}_I^*(h)$. A number of classes of separation distance, d_j , between measurement points are defined. For example,

$$d_1 = 0 - 100 \text{ m}$$

$$d_2 = 100 - 200 \text{ m}$$

$$d_3 = 200 - 300 \text{ m.}$$

For each class, the total number of pairs of points, n_j , whose separation distance falls within that class, and their average separation distance, h_{a_j} , are calculated. Then for each class the average covariance between all pairs of points n_j is calculated by:

$$\text{Cov}(h_{a_j}) = \sum_{m=1}^{n_j} \sum_{n=m}^{n_j} [i(x_m) - m_I](i(x_n) - m_I) \quad (4.35)$$

The $\text{Cov}(h_{a_j})$ is then plotted versus h_{a_j} . An analytical function representing $\text{Cov}^*_I(h)$, such as the exponential function, is then fitted to the plotted points.

Soft data can be used to improve $\text{Cov}^*_I(h)$. This involves the soft-hard indicator cross covariance and the soft indicator covariance. The soft-hard indicator cross covariance, $\text{Cov}^*_{II_s}(h)$ is estimated with the same procedure as $\text{Cov}^*_I(h)$. $\text{Cov}_{II_s}(h)$ is related to $\text{Cov}(h)$ by:

$$\text{Cov}(h) = \frac{\text{Cov}_{II_s}(h)}{p_1 - p_2} \quad (4.36)$$

This relation is only valid if the number of soft data is large. It is developed in more detail in Alabert (1987). It is based upon the following assumptions:

- (1) $I(x)$, $I_s(x)$, p_1 , and p_2 are stationary
- (2) $P(Z(x_1) = 0 | Z(x_2) = 0, Z_s(x_2) = 0) = P(Z(x) = 0 | Z(x_2) = 0)$ and
 $P(Z(x_1) = 0 | Z(x_2) > 0, Z_s(x_2) = 0) = P(Z(x) = 0 | Z(x_2) > 0)$

Assumption (2) states that the information contained in a soft datum at point x_2 , $Z_s(x_2)$, is negligible compared to the information in a hard datum taken at the same point, $Z(x_2)$. A combined estimate of $\text{Cov}(h)$ could be:

$$\text{Cov}^*(h) = \omega \text{Cov}_{I_s}^*(h) + (1 - \omega) \frac{\text{Cov}_{II_s}^*(h)}{(p_1 - p_2)} \quad (4.37)$$

The weight, ω , should be chosen to account for both the number of hard and soft data and the quality of the soft data.

The soft indicator covariance, $\text{Cov}_{I_s}^*(h)$, is again calculated from the soft data using the same procedure as the hard data. $\text{Cov}(h)$ is related to $\text{Cov}_{I_s}(h)$ by:

$$\text{Cov}(h) = \frac{\text{Cov}_{I_s}(h)}{(p_1 - p_2)^2} \quad (4.38)$$

This relationship is developed in detail in Alabert (1987) and is based on the previous two assumptions plus the following additional assumptions:

- (3) $P(Z_s(x) = 0 | Z(y) = 0, Z_s(y) = 0) = P(Z(x) = 0 | Z(y) = 0)$ and
 $P(Z_s(x) = 0 | Z(y) > 0, Z_s(y) = 0) = P(Z(x) = 0 | Z(y) > 0)$

Assumption (3) states that the information contained in $Z_s(y)$ is negligible compared to $Z(y)$.

Assumption (3) is stronger than assumption (2) because it relates to the spatial correlation of the soft information. Assumption (3) would be invalid in the case of a strong spatial correlation in the error $Z_s(x) - Z(x)$. For example, this could occur in the case of subjective guesses which are not made independently of each other.

A combined estimate of $\text{Cov}(h)$ is

$$\text{Cov}^*(h) = \omega_1 \text{Cov}_I^*(h) + \omega_2 \frac{\text{Cov}_{I_s}^*(h)}{(p_1 - p_2)} + \omega_3 \frac{\text{Cov}_{I_s}^*(h)}{(p_1 - p_2)^2} \quad (4.39)$$

The weights ω_j are chosen to sum up to one. They represent the number of pairs used to estimate each of the covariances and the quality of the soft information.

However, a fundamental problem arises in hydrogeology. While there may be enough data to quantitatively estimate μ_i , there will often not be enough data to quantitatively estimate $\text{Cov}(h)$. Even, in cases where there is much data, the measurements are rarely spaced uniformly through the area of interest, but are usually clustered in particular locations. This problem could be tackled through a Bayesian approach where data is combined with geological intuition. For example, $\text{Cov}(h)$ could be estimated by comparing the area of interest to similar areas where much data are available.

Unfortunately, as will be explained in the next Section, the author is unaware of any straightforward Bayesian methodology for carrying this out.

4.5.2 BAYESIAN INFERENCE

Bayesian statistics is philosophically different from classical statistics. The basic approach is that an estimate of a geostatistical, or other parameter, is updated by Bayes' equation as new information becomes available. In this way, an estimate is continually improved as new information becomes available. The Bayesian approach is very powerful because it allows one to combine different types of data. A geological model built from a conceptual understanding of geology can be combined with measured data. With very large data sets, estimates of geostatistical parameters based on the classical and Bayesian methods approach each other.

Utilizing one's conceptual understanding of geology is of great importance in many cases where there is a lack of measured data. Recall from Chapter 3, that there should be a quantitative relationship between μ_I (and $\text{Cov}(h)$) and depositional environment. This relationship could be used to estimate μ_I , or $\text{Cov}(h)$, based on information from a geologically similar area where many data are available. However, as will be discussed in this section, only the mean will be updated here.

The Bayesian updating equation is developed below. Much work has been done on the Bayesian updating of probability density functions of independent random variables. The updating of probabilities for independent random variables is discussed in Section 2.3. However, here we will deal with correlated random variables. Unfortunately, little work has been done on updating probability distributions of multivariate, correlated random variables. Kitanidis (1986) presents a methodology for updating the probability density function of a multivariate Gaussian spatially correlated random process for three different cases of parameter uncertainty.

In the first case, the variance and covariance function are fully known. Therefore, only the mean is updated. In the second case, the covariance function is known except for a multiplicative constant. For example, this case corresponds to an exponential covariance function ($\text{Cov}(h)=\sigma^2\exp(-h/\lambda)$) with known correlation length λ_I . In the final case, only the form of the covariance function is known: the mean and all parameters in the covariance function are unknown.

This thesis will utilize the methodology developed for the second case to update the mean of $I(x)$, even though $I(x)$ is a binary random variable rather than a Gaussian random variable. The methodology should be very applicable to updating the mean of $I(x)$ because it can be developed using only the first two moments and ignoring any distributional assumptions. A spatially correlated binary random variable is fully described by its first moment (or the mean) and covariance structure. The author is

unaware of any Bayesian updating equations developed specifically for multivariate spatially correlated binary random variables. The framework could be updated to incorporate new theoretical probabilistic methods directly applicable to binary random variables as they become available.

The correlation length is not updated for two reasons. The first is to simplify the numerical calculations carried out in the framework. In the first of Kitanidis' two cases the likelihood functions of the parameters can be expressed with a fixed number of sufficient statistics, and conjugate priors can be used in the Bayesian updating. Therefore, the updating breaks down to simply solving a series of algebraic equations. However, Kitanidis' third case is much more difficult because the likelihood function of the parameters cannot be expressed in a fixed number of sufficient statistics. Therefore, no general analytical method is available for calculating the updated parameters. The second reason is that in any field investigation in hydrogeology, it is difficult to get enough data to numerically estimate the correlation structure, let alone update it. If enough data was available, and the effort was warranted, the framework could be adapted so that the covariance function could be updated by Bayes' equation.

The details of the updating procedure for the second case are listed below. Kitanidis (1986) assumes that the random function, $Z(x)$, has the following general linear form:

$$Z(x) = \sum_{j=1}^p f_j(x)\beta_j + \psi(x) \quad (4.40)$$

where,

- x is a spatial point where Z is sampled
- $f_j(x)$ $j=1, \dots, p$ are known functions of x
- β_j $j=1, \dots, p$ are parameters
- $\psi(x)$ is a zero mean spatial random function.

The first term on the right hand side represents the deterministic component of $Z(x)$. The second term on the right hand side represents a zero mean random field. For the special case where $Z(x)$ is a second order stationary random field

$$Z(x) = \mu_z + \psi(x) \quad (4.41)$$

For a vector of n measurements, z ,

$$z = \mathbf{u}\mu_z + \psi \quad (4.42)$$

where \mathbf{u} is a vector of 1's and ψ has zero mean and covariance matrix $\mathbf{Q}_{zz}(\theta)$. $\mathbf{Q}_{zz}(\theta)$ is a function of parameters θ . It is assumed that the form of the covariance function is known except for a multiplicative constant, θ . Therefore,

$$\mathbf{Q}_{zz}(\theta) = \frac{1}{\theta} \mathbf{S}_{zz} \quad (4.43)$$

where \mathbf{S}_{zz} is known. The likelihood function for μ_z and θ , given a measurement vector z , is

$$P(\mu_z, \theta | z) \propto \theta^{r/2} \exp\left[-\frac{\theta}{2} (\mu_z - b_s)^T H_s (\mu_z - b_s)\right] \theta^{v/2} \exp\left(-\frac{1}{2} v q_s \theta\right) \quad (4.44)$$

where

- $H_s = \mathbf{u}^T \mathbf{S}_{zz}^{-1} \mathbf{u}$
- $b_s = \mathbf{u}^T \mathbf{S}_{zz}^{-1} z$
- $r = \text{rank}(H_s)$
- $v = n - r$
- $q_s = (z^T \mathbf{S}_{zz}^{-1} z - b_s^T \mathbf{S}_{zz}^{-1} z) / v$

- α represents "proportional to".

The conjugate prior for μ_z and θ is a normal gamma 2 function:

$$P(\mu_z, \theta) \propto \theta^{v'/2} \exp\left[-\frac{\theta}{2} (\mu_z - m_z')^T H' (\mu_z - m_z')\right] \theta^{v'/2-1} \exp\left(-\frac{1}{2} v' q' \theta\right) \quad (4.45)$$

where

- m_z' = the prior estimated mean
- v' = the rank of H'
- $H' = v'^T S_{zz}^{-1} v'$
- v = vector of ones, n_e long
- n_e = number of prior measurements.

The updated estimated mean, m_z'' is

$$H'' m_z'' = H' m_z' + H_s b_s \quad (4.46)$$

where, $H'' = H' + H_s$. H' and H_s represent weights for the prior and sample estimates of the mean, respectively. The above equation can be rearranged into

$$\begin{aligned} m_z'' &= H''^{-1} [H' m_z' + H_s b_s] \\ &= [H' + H_s]^{-1} [H' m_z' + u^T S_{zz}^{-1} z] \\ &= [H' + u^T S_{zz}^{-1} u]^{-1} [H' m_z' + u^T S_{zz}^{-1} z] \end{aligned} \quad (4.47)$$

Refer to Kitanidis (1986) for a more detailed development of the updating equations. The Bayesian updating in this thesis will be carried out using a modified version of the above equations. This modified version is developed below.

Since $I(x)$ is assumed to be a second order stationary random variable, it will have the following form:

$$I(x) = \mu_I + \varphi(x) \quad (4.48)$$

where $\varphi(x)$ is a zero mean binary random variable with variance $\mu_I(1 - \mu_I)$. Therefore, the equation used to update m_I , has the following form:

$$m_I'' = [H' + \mathbf{u}^T \mathbf{S}_{II}^{-1} \mathbf{u}]^{-1} [H' m_I' + \mathbf{u}^T \mathbf{S}_{II}^{-1} \mathbf{i}] \quad (4.49)$$

where \mathbf{i} is a vector of data n long, and the term $\mathbf{u}^T \mathbf{S}_{II}^{-1} \mathbf{u}$ represents the weighting of existing measurements (or H_s). The variance is directly updated from the updated mean by equation (4.11).

To incorporate a geological estimate of the mean with measured data, m_I' would represent the estimate of μ_I based on the geological model. The confidence in the prior estimate of the mean can be quantified through an equivalent number of n_e measurements which are spaced enough apart to be independent.

Therefore, H' can be calculated by

$$H' = \mathbf{v}^T \mathbf{S}_{II}^{-1} \mathbf{v} \quad (4.50)$$

where \mathbf{v} is a vector of ones n_e long and \mathbf{S}_{II} is the covariance matrix between the n_e measurements. Since the n_e measurements are independent, \mathbf{S}_{II} only contains σ_I^2 terms along the diagonal, and all other terms are zero. Therefore, the above equation simplifies to

$$H' = n_e/\sigma_1^2 \quad (4.51)$$

Equation (4.49) can also accommodate the case where no prior knowledge is assumed. No prior knowledge is also termed a diffuse prior. In this case H' is set to zero and equation (4.49) collapses to

$$m_I'' = [u^T S_{II}^{-1} u]^{-1} [u^T S_{II}^{-1} i] \quad (4.52)$$

One problem in using equation (4.49) in this framework is that it does not directly accommodate soft data because soft data is biased. The development of a Bayesian updating equation that will simultaneously handle both hard and soft spatially correlated data is a current research topic. If the number of soft data is small relative to other information, or its quality is poor, then its affect on the updated mean could be small. Under these circumstances, the soft data could be excluded from the updating, or estimation of the mean.

However, if the soft data provides a substantial quantity of information, then it should be incorporated into the estimation of the mean. The incorporation could be carried out by assuming that the soft data forms an independent data set from the hard data. The estimation of the mean would then be carried out in two steps. In the first step, the prior geologically estimated mean, m_I' , would be updated by the soft data alone. The updating would be done by modifying equation (4.49). Since $[u^T S_{I_s I_s}^{-1} u][u^T S_{I_s I_s}^{-1} u]^{-1}$ equals an identity matrix, equation (4.49) can be rearranged into

$$m_I'' = [H' + u^T S_{II}^{-1} u]^{-1} [H' m_I' + [u^T S_{I_s I_s}^{-1} u][u^T S_{I_s I_s}^{-1} u]^{-1} u^T S_{II}^{-1} i] \quad (4.53)$$

where $S_{I_s I_s}$ is the covariance matrix between the soft data. Using equations (4.52) and (4.50), the above equation can be reduced to

$$m_I'' = [H' + H_s]^{-1} [H' m_I' + H_s m_I] \quad (4.54)$$

where H is the precision matrix of the soft data and m_I is the estimate of the mean from the soft data alone. The updated mean, m_I'' , is simply the weighted average of the prior mean, m_I' , and the sample mean, m_I , from the soft data weighted by the precision matrices.

However, m_I is still biased from the sample precision. Therefore, the above equation is modified using equation (4.32) to unbiased m_I , to form

$$m_I'' = [H' + H_s]^{-1} [H' m_I' + H_s \frac{m_I - p_2}{p_1 - p_2}] \quad (4.55)$$

The above equation can then be used to update the mean using the soft data. In the second step, the final estimate of the mean, m_I''' , would be estimated by updating m_I'' with the hard data using equations (4.49) or (4.54). Note that for hard data, equation (4.55) and equation (4.54) are equivalent because for hard data $p_1 = 1$ and $p_2 = 0$ allowing the precision terms in (4.55) to drop out.

Note, that the updating of the mean is independent of the exact value of the variance of $I(x)$, which is used to calculate the matrix S_{II} and hence the weights, H' and H_s . The magnitudes of both H' and H_s are affected by the variance, but their relative sizes remain unchanged.

Even though the mean is updated using equations developed for Gaussian random variables, in reality its estimate will follow a Beta distribution, which is continuous between zero and one.

4.5.3 SUMMARY OF INFERENCE OF GEOSTATISTICAL PARAMETERS

Both Bayesian and non-Bayesian approaches can be used to estimate the geostatistical parameters.

Non-Bayesian approaches utilize measured data only, where Bayesian updating allows one to incorporate geological intuition into the estimate. Both approaches have advantages and disadvantages. The non-Bayesian methods are the most theoretically complete and will readily incorporate both hard and soft data. However, they cannot incorporate geological intuition which can be critical, particularly in the case of sparse data sets. Nor do they provide a methodology for updating estimates as new information becomes available; therefore, they do not directly fit into the Bayesian data worth framework used here.

Bayesian updating can handle geological intuition and will readily fit into the Bayesian data worth framework. Unfortunately, work on the Bayesian estimation of geostatistical parameters of correlated random variables is not as complete as that of non-Bayesian methods. Only the mean can be readily updated and not the correlation length. In this thesis, the correlation length will be estimated by the non-Bayesian approach and is assumed to remain constant. The correlation length is not updated because the numerical complexity of carrying out the calculations is extreme and because the required number of data to carry out effective updating will rarely be available. The updating equation does not simultaneously handle hard and soft data, but it has been modified to handle hard and soft data in two different steps.

4.6 LIMITATIONS OF SIS ALGORITHM

There are several factors which provide limitations on the SIS algorithm. First, a number of geostatistical assumptions have been made to make the statistics tractable. Secondly, in reality the aquitard realizations are finite in size when theoretically they are assumed to be infinite. Thirdly,

volume variance relationships do not work for the form of the SIS algorithm used here. Finally, some kinds of uncertainty are ignored by the SIS algorithm and there is a practical limit to the number of conditioning data points.

4.6.1 GEOSTATISTICAL ASSUMPTIONS

Geostatistical assumptions which have been made include those of ergodicity, stationarity, and isotropy. These assumptions were explained in detail in Section 4.2.

If ergodicity is not true then geostatistics breaks down. The assumption of ergodicity is axiomatic and must be taken for granted. It is apparently just accepted in the geostatistical community as being valid and there is no standard way of testing its validity (Sinclair, 1991).

In many cases, $I(x)$, may not be second order stationary, resulting in aquitard realizations which are not representative of the true state of nature. An example would be a facies change in the area of interest. The result would be a trend in aquitard continuity. There are a number of ways of dealing with conditions that are not second order stationary. For example low order trends in the mean could be filtered out, leaving a residual which could be second order stationary. Completely non-second-order stationarity conditions could possibly be handled by replacing the SIS algorithm with a different scheme for numerically generating aquitards. One such approach might be to use an algorithm based on fractal-based geostatistics such as have been carried out in the petroleum industry (refer to Hewett and Behrens, 1988).

The assumption of isotropy is not critical. If anisotropic conditions exist, they can easily be built into the SIS algorithm. However, with limited data sets, anisotropy can be difficult to detect and even more difficult to estimate.

4.6.2 FINITE SIZE OF AQUITARD REALIZATIONS

Simulation algorithms assume that the domain is infinite when in reality it is bounded and finite. The boundaries reduce the variability of the realizations, damping the sample covariance function of the realizations below its true covariance function. To reduce this effect, the total size of the discretized aquitard must be approximately four times greater than the correlation length used in generating the realizations.

4.6.3 VOLUME VARIANCE RELATIONSHIP

Several kinds of data representing different volumes, or scales, may be available at a given site to condition the indicator simulations. These include:

- boreholes, which are point size,
- geophysical surveys, which cover a large area, and
- previously simulated blocks, which can be up to hundreds of meters in size.

Recall, that the SIS algorithm sequentially simulates the aquitard blocks so that a simulated block is conditioned on the previously simulated blocks. The weighting of a datum in estimating $I(x)$ at point x is dependent upon the volume of the measurement because of the volume variance relationship. A datum with a large volume will have more weight in estimation than a datum with a small volume, given that the two data are equidistant from the point of estimation. If $I(x)$ was a continuous random variable, then this problem could be tackled using volume variance relationships. However, in this thesis, $I(B_j)$ is a discrete random variable with a value of either 0 or 1. The entire block represents either aquitard or a window. Under these circumstances, $I(B_j)$ is insensitive to the volume of B_j .

Therefore, volume variance relationships do not apply (Strivastava, 1990). Therefore, the methods outlined in this thesis are only able to handle measurements of one volume. This volume is set equal to the volume of the simulated blocks. $I(x)$ would be a continuous random variable if it represented the average point value of $I(x)$ averaged over every point within an aquitard block.

Measurements with different volumes will be accounted for as follows. It will be assumed that the outcome of a borehole can be extrapolated to the entire block. This will be realistic if the size of the block is small and the minimum size of any clay layer is on the order of the size of the block. It is further assumed that there will only be one borehole taken per block. Geophysical measurements covering a large area will be handled by breaking up the area into a number of blocks covering the area.

4.6.4 TYPES OF UNCERTAINTY HANDLED

There are three types of uncertainty: natural, statistical, and model (Benjamin and Cornell, 1970).

Natural uncertainty represents the uncertainty in the random variable itself. Statistical uncertainty is the uncertainty in the parameters, such as mean and variance, governing the probability distribution. Model uncertainty is the uncertainty in the exact form of the probability density function, e.g. "does a random variable really follow a normal distribution, or does it follow a Gamma distribution?"

Simple kriging only accounts for the natural uncertainty and ignores the statistical and model uncertainty because it assumes that μ_I and $Cov(h)$ are known. The statistical uncertainty in the assumed parameters can be accounted for by using their Bayesian distributions (Benjamin and Cornell, 1970). Kitanidis (1986) presents a series of matrix equations for estimating spatially correlated random variables that accounts for the uncertainty in the different parameters. There is no straightforward procedure to account for model uncertainty (Benjamin and Cornell, 1970). As an initial first order approximation, model and statistical uncertainty will be ignored in this thesis.

4.6.5 NUMBER OF CONDITIONING DATA

Recall that there is potentially a large amount of data to condition the estimate of $I(B)$ at some block, B . These data will not only include measured data, but previously simulated blocks. Ideally the estimate should be conditioned on all data. However, this is impractical since each conditioning data point adds one equation to the system that must be solved for the weights a_j , $j=1, \dots, n$. The solution quickly becomes numerically awkward as n increases because the effort needed to solve this system of equations is proportional to n^2 .

Therefore, the number of conditioning data points is restricted to the ones nearest to the estimation point. This limitation will not cause numerical problems because data points that are far away from the estimation point, or have other data points in between themselves and the estimation point, will have little effect on the estimation result. For one-dimensional simulations, the limit is the five nearest previously simulated blocks and/or measured data on either side of the block being simulated. In two dimensional simulations, the 10 to 20 nearest measured data points or previously simulated blocks are used.

4.7 ALTERNATIVE SIMULATION ALGORITHMS

There are several standard methods for generating realizations of correlated random variables. These include turning bands (see Mantoglou, 1987) and Cholesky decomposition (see Clifton and Neumann, 1982; Alabert, 1987; and Davis 1987). These methods deal with continuous random variables rather than discrete random variables, and assume that the random variable comes from a multi-variate Gaussian distribution. It would be possible to use any of these alternative methods for dealing with

aquitard continuity by generating realizations of aquitard block thickness. Holes would exist if the aquitard thickness was below some critical value.

However, the SIS algorithm has several distinct advantages over these methods. The first is that the conditioning of realizations on both hard and soft data is built into the SIS algorithm. There is no straightforward method for conditioning the realization from the standard methods on soft data. A second important advantage is that the SIS algorithm does not require that the simulated random variable come from a multivariate Gaussian distribution.; a wide range of different probability density functions can be handled (Gomez-Hernandez and Srivastava, 1990). Aquitard thickness may not follow a Gaussian distribution. For example, if there is a finite chance of a hole, i.e. thickness equal to zero, then the thickness cannot follow a Gaussian distribution because the probability of the random variable having a particular value is zero.

Another important advantage of the SIS algorithm is that it deals with extreme values much better than the Gaussian based methods. This is of direct interest here because one extreme thickness, or window, can have a major impact on the flow system and transport of contaminants. One of the specific purposes of IK, on which the SIS algorithm is based, is to handle extreme values (Journel, 1983). The Gaussian assumption has a damping effect which greatly reduces the probability of extreme outliers. In addition, the Gaussian assumption does not allow for the spatial correlation of extreme values (Journel, 1989), which again is one of the specific purposes of the SIS algorithm. Including the spatial correlation of extreme values is of utmost importance because it provides valuable information on predicting the locations of extreme values.

The advantage of the Gaussian-based methods is that they are very straight forward to apply. If the framework were used to evaluate the worth of hydraulic conductivity measurements, which are

generally assumed to follow a multivariate log-normal distribution, then the SIS algorithm could be readily replaced with one of the above standard methods.

4.8 GEOSTATISTICAL NATURE OF CLAY LAYERS

In general, little work has been done in quantifying the geostatistical nature of clay/shale layers, or relating it to depositional environments. Desbarats (1987a) found that, while the shale layers in the vertical direction had no correlation, they were exponentially correlated in the horizontal direction with a range of 15 m and no apparent nugget effect. The shales were deposited in an alluvial environment (Desbarats, 1987b). He noted that the physical significance of the range was not clear because indicator variography expresses spatial continuity of shales and sands rather than shale continuity alone. The range does not correspond to the average shale length.

In the only other study relating spatial correlation and geology that the author is aware of, Phillips and Wilson (1989) produce a method for estimating the correlation length of hydraulic conductivity based on the dimensions of geologic units. However, they did not study shale continuity, nor did they study the spatial correlation as it relates to specific depositional environments.

4.9 NOTATION

a	range of covariance function
a_j	j^{th} kriging weight or declustering weight
B_j	j^{th} aquitard block generated by sequential indicator simulation algorithm
C_{jk}	covariance coefficient between $I(x_j)$ and $I(x_k)$
$\text{Cov}(h)$	covariance function of $I(x)$
$\text{Cov}_I^*(h)$	estimated covariance function of $I(x)$

$\text{Cov}^*_{\Pi_s}(h)$	estimated cross covariance function between $I(x)$ and $I_s(x)$
$\text{Cov}_{\Pi_s}(h)$	cross covariance function between $I(x)$ and $I_s(x)$
$\text{Cov}_{I_s}(h)$	covariance function of $I_s(x)$
$\text{Cov}^*_{I_s}(h)$	estimated covariance function of $I_s(x)$
d_j	j^{th} distance class
$f_j(x)$	known function of x representing drift in $Z(x)$
$F(0)$	cumulative probability distribution of $I(x)$
$F^*(0)$	estimate of $F(0)$
$F^*_{I_s}(0)$	estimate of $F(0)$ from hard data
$F^*_{I_s}(0)$	estimate of $F(0)$ from soft data
h	separation distance
h_{a_j}	average separation distance of data points within distance class d_j
H_s	weight of measured sample data
H'	weight of prior data
H''	updated weight of data
i	vector of data $i(x)$
$i(x)$	value of indicator random variable $I(x)$
$i(x)^*$	estimated value of indicator random variable $I(x)$
$i(x)_T$	true value of indicator random variable $I(x)$
$I(x)$	indicator random variable at point x
$I_s(x)$	soft indicator random variable at point x
m_I	estimate of μ_I
m_I'	prior estimate of μ_I
m_I''	updated estimate of μ_I
m_z'	prior estimate of μ_z
m_z''	updated estimate of μ_z

n_e	equivalent number of data
n_j	number of data point in d_j
n_h	number of hard data
n_s	number of soft data
p	random number drawn from uniform random number generator
$p_1(x)$	probability that a window will be sampled at point x , given that one exists, $P(I_s(x)=1 I(x)=1)$
p_1	stationary form of $p_1(x)$
$p_2(x)$	probability that a window will be sampled at point x , given that one does not exist, $P(I_s(x)=1 I(x)=0)$
p_2	stationary form of $p_2(x)$
$Q_{zz}(\theta)$	covariance matrix of $Z(x)$
$S_{II}(\theta)$	known covariance matrix of $I(x)$, except for unknown multiplicative constant
$S_{zz}(\theta)$	known covariance matrix of $Z(x)$, except for unknown multiplicative constant
u	vector of 1's
v	vector of 1's
z	vector of measurements of z
$z(x)$	value of $Z(x)$ at point x
z_c	critical cutoff
$Z(x)$	continuous random regional variable at location x
θ	unknown parameter
λ_I	correlation length of $I(x)$
μ_I	mean of random variable $I(x)$
μ_{I_s}	mean of random variable $I_s(x)$
μ_Z	mean of random variable $Z(x)$
σ_I^2	variance of $I(x)$
σ_Z^2	variance of $Z(x)$

$\varphi(x)$	zero mean binary random function
$\psi(x)$	zero mean continuous random function
ω	relative weight of hard data

CHAPTER 5: CONTAMINANT TRANSPORT

5.1 INTRODUCTION

Recall that failure occurs when contaminants from the landfill penetrate an aquitard and spread to a lower aquifer. The failure time is needed in the objective function so that future costs can be converted into present day dollars. The purpose of this chapter is to explain how contaminant transport is modeled and failure times calculated for an aquitard realization generated by the SIS algorithm.

For simplicity it is assumed that the contaminants are miscible in water, are at low concentrations which do not significantly change the density of groundwater, and are non reactive and non-radioactive. It is further assumed that groundwater flow conditions are fully saturated and at steady state. More complicated contaminants or flow conditions could easily be incorporated into the framework by increasing the complexity of the numerical model needed to calculate failure times.

A brief overview of contaminant transport processes pertinent to this thesis will be given first. For a more detailed discussion on contaminant transport processes refer to Domenico and Schwartz (1990), Freeze and Cherry (1979), or any other standard text on hydrogeology. A description of how contaminant transport and failure times are calculated in both the two dimensional and three dimensional cases follows.

5.2 TRANSPORT PROCESSES

The transport of a contaminant that is miscible, at low concentrations, and non reactive, is governed by an advection dispersion equation of the following form (de Marsily, 1986):

$$\nabla \bullet (\mathbf{D} \nabla C - C \mathbf{v}) = \frac{\partial C}{\partial t} \quad (5.1)$$

where

- \mathbf{D} is the dispersion tensor (L^2/T)
- C is the concentration (M/L^3)
- \mathbf{v} is the average linear velocity vector of the groundwater flow (L/T)
- t is time (T)

Bold upper case letters represent tensors and bold lower case letters represent vectors. For one dimensional transport in the x direction, in a homogeneous medium, equation (5.1) becomes:

$$D_x \frac{\partial^2 C}{\partial x^2} - v_x \frac{\partial C}{\partial x} = \frac{\partial C}{\partial t} \quad (5.2)$$

The first term on the left hand side represents the hydrodynamic dispersive component of transport while the second term accounts for the advective component. These different components are discussed in more detail below.

5.2.1 ADVECTION

The advective component represents the amount of dissolved contaminant physically transported by flowing groundwater at the average linear velocity of the groundwater. The average linear velocity of groundwater is calculated using Darcy's law:

$$\mathbf{v} = - \frac{\mathbf{K}}{n} \nabla h \quad (5.3)$$

where \mathbf{K} is the hydraulic conductivity tensor, n is the effective porosity, and h is the hydraulic head.

From equation (5.3) it is seen that the rate of advective transport is dependent upon the hydraulic conductivity, the porosity, and the hydraulic gradient. If the co-ordinate axes coincide with the principal directions of anisotropy, then the off diagonal components of \mathbf{K} become zero. Therefore,

$$\mathbf{K} = \begin{pmatrix} K_{xx} & 0 & 0 \\ 0 & K_{yy} & 0 \\ 0 & 0 & K_{zz} \end{pmatrix} \quad (5.4)$$

Darcy's law has the following form for flow in the x direction:

$$v_x = - \frac{K_{xx}}{n} \frac{\partial h}{\partial x} \quad (5.5)$$

The hydraulic head field is determined by solving the flow equation, which has the following form for steady state flow:

$$\nabla \cdot \mathbf{K} \nabla h = 0 \quad (5.6)$$

5.2.1 HYDRODYNAMIC DISPERSION

Hydrodynamic dispersion accounts for the spreading of contaminants as they are transported. As a result, it is a dilution process; however, contaminants can arrive at a particular point faster than they would by simple advection at the average linear velocity. Hydrodynamic dispersion has two components: diffusion and mechanical dispersion.

Diffusion is transport due to concentration gradients. The rate of diffusion is governed by Fick's law:

$$f_d = -D_d \nabla C \quad (5.7)$$

where

- f_d is the mass flux of contaminant flowing through a unit area of aquifer per unit time, and
- D_d is the apparent diffusion coefficient of the porous media.

Mechanical dispersion is a spreading process caused by local variations in groundwater velocity. These local variations are the result of flow through heterogeneities that occur at both the microscopic and macroscopic scale.

On the pore scale, mixing occurs for a number of reasons. First, fluid in the center of a pore will flow faster than at the edges because of boundary effects. In addition groundwater will flow faster through some pores than others due to pore size and pore geometry. Finally, the path through any pore system will be tortuous and branching, causing flow through the pore system to keep dividing.

On larger scales, groundwater will flow faster through more permeable parts of a flow system, such as a sand lens, than through less permeable parts of the flow system. As a contaminant travels farther through a flow system, dispersion is increasingly controlled by larger scale heterogeneities.

Mechanical dispersion typically predominates over molecular diffusion in most groundwater flow situations. Diffusion is only an important process at low groundwater velocities.

5.2.3 IMPORTANCE OF ADVECTION

Massmann (1987) reported from a study of ten case histories, that the advection component generally predominates over the dispersive component if the average linear groundwater velocity is greater than several meters per year. He further notes that hydraulic conductivities of between 10^{-2} and 10^{-4} m/s are

needed for this to occur. This range of values would apply to sands and gravels for unconsolidated deposits. For simplicity, it is assumed in this thesis that the average linear groundwater velocities are high enough that advection predominates, allowing dispersion to be ignored. Travel paths from the landfill through the upper aquifer and through an existing window in the aquitard to the lower aquifer are assumed to occur in sand and gravel.

This thesis assumes that contaminant transport occurs only by advection. Nevertheless, if dispersion is an important component of transport, it would be a simple matter to incorporate it into the framework.

5.3 MODELING OF CONTAMINANT TRANSPORT

Contaminant transport is modeled by first solving the steady state flow equation (5.6) for the hydraulic head field using a finite element or finite difference model. The advective velocity field is then calculated from the hydraulic head field. The travel time for a plume to reach a point of failure in the lower aquifer is then calculated from the velocity field by a particle tracking routine. Recall that all factors governing contaminant transport are assumed known, except for aquitard continuity.

The modeling of contaminant transport for the two different cases (two-dimensional and three-dimensional) covered in this thesis will now be discussed. Two dimensional modeling is used in Chapter 6 for explanatory purposes only. Three-dimensional modeling is used in both Chapters 7 and 8.

5.3.1 2-D MODELING OF SOLUTE TRANSPORT

A Galerkin finite element model is used to calculate the two-dimensional hydraulic head field from equation (5.6). The boundary conditions on the flow field are shown in Figure 5-1. The flow field is split into three regions. The central region is the zone of interest where aquitard continuity is unknown.

The aquitard in this region is generated by the SIS algorithm. The purpose of the outer regions on either side of the central region is to reduce the effect of the vertical boundary conditions on flow in the central zone of interest. The aquitard in these regions is assumed to be continuous.

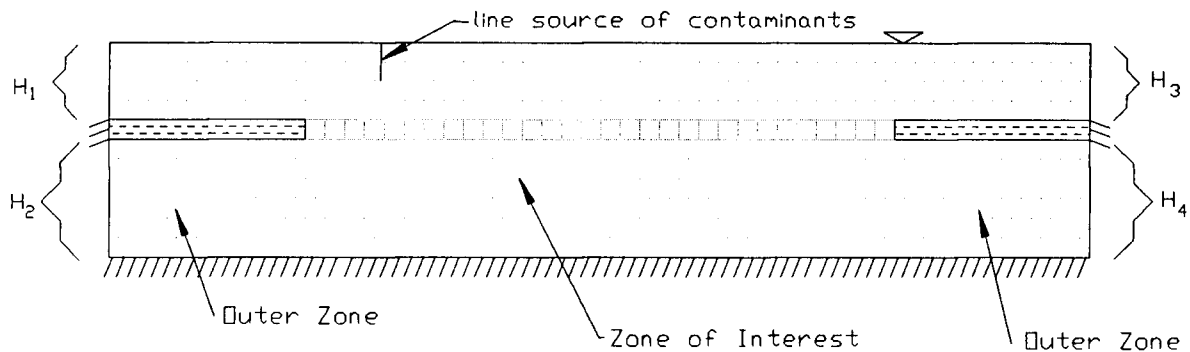


Figure 5-1: Boundary conditions on two-dimensional flow field.

The bottom of the system is an impermeable boundary. On the vertical sides, constant head boundaries, H_1 , H_2 , H_3 , and H_4 occur on the edges of the aquifers while impermeable boundaries occur on the edges of the aquitard. H_1 , H_2 , H_3 , and H_4 have been chosen so that flow is from left to right and is vertically downward across the aquitard at the right hand side. The top boundary is a fixed water table which is assumed to vary linearly between the two vertical constant head boundaries on either side of the upper aquifer. The contaminant source is represented as a vertical line over which particles are released at a uniform spacing. A vertical line source was chosen to spread the plume over a large thickness of the upper aquifer.

Linear triangular elements spaced on a rectangular mesh are used in the finite element model (Fig. 5-2). A variable mesh size can be used so that a finer mesh can exist in the central region than in the two outer regions. The aquitard layer is represented by two or more layers of elements.

Once the hydraulic head field has been calculated by the finite element model, the average element linear velocities are calculated by (Frind and Matanga, 1985):

$$v_x = \frac{-K_x}{n} \frac{\partial}{\partial x} \sum_j h_j w_j \quad (5.8)$$

$$v_y = \frac{-K_y}{n} \frac{\partial}{\partial y} \sum_j h_j w_j \quad (5.9)$$

where,

- h_j is the hydraulic head at node j ,
- n is the porosity, and
- w_j is the basis function for node j .

The element velocities are transferred to a rectangular grid of cells to simplify the particle tracking. This is done by assigning to the grid point the velocity of the element that contains the grid point. The velocity of the particle, v_p , at any point (x,y) in some cell is then calculated by linear interpolation of the velocities at the four grid points at the cell corners. Particles are tracked through the velocity field by the tangent, or Euler, method (see Boyce and DiPrima, 1969):

$$x_p(t) = x_p(t - \Delta t) + v_{px}[x_p(t - \Delta t), y_p(t - \Delta t)]\Delta t \quad (5.10)$$

$$y_p(t) = y_p(t - \Delta t) + v_{py}[x_p(t - \Delta t), y_p(t - \Delta t)]\Delta t \quad (5.11)$$

where

- $x_p(t)$ is the x co-ordinate of the particle at time t ,
- $y_p(t)$ is the y co-ordinate of the particle at time t ,

- Δt is the time step, and
- $v_{px}[x_p(t), y_p(t)]$ is the x component of the particle velocity at point $[x_p(t), y_p(t)]$.

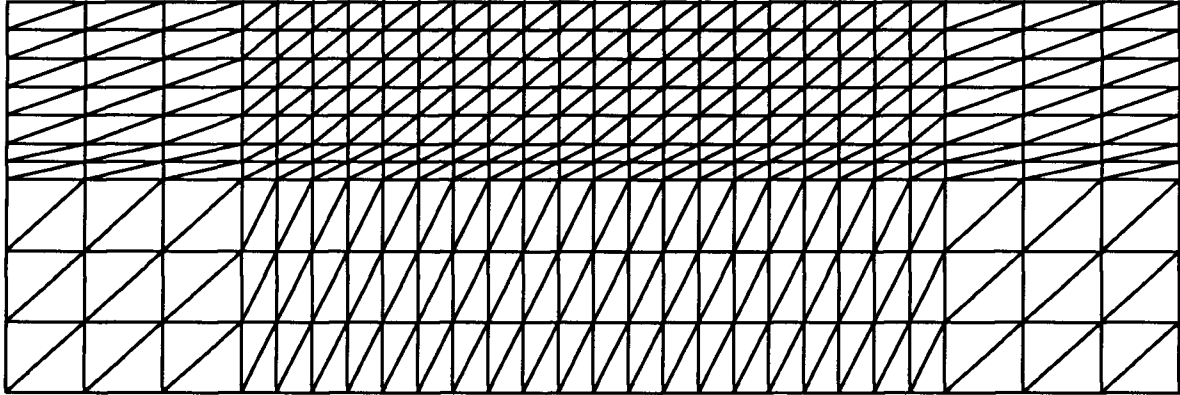


Figure 5-2: Sample finite element grid for two dimensional vertical cross section.

The time step, Δt , is kept small so that it takes at least ten steps for a particle to cross one cell. This is to keep particles from jumping streamlines. A number of particles are released at different points in the source area and are tracked through the flow region. Failure occurs if any of the particles reaches the lower aquifer. It is assumed that any of the particles reaching the lower aquifer represents a major breakthrough of contamination.

There are several limitations associated with the approach carried out here for modeling contaminant transport and groundwater flow. For example, the position of the water table is fixed. In reality the position of the water table is dependent upon the geometry of the aquitard used in the flow model. This could cause errors in the calculated hydraulic head field. Another potential numerical problem is created by tracking particles through the velocity field using the Euler or tangent method. For large time steps, particularly in non smooth velocity fields, particles could jump stream lines resulting in an incorrect paths being followed.

Both of these limitations could be removed by making the analysis more complicated and numerically intensive, thus increasing the reliability of the calculated failure times. For example, a free surface model would account for a changing water table. Problems of particles jumping stream lines could be solved by having a very fine finite element mesh or by tracking the particle using a modified Euler or Runge Kutta approach. However, the purpose of the two dimensional cross section is to provide a simple test case on which to build the more complicated and more realistic three dimensional case. Hence, we are only concerned with first order accuracy for this case, and for simplicity, inaccuracies due to the above numerical problems will be ignored. The overall reliability of estimated worths will be more greatly affected by uncertainty in other factors such as aquitard heterogeneity and boundary conditions on the flow model.

5.3.2 3-D MODELING OF SOLUTE TRANSPORT

In the three-dimensional modeling, the hydraulic head field is solved using the USGS finite difference MODFLOW package. MODFLOW is a commercially available computer model that has been widely used throughout the groundwater world over the last 20 years and has been well validated.

The transport of contaminant is solved using the USGS MODPATH particle tracking routine.

MODPATH assumes that advective transport dominates other forms of transport. MODPATH uses flow velocities calculated directly by MODPATH to move particles of contamination through the flow field.

For a detailed description of MODFLOW or MODPATH , refer to McDonald and Harbaugh (1989) and Pollack (1989), respectively.

5.4 NOTATION

C	concentration of contaminant
D	dispersion tensor
D_d	apparent diffusion coefficient of the porous media
D_x	dispersion in the x direction
f_d	mass flux of contaminant flowing through a unit area of aquifer per unit time
h	hydraulic head
K	hydraulic conductivity tensor
K_{xx}	hydraulic conductivity in x direction
K_{yy}	hydraulic conductivity in y direction
K_{zz}	hydraulic conductivity in z direction
n	porosity
t	time
v	average linear velocity of groundwater flow
v_x	average linear velocity of groundwater flow in x direction
v_{px}	x component of particle velocity
w_j	basis function for node j
$x_p(t)$	x co-ordinate of particle at time t
$y_p(t)$	y co-ordinate of particle at time t

CHAPTER 6: OUTLINE OF FRAMEWORK

6.1 INTRODUCTION

Chapter 6 ties together the different components introduced in Chapters 2 through 5 into the data worth framework. The framework is able to evaluate the worth of hard, point measurements and soft, areal measurement. A soft, areal measurement could consist of some type of geophysical survey such as a shallow seismic, or a radar survey. Soft, point measurements cannot be handled.

Different methods of measuring aquitard discontinuities are discussed in Section 6.2. Section 6.3 describes how the framework evaluates the worth of a single hard measurement. Section 6.4 discusses the sensitivity of this estimate to numerical artifacts of the methodology. Section 6.5 presents how the methodology developed in Section 6.3 can be used to estimate the worth of a soft geophysical survey which covers a large area. Section 6.6 discusses how the framework could be modified to handle data worth problems in other disciplines, such as mining engineering and reservoir engineering.

6.2 MEASURING AQUITARD DISCONTINUITIES

Aquitard continuity can be measured directly using hard data provided by boreholes, or soft data provided by geophysical surveys, or by other methods. It can also be measured indirectly by methods such as hydraulic head measurements, pump tests, barometric efficiency, and age dating of water.

Boreholes provide both hard and soft point measurements. If the borehole is continuously cored, the presence of a distinct aquitard should be determined with certainty. However, if one meter split spoon samples were taken every two meters, a thin aquitard could be missed. Geophysical measurements could range from areal surveys covering the entire region of interest, such as radar or seismic surveys, to point

measurements such as geophysical logs in a borehole. It is assumed that geophysical measurements will be imprecise. No specific geophysical technique is targeted in this thesis. However, several methods would be applicable such as seismic, resistivity, and radar surveys, and gamma ray or self potential logs.

Measurements of hydraulic head, H , are available in virtually all hydrogeological investigations. They can be used in two forms to predict aquitard continuity. In the first form, many H measurements are taken throughout the aquifer, but at the same time. They can be used to estimate, or constrain, patterns of hydraulic conductivity through inverse techniques (see Yeh, 1986; Kitanidis and Vomvoris, 1983; and Clifton and Neuman, 1982). However, these techniques are not widely used because their numerical complexity is high and stability problems can lead to a difficulty in obtaining solutions. Previous work has also shown that such measurements of H are not very effective in determining the continuity of aquitards or aquifers. Fogg et. al. (1979), quoted by Rouhani (1985), found that radical changes in transmissivity created only small changes in hydraulic head, while Fogg (1986) reported that hydraulic heads give little indication of interconnected zones of aquifer/aquitard systems, even with carefully calibrated models. Duffield et. al. (1989) confirmed these results in their study of the Savannah River Site in South Carolina. They found that windows and faults in aquitards, with significant vertical gradients across them, produced only small changes in the H field which were difficult to detect without closely spaced monitoring wells in the vicinity of the window.

In the second form, H measurements taken from a single well at different points in time form a time series. H measurements in this form are potentially a very valuable way of investigating aquitard continuity. The fluctuations in hydraulic head, both natural and induced, will be correlated for two aquifers that are hydraulically connected. Fluctuations in hydraulic head for aquitards that are not hydraulically connected should be independent or show a significant time lag.

Pump tests can be valuable in testing aquitard continuity. A well in one aquifer can be pumped while drawdown is observed in adjoining aquifers. A large drawdown is a good indication of hydraulic

connection. Such a connection may be caused by an aquitard discontinuity between the aquifer with the pumping well and the aquifer with the observed drawdown. However, no analyses are known to the author that determine exactly how a window will affect a pump test.

The age dating of water through isotope analysis could be very useful in predicting aquitard continuity. If the water in two adjacent aquifers have greatly different residence times, then the aquitard separating them is probably continuous. For a more detailed explanation of the age dating of groundwater, refer to Domenico and Schwartz (1990) or Fritz and Fontes (1980).

Barometric efficiency, B_e , could potentially be used to establish the continuity of aquitards that act as confining layers for near-surface aquifers. B_e relates the decline in peizometric head in an aquifer to a given increase in air pressure. It is defined by:

$$B_e = \frac{\gamma dh}{dP_a} \quad (6.1)$$

where

- γ is the specific weight of water
- dh is the change in the peizometric level, and
- dP_a is the change in the air pressure.

The greater is the value of B_e , the greater is the confining ability of the aquitard and the greater the likelihood of its continuity. Refer to Freeze and Cherry (1979) for a more detailed explanation of barometric efficiency.

Some of the above methods could be very promising in helping to predict aquitard continuity. However, as a first step, only the worth of boreholes, geophysical surveys, and/or local geological information will

be directly evaluated in this thesis. Other types of data could be added to the framework later if desired. However, such additions could involve a great deal of numerical complexity.

As noted in Chapter 3, a regional geological understanding of how an aquitard was formed can be very valuable in predicting continuity. In this thesis prior geological understanding can be incorporated into the framework, but its worth will not be evaluated.

In this thesis, only the presence or absence of aquitard is of interest; aquitard thickness is ignored. Therefore, data consists of a set of yes or no values; either the aquitard is present beneath a location (x_i) or it is not. If desired, aquitard thickness could be put into the framework through co-kriging or probability kriging. However, this will not be done for two reasons. First, it is unclear whether a relationship exists between layer thickness and continuity (see Chapter 3). Secondly, co-kriging will substantially increase the complexity of the framework, but is expected to bring little improvement over simple indicator kriging (Journel, 1983). Practice in probability kriging has shown that generally the increase in precision over normal indicator kriging is small and not worth the increased effort (Sinclair, 1990). For a detailed discussions on cokriging or probability kriging refer to Journel and Huijbregts (1978) or Sullivan (1985), respectively.

6.3 EVALUATING THE WORTH OF HARD, POINT MEASUREMENTS

This section ties together all of the ideas presented earlier to show how the framework evaluates the worth of a sampling program for hard, point measurements. This presentation uses an example design where the worth of a single hard measurement is evaluated. The example design is presented below.

6.3.1 EXAMPLE DESIGN

The example design is similar to the landfill presented in Chapter 2. The boundary conditions, hydrogeological and geostatistical parameters are shown in Figure 6-1. The confidence in the estimates of the mean is arbitrarily set to be equal to that of 15 prior measurements. (Recall, that the updating of the mean and the confidence in the prior estimate of the mean are discussed in Section 4.5.2.) The finite element mesh is shown in Figure 6-2. The mesh consists of 2 520 elements and 1 397 nodes. The worth of a single, hard measurement is evaluated. The hard measurement in this case will represent a borehole which is cored and logged in its entirety. It is taken 75 m (block 5) from the left hand side of the zone of interest.

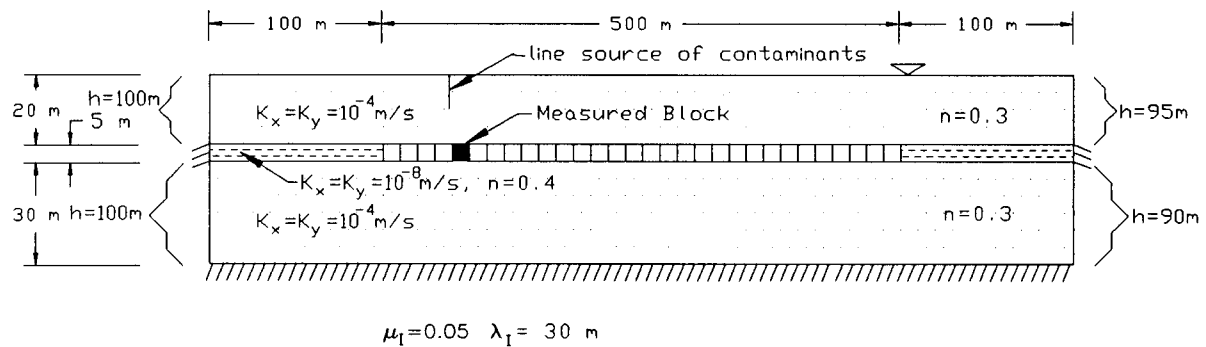


Figure 6-1: Boundary conditions, hydrogeological and geostatistical parameters used in the example design.

The two design alternatives are again to have either a liner or no liner. The economic parameters are shown in Table 6-1 while numerical parameters are shown in Table 6-2. A discount rate of 10% is used. A minimum of 100 realizations is used to estimate the objective function of an alternative for each prior analysis for a particular set of sample outcomes in the preposterior analysis. The number of realizations needed to obtain a reliable estimate of the objective function for an alternative is discussed in Section 6.4. Five particles were released from the source. Experimentation indicated that five was the minimum number of particles released from the source which yielded consistent data worth estimates. Results were not significantly improved by using more than five particles.

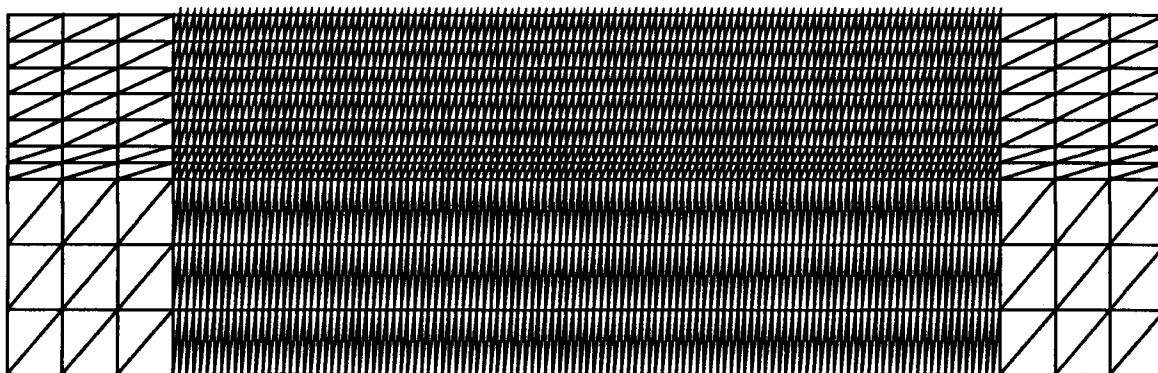


Figure 6-2: Finite element mesh used in example design with eight times vertical exaggeration.

Alternative	Benefits (millions \$)	Costs (millions \$)	Cost of Failure (millions \$)
Liner	10.	5.	1.
No Liner	10.	0.	10.

Table 6-1: Economic parameters used in example design.

Parameter	Value
minimum number of realizations to estimate Z	100
number of particles released from source	5
# of aquitard blocks	30
starting seed	6874462
first aquitard block generated	2
minimum number of conditioning data points on either side of est. pt.	5

Table 6-2: Numerical parameters used in example design.

6.3.2 TWO METHODS OF GENERATING REALIZATIONS FOR THE FRAMEWORK

Recall that there are two basic components in analyzing the worth of a sampling pattern: the prior analysis and the preposterior analysis. Aquitard realizations generated in the prior analysis are created by the SIS algorithm using the prior estimates of the geostatistical parameters. Aquitard realizations

generated during the preposterior analysis are created by the SIS algorithm using estimates of the geostatistical parameters updated from sample outcomes.

In a straightforward application of the principles discussed in Chapter 2, aquitard realizations would be first generated during the prior analysis. A second set of realizations would then be generated during the preposterior analysis. An alternative way is to generate realizations during the preposterior analyses and then "reuse" them in the prior analyses. The advantages and disadvantages of each method are discussed below. It will be shown that numerical problems lead to the abandonment of the first method.

6.3.2.1 Realizations Generated During Both Prior and Preposterior Analysis (Abandoned Approach)

6.3.2.1.1 The Prior Analysis

The prior analysis can be visualized by a decision tree (Fig. 6-3) that is slightly different from the one presented in Chapter 2 (Fig. 2-2). In Figure 2-2, a design alternative only had two possible outcomes: failure or no failure. The true outcome was uncertain. Here, the design alternative has as many outcomes as realizations that are generated. Each outcome is assumed to be equally likely. To simplify the rest of the Figures presented in this Chapter, the effect of all of the possible outcomes is represented by the expected value of the objective. The prior analysis is shown as the upper limb in Figure 6-4.

Using the objective function given as equation (2.3) and the data from Table 6-1, the prior best design, A_D , is the no liner alternative with $E(Z(A_{NL})) = \$7.743 \times 10^6$ and $E(\text{Reg}(A_{NL})) = \2.195×10^5 . The prior probability of failure is 0.37.

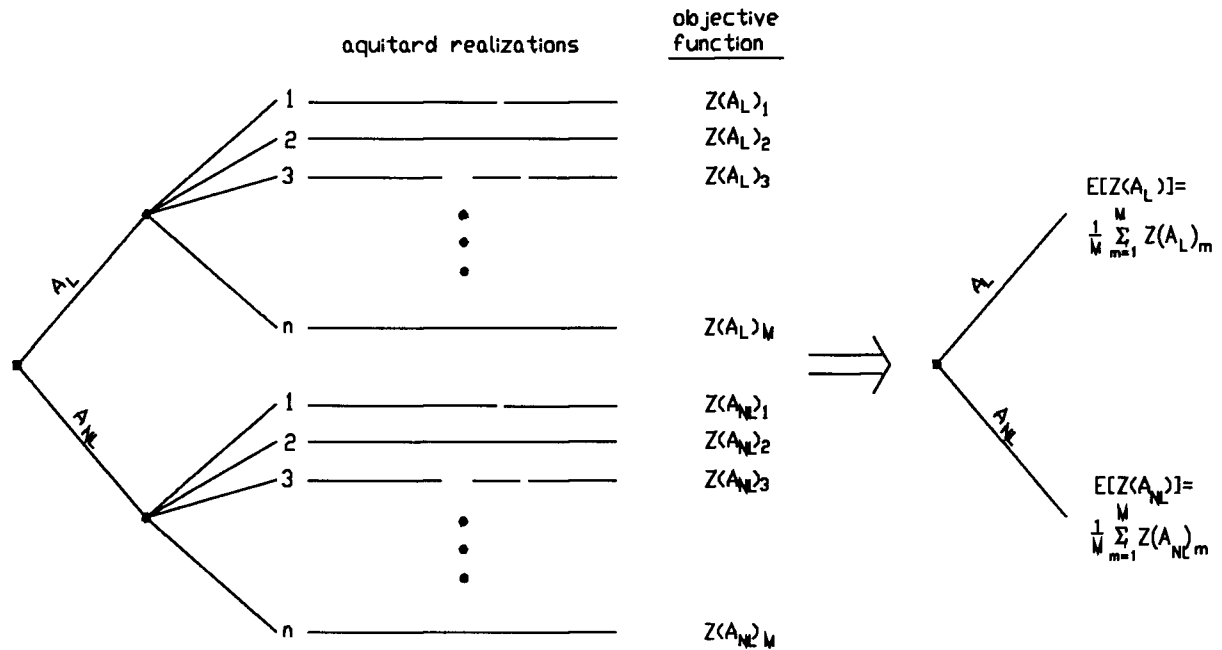


Figure 6-3: Decision tree used in prior analysis and its simplified version to right.

6.3.2.1.2 Preposterior Analysis

The preposterior analysis is carried out in the following basic steps:

- 1) A pattern of n measurements is proposed.
- 2) The 2^n combinations of different sample outcomes S_j are calculated.
- 3) The mean is updated, based on sample outcome S_j .
- 4) A series of M aquitard realizations, R_{mlj} , are generated using the updated parameters and conditioned on S_j . (The subscript mlj on R refers to m^{th} realization which is conditioned on sample outcome S_j .)
- 5) For each realization, R_{mlj} , contaminant transport is modeled for each alternative, A_i , to determine if failure occurs for A_i . Failure times are calculated.
- 6) The failure time is then used to calculate the objective function, $Z(A_i, R_{mlj} | S_j)$, for each A_i , for all M realizations, R_{mlj} .

- 7) The alternative, A_D' , with the highest expected objective function, over all M realizations is then selected.

$$E(Z(A_D')) = \frac{1}{M} \sum_{m=1}^M Z(A_D', R_{mlj} | S_j) \quad (6.2)$$

$Z(A_D', R_{mlj} | S_j)$ is the objective function of the posterior best design alternative for realization R_{mlj} , given S_j .

- 8) Steps 3 through 7 are repeated for each of the 2^n sample outcomes S_j .
- 9) The expected expected objective function of the best preposterior design is calculated by

$$E[E(Z(A_D'))] = \frac{1}{2^n} \sum_{j=1}^{2^n} \sum_{m=1}^M \frac{Z(A_D', R_{mlj} | S_j)}{M} P(S_j) \quad (6.3)$$

- 10) The worth of the sampling pattern is calculated from

$$\text{Worth} = E[E(Z(A_D'))] - E(Z(A_D)) \quad (6.4)$$

Recall that all hard measurements are assumed to be taken at the same scale as the blocks that form the discretized stratigraphic horizon containing the aquitard. If a measurement is taken at a block, the outcome of the measurement is assumed to apply to the entire block.

In step 2, it is assumed that there are only two possible outcomes at any sampled block: either an aquitard is measured or a window is measured. Since there are n sampling locations, there are 2^n possible combinations of sample outcomes.

For the preposterior analysis of the borehole taken at B_5 , there are only two possible outcomes: S_W or S_{NW} . Each sample outcome is used in turn to update the geostatistical parameters. The updating of geostatistical parameters was discussed in Section 4.5.2. One hundred new realizations are generated for each set of updated geostatistical parameters. The new best design, A_D' , is chosen for each set of realizations. These results are summarized in Figure 6-4.

The worth, W_1 , of the borehole from the expected increase in the maximum expected objective function is

$$\begin{aligned}
 W_1 &= E[E(Z(A_D'))] - E[Z(A_D)] & (6.5) \\
 &= [(\$4.355 \times 10^6)(0.05) + (\$7.802 \times 10^6)(0.95)] - \$7.743 \times 10^6 \\
 &= \$-112\,700.
 \end{aligned}$$

The worth, W_2 , of the borehole from the expected decrease in the minimum expected regret is

$$\begin{aligned}
 W_2 &= E[\text{Reg}(A_D)] - E[E(\text{Reg}(A_D'))] & (6.6) \\
 &= \$2.195 \times 10^5 - [(\$0)(0.05) + (\$2.158 \times 10^5)(0.95)] \\
 &= \$145\,000.
 \end{aligned}$$

Note, that even though the two methods ought to be equivalent (see Chapter 2), here they give different worths for the same borehole. W_1 even has a negative value, which is impossible. The minimum possible worth for a measurement is zero. This difference is caused by changes in the system between the prior and the preposterior analysis. The system refers here to the entire set of parameters used in either the preposterior or the prior analysis. These include the geostatistical parameters, the expected value of the objective function of the different alternatives, and the probability of failure. If anyone of these parameters changes between the prior and the preposterior analysis, the system has changed. It is explained below how the system has changed.

The properties of the ensemble of realizations used in the prior analysis must be identical to the properties of the ensemble of realizations used in the preposterior analysis; no sample in reality has been taken to change the ensemble of realizations. Therefore, all parameters must remain consistent between the prior and preposterior analysis; their expected values in the prior analysis must equal their expected values in the preposterior analysis. However, in the example analysis, the probability of failure and objective functions for the different alternatives are inconsistent (Table 6-3). Only the geostatistical parameters remain consistent.

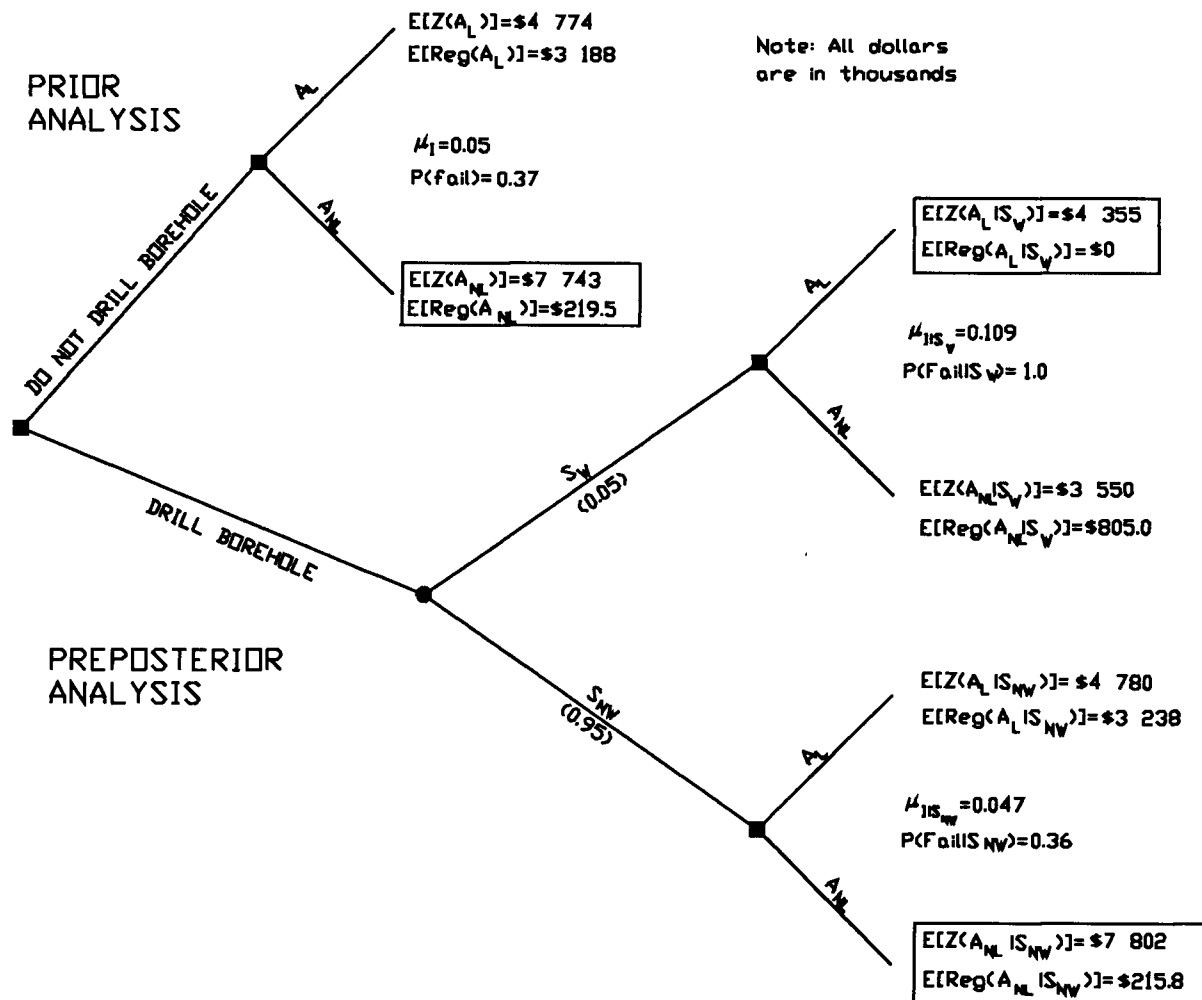


Figure 6-4: Preposterior analysis of example design when realizations are generated in both the prior and the preposterior analysis.

Theoretically, the generated realizations are only dependent upon the geostatistical parameters; therefore, the properties of the prior and preposterior ensemble of realizations would approach each other as the number of generated realizations increased, since the geostatistical parameters remain consistent. Therefore, if a huge number of realizations were generated, the ensembles of realizations would be almost identical.

Parameter	E[Prior Value]	E[E(Preposterior Value)]	
m_I	0.05	0.05	$=(.05)(.109)+(.95)(.047)$
λ_I	30	30.	$=(.05)(30)+(.95)(30)$
$Z(A_L)$	$\$4.774 \times 10^6$	$\$4.759 \times 10^6$	$=(.05)(\$4.355 \times 10^6)+(.95)(\$4.780 \times 10^6)$
$Z(A_{NL})$	$\$7.743 \times 10^6$	$\$7.589 \times 10^6$	$=(.05)(\$3.550 \times 10^6)+(.95)(\$7.802 \times 10^6)$
$P(\text{failure})$	0.37	0.392	$=(.05)(1.)+ (.95)(0.36)$

Table 6-3: The values of parameters used in the prior analysis and the expected value of parameters used in the preposterior analysis.

Unfortunately, in reality this does not happen. The realizations are only pseudo-random and are dependent upon a number of "artificial" parameters, which are functions only of the algorithm used to generate the realizations. These parameters are: the starting seed, the number of the first aquitard block generated, the order in which the aquitard blocks are generated, and the number of aquitard blocks generated. Change any of these parameters and a different set of realizations are generated. This effect is defined as noise in this thesis. Because of this pseudo-randomness, the properties of the ensemble of realizations generated during the prior and the preposterior analyses will not be exactly identical, regardless of how many realizations are generated. Given the sensitivity of the system, even these very small inconsistencies in $Z(A_L)$, $Z(A_{NL})$, and P_f are enough to cause the large discrepancies in data worth noted in equations (6.5) and (6.6).

The geostatistical parameters remained consistent because the updating of the mean is carried out directly by Bayes' equation and is unaffected by parameters used in the SIS algorithm. The correlation length is

not updated, and therefore, must be consistent. The updating of geostatistical parameters is discussed in Section 4.5.2.

In view of the foregoing, it was therefore recognized that this method of generating realizations would not work.

6.3.2.2 Realizations Generated During the Preposterior Analysis (Method Used in Thesis)

In this method, all realizations are generated during the preposterior analysis. For each combination of sample outcome, the geostatistical parameters are updated and 100 realizations are produced. The ensemble of realizations used in the prior analysis is formed from the sum of the realizations generated during the preposterior analysis, weighted by the probability of the different sample combinations occurring. Therefore, the ensemble of realizations used in the prior and preposterior analysis are identical. The preposterior analysis is carried out in the following basic steps:

- 1) A pattern of n measurements is proposed.
- 2) The 2^n combinations of different sample outcomes S_j are calculated.
- 3) The mean is updated, based on sample outcome S_j .
- 4) A series of M aquitard realizations, R_{mlj} , are generated using the updated parameters and conditioned on S_j . (The subscript mlj on R refers to m^{th} realization which is conditioned on sample outcome S_j .)
- 5) For each realization, R_{mlj} , contaminant transport is modeled for each alternative, A_i , to determine if failure occurs for A_i . Failure times are calculated.
- 6) The failure time is then used to calculate the objective function, $Z(A_i, R_{mlj} | S_j)$, for each A_i , for all M realizations R_{mlj} .
- 7) The alternative, A_D' , with the highest expected objective function, over all M realizations is then selected.

$$E(Z(A_D)) = \frac{1}{M} \sum_{m=1}^M Z(A_D', R_{mlj} | S_j) \quad (6.7)$$

$Z(A_D', R_{mlj} | S_j)$ is the objective function of the posterior best design alternative for realization R_{mlj} , given S_j .

- 8) Steps 3 through 7 are repeated for each of the 2^n sample outcomes S_j .
- 9) The expected expected objective function of the best preposterior design is calculated by

$$E[E(Z(A_D'))] = \frac{1}{2^n} \sum_{j=1}^{2^n} \sum_{m=1}^M \frac{Z(A_D', R_{mlj} | S_j)}{M} P(S_j) \quad (6.8)$$

- 10) The prior expected objective function of each alternative is calculated by

$$E(Z(A_I)) = \sum_{j=1}^{2^n} \sum_{m=1}^M \frac{Z(A_I, R_{mlj} | S_j)}{M} P(S_j) \quad (6.9)$$

The alternative with the highest objective function is the prior best design, A_D .

- 11) The worth of the sampling pattern is calculated from

$$\text{Worth} = E[E(Z(A_D'))] - E(Z(A_D)) \quad (6.10)$$

The steps are identical to those presented in Section 6.3.2.1., except a new step 10 has been inserted.

This new step carries out the prior analysis using realizations generated during the preposterior analysis.

Since the ensemble of realizations used in the prior analysis and the preposterior analysis are the same,

the expected objective function for an alternative is identical for both the prior and the preposterior analysis. Therefore, using step 10

$$\begin{aligned}
 E(Z(A_L)) &= E(Z(A_L|S_W))P(S_W) + E(Z(A_L|S_{NW}))P(S_{NW}) \\
 &= (\$4.3550 \times 10^6)(0.05) + (\$4.7802 \times 10^6)(0.95) \\
 &= \$4.7590 \times 10^6
 \end{aligned} \tag{6.11}$$

and

$$\begin{aligned}
 E(Z(A_{NL})) &= E(Z(A_{NL}|S_W))P(S_W) + E(Z(A_{NL}|S_{NW}))P(S_{NW}) \\
 &= (\$3.5501 \times 10^6)(0.05) + (\$7.8024 \times 10^6)(0.95) \\
 &= \$7.5900 \times 10^6
 \end{aligned} \tag{6.12}$$

Therefore, the prior best alternative is to have no liner. Using the results shown Figure 6-5, the worth of data from the expected increase in maximum expected objective function is

$$\begin{aligned}
 W_1 &= E[E(Z(A_D'))] - E(Z(A_D)) \\
 &= [(\$4.3550 \times 10^6)(0.05) + (\$7.8024 \times 10^6)(0.95)] - \$7.5900 \times 10^6 \\
 &= \$40\,000
 \end{aligned} \tag{6.13}$$

The worth of the borehole from the expected decrease in the minimum expected regret is

$$\begin{aligned}
 W_2 &= E(\text{Reg}(A_D)) - E[E(\text{Reg}(A_D'))] \\
 &= \$2.4526 \times 10^5 - [(\$0)(0.05) + (\$2.1580 \times 10^5)(0.95)] \\
 &= \$40\,000
 \end{aligned} \tag{6.14}$$

The worth of the borehole by both the above methods is \$40 000.

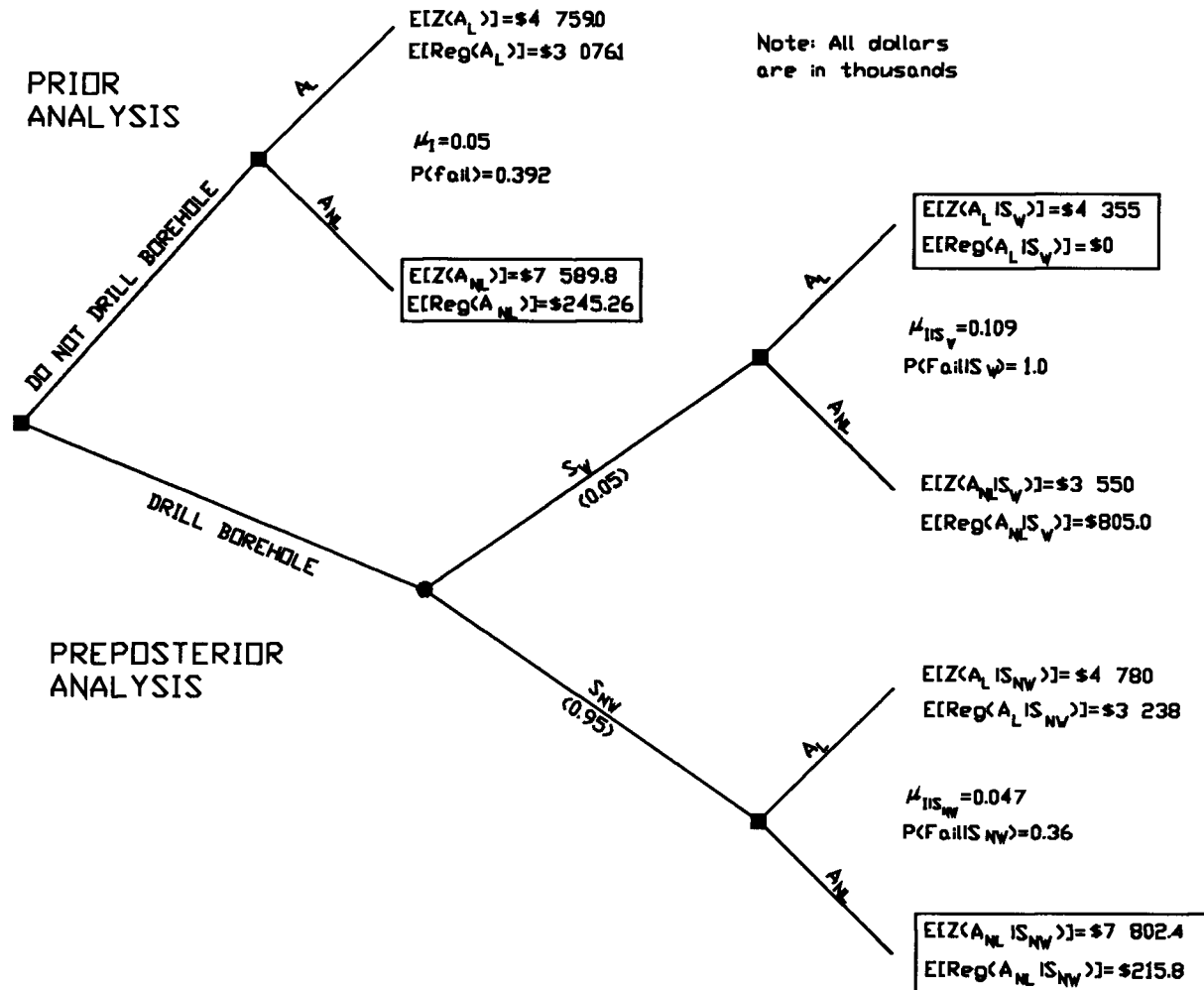


Figure 6-5: The preposterior analysis for example design for case where realizations are generated during preposterior analysis only.

One problem is that the total number of required realizations limits the number of sample locations. For example, if a minimum of 100 realizations is needed per sample outcome, then 3 200 realizations would be needed for a sampling pattern of five hard measurements. (Recall that there are 32 (ie. 2^5) possible combinations of sample outcomes for a pattern of five measurements.) The practical upper limit of the sampling pattern is six to seven boreholes. It may well be that phased site investigation programs often consider suites of this order of magnitude.

6.4 SENSITIVITY OF ESTIMATED WORTH OF SINGLE HARD MEASUREMENT TO NUMERICAL ARTIFACTS

There are many numerical parameters which are only artifacts of the methodology used in the framework. These parameters affect the estimated worth, W , of a proposed sample. The purpose of Section 6.4 is to study the sensitivity of W to these parameters and to determine if they could affect the decision of whether a sample is cost effective or not.

Numerical parameters are used in both the deterministic modeling of contaminant transport and the stochastic generation of the aquitards. Some numerical parameters used in the deterministic modeling of contaminant transport are

- 1) the density of the mesh used in the numerical model to solve for hydraulic head
- 2) the number of particles released at the contaminant source for particle tracking
- 3) the distance of vertical boundaries from the zone of interest
- 4) the absolute difference used to stop iterative head calculations (used in MODFLOW).

In this thesis, it is assumed that the correct values of the above parameters have been set by sensitivity analyses and that the deterministic transport of contamination is correctly modeled.

The remainder of this section is concerned with numerical parameters that affect the generation of the aquitards. These parameters are

- 1) the number of realizations generated per sample outcome
- 2) the starting seed used in the random number generator
- 3) the number of the first aquitard block generated
- 4) the number of blocks into which the aquitard is discretized.

The sensitivity of the worth of a single borehole to each of the above parameters will be discussed below.

The total effect of these numerical parameters on the estimated worth will be discussed last.

6.4.1 THE NUMBER OF REALIZATIONS GENERATED PER SAMPLE OUTCOME

In the example design, 100 aquitard realizations were used to estimate W . However, W is dependent upon the number of realizations used to estimate it. In the example presented here, as the number of realizations increases W decreases and becomes asymptotic after 50 realizations (Fig 6-6); however, there remains an irreducible fluctuation. Therefore, it is assumed that if enough realizations are generated W will be unbiased, but there will be a random error. The standard deviation of the random error, σ_w , is estimated to be \$830. This corresponds to a 2% fluctuation from the average W of \$44 200; therefore, for the example design, the random error will have a small effect on W .

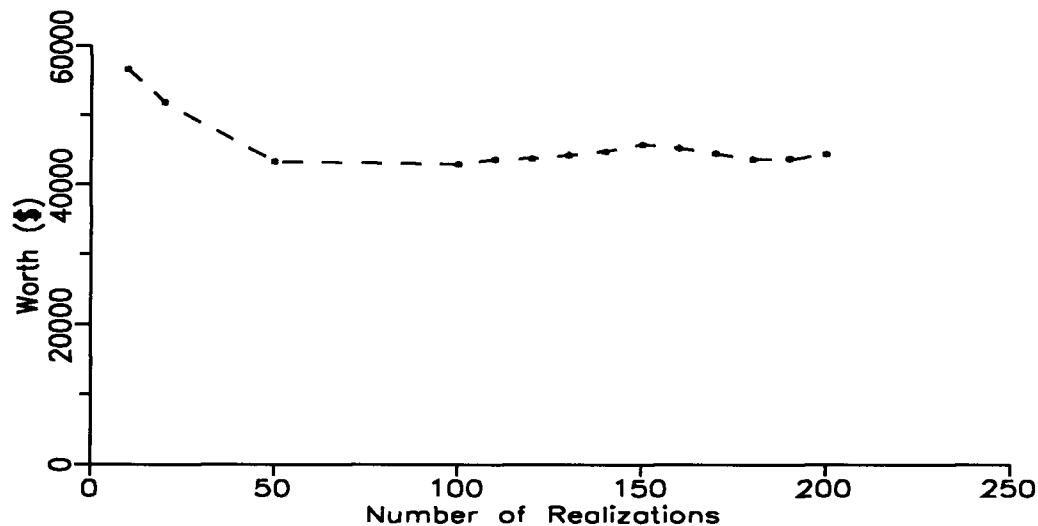


Figure 6-6: Sensitivity of the worth and median failure time to number of realizations per sample outcome.

6.4.2 STARTING SEED USED IN RANDOM NUMBER GENERATOR

Ideally the realizations generated by the SIS algorithm should be completely random. Unfortunately, they are not because they are dependent upon the $U(0,1)$ random number generator. The $U(0,1)$ random number generator generates pseudo-random, rather than truly random, sequences of numbers which are dependent upon a starting seed. The pseudo-random sequence changes for every different starting seed. The result of this incomplete randomness is that the ensemble of realizations generated with one starting seed will be different from an ensemble generated with another starting seed. Every different ensemble of realizations will yield a slightly different probability of failure and a different set of failure times, and hence, a different estimated worth for a sample.

As the starting seed increases, W moves randomly about a constant mean value (Fig 6-7). Therefore, as in the above case, varying the starting seed is assumed to create a random error, but will not bias W . The standard deviation in W , σ_w , is estimated to be \$1 440, which corresponds to a 3.5% fluctuation about the average W of \$41 500. Therefore, for this example the random error will again have a small effect on W .

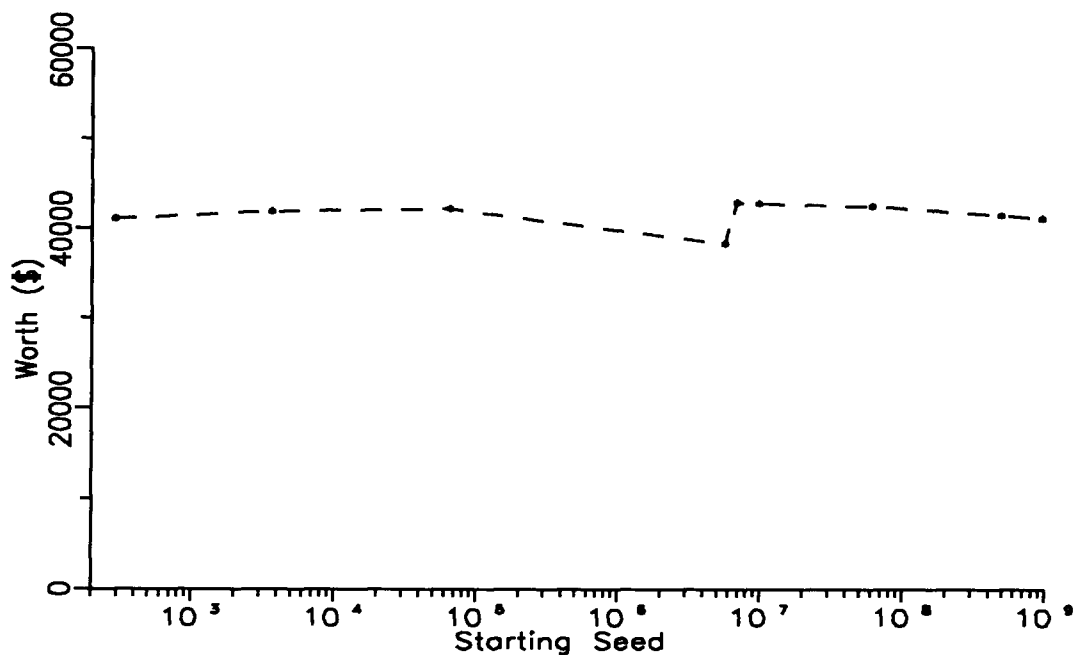


Figure 6-7: Sensitivity of the worth to the starting seed used in the random number generator.

6.4.3 NUMBER OF FIRST AQUITARD BLOCK GENERATED

The realizations are also dependent upon a congruential random generator used to determine the order in which the aquitard blocks in a realization are generated. The order is dependent upon the number of the first block generated, which is supplied by the user. A different order, and consequently a different set of realizations, will result for each different starting block number.

W again varies randomly about a constant mean as the first aquitard block generated changes (Fig 6-8). Therefore, the starting block number will not bias W, but will create a random error with standard deviation equal to \$2 080. This corresponds to a 4.4% fluctuation about the average W of \$44 500.

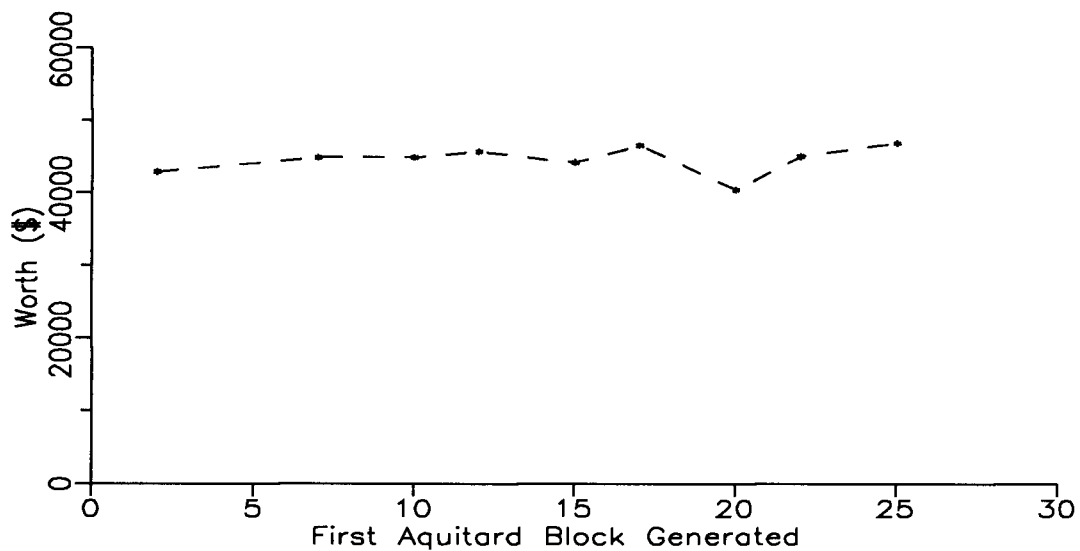


Figure 6-8: Sensitivity of the worth to first aquitard block in starting path.

6.4.4 NUMBER OF BLOCKS INTO WHICH AQUITARD IS DISCRETIZED

W is dependent upon the number of blocks into which the aquitard is discretized. Fortunately, W varies randomly around a mean of \$42 760 (Fig. 6-9). Therefore, at least for this example, W is unbiased by the

number of aquitard blocks, but there is a random error with a standard deviation of \$2 630, which is 6% of the average worth.

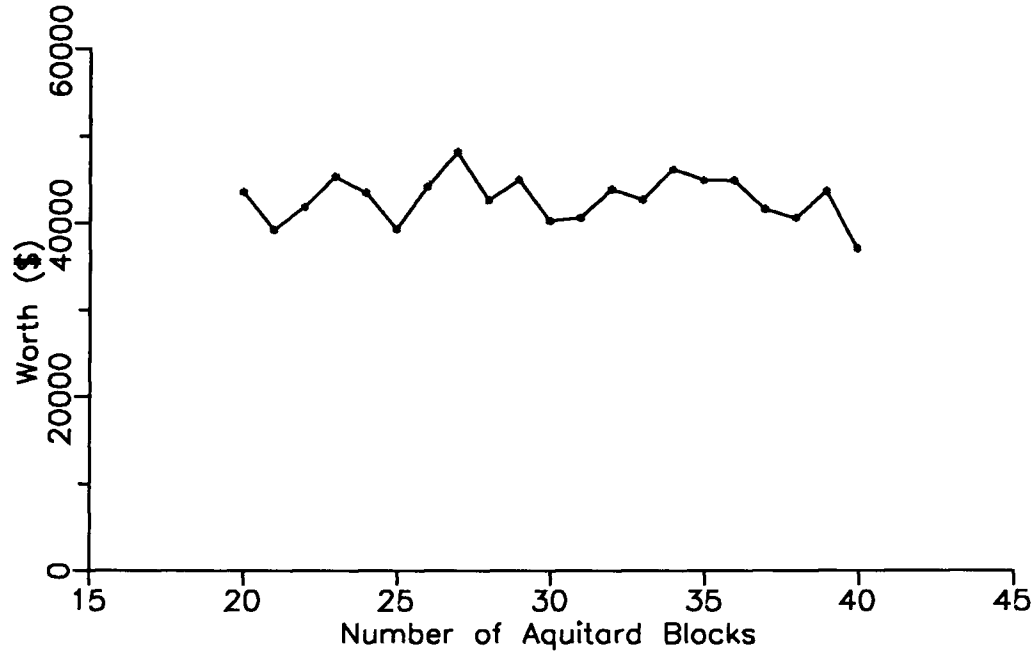


Figure 6-9: Sensitivity of W to the number of blocks that the aquitard is discretized into.

6.4.5 COMBINED AFFECT ON RELIABILITY OF DATA WORTH

For the example design case studied here, if the numerical parameters are set correctly, W will be unbiased, but each will contribute to a random error in it. Assuming that the errors caused by any one parameter are independent of the others and normally distributed, then the standard deviation of the total random error, σ_w , in W can be estimated by the central limit theorem. Therefore,

$$\sigma_w^2 = \sum_{j=1}^n \sigma_{w_j}^2 \quad (6.15)$$

where $\sigma_{w_j}^2$ is the variance in W caused by parameter j. For the example design presented here,

$$\begin{aligned}
\sigma_w^2 &= (\$830)^2 + (\$1\,440)^2 + (\$2\,080)^2 + (\$2\,060)^2 \\
&= (\$3\,400)^2
\end{aligned}$$

The σ_w is only \$3 400 compared to an overall average W which is in excess of \$40 000. Therefore, for the example presented here the total random error in W is small compared to the average W . The magnitude of the random error may be site dependent; therefore, it should be estimated for each site. In addition, possible bias in W due to numerical artifacts should be checked for each site.

6.5 PREPOSTERIOR ANALYSIS OF A SOFT, AREAL SURVEY

Section 6.5 discusses how the framework is used to evaluate the worth of a soft, geophysical survey which covers a large area. The survey must cover the entire area where potential windows could cause not only failure, but a failure which would alter the prior best design alternative. These latter type of windows are denoted as W_{fd} . Some windows may allow failure (i.e. contamination to reach the lower aquifer), but the cost of the failure may not be high enough to change the prior best design alternative. As will be shown in Chapter 8, this area is not fixed, but is a function of other factors such as the cost of failure.

Since the survey covers the entire area where W_{fd} may occur, it is assumed that the survey will sample any such window, given that one exists, with some probability, $P(S_{W_{fd}} | W_{fd})$. A false outcome may also be possible. Its probability is denoted by $P(S_{W_{fd}} | \neg W_{fd})$. These two probabilities represent the likelihood functions (or the precision p_1 and p_2) of the survey. They must be estimated a priori for the data worth analysis to be carried out; however, this will not be a simple task for two reasons. The first is that geophysicists generally do not quantify the precision, or quality, of geophysical surveys in these terms (Cross, 1992). Therefore, there are no readily available estimates. Secondly, they depend on may

factors which may be poorly understood, such as stratigraphy and material properties of geological materials.

The above assumption allows the multivariate Bayesian updating problem described previously for hard, point measurements to break down to a univariate case. The worth of the survey can then be estimated using the methodology for univariate random variables outlined in Chapter 2. The following information is needed to carry out the analysis: the prior probability of failure, the updated probability of failure for each sample outcome, the expected value of the objective functions for the alternatives for both failure and no failure, and the likelihood functions of the measurement. As previously mentioned, the likelihood functions of the survey must be estimated. All the remaining information is calculated or derived from the prior analysis, which is carried out by the framework.

The prior analysis directly evaluates the prior probability of failure and the expected value of the objective functions for the alternatives for both failure and no failure. Note that the expected values of the objective functions of the design alternatives now have a different form from that used for the hard, point measurements. Instead of simply calculating the total expected value of an alternative, such as $E(Z(A_C))$, the expected value is calculated twice for each alternative, once for the realizations that fail and once for the realizations that don't fail, i.e. $E(Z(A_C)|\text{Failure})$ and $E(Z(A_C)|\text{No Failure})$. Recall, from Section 6.3.2 that the expected values of the objective functions for the different alternatives, given failure or no failure, remain unchanged by sampling.

The prior probability of failure is updated by Bayes' equation for the univariate case, using the likelihood functions. The probability of sampling different outcomes is calculated using the likelihood functions and the prior probability of failure. An example analysis is carried out for the case study in Section 8.5.

Note, because of the uncertainty in the estimated likelihood functions, there will be uncertainty in the estimated worth of a geophysical survey. Therefore, instead of concentrating on the actual worth of a

geophysical survey, the break even point, or minimum precision for the survey to be cost effective, will be estimated. The minimum precision of the survey should be much easier to estimate than the actual precision of the survey.

6.6 MODIFICATION TO FRAMEWORK TO HANDLE DATA WORTH PROBLEMS IN OTHER DISCIPLINES

The framework forms a foundation for addressing data worth questions in both groundwater and other disciplines, that deal with heterogeneous geological environments. For example, if one were interested in determining the patterns of hydraulic conductivity within an aquifer, the framework could be easily modified to deal with this situation. Hydraulic conductivity is generally assumed to behave as a multivariate lognormal distribution. The framework could be modified to handle it by replacing the SIS algorithm with a turning bands algorithm. Flow or transport could still be simulated using the numerical model.

It could also be modified for use with exploration programs used in petroleum reservoir engineering. The major factor in controlling flow in a petroleum reservoir is often patterns of sand/shale continuity. This factor is particularly true in enhanced oil recovery programs. The SIS algorithm could still be used to simulate the reservoir geology. The major modification would be replacing the numerical contaminant transport model with a numerical multiphase flow model.

One could address a question such as: Will the increased recovery and information gained from a new well justify the cost of installing the well? The framework could be particularly applicable to petroleum engineering because the economic consequences of decisions are high. An oil well can cost \$10's millions, but increased recovery could be worth \$100's millions. In addition, the economic consequences are more straightforward to quantify than those in groundwater contamination because one does not have

to deal with factors which are hard to put a monetary value on, such as the loss of a river for recreational use.

It would be straight forward to modify the framework to address data worth questions in mine development. For this case, only an algorithm for simulating ore bodies would be required. Again, if grade/tonnage of the ore body behaved as lognormal random variable, the SIS algorithm could be replaced by a turning bands algorithm. One could investigate whether one should spend (a) \$100 000 on diamond drill holes, (b) more than a \$1 million on building a shaft and collecting a large bulk sample, (c) nothing and build the mine, or (d) nothing and abandon the site. Mining could be a very appropriate area to adopt the framework for three reasons. The first is that potential mine sites often have much data available. Secondly, geostatistics has been employed for a number of years to many types of mineral deposits; therefore, the geostatistical nature of ore bodies is better understood than that of geological stratigraphy. Finally, there is a need because many poor decisions have been made in mine development. Often \$10's of million have been spent developing a mine, only to find that the mine is uneconomic.

6.7 SUMMARY OF CHAPTER 6

Chapter 6 outlines how the framework evaluates the worth of a sampling program using a design example which involves two dimensional contaminant transport. The framework can only directly evaluate the worth of hard, point measurements. Soft, point measurements cannot be handled. However, the framework can be used to estimate the worth of a soft, geophysical survey which covers the entire area where windows can cause a failure which alters the prior best design alternative.

There are two methods by which realizations might be generated by the SIS algorithm for the framework to estimate W . In the first method, realizations are generated in both the prior and preposterior analysis. This method was rejected because noise in the SIS algorithm causes the data worth calculations to break

down. In the second method, realizations are generated during the preposterior analysis and are "reused" in the prior analysis. This method leads to correct results and was selected for use in this thesis.

The estimated worth of a hard measurement is sensitive to numerical artifacts in the SIS algorithm. However, for the example presented here, this sensitivity is very small compared to average value of the estimated worth.

The framework could be modified to handle other types of data worth problems in both hydrogeology and other disciplines.

6.8 NOTATION

A_D	prior best design alternative
A_D'	posterior best design alternative
A_L	liner alternative
A_{NL}	no liner alternative
B_e	barometric efficiency
h	hydraulic head
K_x	hydraulic conductivity in x direction
K_y	hydraulic conductivity in y direction
m_I	estimate of mean of $I(x)$
NW_{fd}	no window exists which causes failure that changes prior best design, A_D
P_a	air pressure
p_1	probability of sampling a window, given that one exists
P_2	probability of sampling a window, given that one does not exist
$Reg(A_j)$	regret of alternative A_j

R_{mlj}	m^{th} aquitard realization which is condition on sample outcome S_j
S_j	j^{th} sample outcome
W	worth of data
W_{fd}	window exists which causes failure and changes prior best design, A_D
W_1	worth of data from the expected increase in the maximum objective function
W_2	worth of data from the expected reduction in minimum expected regret
Z	objective function
γ	specific weight of water
μ_I	mean of indicator random variable $I(x)$
λ_I	correlation length of indicator random variable $I(x)$
σ_w^2	variance of W
$\sigma_{w_j}^2$	variance of W caused by parameter j

CHAPTER 7: GENERIC DESIGN CASE: A SENSITIVITY ANALYSIS OF DATA WORTH

7.1 INTRODUCTION

Chapter 7 presents a sensitivity study of the different factors affecting the worth, W , of a single, point, hard measurement. The factors include economic, hydrogeological, and geostatistical parameters needed to carry out the data worth analysis, as well as the presence, or absence, of existing data.

Economic parameters include the discount rate, known benefits, known costs and cost of failure for all alternatives. The hydrogeological parameters include the three-dimensional geometry of the hydrostratigraphic units, the distribution of hydraulic conductivity and porosity throughout each unit, and the hydraulic boundary conditions. The geostatistical parameters include the prior estimate of the mean, m_I , the correlation length, λ_I , and the confidence in m_I .

The major purpose of this study is to present an analysis of how and why different factors can affect W . The secondary purpose is to show how sensitive W is to errors in parameter estimates. The effect of this sensitivity on the decision of taking a measurement will be discussed briefly. A measurement will only be taken if its estimated worth is greater than its cost. However, this concept will be ignored until Chapter 8. The decision of whether a measurement should be taken is covered in detail in Chapter 8 using the case history.

W is quantified in this Chapter in terms of method 3 because it is easier to visualize how different factors affect W . Method 3 was presented in Section 2.4.2.3. Recall from equation (2.44) that W was quantified by:

$$W = E[E(Z(A_D'|S)) - E(Z(A_D|S))] \quad (7.1)$$

where,

- A_D is the prior best design
- A_D' is the posterior best design
- $Z(A_D|S)$ is the objective function of A_D , but evaluated with additional sample information S
- $E(Z(A_D))$ is the expected value of $Z(A_D)$.

For the case of two sample outcomes, S_W and S_{NW} , the above equation can be rearranged to form:

$$W = \{E[Z(A_D'|S_W)] - E[Z(A_D|S_W)]\}P(S_W) + \{E[Z(A_D'|S_{NW})] - E[Z(A_D|S_{NW})]\}P(S_{NW}) \quad (7.2)$$

The first set of terms on the right hand side of the above equation represents the contribution of S_W to W .

It is the product between the probability of sampling the window, $P(S_W)$, and the difference between $E[Z(A_D'|S_W)]$ and $E[Z(A_D|S_W)]$. Similarly, the second term on the right hand side represents the contribution of S_{NW} to W .

It is important to note that conclusions drawn in this Chapter may not be extrapolated to every design problem. Parameters which are numerical artifacts of the methodology have already been discussed in Chapter 6. The sensitivity study will be carried out using the two contamination scenarios presented below.

7.2 TWO CONTAMINATION SCENARIOS

7.2.1 SCENARIO NUMBER 1

Scenario 1 is a layered system consisting of an unconfined upper aquifer, an impermeable aquitard and a lower aquifer (Fig. 7-1 and 7-2). Groundwater contamination has been discovered in the unconfined aquifer. A municipal water supply well is located in the lower aquifer 400 m down gradient from the contamination. The well is pumping at a rate of $5 \times 10^{-3} \text{ m}^3/\text{s}$ (79 US gal/min). The clay aquitard is known to exist at the water supply well, but its presence is uncertain elsewhere.

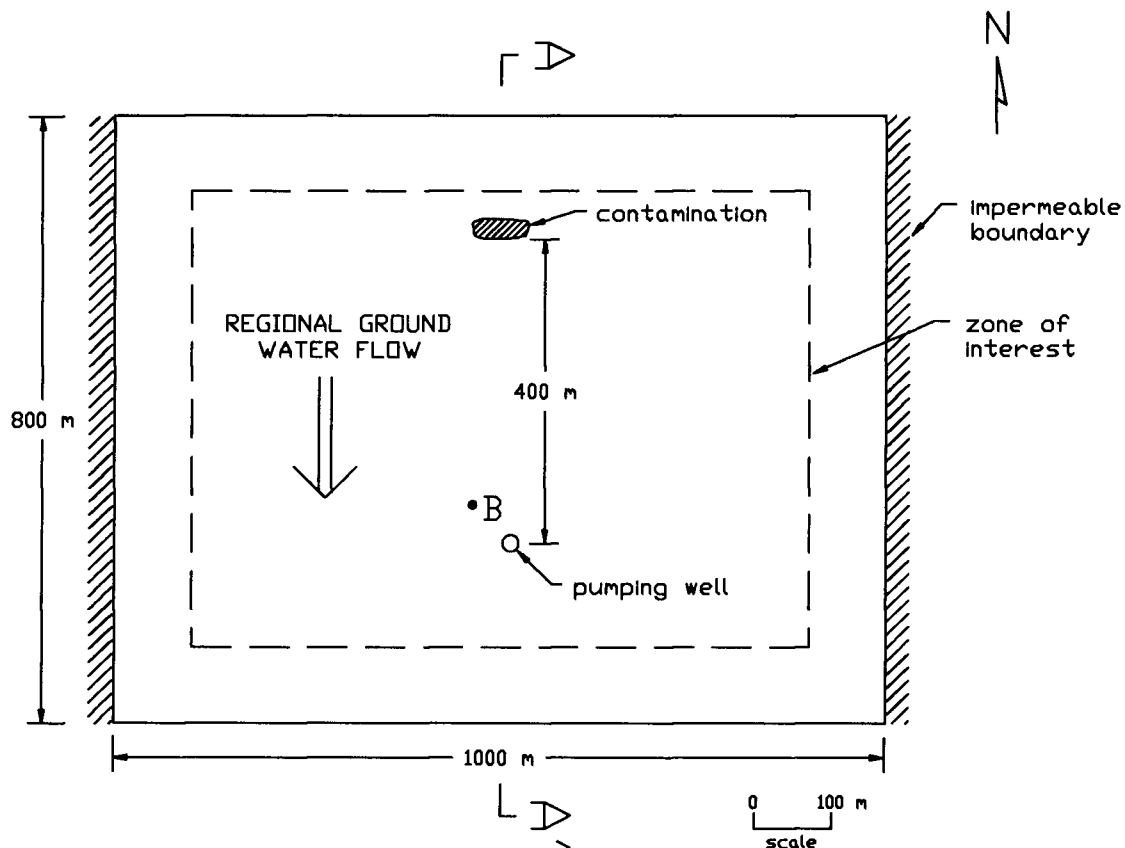


Figure 7-1: Plan view of contaminated aquifer system.

If the contamination reaches the lower aquifer, then the municipal water supply well will be lost and an expensive remediation program will be necessary to protect further water supply wells. Failure is defined here as contamination reaching any part of the lower aquifer. The cost of failure is assumed to be \$40 million. A decision must be made whether to contain the contamination, A_C , with pumping wells, or to provide no containment, A_{NC} , and hope for the best. The containment will be long-term, but its net

present cost is estimated to be \$4 million. It is assumed to be 100% effective. No benefits are associated with either alternative and there are no known costs associated with A_{NC} . The costs and benefits for the alternatives are summarized in Table 7-1. A discount rate of 10% is used in the analysis.

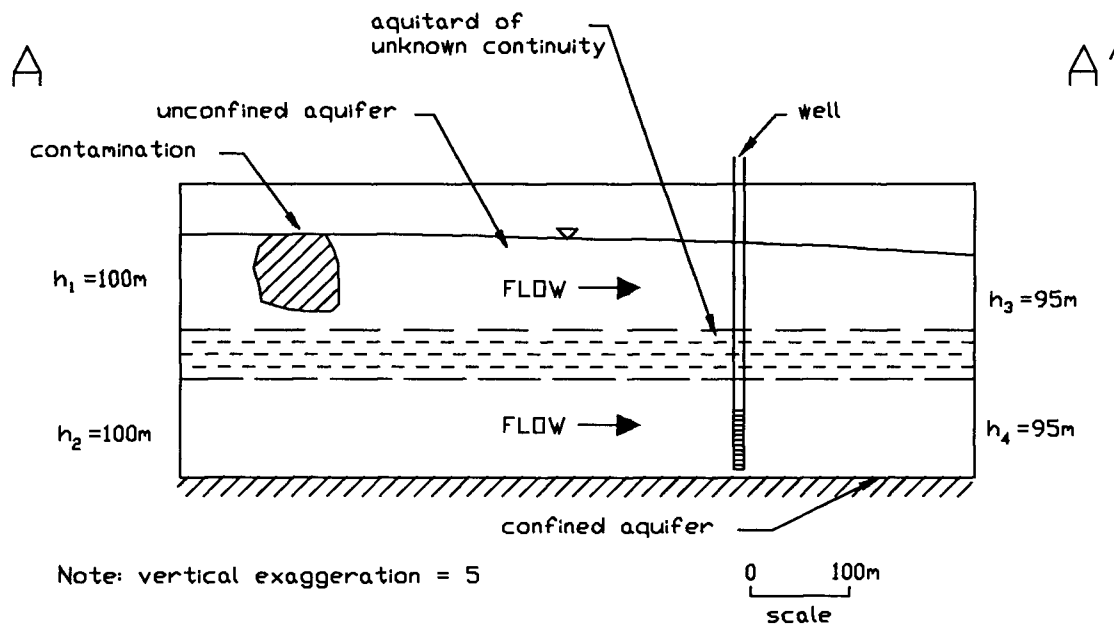


Figure 7-2: Cross section through contaminated aquifer system.

Alternative	Known Benefits (millions \$)	Known Costs (millions \$)	Cost of Failure (millions \$)
A_C	0	4.	0
A_{NC}	0	0.	40.

Table 7-1: Costs and benefits for the containment and no containment alternatives.

The boundary conditions are shown in the cross section through the aquifer/aquitard system (Fig. 7-2) and the hydrogeological parameters are summarized in Table 7-2. The correlation length, λ_I and estimated mean, m_I , are 50 m and 0.03, respectively. The confidence in the prior estimate of m_I is equivalent to 15 independent hard data. The boundary conditions are 100 m away from the zone of interest. Recall, that windows are only generated in the zone of interest. Note that the downward vertical gradient across the aquitard is local in nature because it is due entirely to the pumping well.

Layer	Parameter	Value
Unconfined Aquifer	K_h	2×10^{-5} m/s
	K_v	2×10^{-5} m/s
	Thickness	20. m
	porosity	0.3
Aquitard	K_v	10^{-10} m/s
	Thickness	10. m
	porosity	0.4
Confined Aquifer	K_h	8×10^{-5} m/s
	Thickness	20. m
	porosity	0.3

Table 7-2: Hydrogeological parameters used in Scenario 1.

Two layers of nodes were used in the upper aquifer while one layer of nodes was used in the lower confined aquifer. The clay aquitard was accounted for using a leakage layer. The node spacing in both horizontal directions is 25 m. The contamination source is represented by a series of particles released along an east/west horizontal line in the middle of the upper aquifer. Numerical parameters used in the stochastic simulations are summarized in Table 7-3.

The value of W is evaluated for a single borehole taken at point B, 50 m north and 25 m west of the municipal water supply well (Fig. 7-1).

From the prior analysis, best design alternative is no containment, A_{NC} . Its expected objective function is $E[Z(A_{NC})] = -\$2.45$ million. The expected objective function for the containment alternative, $E[Z(A_C)] = -\$4$ million. W is estimated to be \$25 700. The prior probability of failure is 0.38 and the median failure time is 21.0 years.

Parameter	Value
number of realizations per sam. outcome	100
first aquitard block generated	39
# of aquitard blocks	768
starting seed	687453

Table 7-3: Numerical parameters used in Scenario 1.

7.2.2 CONTAMINATION SCENARIO 2:

The second Scenario is identical to the first, except for the following: no conditioning data are present, the well is absent, m_1 is estimated to be 0.01, and the boundary condition h_4 on the south side of the lower aquifer has been reduced from 95 m to 90 m. Therefore, the vertical gradient is forced entirely by the lower boundary condition, rather than the pumping well. The definition of failure is still contamination of any part of the lower aquifer.

From the prior analysis, $E[Z(A_C)] = -\$4$ million and $E[Z(A_{NC})] = -\$3.01$ million. Therefore, the prior best design is again to have A_{NC} . The value of W for the same borehole as in the first scenario is estimated to be \$55 600. The prior probability of failure is 0.28 and the median failure time is 17.4 years.

7.3. SENSITIVITY TO ECONOMIC PARAMETERS

The sensitivity of W to the known cost of containment, the cost of failure, and the discount rate are studied below for scenario 1.

7.3.1 KNOWN COST OF CONTAINMENT (SCENARIO 1)

W can be very sensitive to the known cost of containment, C_c (Fig. 7-3). Attention is drawn to three points D, E, and F in Figure 7-3 where C_c equals \$2.39, \$2.45, and \$5.27 million, respectively. W is zero for C_c below point D, but rises rapidly to a maximum of \$60 000 at point E. W then more gradually drops off to \$0 at point F where $C_c = \$5.27$ million.

The significance of the three containment costs at D, E, and F can be visualized in Figure 7-4. Here, the expected prior objective functions of the two alternatives are shown in solid lines. The expected

expected objective function of the posterior best design, $E[E(Z(A_D'))]$, is shown in a dashed line. Recall, that W is positive only if $E[E(Z(A_D'))]$ is greater than the expected objective function of the prior best design, $E[Z(A_D)]$. W increases with this difference.

The containment cost at point E represents where $E(Z(A_C)) = E(Z(A_{NC}))$ (Fig. 7-4). Below E, A_C is the best alternative, while above E, A_{NC} is the best alternative. Point E also marks an instability in the data worth analysis. Any data worth analysis carried out near it can be unreliable. There will always be uncertainty in most parameters, such as C_c . Therefore, if C_c is estimated to be close to point E, it is possible that the true value of W could be dramatically different from its calculated value.

This instability in W , at the point where $E(Z(A_C)) = E(Z(A_{NC}))$, will be seen for different parameters throughout this sensitivity study.

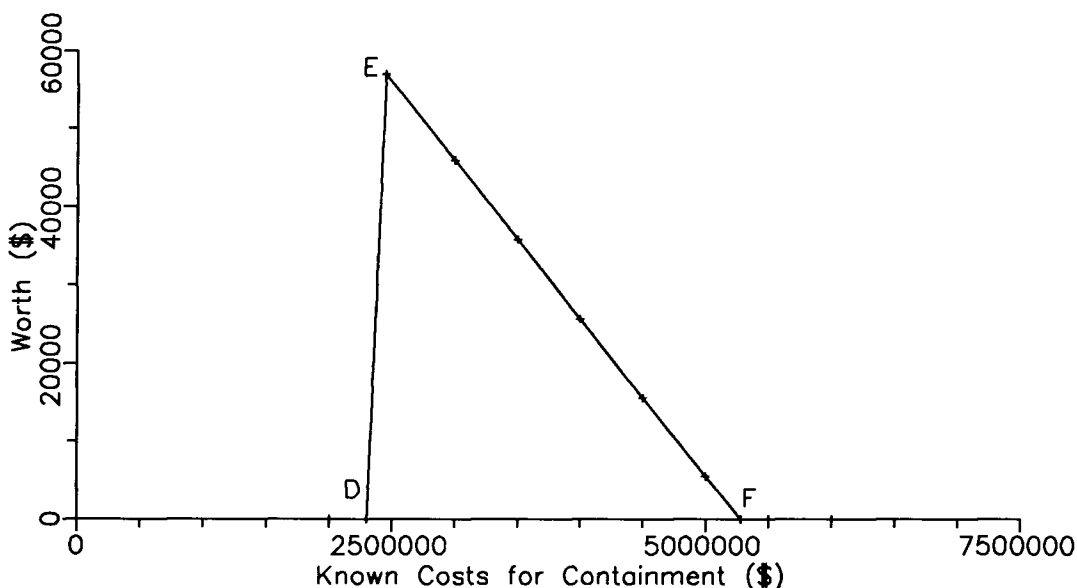


Figure 7-3: Sensitivity of W to the known cost of containment.

For a positive W , the true cost of containment must lie between \$2.45 million (E) and \$5.27 million (F).

It is informative to graphically examine the effect of each sample outcome on the prior and posterior objective functions of the alternatives, and hence on W . The effect of sampling a window, S_W , is shown in Figure 7-5. Recall that S_W determines that failure will occur with certainty. The prior and posterior objective functions are again shown in solid and dashed lines, respectively. Note that $Z(A_C)$ is constant, therefore, $E(Z(A_C)) = E(Z(A_C|S_W))$. For C_c between E and F , S_W results in a change in decision. A_D changes from A_{NC} to A_C when the certainty of failure is determined. Sampling a window stops a poor design from being carried out. For C_c greater than F and less than E , S_W has no effect on A_D .

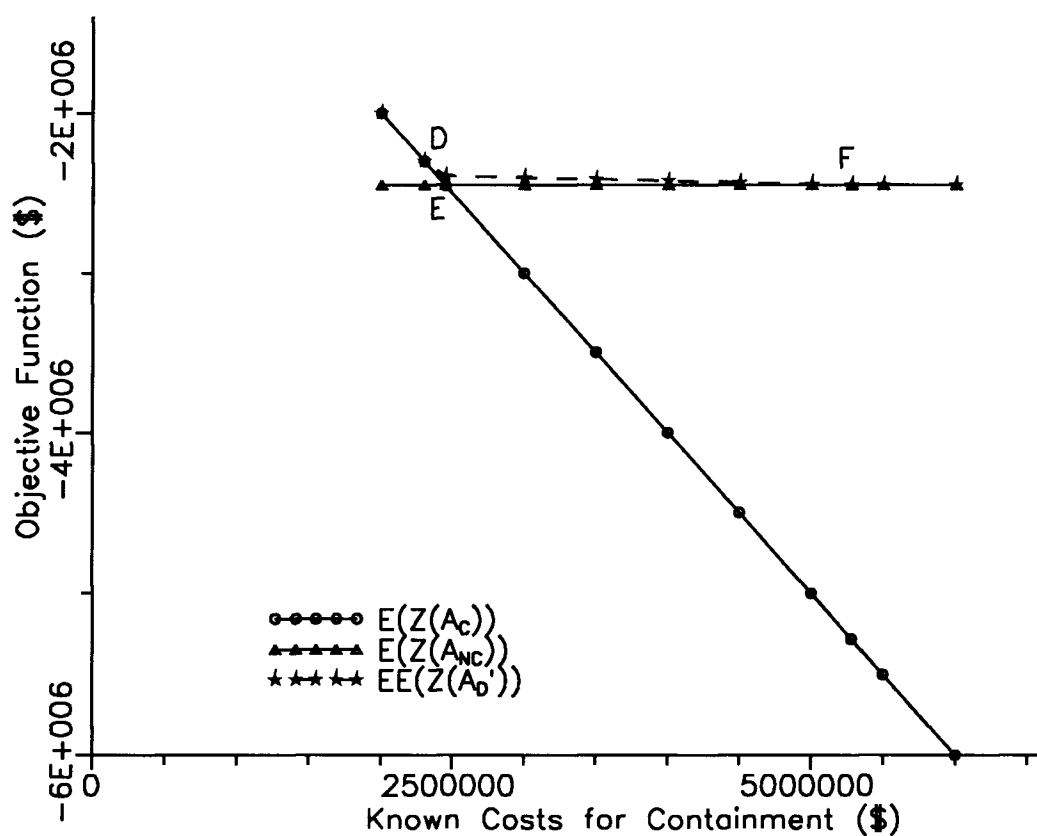


Figure 7-4: The expected prior objective function of the two alternatives and the expected expected objective function of the posterior best design alternative versus known cost of containment.

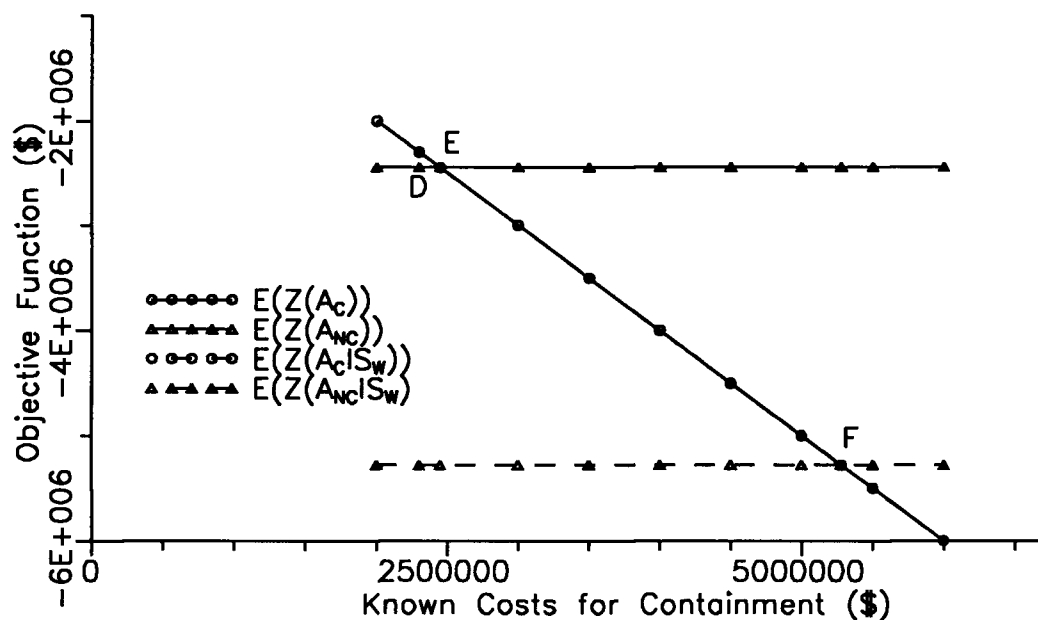


Figure 7-5: The effect of sampling a window on the objective functions of the different alternatives.

Similarly in Figure 7-6, S_{NW} , only results in a change in the prior design alternative for C_c between D and E. For C_c greater than E and less than D, S_{NW} has no effect on the prior design decision.

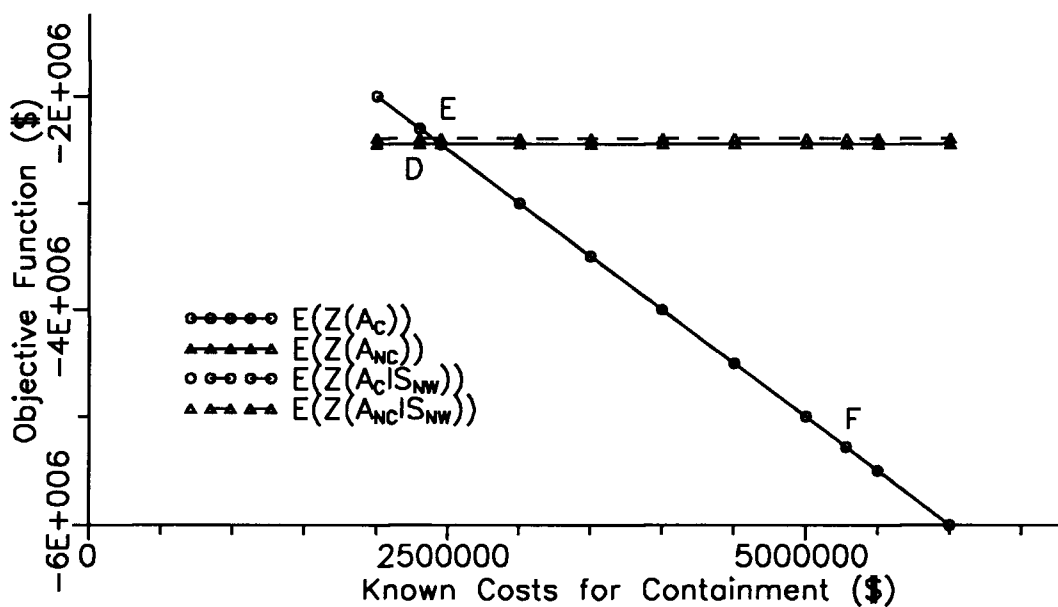


Figure 7-6: The effect of sampling no window on the objective functions of the different alternatives.

Consequently, for C_c below D and above F, neither S_W or S_{NW} affects A_D and $W = \$0$. $W > \$0$ for C_c between D and F. For C_c between D and E, only S_{NW} affects A_D , while for C_c between E and F, only S_W affects A_D . Recall from Chapter 2, that a sample only has worth if its outcome results in a change in A_D .

7.3.2 COST OF FAILURE (SCENARIO 1)

The value of W exhibits a similar sensitivity to the cost of failure, C_f (Fig 7-7). W is very unstable at point E ($C_f = \$67$ million) where A_D changes ($E(Z(A_C)) = E(Z(A_{NC}))$) (Fig. 7-8). For C_f between E and F ($C_f = \$30.4$ million) W drops from a maximum to zero with less than a 3% change in C_f . For C_f between D ($C_f = \$30.4$ million) and E, W rises more slowly. For positive W , $\$30.4 \text{ million} < C_f < \65.4 million .

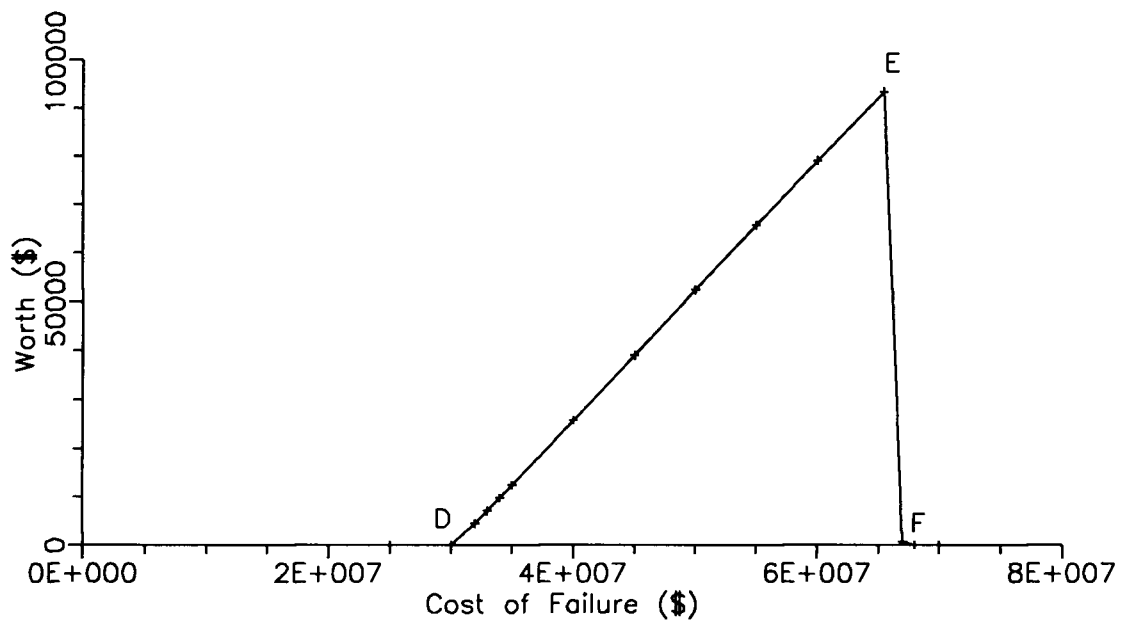


Figure 7-7: W versus cost of failure.

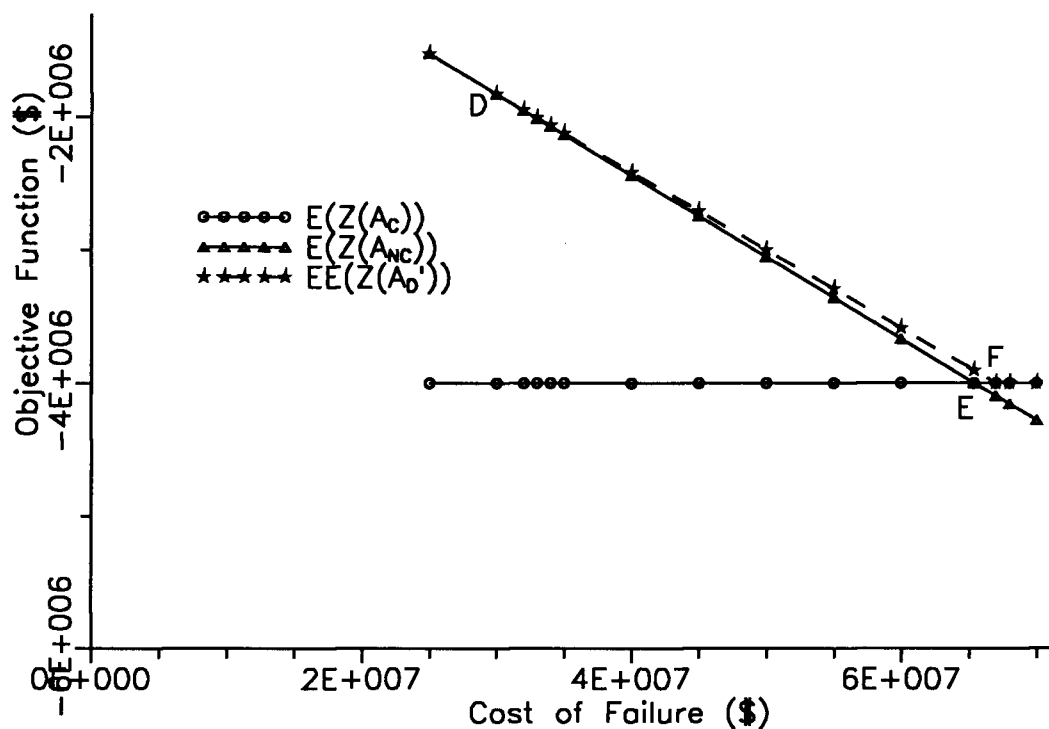


Figure 7-8: The expected prior objective function of the two alternatives and the expected expected objective function of the posterior best design alternative versus cost of failure.

7.3.3 DISCOUNT RATE (SCENARIO 1)

The value of W is very sensitive to the discount rate (Fig 7-9). It rises from \$0 at $i=0.066$ (D) to \$110 000 at $i=0.0675$ (E). It then gradually drops to zero at $i=0.114$. The maximum W at $i=0.0675$ (E) again represents an instability point for W where A_D changes (Fig. 7-10). For a positive W , the discount rate must lie between 0.0675 (E) and 0.114 (F).

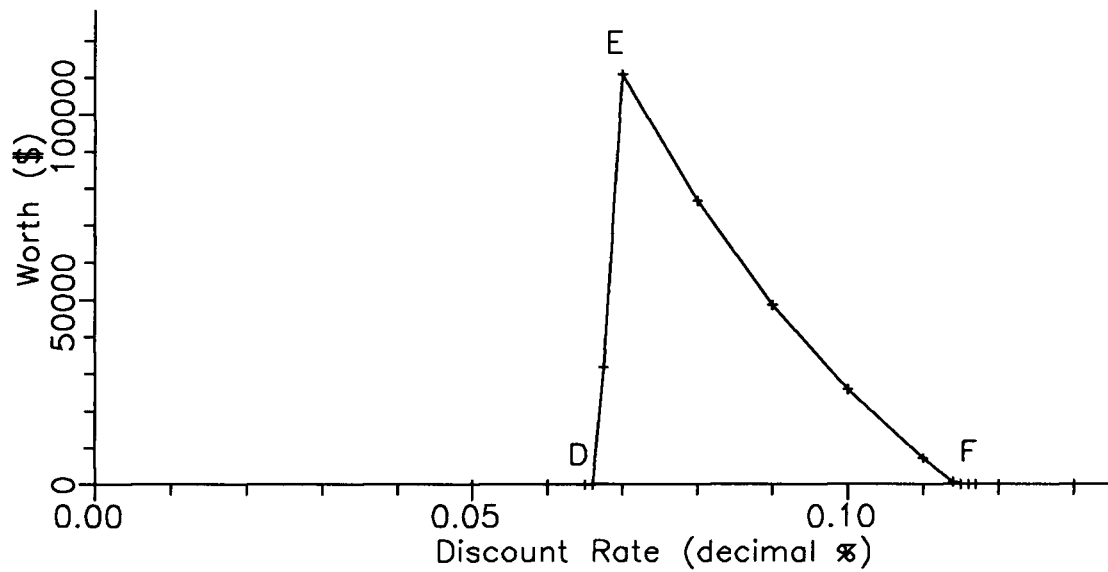


Figure 7-9: W versus discount rate.

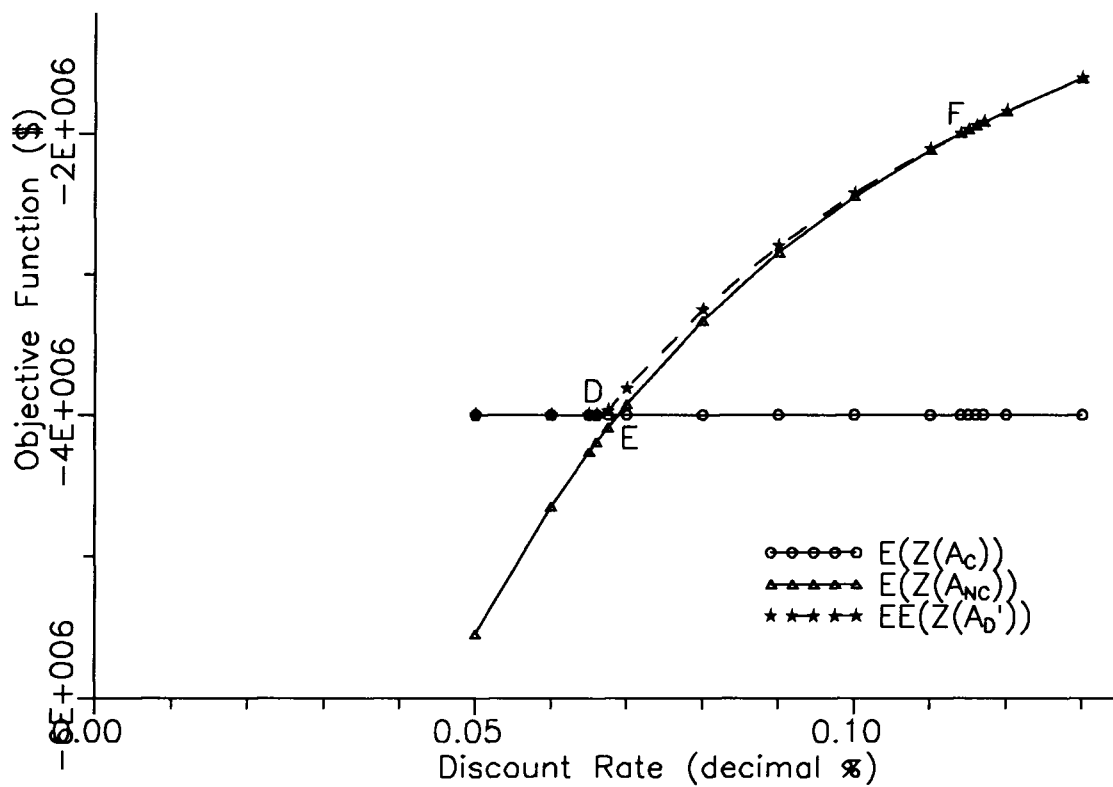


Figure 7-10: The expected prior objective function of the two alternatives and the expected expected objective function of the posterior best design alternative versus discount rate.

The change in W with discount rate demonstrates an important point. Different parties may view

discount rates differently, and consequently can get large differences in W . For example, an owner operator of a land fill will be interested in making a profit. Therefore, future cost could be discounted back into present day dollars by some acceptable market discount rate. At a discount rate of 0.1, W is \$25 700. However, for an environmentalist, a future failure is just as important as present day failure. Therefore, an environmentalist would be more inclined to use a discount rate of 0 and would evaluate $W = \$0$. For a discount rate of 0, the best prior alternative is A_C under all circumstances.

7.4 SENSITIVITY TO HYDROGEOLOGICAL PARAMETERS

The sensitivity of W to the vertical hydraulic conductivity (K_v) of the clay aquitard, the horizontal hydraulic conductivity (K_h) of the lower aquifer, and the fixed boundary condition (h_4) are studied using Scenario 2.

7.4.1 VERTICAL HYDRAULIC CONDUCTIVITY OF AQUITARD (SCENARIO 2)

The value of K_v is quantified here in terms of a leakage coefficient, L_c , which is defined as K divided by the aquitard thickness.

At low L_c , W is relatively constant at over \$55 000 (Fig. 7-11). However, W drops to \$0 as L_c increases above 10^{-8} 1/s. As the aquitard becomes more permeable at high L_c , contamination can penetrate the aquitard, regardless of the presence or absence of windows. This is shown by the prior probability of failure climbing to 1 at high L_c (Fig. 7-11). When the probability of failure is 1, it is certain that the best design is A_C and W is zero.

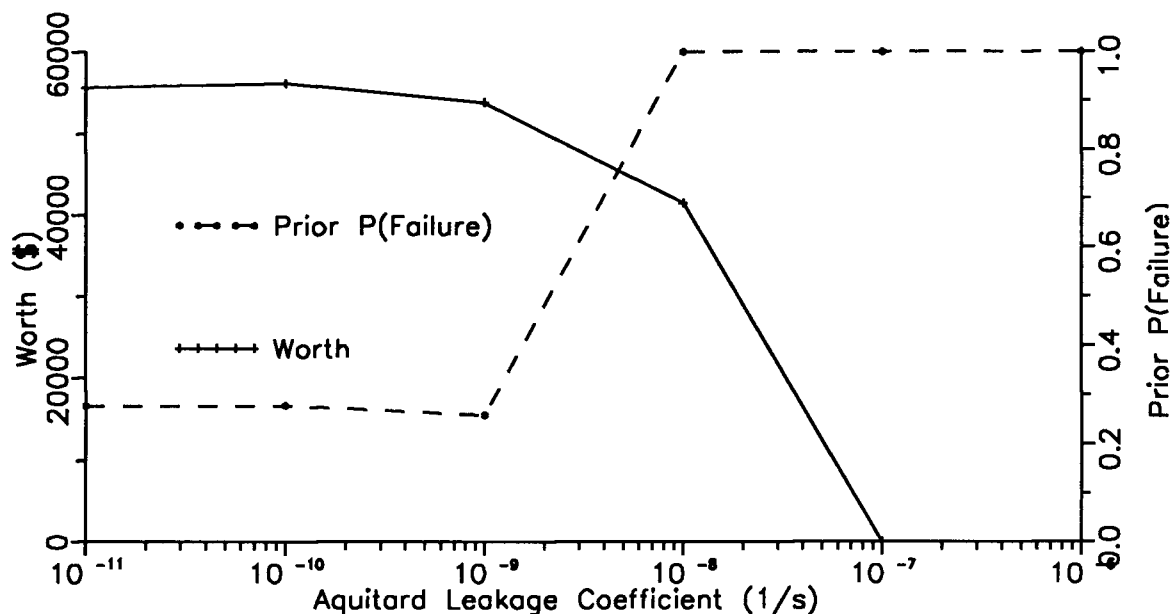


Figure 7-11: The sensitivity of W and prior probability of failure to aquitard hydraulic conductivity for Scenario 2.

Therefore, for this case it is important to know if L_c , or K_v , is above or below a threshold value.

Knowing its actual value is less important.

7.4.2 HORIZONTAL HYDRAULIC CONDUCTIVITY OF LOWER AQUIFER (SCENARIO 2)

The horizontal hydraulic conductivity of the lower aquifer has been quantified in terms of the transmissivity, T , which is equal to the product of the hydraulic conductivity times the aquifer thickness. At high T , W is relatively insensitive to changes in T (Fig 7-12). As T decreases, W starts to decrease more rapidly and then becomes zero at $T = 10^{-5} \text{ (m}^2/\text{s)}$. The reason for this decrease lies in the interaction between the downward vertical gradient across the aquitard and the transmissivity of the lower aquifer. At very low T , the lower aquifer can transmit little water and there is little leakage, and hence little vertical gradient across the aquitard. With little vertical gradient across the aquitard, there is little tendency for contamination to be pulled through it to the lower aquifer and for failure to occur, even if a window is present. Since failure cannot occur it is certain that the best design is A_{NC} and W is zero.

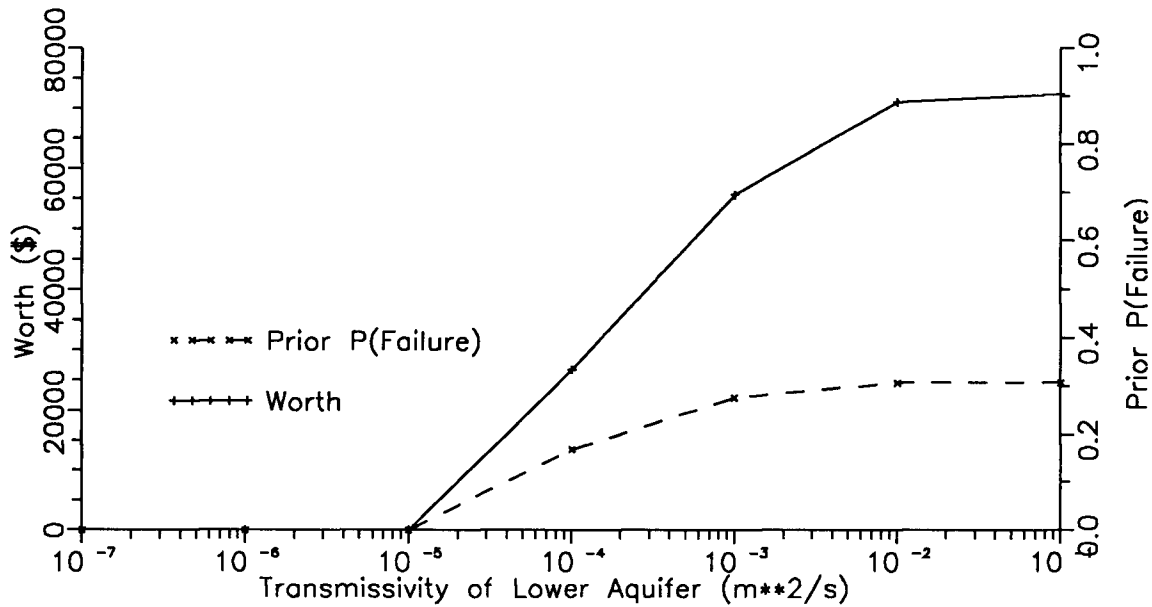


Figure 7-12: The sensitivity of W and prior probability of failure to the transmissivity of the lower aquifer.

However, as T increases, a critical point is reached ($T = 10^{-4} \text{ m}^2/\text{s}$) when a significant vertical gradient across the aquitard is created and significant leakage can occur through a window. The prior probability of failure increases from 0 to 0.168 and the prior design alternative of A_{NC} could now be in error. W then increases from \$0 to \$26 700. However, as T increases further, it has little effect on the prior probability of failure. At this point, the probability of failure is controlled predominantly by the presence or absence of windows in the aquitard and not by the vertical gradient.

Therefore, it is more important to know whether T , or K_h , is above or below a critical value rather than knowing its actual value. However, for this case, the transition to the critical value is not as sharp as was the case for the hydraulic conductivity of the aquitard. Alternatively, if a strong vertical gradient is known to exist across the aquitard, knowledge of T , or K_h , of the lower aquifer may not be important, at least for the definition of failure used here.

7.4.3 CONSTANT HEAD BOUNDARY CONDITION, h_4 , IN LOWER AQUIFER (SCENARIO 2)

Several different boundary conditions could affect the flow model and the transport of contamination. The two Scenarios only account for a few of the possible boundary conditions. For example, the upper boundary could be a recharge boundary rather than a water table boundary and the vertical boundaries could be flow boundaries rather than constant head boundaries. However, to simplify the situation, only the constant head boundary condition h_4 , will be investigated here. All other boundary conditions are kept constant.

The value of h_4 was gradually reduced below the boundary condition, h_3 , on the aquifer above, increasing the downward vertical gradient across the south end of the aquitard. The value of W is plotted versus the difference in h_3 and h_4 (Fig. 7-13). The results are very similar to those encountered in the last section in the study of the hydraulic conductivity of the lower aquifer. At very low differences in head across the aquitard, little vertical gradient exists, and failure does not occur. Consequently, W equals \$0. As the difference increases to 1 m, a critical vertical gradient is achieved and failure can occur. At a head difference of two meters W suddenly increases to approximately \$8 000. W then increases more or less linearly with the difference in hydraulic head.

Therefore, it is critical to know if the vertical gradient across the aquitard is above a critical value. Since W increases with the difference in h_3 and h_4 , if h_3 is known it can be important to know the actual value of h_4 .

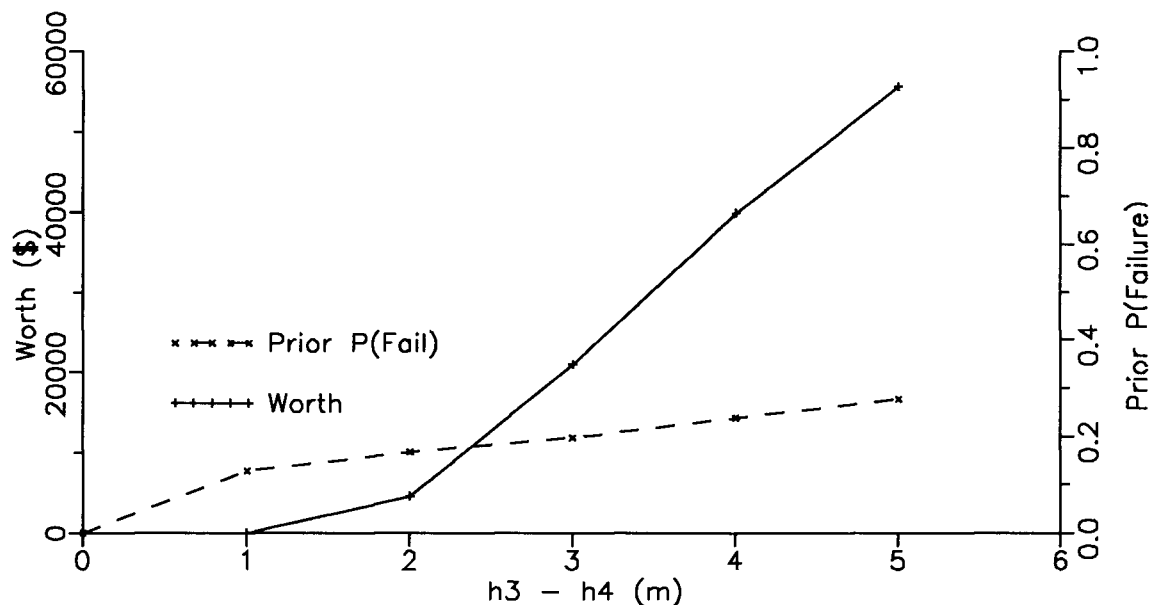


Figure 7-13: The sensitivity of W to the constant head boundary condition in lower aquifer.

7.5 SENSITIVITY TO GEOSTATISTICAL PARAMETERS

The sensitivity of W to the prior estimate of the mean, m_I , the correlation length λ_I , and the prior confidence in m_I are presented in this section using Scenario 1 and 2.

7.5.1 PRIOR ESTIMATE OF MEAN OF $I(x)$ (SCENARIO 1)

The value of W increases almost linearly with m_I from \$0 at $m_I = 0$ to over \$100 000 for $m_I = 0.15$ (Fig. 7-14). Data worth is totally due to sampling a window, S_W . S_W again switches A_D from A_{NC} to A_C (Fig 7- 16). S_{NW} makes no contribution to W for all m_I tested because, A_{NC} is the best alternative regardless of the sample outcome (Fig. 7-15).

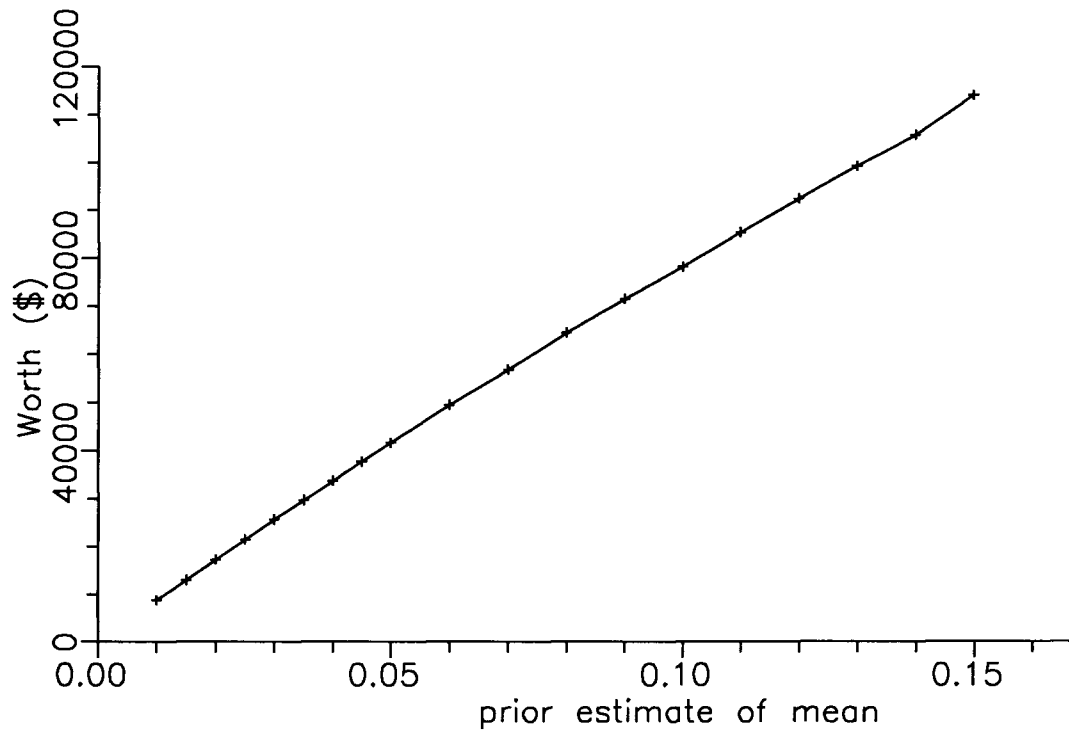


Figure 7-14: Sensitivity of W to the prior estimate of the mean.

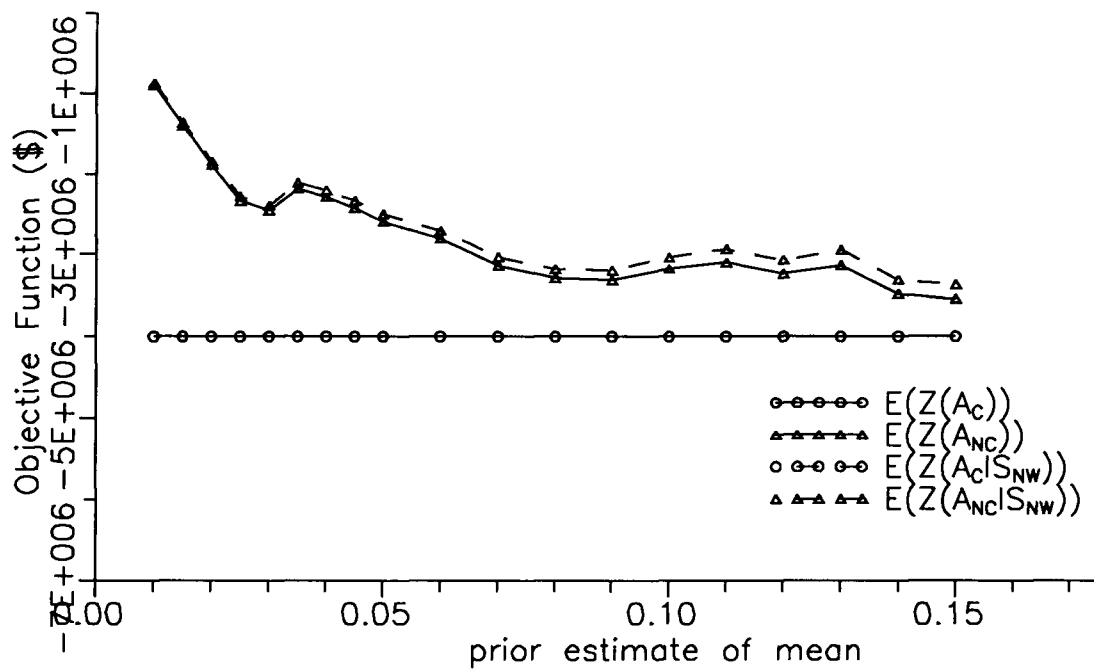


Figure 7-15: Effect of sampling no window on the prior and posterior objective function of the containment and no containment alternatives.

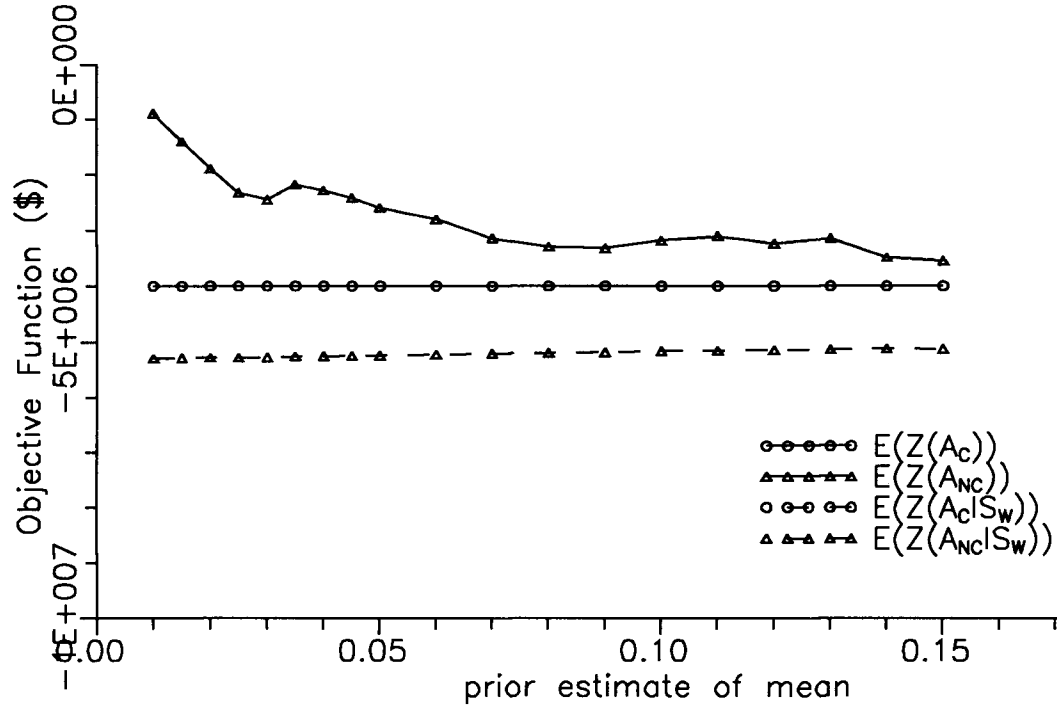


Figure 7-16: Effect of sampling a window on the prior and posterior objective functions of the containment and no containment alternatives.

The reason for this increase can be visualized as follows. W from equation (7.2) is

$$W = \{E[Z(A_D'|S_W)] - E[Z(A_D|S_W)]\}P(S_W) + \{E[Z(A_D'|S_{NW})] - E[Z(A_D|S_{NW})]\}P(S_{NW}) \quad (7.3)$$

The prior design decision is no containment, hence $A_D = A_{NC}$. If a window is sampled, $A_D' = A_C$ and if no window is sampled then $A_D' = A_{NC}$. Therefore, the above equation can be rewritten as

$$W = \{E[Z(A_C|S_W)] - E[Z(A_{NC}|S_W)]\}P(S_W) + \{E[Z(A_{NC}|S_{NW})] - E[Z(A_{NC}|S_{NW})]\}P(S_{NW}) \quad (7.4)$$

Note that the second difference term is zero, and the above equation simplifies to

$$W = \{E[Z(A_C|S_W)] - E[Z(A_{NC}|S_W)]\}P(S_W) \quad (7.5)$$

From Figure 7-16, one can see that the difference in $E[Z(A_C|S_W)]$ and $E[Z(A_{NC}|S_W)]$ is almost constant.

Therefore, the increase in W with m_I is caused by the increase in $P(S_W)$ with m_I (Fig. 7- 17).

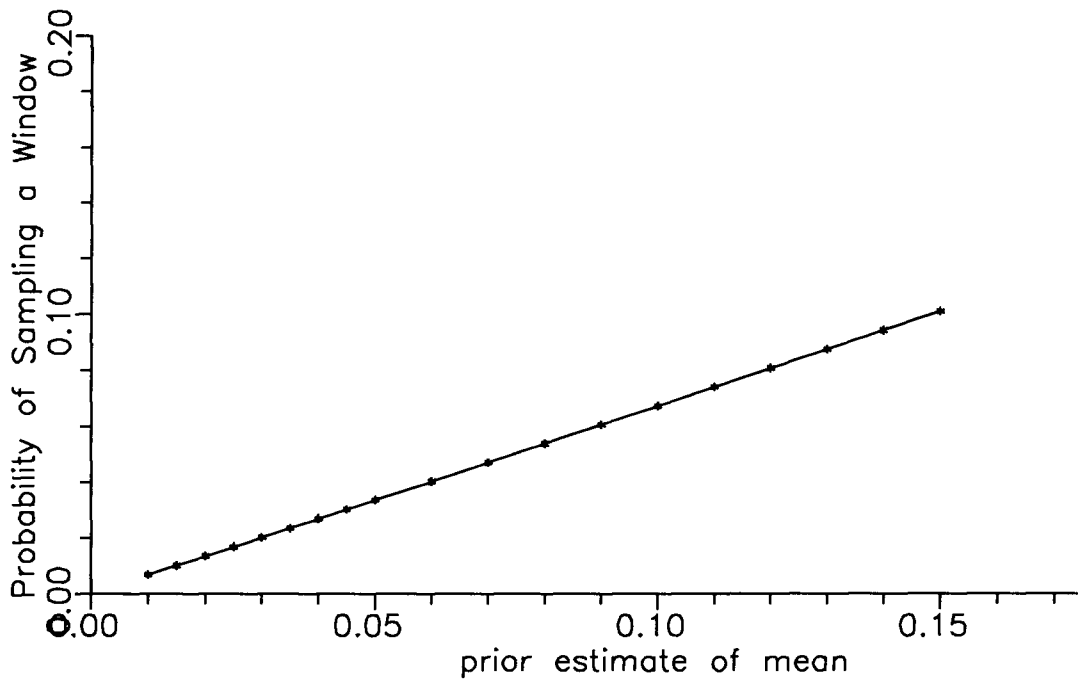


Figure 7-17: Probability of sampling a window versus the mean chance of a window.

7.5.2 CORRELATION LENGTH of $I(x)$ (SCENARIO 2)

The value of W rises from \$0 at $\lambda_I = 40$ m to over \$50 000 at $\lambda_I = 45$ m (Fig. 7-18). W then rises slightly, but then slowly drops off as λ_I increases. As λ_I increases, the realizations become increasingly constrained resulting in fewer windows. Consequently, the prior probability of failure decreases (Fig. 7-18). At low λ_I , the probability of failure is so high that A_C is the only viable alternative, regardless of the outcome of the sampling program, and $W = \$0$. At $\lambda_I = 45$ m, the probability of failure is low enough

that A_D becomes A_{NC} . W jumps to over \$50 000 because sampling a window will find that A_{NC} was a poor choice.

For this case, it is more important to know whether λ_I is above or below a critical threshold, rather than its actual value.

The decrease in W with increasing λ_I at higher values of λ_I is contradictory to what might have been expected. Intuitively, one would expect that W would increase with λ_I . As λ_I increases, information from the sample can be extrapolated over a larger area and the effect of the sample on the system increases. However, the trend in W has more factors affecting it than simply λ_I . It is worth noting, however, that in the case history described in Section 8.4.3, W increases with λ_I .

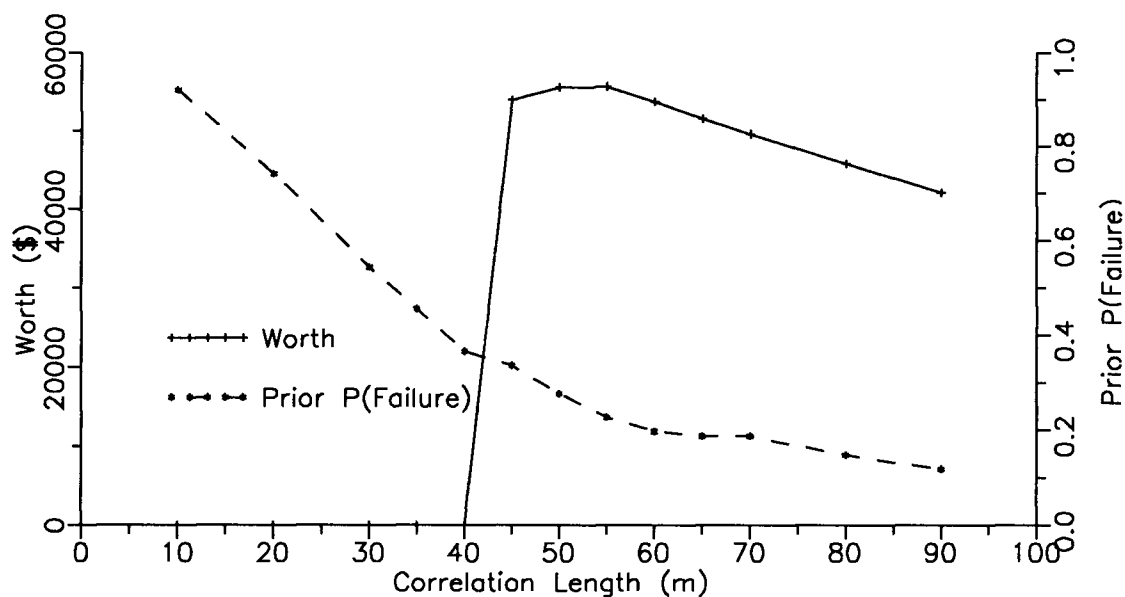


Figure 7-18: Sensitivity of W and prior probability of failure to correlation length.

7.5.3 CONFIDENCE IN THE PRIOR ESTIMATE OF MEAN (SCENARIO 1)

Recall, that the prior confidence in m_I is quantified by relating it to an equivalent number of prior

independent hard measurements, n_e . The value of W initially increases with increasing confidence in m_I , or n_e , but then becomes asymptotic for n_e greater than 15 (Fig 7-19). Therefore, for scenario 1 the confidence in the prior estimate of the mean is relatively unimportant.

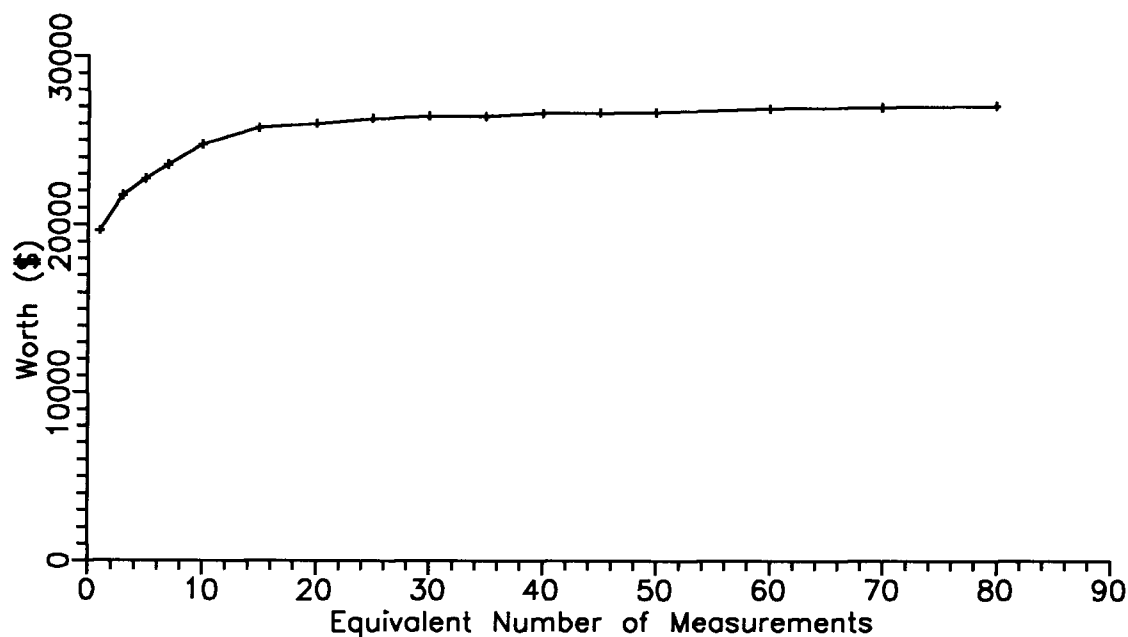


Figure 7-19: Sensitivity of W to the prior confidence in the estimates of the geostatistical parameters.

As with the correlation length, W reacts in an opposite manner to what might have been expected. As n_e increases, the measurement outcome has less effect on the updated estimate of the mean (Fig. 7-20). As the measurement has less effect on the updated mean, one would expect that W would decrease. This paradox is explained below.

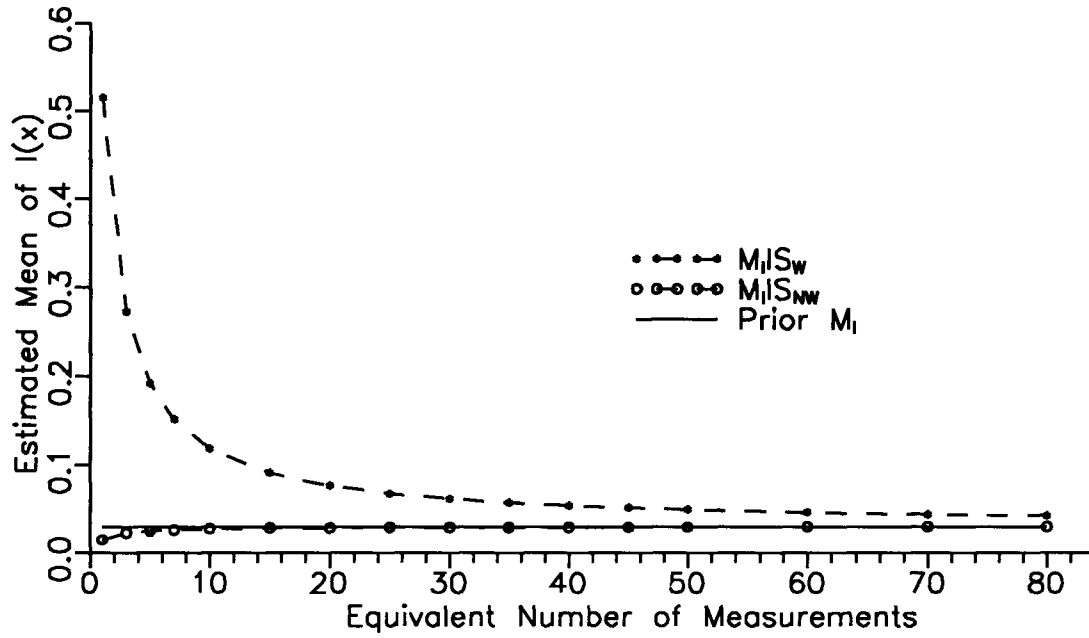


Figure 7-20: The updated mean versus n_e .

Since W is completely due to S_W , $A_D = A_{NC}$, and $A_D' = A_C$, given S_W , equation (7.2) simplifies to

$$W = \{E[Z(A_C|S_W)] - E[Z(A_{NC}|S_W)]\}P(S_W)$$

$P(S_W)$ is controlled by the prior estimate of m_1 and λ_1 and is independent of n_e . Therefore, the increase in W is due completely to the difference between $E[Z(A_C|S_W)]$ and $E[Z(A_{NC}|S_W)]$, which decreases for increasing n_e (Fig. 7-21).

$E[Z(A_C|S_W)]$ stays constant, but $E[Z(A_{NC}|S_W)]$ decreases. The objective function for A_{NC} will have the following form since its known costs and known benefits are equal to zero:

$$Z(A_{NC}|S_W) = - \frac{P_f C_f(t)}{(1+i)^t} \quad (7.6)$$

The cost of failure, $C_f(t)$ is fixed and the probability of failure, P_f , remains constant at one. The only

variable is the failure time, t . Therefore, the decrease in $E[Z(A_{NC}|S_W)]$ with increasing n_e is due entirely to a corresponding increase in t with n_e (Fig. 7-21).

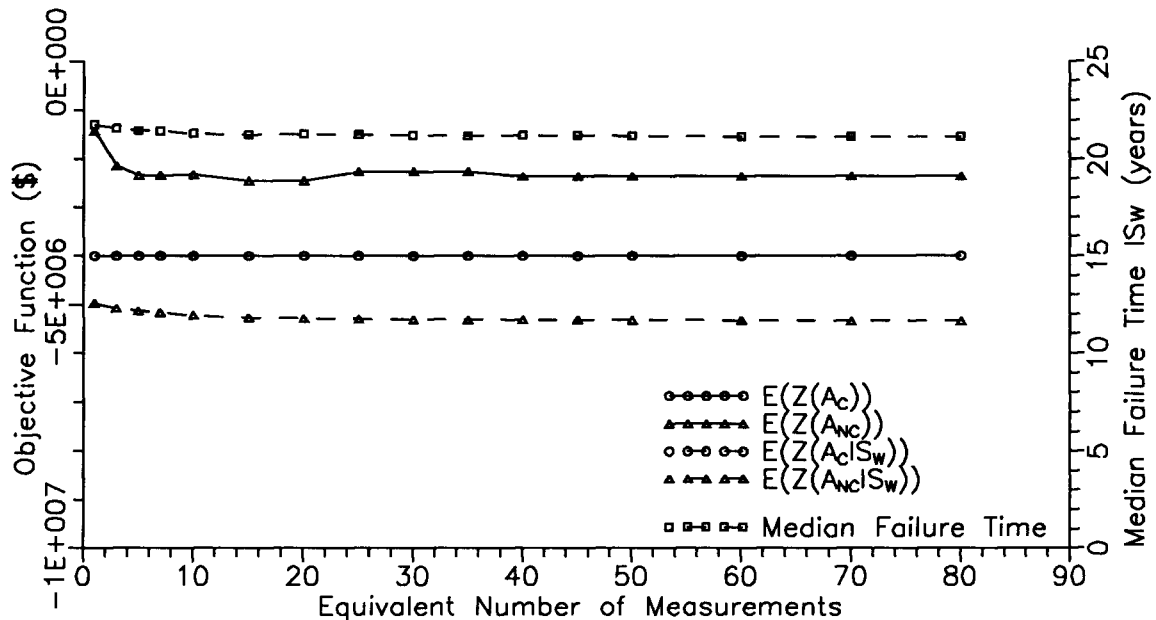


Figure 7-21: Effect of sampling a window on the objective functions

The reason for this decrease in t lies in the interaction between the vertical gradient through the window and the velocity in the upper aquifer at which the flow approaches the window. At high n_e , when the updated mean approaches its prior value of 0.03, only 3% of the aquitard blocks will represent windows. Leakage will be concentrated through a few windows. Consequently, the vertical gradient through the windows will be strong. Therefore, the contaminant will be transported more quickly as it approaches towards and travels through the window in the aquitard. At $n_e=1$, the updated mean is 0.515; therefore, approximately 50% of the blocks will represent windows. Leakage through the aquitard is distributed through many windows; therefore, the vertical gradient pulling contaminant towards and through the window is small. Hence contaminants will not travel as quickly towards and through the window.

7.6 SENSITIVITY TO EXISTING HARD DATUM

The sensitivity of the worth of a single borehole to an existing datum was studied for Scenario 1. The worth was calculated of single hard measurements taken on a 25 m spacing along an east west line through the hard datum located at the well. These results are shown in Figure 7-22. The well is located at 512.5 m. As expected, W is zero at the well, where the existing hard datum is located. There is no point in taking a measurement at a location where the aquitard is already known to exist with certainty.

As the measurement gets further from the existing datum, uncertainty about the presence, or absence, of aquitard increases and hence, W increases. However, on either side W reaches a maximum about 50 m from the datum and then decreases to zero. As windows get further from the well the vertical gradient induced by the well through them will decrease and failure is less likely to occur, accounting for the decrease in W. Note that the plot of W versus distance is not symmetric about the existing datum. This lack of symmetry is because the well does not lie in the middle of the path of contaminants, but off to the right hand side.

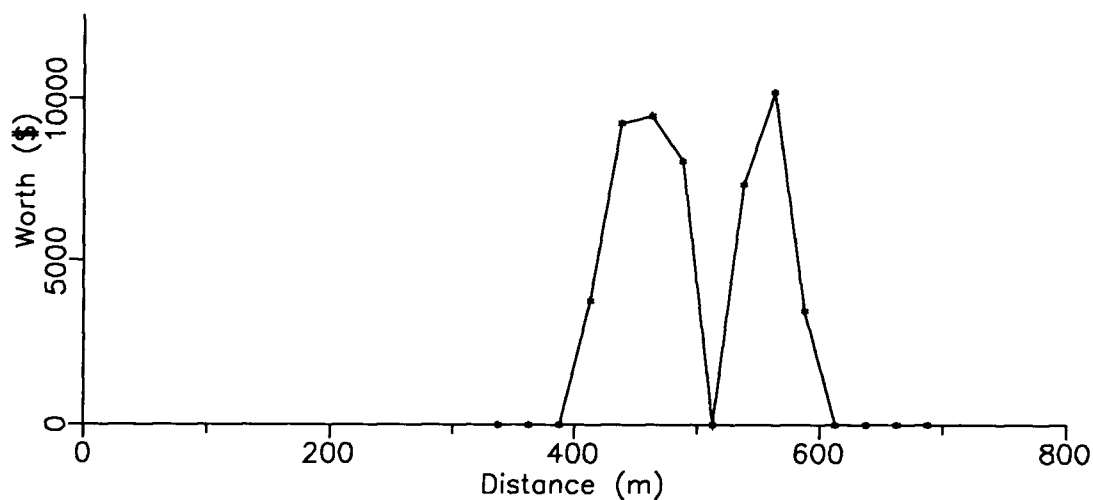


Figure 7-22: Effect of an existing hard datum on the worth of single borehole taken along an east-west line through the datum.

7.7 SUMMARY OF CHAPTER 7

Chapter 7 presents a sensitivity analysis of the worth of a single, hard measurement to economic, hydrogeological, and geostatistical parameters. The economic parameters include the cost of failure, the discount rate, and the known cost of containment. The hydrogeological parameters include a constant head boundary condition in lower aquifer, the vertical hydraulic conductivity of the aquitard, and the horizontal hydraulic conductivity of the lower aquifer. The geostatistical parameters include the correlation length, the mean, and the confidence in the estimate of the mean.

The worth is much more sensitive to the economic parameters than to the geostatistical or to the hydrogeological parameters. For the hydrogeological parameter in general, it is much more important to know whether the value of the parameter is above or below some threshold value, rather than knowing its actual value. For the geostatistical parameters, the worth is relatively insensitive to the correlation length and the confidence in the prior estimate of the mean, but is sensitive to the estimate of the mean. As the measurement point approaches an existing datum point, spatial correlation causes W to decrease until $W=\$0$ where the measurement and existing datum coincide.

The estimated worth of a measurement can be unstable when the objective function of the prior best design alternative is close in value to that of another prior design alternative.

Different parties, which view discount rates differently, may get very different estimates of W .

7.8 NOTATION

A_C	containment alternative
A_D	prior best design alternative
A_D'	posterior best design alternative
A_{NC}	no containment alternative

C_c	cost of containment
C_f	cost of failure
h	hydraulic head
i	discount rate
K_h	hydraulic conductivity in horizontal direction
K_v	hydraulic conductivity in vertical direction
L_c	leakage coefficient
m_I	estimate mean of $I(x)$
n_e	number of equivalent measurements
P_f	probability of failure
S_{NW}	outcome of sampling no window
S_W	outcome of sampling a window
t	time
T	transmissivity
W	worth of a sampling program
Z	objective function
λ_I	correlation length of indicator random variable $I(x)$
μ_I	mean of indicator random variable $I(x)$

CHAPTER 8: SAVANNAH RIVER SITE CASE HISTORY

8.1 INTRODUCTION

Chapter 8 uses the Savannah River Site (SRS) to demonstrate as realistically as possible how the framework developed in this thesis can be used to evaluate the worth of data in a hydrogeological design problem. The design problem utilized here is the closure of the H-Area seepage basins at the Savannah River Site (SRS). The SRS is a nuclear weapons production facility approximately 3 400 square km in size which is located in South Carolina on the Savannah River (Fig 8-1). The H-Area seepage basins are located in the General Separations Area (GSA) of the SRS (Fig. 8-2). The H-Area seepage basins are unlined earth basins that were used for the disposal of effluent water for nearly 30 years. The effluent contained dissolved tritium and other radioactive and nonradioactive species (Buss et al. 1987). The effluent would seep through the soil to the water table where it would then travel to nearby streams. Contaminants in the disposed effluent water were filtered by the soil as it infiltrated through the soil.

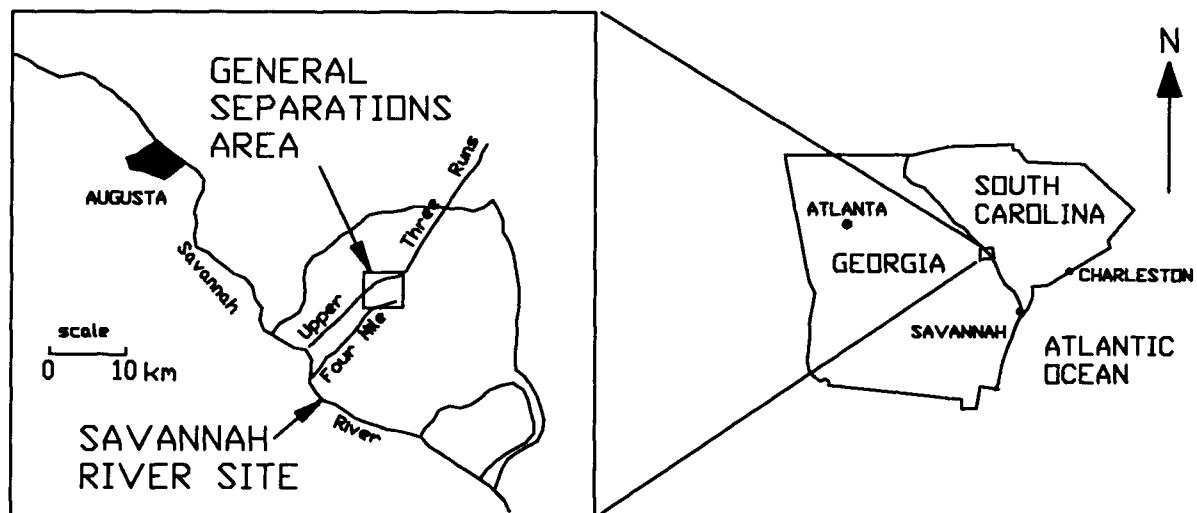


Figure 8-1: Location map of the Savannah River Site (modified from Duffield et al., 1990).

The seepage basins are presently no longer being used for waste disposal. However, if simply abandoned, they pose a potential long term threat to the local environment and water supplies. It is possible that the contaminants remaining in the soil could be remobilized in the future by infiltrating precipitation. This remobilization could provide a contaminant source over the next several hundred years. To deal with this potential long term threat, various options were considered for the closure of the seepage basins. These options ranged from basically leaving the basins "as is" to removing all of the contaminated soil.

The remobilized contaminants pose two environmental problems. Firstly, they could be transported to Four Mile Creek (Fig. 8-2), which would cause it to become contaminated. Secondly, the contaminants could be transported through the aquitard discontinuities to lower aquifers, causing the contamination of clean aquifers. This case study will focus only on lower aquifers. The continuity of only one aquitard will be dealt with.

The remainder of this introduction will discuss the general GSA geology, physiography, and hydrogeology. Section 8.2 defines the base case, and presents all parameters needed by the framework to evaluate the worth of data. The prior analysis is carried out in Section 8.3. The preposterior analyses of hard, point data and soft, areal geophysical surveys are carried out in Sections 8.4 and 8.5, respectively. The case study is presented here for demonstration purposes only. It is not for determining the true closure design, which has already been invoked. The case study is as realistic as possible, but idealizations have been carried out to simplify the numerical modeling. In addition, values of certain parameters which are difficult to estimate, such as the cost of failure and the mean of $I(x)$ have been set to be realistic, but also to force the worth of data to have a positive value.

8.1.1 PHYSIOGRAPHY AND GEOLOGY

The GSA is approximately 5.5 km by 3.7 km in dimension (Fig. 8-2). The surface topography is characterized by gently rolling hills. It is bounded on the north by Upper Three Runs Creek, on the south by Four Mile Creek and on the east by the McQueen Branch.

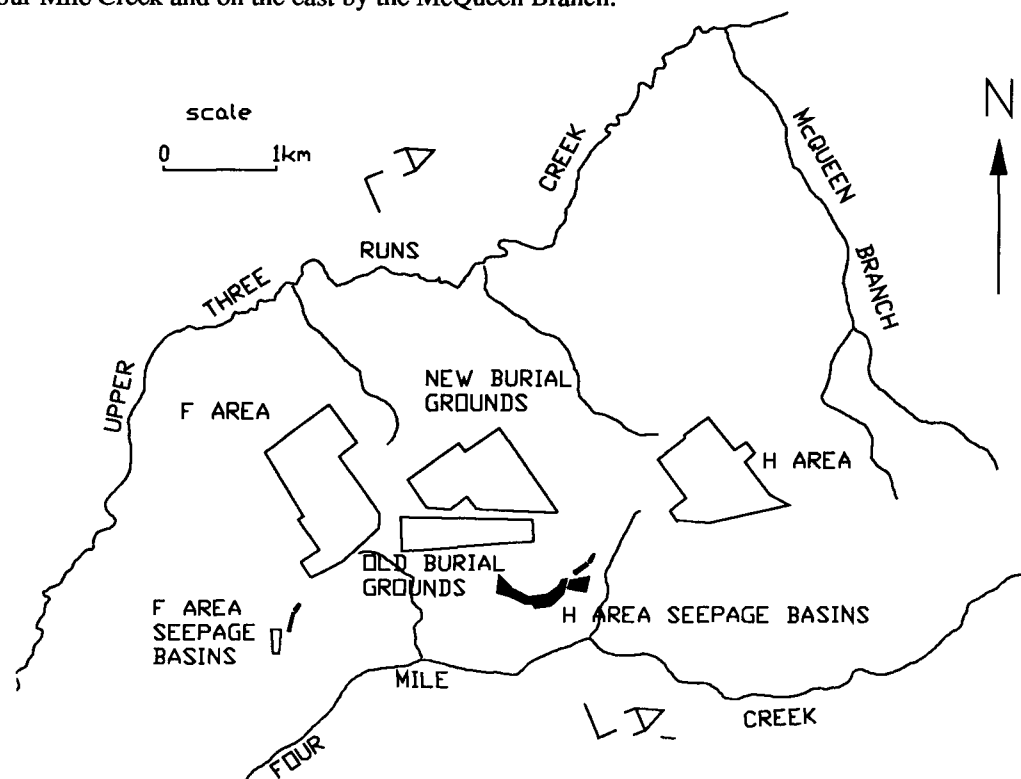


Figure 8-2: H-Area seepage basins in the General Separations Area (modified from Parizek and Root, 1986)

It is underlain by a thick sequence of unconsolidated sediments which form a layered system of aquifers and aquitards, that dip to the south east at 1.6 to 2 m per km. Sediments range in depth from 150 to 400 m (Duffield et al. 1989). The sediments were deposited during periods of successive transgressions and regressions (Cooke, 1936, quoted by Parizek and Root, 1986). This time period also included several periods of erosion. This study will focus on the stratigraphic units which form the upper three aquifers and upper two aquitards. Several types of nomenclature have been used to describe the stratigraphy of the SRS. The nomenclature used by Parizek and Root (1986) is used here.

The Congaree Formation forms the lowermost aquifer studied (Fig. 8-3). It is about 30 m in thickness and consists of mostly well sorted sand. The Congaree Formation is of marine origin and was deposited

during a transgression (Price, 1989). The Congaree is bounded from below by the Ellenton Formation, which is a thick, areally extensive clay unit. The Green Clay was deposited on top of the Congaree as the transgression continued, forming an aquitard. The Green Clay is generally continuous throughout the GSA and its thickness ranges from 0.3 to 6.1 m. It consists of a grey to green dense clay. Glauconite present within the Green Clay confirms that it is of marine origin (Price, 1989). However, the Green Clay is not always green or a clay. It is typically recognized by a very fine grained material (Parizek and Root, 1986). The Green Clay is the aquitard of interest in this study.

A regression then occurred during which the McBean Formation was deposited. It forms an aquifer; however, the lower part of the McBean is carbonaceous and fine grained and could act as a confining layer with the Green Clay. Glauconite in the carbonaceous zone can make it appear Green. It consists of well sorted to clayey sand and ranges in thickness from 20 to 25 m. Siple (1967), quoted by Parizek and Root (1986), determined that the McBean is of marine origin. Clay and silt lenses are widely distributed throughout the McBean.

The McBean Formation is bounded from above by the Tan Clay, which forms the uppermost aquitard. It is a discontinuous layer that occurs throughout the GSA. Its thickness ranges from between 0.3 and 3 m. The Congaree Formation, Green Clay, McBean Formation and Tan Clay were all deposited during the Eocene period from 49 to 35 million years ago.

The Barnwell formation forms the uppermost aquifer. It consists of clayey to well sorted sand. Discontinuous clay and silt lenses occur throughout. It is about 30 m in thickness. The bottom of the Barnwell could have formed in a near shore marine environment. Nystrom and Willoughby (1982), quoted by Parizek and Root (1986), reported broad scour features at the base of the Barnwell Formation. Parizek and Root (1986) suggest that the deposition of the Tan Clay on this irregular feature could account for its discontinuous nature. The Barnwell was formed during the Oligocene from 35 to 22 million years ago.

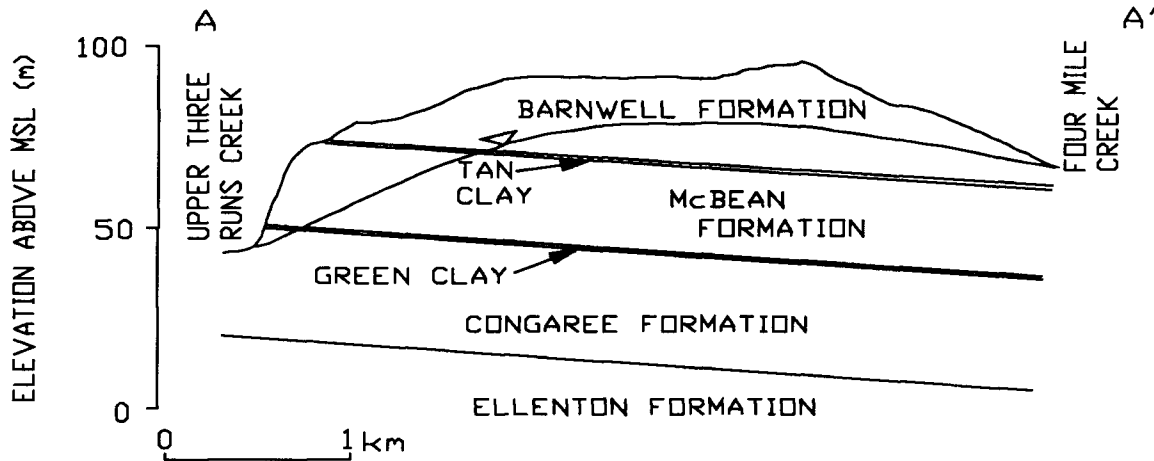


Figure 8-3: Geologic cross section through the General Separations Area (modified from Parizek and Root, 1986). (The location of the cross section is shown in Figure 8-2.)

A major potential cause of discontinuities in the Green Clay would be erosion by channeling (Price, 1989). Channeling could occur during any post Eocene period of unconformity or alluvial action. Several such periods of alluvial action did occur. For example, the Barnwell is overlain by an unconformity and much alluvial activity occurred during the Late Tertiary periods. For a more detailed description of the site geology, refer to Parizek and Root (1986).

8.1.2 HYDROGEOLOGY

The water table is predominantly located in the Barnwell, but also in some parts of the McBean and Congaree near Upper Three Runs Creek (Fig. 8-3). In general, water enters the system through infiltration into the Barnwell. The three bounding creeks form discharge zones. The hydraulic head distribution in the Barnwell and McBean is strongly influenced by all three creeks. In the Congaree, only Upper Three Runs Creek has an influence on the hydraulic head distribution.

The vertical hydraulic gradient is downward across both the Tan Clay and the Green Clay. Groundwater flows from the Barnwell either laterally to discharge in the surrounding creeks or vertically across the

Tan Clay into the McBean. The groundwater in the McBean predominantly moves laterally towards the three creeks. However, some groundwater will penetrate the Green Clay and pass into the Congaree.

In general, the Tan Clay does not appear to be a significant confining layer or to greatly affect the hydrogeological system. Hydrogeological modeling studies by Parizek and Root (1986) and a comparative study of hydrographs from the McBean and Barnwell suggest that the two formations act as one hydrostratigraphic unit. The Tan Clay best acts as a confining layer in H-Area where the hydraulic head difference across the aquitard is up to 5 m. The Green Clay acts as a very strong confining layer. The hydraulic head difference across the Green Clay is as high as 25 m. Parizek and Root (1986) report that this head difference is persistent throughout the GSA and, therefore, it is unlikely that the Green Clay is extensively discontinuous. However, Duffield et al. (1989) found that small discontinuities in the Green Clay in the GSA could be difficult to detect with hydraulic head data because the perturbations that they created in the hydraulic head field were small.

Groundwater in the Congaree comes from leakage through the Green Clay and from horizontal flow from off site towards the south east. Groundwater in the Congaree flows laterally north west where it discharges into Upper Three Runs Creek. The leakage across the Green Clay is probably not great (Parizek and Root, 1986). The Congaree is bounded from below by the Ellenton Formation, which is a thick, areally extensive aquitard. The Ellenton Formation is assumed to be completely impermeable in this thesis.

The clay and silt lenses in the Barnwell and the McBean will cause the hydraulic conductivity to be anisotropic.

Groundwater flow velocities in both the Barnwell and the McBean are up to 100 m/yr. Therefore, the assumption of advective transport dominating dispersive transport will be valid. The dominance of advective transport over dispersive transport was discussed in Chapter 5.

For a more detailed description of the site hydrogeology, refer to Parizek and Root (1986).

8.2 SET UP OF BASE CASE

Section 8.2 sets up the base case, or the basic modeled system. Setting up the modeled system requires: (a) determining the closure design alternatives, (b) determining how to model contaminant transport near the H-Area seepage basins, (c) analyzing available Green Clay data, and (d) evaluating the geostatistical parameters using the available Green Clay data.

8.2.1 ALTERNATIVE CLOSURE DESIGNS

Three design alternatives were considered for closure: (a) low permeability clay cap, (b) no clay cap (or no action), and (c) waste removal and low permeability clay cap (Killian et al. 1987). For simplicity, this thesis will only deal with the first two alternatives. In the low permeability clay cap option, A_{CC} , the basins would be back filled with soil and compacted. A low permeability cap would then be placed on the top to reduce infiltration. The basins would be fenced off and maintenance would be carried out for 30 years. Maintenance would consist of mowing grass in the basins, checking for soil erosion, and monitoring groundwater. This alternative is assumed to be 100% efficient in stopping the contaminant source. The basins were closed with this option.

In the no clay cap alternative, A_{NC} , the basins would be fenced off and maintenance similar to the A_{CC} alternative would be carried out. With this alternative the seepage basins represent an active source of contamination. Therefore, failure, or contamination of the lower aquifer can only occur for A_{NC} .

The total estimated costs in fourth quarter 1985 dollars for A_{CC} , and A_{NC} are \$22.8, and \$3.3, respectively (Killian et al., 1987). The benefits of all alternatives are zero (that is they do not lead to any direct income to the decision maker). Unless stated otherwise, all monetary values used in Chapter 8 are in fourth quarter 1985 dollars.

Preventing contamination of the Congaree is important for several reasons. Firstly, under existing regulations, if contamination occurs, it will have to be cleaned up. Secondly, contamination will result in regulatory penalties and bad publicity for the SRS. The critical factor in preventing contamination of the Congaree is the continuity of the Green Clay.

The author is unaware of any study that has directly estimated the cost of contamination of the Congaree by the H-Area seepage basins, and determining a cost of failure is difficult. The easiest of the above cost factors to estimate will be regulatory penalties. However, even these may not be that straight forward to estimate because failure may not happen for several years and it then may not be detected for several more years. The penalties will be dependent upon future laws which may be different than those now in effect.

Clean up costs are difficult to estimate. Again, since failure may happen a number of years into the future, the clean up costs will be highly dependent upon future, unknown clean up standards and techniques. Based on present clean up standards and techniques, the clean up costs will be very expensive. Clean up costs at some contamination sites have reached over \$100 million. However, it is suggested here that this is an absolute maximum of any possible clean up cost for two reasons.

Firstly, present clean up standards are unrealistically strict. For example, under some legislation the contaminated aquifer must be cleaned up to drinking water standards. Practice has shown that in most cases, this is an impossible goal. In the future, clean up standards will likely be relaxed. Secondly, much

of the past clean up costs have been spent on litigation rather than the actual clean up. It is also likely in the future as legislation improves, that these costs will be reduced.

The costs associated with bad publicity are extremely difficult, if not impossible to quantify.

Therefore, since the cost of failure is unknown and very difficult to estimate, and this case study is presented for demonstration purposes only, two costs of failure will be assessed, and these will be arbitrarily set at \$70 million and \$45 million. These values were chosen after some preliminary sensitivity analyses of the case history were carried out. The \$70 million cost of failure was chosen to force data to have a large stable positive net worth. Recall from Chapter 7 that if the prior best design alternative is unstable, the estimated W is unstable. The \$45 million cost of failure still gives a positive net worth, but it is less stable. From the sensitivity analysis carried out in Section 8.4.2.2, a cost of failure of approximately \$35 million results in a net data worth of \$0.

The costs and benefits associated with the three alternatives are summarized in Table 8-1. A discount rate of 0.10 is used in the analysis. A discussion on the choice of different discount rates is presented by Massmann and Freeze (1987a and 1987b).

8.2.2 MODELING OF CONTAMINANT TRANSPORT NEAR H-AREA SEEPAGE BASINS

Root (1987) and Parizek and Root (1986) carried out comprehensive hydrogeological studies of the GSA.

Other studies include: Duffield et al. (1990), Duffield et al. (1989), and Duffield et al. (1987).

Alternative	Benefits (million \$)	Known Costs (million \$)	Cost of Failure (million \$)
A_{CC}	0	22.8	0
A_{NC}	0	3.3	70

Table 8-1: Summary of cost and benefits associated with the no action and waste removal alternatives.

Ideally, the flow within the entire GSA should be modeled because of the presence of the three bounding creeks makes the boundary conditions on all sides easy to define . However, it is impractical to model such a large area because of the number of Monte-Carlo realizations needed for the data worth analysis. Therefore, flow in a much smaller region around the H-Area seepage basins will be modeled instead (Fig. 8-4). Steady state flow conditions are assumed.

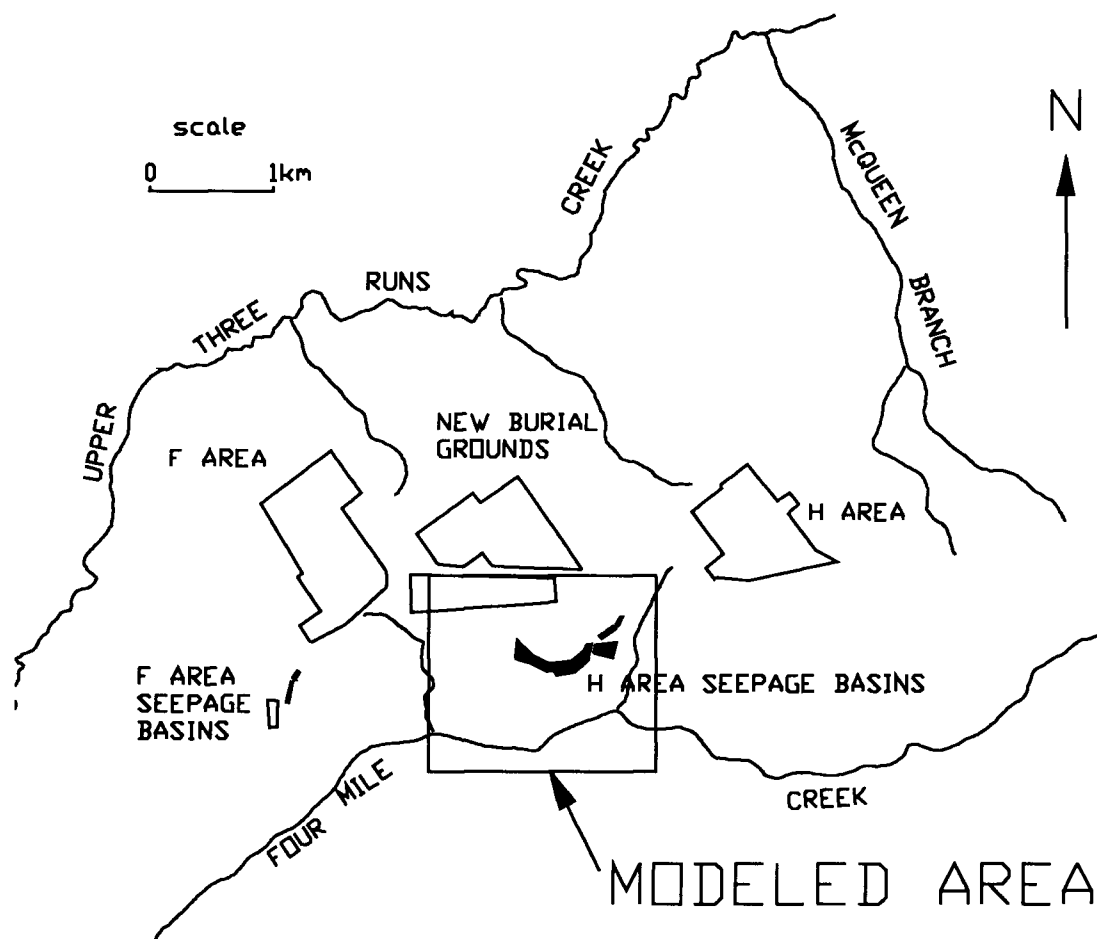


Figure 8-4: Area where flow and transport are modeled around the H-Area seepage basins.

The Tan clay was not included in the numerical model of the site hydrogeology. The Tan Clay has a very weak influence on the hydrologic system (see Section 8.1.2) and it is very discontinuous and does not prevent contamination from entering the McBean Formation. Yet, it is almost as thick as the Green clay and its vertical hydraulic conductivity was estimated by Parizek and Root (1986) and Duffield et al.

(1987) to be of the same order of magnitude as the Green Clay. Therefore, if it were included as a continuous layer, it would exert an artificially strong influence on the vertical movement of groundwater and prevent contamination from entering the McBean Formation. Alternatively, it could be included as a distinct layer with discontinuities placed in it. However, it is not known where these discontinuities are; therefore, this approach was rejected.

However, leaving out the Tan Clay completely will artificially increase the vertical transport of contaminants. Contamination is generally transported horizontally in the Barnwell and upper part of the McBean (Duffield et al. 1989). To maintain transport in the upper portions of the system, the vertical hydraulic conductivity of the Green Clay was arbitrarily decreased by a factor of two from that estimated by Parizek and Root (1986).

All vertical boundaries on the edges of the flow region are defined as constant head boundaries. Since the Tan Clay is assumed to not be present, the vertical boundary conditions in the McBean and the Barnwell will be identical. However, those in the Congaree will be different because of the presence of the Green Clay.

The southern and eastern boundaries in the McBean and Barnwell are placed along Four Mile Creek and the unnamed creek, respectively. The western boundary was placed so that approximately 50% of it overlapped with another unnamed creek. The northern boundary was placed approximately 600 m north of the main seepage basin. The hydraulic head along all boundaries was set equal to the elevation of the 1982 water table, presented by Parizek and Root (1986).

In the Congaree, all vertical boundaries are placed along the edges of the modeled flow region. The values on the constant head boundaries are set by interpolation from a 1982 contour map of hydraulic head in the Congaree presented by Parizek and Root (1986).

The water table represents the upper boundary of the hydrogeological system. The recharge to the water table was estimated by Parizek and Root (1986) to be 38.1 cm/yr. Ideally, with the clay cap alternative, infiltration will be reduced over the seepage basins, creating a depression in the water table. However, for simplicity this change in boundary condition for the clay cap alternative will be ignored. The bottom of the Congaree is assumed to be impermeable.

The only two hydrogeological studies of the GSA presented in enough detail to sufficiently follow the important modeling steps are Parizek and Root (1986) and Duffield et al. (1987). (Root (1987) and Parizek and Root (1986) present equivalent hydrogeological information.) Parizek and Root (1986) modeled the same system of aquifers and aquitards modeled here. Duffield et al. (1987) included the aquifer and aquitard below the Congaree in their modeling study. The modeling carried out in this thesis will closely follow that of Parizek and Root (1986) rather than Duffield et al. (1989) because of the greater similarity of the system modeled and the more comprehensive nature of the presentation.

The same layering of nodes used by Parizek and Root (1986) will be used in this thesis. The Barnwell will be represented by a single layer of nodes, while the McBean will be represented by two layers of nodes to account for vertical gradients. The Green Clay is represented as a leakage layer, and the Congaree is represented by a single layer of nodes. This density of nodes should be sufficient to model the groundwater velocities as accurately as needed here. More layers are used here than are used in the particle tracking study carried out by Duffield et al. (1987) in the same area.

A nodal spacing of 29 m has been used in the horizontal discretizations of the aquifer and aquitard units. Therefore, the aquitard has been discretized into 29 m square blocks. This discretization corresponds to 60 columns and 50 rows. The effect of the density of discretization on the worth of data is investigated in Section 8.4.2.1.

The hydraulic parameters used in this thesis for the hydrostratigraphic units are summarized in Table 8-2. Except the hydraulic conductivity of the Green Clay, all of the values were taken directly from the results of a steady state calibration by Root (1986). Recall that the hydraulic conductivity of the Green Clay was reduced by a factor of two. Root's calibration was carried out by trial and error. The calibration was carried out by matching the calculated hydraulic head with maps of hydraulic head in the three aquifers that were produced from 150 measurements.

The contaminant source is represented by 33 particles spaced along a line centered in each of the four seepage basins. The particles are all initially released from an elevation corresponding to 99% of the saturated thickness of the Barnwell. The flow solution and the paths of contaminant particles tracked are shown in Figure 8-5, for the case where no windows are present in the Green Clay.

hydrostratigraphic unit	parameter	Estimate
Barnwell	K_h	8.8×10^{-6} (m/s)
	K_v	7.4×10^{-8} (m/s)
	porosity	0.2
Upper McBean	K_h	1.8×10^{-5} (m/s)
	K_v	1.5×10^{-7} (m/s)
	porosity	0.2
Lower McBean	K_h	8.8×10^{-6} (m/s)
	K_v	7.4×10^{-8} (m/s)
	porosity	0.2
Green Clay	K_v	1.75×10^{-10} (m/s)
	porosity	0.4
Congaree	K_h	2.2×10^{-4} (m/s)
	K_v	2.2×10^{-5} (m/s)
	porosity	0.2

Table 8-2: Hydraulic parameters of hydrostratigraphic units used in the base case.

Windows will be generated in the Green Clay up to 50 m from the fixed boundary conditions in the McBean and Barnwell.

8.2.3 GREEN CLAY DATA BASE

This thesis will utilize the same Green Clay data base presented by Parizek and Root (1986). It consists of 147 boreholes which penetrated the Green Clay horizon. They are summarized in Appendix 1. All of the boreholes had lithologic logs available while 47 boreholes also had geophysical logs. More Recent boreholes have been taken, but they will not be used because their results are not readily available. The boreholes have been split into both hard and soft data.

The hard data comprises the 47 boreholes which have geophysical logs. The geophysical logs include gamma ray, self potential, and resistivity logs. These boreholes are defined as hard data because the gamma ray signature of the Green Clay is relatively consistent and widespread throughout the GSA (Parizek and Root 1986) and is easy to pick out (Aaland, 1989). All of these boreholes found Green Clay present. The data points are mostly concentrated near H-Area, but a few are spread throughout the GSA; however, only one is located near the H-Area seepage basins (Fig. 8-6).

The soft data comprises the remaining 100 boreholes which have only lithologic logs. These data are defined as soft because often only a percentage of the core was recovered in many boreholes (Parizek and Root, 1986). The quality of the logging and the amount of core recovered varied over time with earlier boreholes having poorer core recovery and a poorer quality of logging than the later boreholes. However, for simplicity, this variation is ignored. Thirty four of these boreholes (34%) did not encounter the Green Clay. Their locations are again concentrated in particular areas of interest, but some locations are scattered throughout the GSA (Fig. 8-7). It is worth noting that boreholes that did not encounter the Green Clay are generally located within 100 m of a borehole that definitely did encounter the Green Clay.

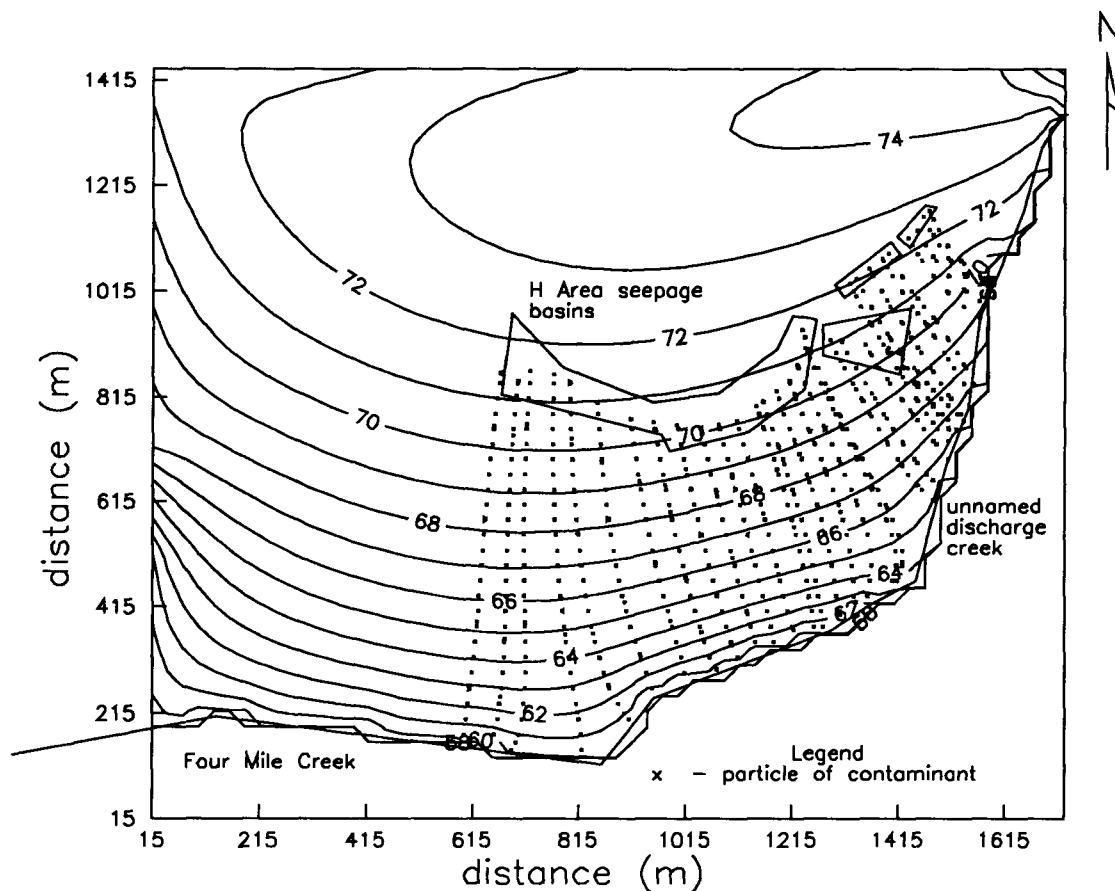


Figure 8-5: Contours of hydraulic head in Barnwell Formation and paths of particles of contamination near the H Area seepage basins. (Contour interval is 1 m.)

The Green Clay data base has been split into two categories. The 147 boreholes taken through out the GSA will be referred to as global data. They are used to estimate μ_I and λ_I . (The estimation of μ_I and λ_I is covered in the next Section.) A subset of the global data (14 soft and 1 hard) are located within the region where flow and transport are modeled (Fig. 8-8). These are referred to as local data. The aquitard realizations are conditioned on local data only.

Recall from Chapter 4 that the reliability, or quality, of the soft data is quantified by

$$p_1 = P(I_s(x) = 1 | I(x) = 1) = P(S_W | \text{Window is present})$$

$$p_2 = P(I_s(x) = 1 | I(x) = 0) = P(S_W | \text{No window is present})$$

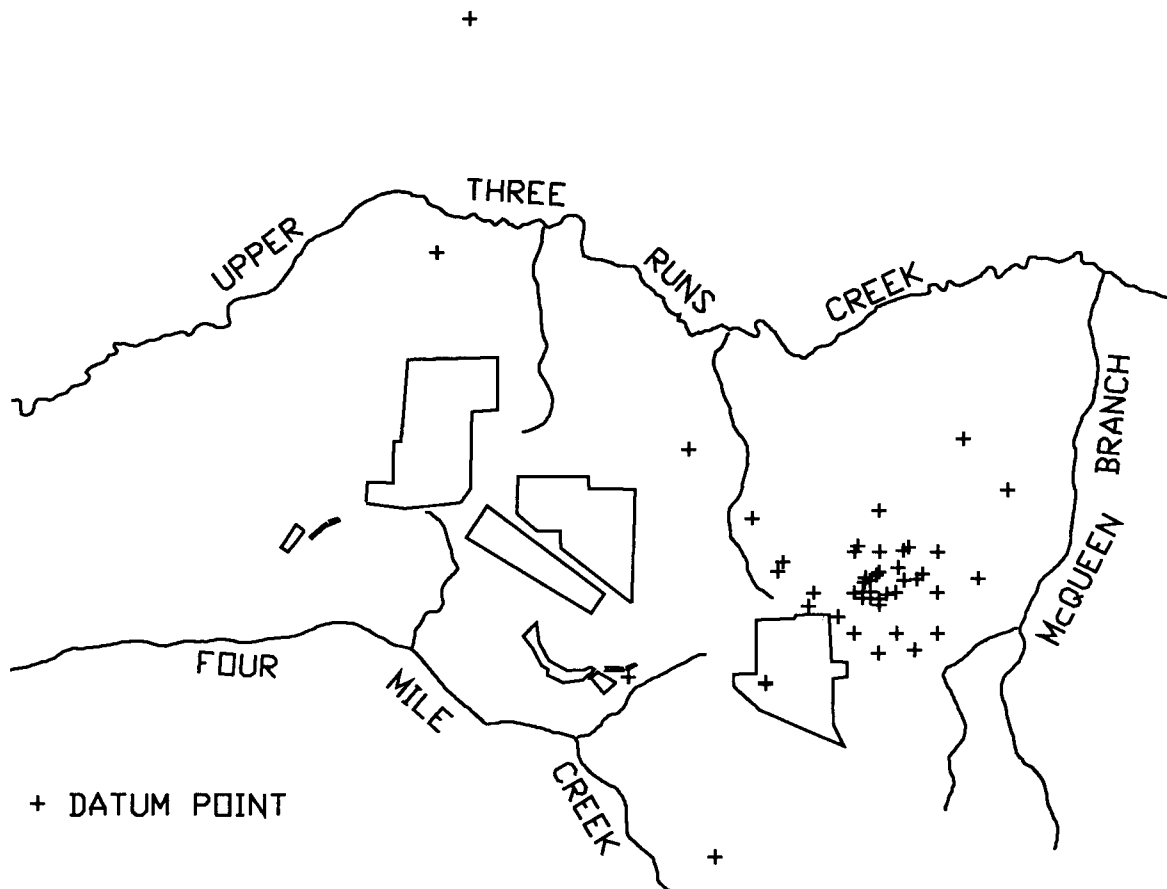


Figure 8-6: Locations of global hard data.

where p_1 represents the probability that the lithologic log will indicate a window given that a window is really present. In other words, p_1 represents the probability that the sample outcome is correct. In this thesis it is assumed that $p_1 = 1$. The value of p_2 represents the probability that the lithologic log indicates a window is present, while in reality Green Clay is present. In other word, p_2 represents the probability that the sample outcome is wrong. Here, p_2 is estimated from the lithologic logs of the 47 hard data. Of all the hard data sampled, 18, or 38%, of these lithologic logs report a window even though the geophysical logs indicate aquitard; therefore, $p_2 = 0.38$. Hence, it is expected that 38% of the soft data will show a window when aquitard is actually present.

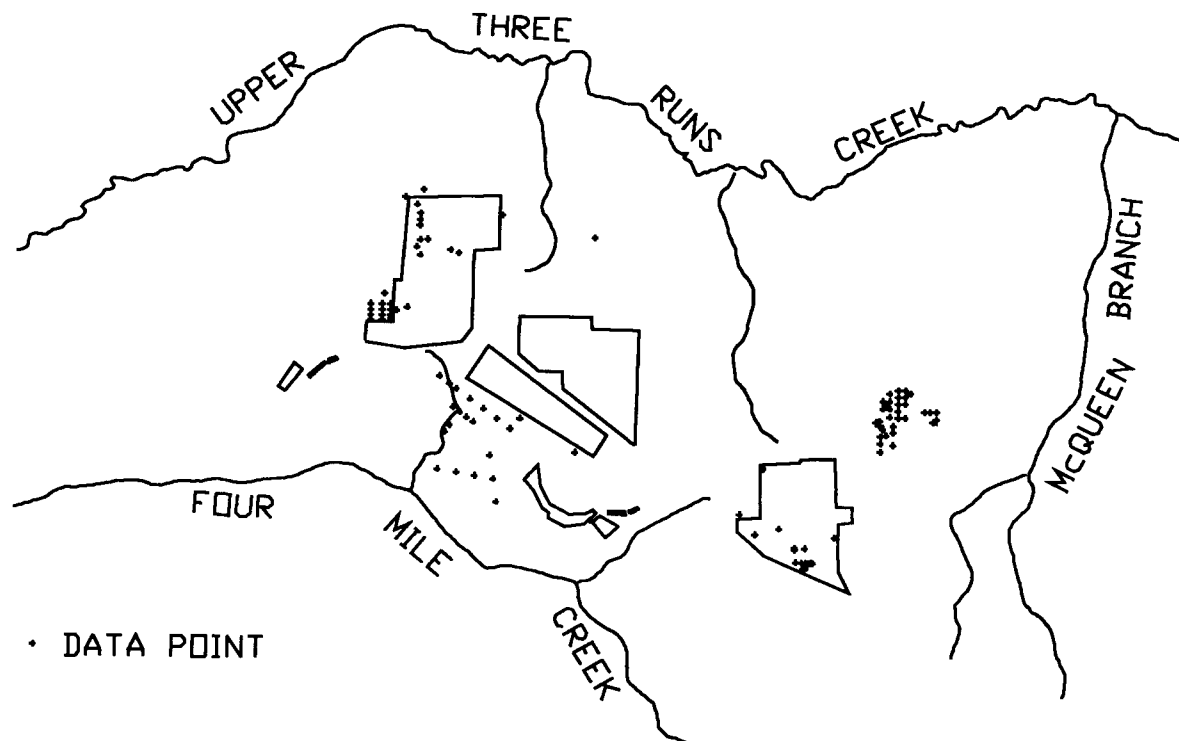


Figure 8-7: Locations of global soft data.

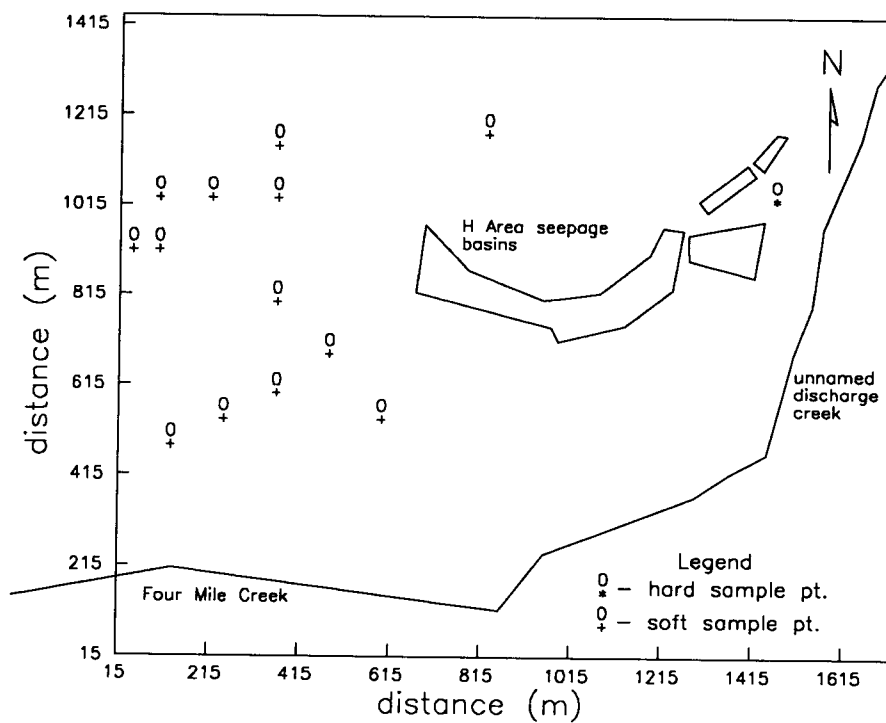


Figure 8-8: Local hard and soft data used to condition aquitard realizations.

It is likely that none of the soft data truly sampled a window. Since, $p_2 = 0.38$, it is expected that 38% of the lithologic logs will indicate a window even when Green Clay is actually present. If some lithologic logs are truly finding windows, then it would be expected that more than 38% of the logs would indicate windows. However, only 34% of the lithologic logs alone indicate windows, which is below the expected 38%. Furthermore, all of the lithologic logs of the hard data which indicate a window are apparently wrong. It is assumed that leakage will not occur through existing boreholes.

8.2.4 INFERENCE OF GEOSTATISTICAL PARAMETERS

Recall from Section 4.3.3 that the mean will be estimated by Bayesian updating, while the correlation length must be estimated by non Bayesian methods. The Bayesian estimation of μ_I is dependent upon λ_I ; therefore, λ_I must be estimated first. However, the estimation of λ_I presents a problem because it cannot be directly estimated from the data. This problem and the method used to circumvent it are discussed in the next Section.

8.2.4.1 Inference of Correlation Length.

The correlation length cannot be directly estimated for either the hard or soft data. All of the hard data encounter aquitard; therefore, there is no variability in the data and a covariance function cannot be calculated. The soft data does have variability in the data; however, as discussed in Section 8.4, all of the encountered windows are probably due to false sample outcomes. Therefore, the variability is likely due to false sample outcomes, rather than representing any true variability in the aquitard. A covariance function based on these data would be completely misleading as to the true spatial variability of the Green Clay.

In lieu of data to estimate the correlation length, it will be arbitrarily assumed that λ_1 is equal to 200 m.

It assumed that the correlation will be large since the Green Clay was deposited in a marine environment.

Fortunately, as will be shown in Section 8.4.2.3, the worth of a sample is relatively insensitive to the correlation length.

8.2.4.2 Inference of Mean and Variance

There are three sources of information available to estimate the mean: geological intuition, global soft data and global hard data. The mean will be first estimated based on geological intuition. A combined estimate using all of the information will be obtained by updating the geologically based estimate in two separate steps, one for the soft data and one for the hard data, using equation (4.55) which is presented below:

$$m_I'' = [H' + H]^{-1} [H' m_I' + H \frac{m_I - p_2}{p_1 - p_2}] \quad (8.1)$$

where

- $H' = [u^T S_{IsIs}^{-1} u]^{-1}$, or the weight of the prior data
- $H = u^T S_{II}^{-1} i$, or the weight of the sample data
- m_I' is the prior mean
- m_I is the sample mean
- m_I'' is the updated mean
- p_1 and p_2 represent the precision of the measurement.

It is believed that the Green Clay was deposited over 35 million years ago. Since then, unconformities and periods of alluvial action have occurred which could have eroded a discontinuity in the Green Clay. Upper Three Runs Creek is a present day example of channeling creating a discontinuity in the Green Clay. Therefore, based on the geology alone, it could be estimated that 5% of the Green Clay under the

GSA has been eroded by channeling in the past 35 million years. Therefore, the geological estimate of the mean, m_1' , is 0.05. The confidence in the prior estimate is assumed equivalent to five independent hard measurements.

Updating the geological estimate with the 100 global soft data yields:

$$\begin{aligned} m_1'' &= \frac{(105.26)(0.05) + (132.116)(0)}{105.26 + 132.116} \\ &= 0.0222 \end{aligned} \quad (8.2)$$

Note that the unbiased estimate of the sample mean based on soft data alone is 0 and that the weight of the soft data, H , is 132.1 compared to the weight, $H' = 105.3$ for geological intuition.

The second updating step using the 47 global hard data yields:

$$\begin{aligned} m_1''' &= \frac{(0.0222)(237.38) + (336.18)(0)}{237.38 + 336.18} \\ &= 0.0092 \end{aligned} \quad (8.3)$$

Note, that the sample mean based on the hard data alone is zero and that the weight of the hard data alone, H , is 336.2 which is three times the weight of the soft data alone and over three times the weight of the geological estimate.

The overall updated mean, m_1''' , is 0.0092. The updated estimate of the variance is

$$\begin{aligned} \sigma^{2'''} &= 0.0092 (1 - 0.0092) \\ &= 0.00912 \end{aligned}$$

The geostatistical parameters used in the base case are summarized in Table 8-3.

Parameter	description
mean	0.0092
variance	0.00912
correlation length	200 m
confid. in geol. est. of mean	5 ind. samples

Table 8-3: Summary of geostatistical parameters used in base case.

8.3 PRIOR ANALYSIS

A prior analysis is carried out using the base case set up in Section 8.2. Recall from Section 6.4 that the prior analysis is calculated using the same realizations generated for the preposterior analysis. One hundred realizations are used for each sample outcome in the preposterior analysis; therefore, a total of 200 realizations are used in the prior analysis.

A decision tree illustrating the prior analysis is shown in Figure 8-9 for $C_f = \$70$ million. A_{NC} is the best alternative with an expected objective function of $-\$11.296$ million. The expected objective function for A_C is $-\$22.8$ million. The prior probability of failure is 0.226. The expected regret of the clay cap alternative is $\$3.79$ million; therefore, no more than approximately $\$3.79$ million should be spent on any exploration program. Note that the expected regret of the prior best design alternative is equal to the expected value of perfect information, EVPI.

When $C_f = \$45$ million, the clay is still the best alternative with an objective function of $-\$8.44$ million. The expected objective function for the clay cap alternative is still $-\$22.8$ million. The prior probability of failure is still 0.226, but the expected regret of the clay cap alternative is $\$1.19$ million. No more than approximately $\$1.19$ million should be spent on any exploration program.

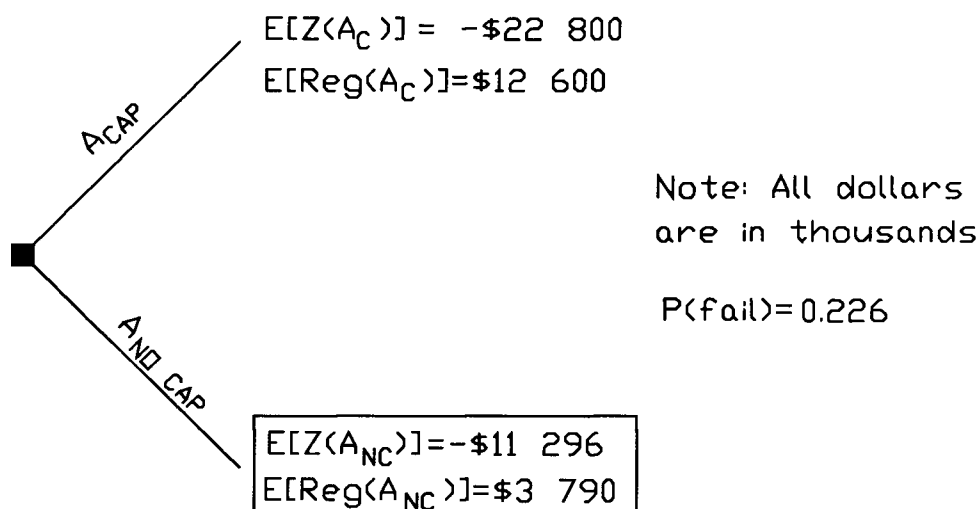


Figure 8-9: Decision tree used in prior analysis, where Cost of failure = \$70 million.

Note that reducing C_f from \$70 million to \$45 million has reduced the estimate of maximum expenditure for an exploration program by over three times. C_f could be very difficult to estimate. Failure can happen decades into the future; therefore, the cost of failure is dependent upon many future factors which are unknown at present, such as legislation and clean up techniques. Therefore, the estimated maximum expenditure is highly uncertain.

8.4 PREPOSTERIOR ANALYSIS OF HARD DATA

Section 8.4 presents the preposterior analysis of hard data. This analysis includes estimating data worth for both $C_f = \$70$ and \$45 million. For simplicity, $C_f = \$70$ million and $C_f = \$45$ million, will be referred to as C_{f7} and C_{f4} , respectively. The framework is used in Section 8.4.1 to determine whether a single hard measurement is cost effective, or in other words should it be taken. The robustness of this decision is studied in Section 8.4.2. In Section 8.4.3, the framework is used to prioritize sampling locations and to determine the maximum area around the seepage basins where hard measurements should be taken. Finally, in Section 8.4.4, the worth patterns of multiple hard measurements is studied. It is assumed in this Chapter that a hard measurement is identical to existing hard data and consists of a borehole and

geophysical logs including: gamma ray, self potential, and resistivity. The preposterior analysis of a soft geophysical survey that covers a large area is carried out in Section 8.5.

8.4.1 SINGLE HARD MEASUREMENT

The framework is used in this Section to determine whether a single hard measurement should be taken at point B, approximately 300 m south of the seepage basins (Fig. 8-10). A decision tree for the preposterior analysis of this measurement is shown in Figure 8-11, for C_{f7} . The expected expected objective function of the posterior best design alternative is

$$\begin{aligned}
 E[E(Z(A_D^*))] &= E(Z(A_D^*)|S_W)P(S_W) + E(Z(A_D^*)|S_{NW})P(S_{NW}) \quad (8.4) \\
 &= (-\$22\,800\,000)(0.00730) + (-\$11\,034\,000)(0.99270) \\
 &= -\$11\,119\,892
 \end{aligned}$$

Therefore, W from equation (2.30) is

$$\begin{aligned}
 W &= E[E(Z(A_D^*))] - E(Z(A_D)) \quad (8.5) \\
 &= -\$11\,119\,892 - (-\$11\,296\,000) \\
 &= \$176\,100
 \end{aligned}$$

For C_{f4} , W is reduced to \$62 400.

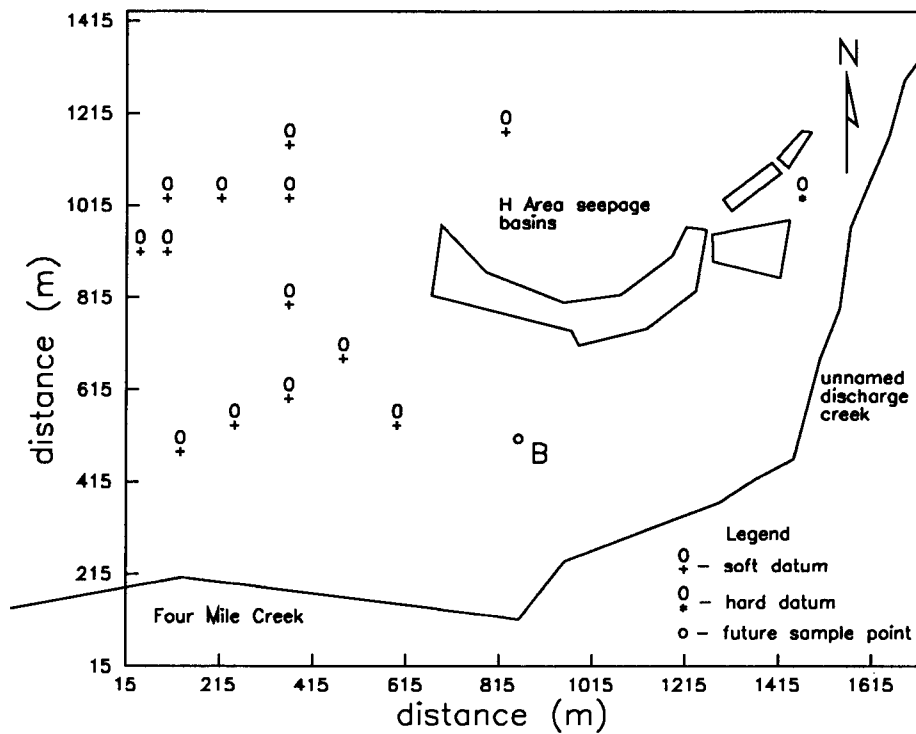


Figure 8-10: Location of hard measurement taken at point B.

We are really interested in the net worth, W_{net} of the hard measurement, where W_{net} is defined as the difference between W and the cost of taking the measurement. It represents whether the measurement is cost-effective or not. It is assumed that if the measurement, or borehole, is taken, a monitoring well will also be installed. The cost of installing a monitoring well at the SRS in 1989 dollars is approximately \$420/m. This cost includes drilling, materials, and oversight by a state registered geologist. The depth to the Green Clay at point B is approximately 33m, but it is assumed that the borehole will be drilled a further 20 m into the Congaree to ensure that the Green Clay horizon is penetrated and to get a sampling point for the hydraulic head towards the lower half of the Congaree Formation. Therefore the total cost of the borehole and monitoring well is 22 260 (\$420/m x 53m) 1989 dollars.

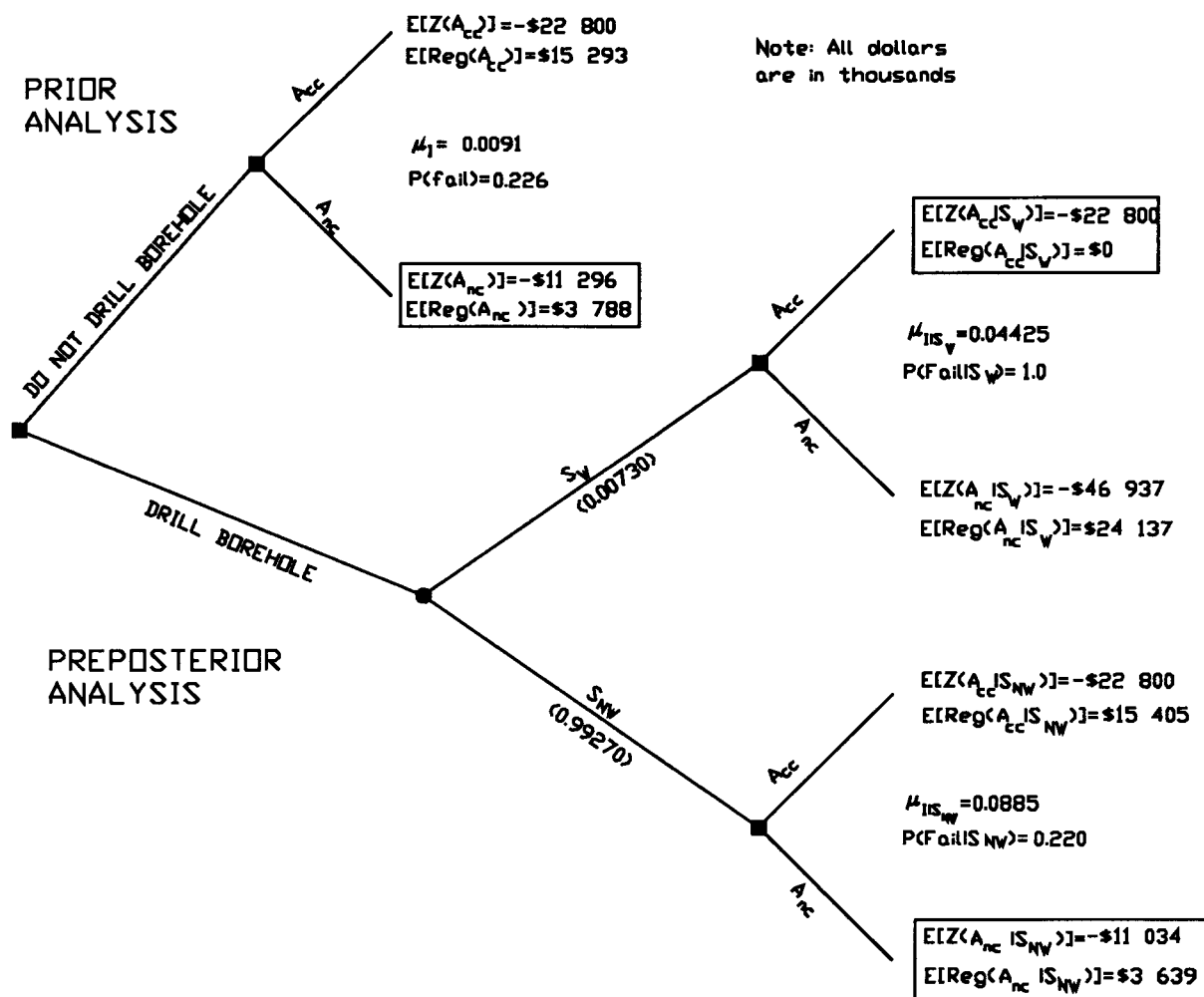


Figure 8-11: Decision tree used in preposterior analysis of hard measurement taken at point B, for cost of failure = \$70 million.

The cost of taking the geophysical logs in one borehole 50 m deep at the beginning of 1992 will be on the order of \$700 (Sperling, 1992). When all costs are discounted back at the annual rate of inflation, the total cost of the hard datum is approximately 20 000 third quarter 1985 dollars. Hence, for C_{f7} W_{net} is approximately \$156 100 (= \$176 100 - \$20 000) in third quarter 1985 dollars. For C_{f4} , W_{net} is reduced to \$42 400 (= \$62 400 - \$20 000). Note that the cost of the data worth analysis is assumed to be zero.

8.4.2 SENSITIVITY OF NET WORTH OF HARD SINGLE HARD MEASUREMENT TAKEN AT POINT B TO PARAMETERS SET UP IN BASE CASE.

In Section 8.4.1, it was determined that the hard measurement taken at point B was cost effective, or hence, that it should be taken. For this data worth analysis to be carried out, values had to be assumed for all parameters in the base case (Section 8.2). These included geostatistical parameters, hydrogeological parameters, economic parameters, and numerical artifacts of the SIS algorithm. Errors, or variations, in estimates of these parameters will cause variations in the estimated net worth of the measurement.

The purpose of the this Section is two fold. First, and foremost, it is to test the robustness of the decision made in the last Section that the measurement is cost effective. Recall that for the measurement to be cost effective, $W_{\text{net}} > \$0$. The second reason is to get an idea of how large these variations in W_{net} can be. Both of these purposes are accomplished by carrying out a sensitivity of W_{net} of the measurement taken at point B to parameters set up in the base case. These parameters include: economic and geostatistical parameters, and numerical artifacts of the SIS methodology. The sensitivity of W to hydrogeological parameters will not be studied. Recall from Chapter 7 that the following two conditions are important with respect to the hydrogeology:

- (1) The aquitard is impermeable enough to prevent major vertical migration of contamination, except where windows are present.
- (2) The vertical gradient across the aquitard is sufficient to draw contamination through a window, if present, to the lower aquifer.

The GSA hydrogeology is well understood; therefore, both of these conditions are known to be true (Refer to Section 8.1). Therefore, for simplicity it was decided not to carry out a sensitivity analysis for the hydrogeological parameters.

8.4.2.1 Numerical Artifacts

Parameters which are numerical artifacts of the SIS methodology include the number of blocks into which the aquitard has been discretized, the starting seed, the number of the first aquitard block generated, and the number of realizations generated.

The sensitivity of the net worth to aquitard discretization was studied by carrying out the preposterior analysis using five different densities of aquitard discretization, or finite difference mesh (Table 8-4).

Recall, each finite difference cell represents one aquitard block.

grid size	aquitard block dimension (m)
40 x 33	43
50 x 42	35
60 x 50	29
70 x 59	25
80 x 67	21

Table 8-4: Aquitard discretizations used in evaluating net worth of hard measurement taken at point B.

For C_{f7} as the aquitard block size changes, W_{net} fluctuates randomly and very slightly about its mean value (Fig. 8-12) with a standard deviation of \$3 820. This standard deviation is only 2.6% of the mean of \$151 040. For C_{f4} the fluctuations are similar with a standard deviation of \$2017. This standard deviation corresponds to only 3.4% of the mean of \$58 900. Note, that a block size of 29 m is used in the base case.

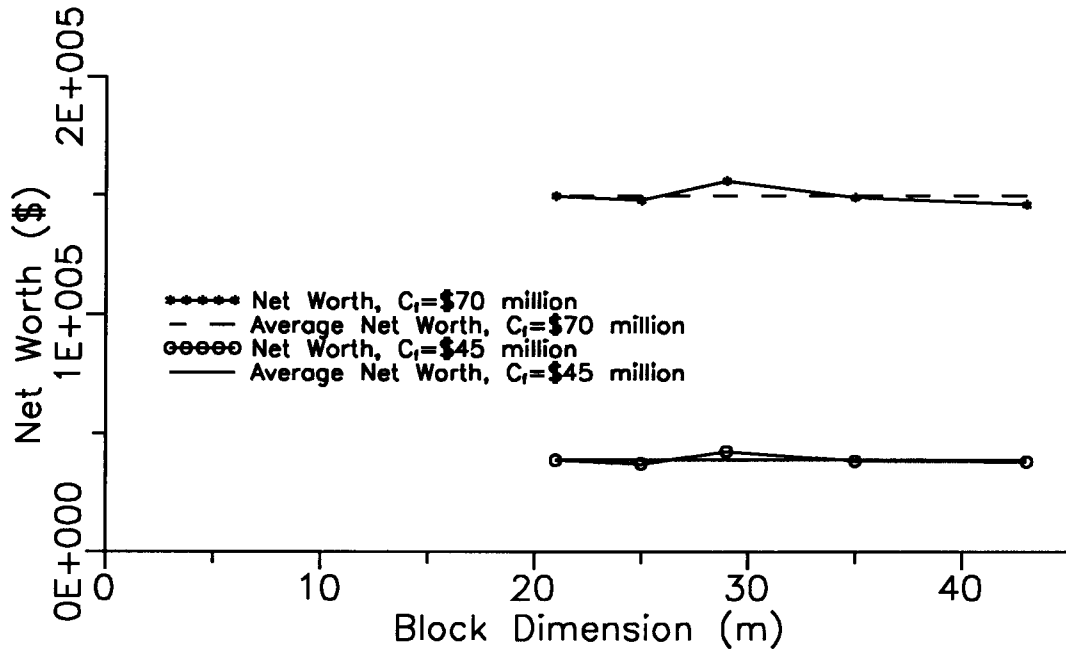


Figure 8-12: Sensitivity of net worth to aquitard block discretization.

For both C_{f7} and C_{f4} , W_{net} has very little sensitivity to the starting seed, the number of the first aquitard block generated, or the number of realizations. For all cases, it fluctuates randomly and slightly about its mean value. The standard deviations of the fluctuations are \$835, \$3 147, and \$3 121 for the number of realizations, the starting seed, and the number of the first aquitard block generated, respectively. The standard deviation of the total random error from all of the numerical artifacts in W_{net} from equation (6.15) is

$$\begin{aligned}
 \sigma_{W_{net}} &= \left(\sum_{i=1}^4 \sigma_{W_{net_i}}^2 \right)^{1/2} \\
 &= (\$3\,820^2 + \$835^2 + \$3\,147^2 + \$3\,121^2)^{1/2} \\
 &= \$5\,910
 \end{aligned}
 \tag{8.6}$$

Therefore, the standard deviation of the total random error is only 3.4% of W_{net} of \$156 400 evaluated for the hard datum taken at point B. For C_{f4} , the standard deviations of the fluctuations are \$474, \$1917,

and \$1968 for the number of realizations generated, the starting seed, and the number of the first aquitard block generated. The total standard deviation is \$3441 which is only 12.3% of the W_{net} of \$42 000.

In summary, for both costs of failure, parameters which are numerical artifacts will only have a small effect on W_{net} of the measurement taken at point B and hence will not affect whether it is cost-effective or not.

8.4.2.2 Economic Parameters

The value of W_{net} is almost equally sensitive to the discount rate for both costs of failure (Fig. 8-13). As the discount rate increases, W_{net} decreases. The bounds over which the measurement is cost-effective is wide for both cost of failure. For C_{f4} , the discount rate must increase to 0.15, while for C_{f7} , it must increase to greater than 0.15, before the measurement is no longer cost-effective.

Errors of more than a few percent in the discount rate are unlikely; therefore, W_{net} will have a positive value for all likely discount rates. Therefore, for the example carried out here, the discount rate is not a critical parameter in determining whether the measurement is cost-effective or not. However, as C_f decreases, it will become more important.

Turning now to the cost of failure, W_{net} is zero for $C_f < \$35$ million, but then increases linearly with C_f (Fig. 8-14). C_f could be a critical parameter in determining whether the datum is cost-effective. A 50% decrease in the base case C_f of \$70 million would result in $W_{\text{net}} = \$0$. Unfortunately, a 50% error in the estimated C_f is possible since as discussed in Section 8.3, it is very hard to estimate.

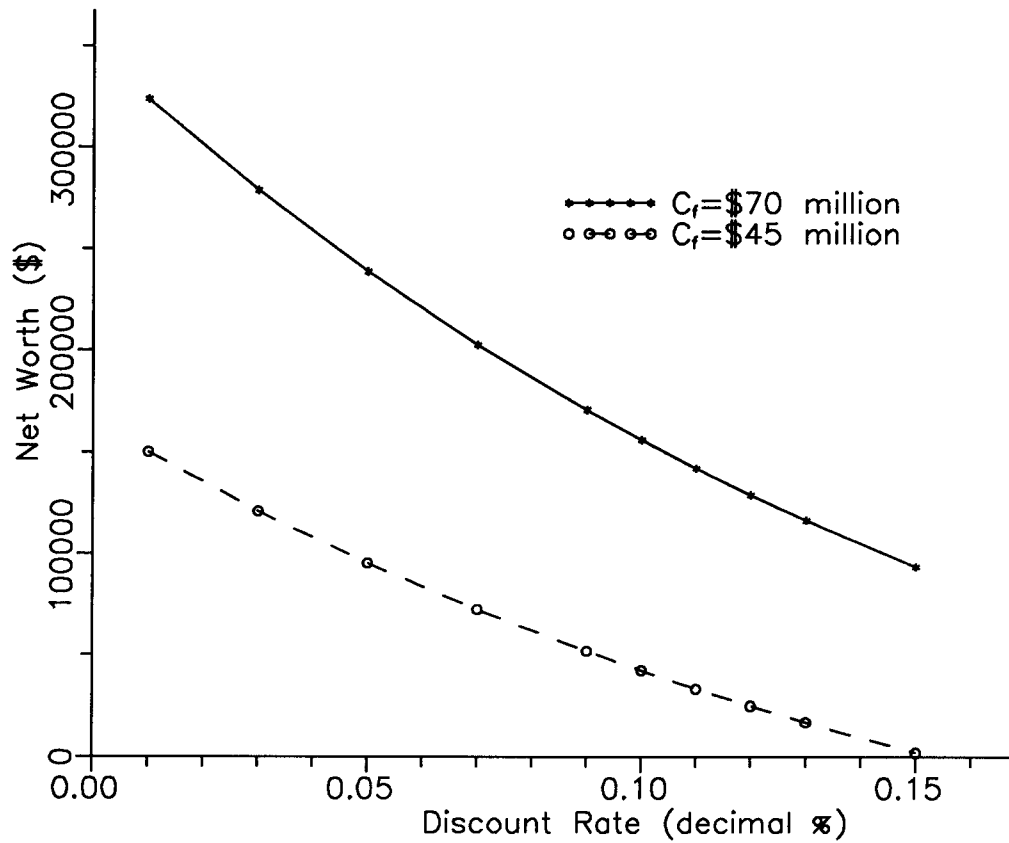


Figure 8-13: Sensitivity of net worth to the discount rate.

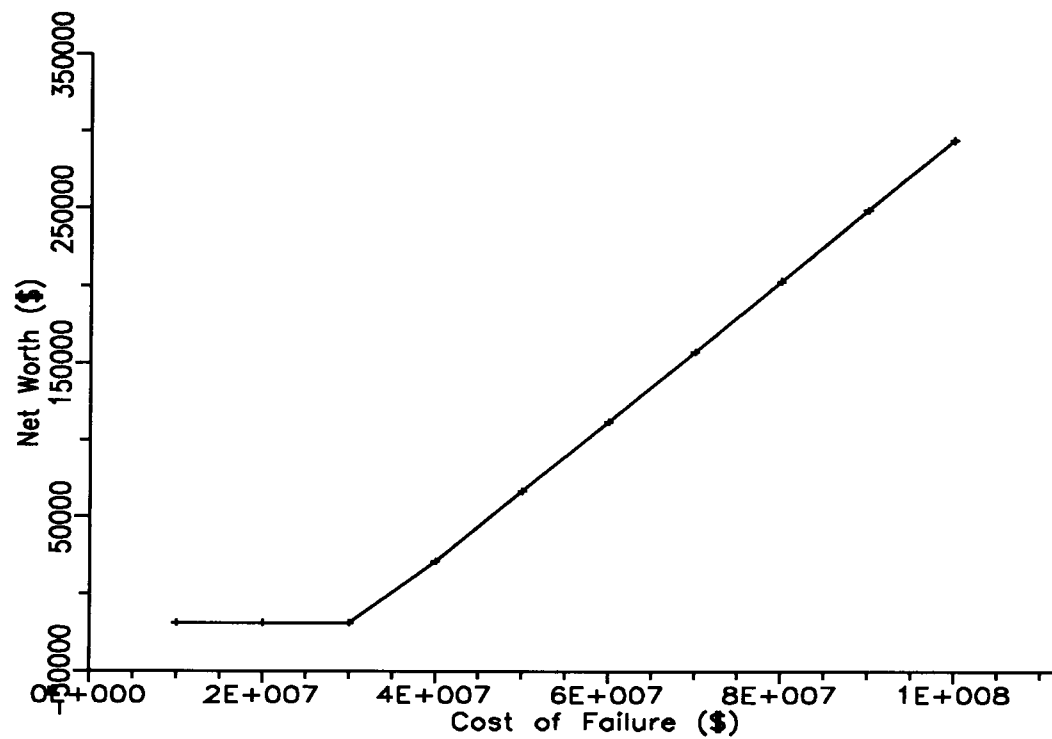


Figure 8-14: Sensitivity of net worth to cost of failure.

With respect to the known cost of failure, W_{net} has a similar sensitivity to the cost of the clay cap, C_{cc} , for both C_{f7} and C_{f4} (Fig. 8-15). For C_{f7} , the measurement is cost-effective for C_{cc} between \$15 million and \$40 million. The estimated base case value of C_{cc} is \$22.3 million. Therefore, an underestimate of 50% or an over estimate of 100% is necessary to reduce the W_{net} to zero. For C_{f4} , C_{cc} has a greater impact on the measurement's cost-effectiveness. The measurement is cost-effective for C_{cc} between \$10 and \$29 million. The base case value of C_{cc} now only has to increase by 30% to make the measurement no longer cost-effective.

The value of C_{cc} will be much easier to estimate than C_f because the time horizon of construction will be much shorter and will involve many fewer uncertainties. Therefore, for high C_f , C_{cc} will likely have little impact on the cost-effectiveness of the measurement. However, this impact will grow as the cost of failure decreases.

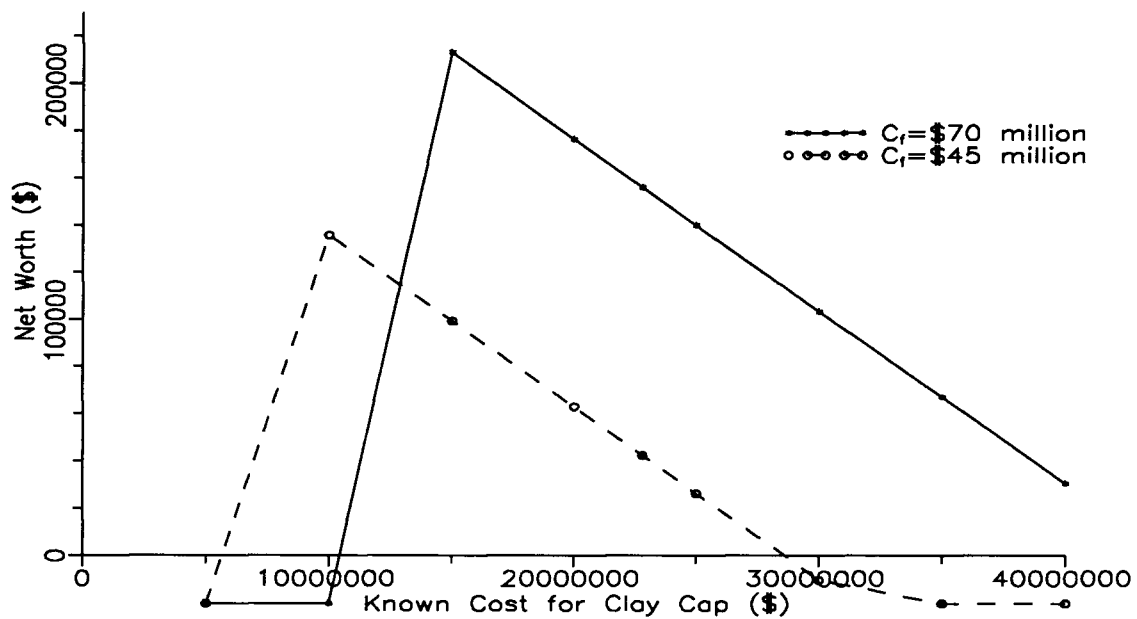


Figure 8-15: Sensitivity of net worth to known cost of lay cap alternative.

The value of W_{net} has an identical sensitivity to the known cost of the no clay cap alternative, C_{nc} for both C_{f7} and C_{f4} . The measurement is cost-effective for $C_{\text{nc}} < \$10$ million, for both costs of failure. Therefore, C_{nc} must at least triple before the measurement is no longer cost-effective. The value of C_{nc} should be easy to estimate. Therefore, uncertainty in C_{nc} is unlikely to affect the measurement's cost-effectiveness.

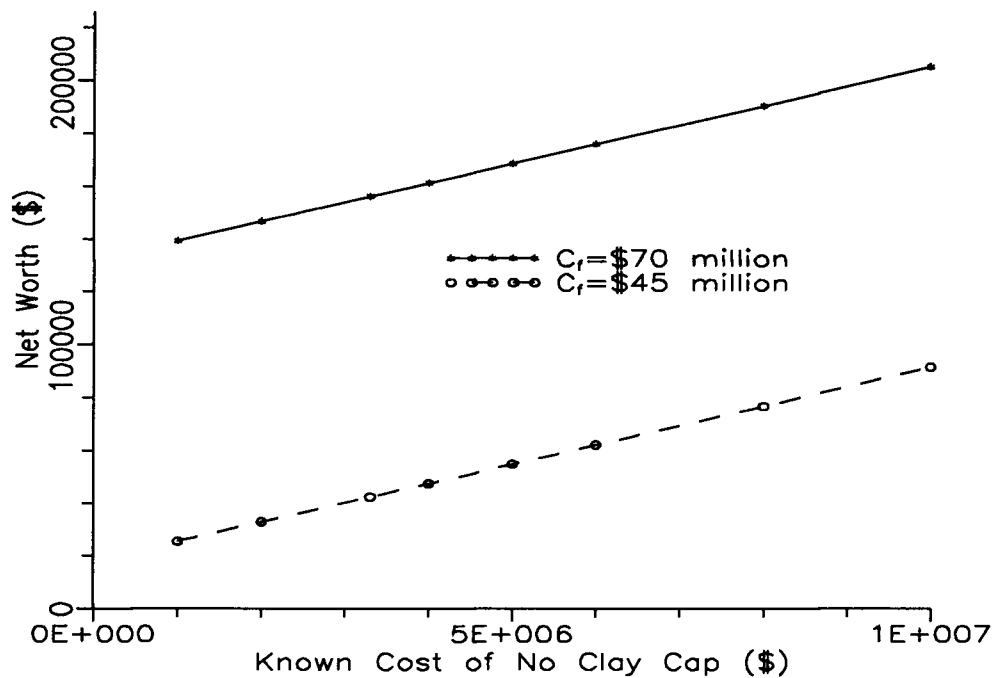


Figure 8-16: Sensitivity of net worth to known cost of no clay cap alternative.

8.4.2.3 Geostatistical Parameters

The sensitivity of W_{net} to the geological estimate of the mean, m_I , is shown in Figure 8-17, for both costs of failure. The measurement is cost-effective for $0 < m_I < 0.16$ for C_{f7} and for all values of m_I tested for C_{f4} . Therefore, there is a large margin of error over which the net worth will maintain a positive value and measurements will be cost-effective. However, it is impossible to estimate possible errors in the

geological estimate of the mean because of a lack of available data. The geological estimate of the mean could potentially be a critical parameter in determining whether the measurement is truly cost-effective.

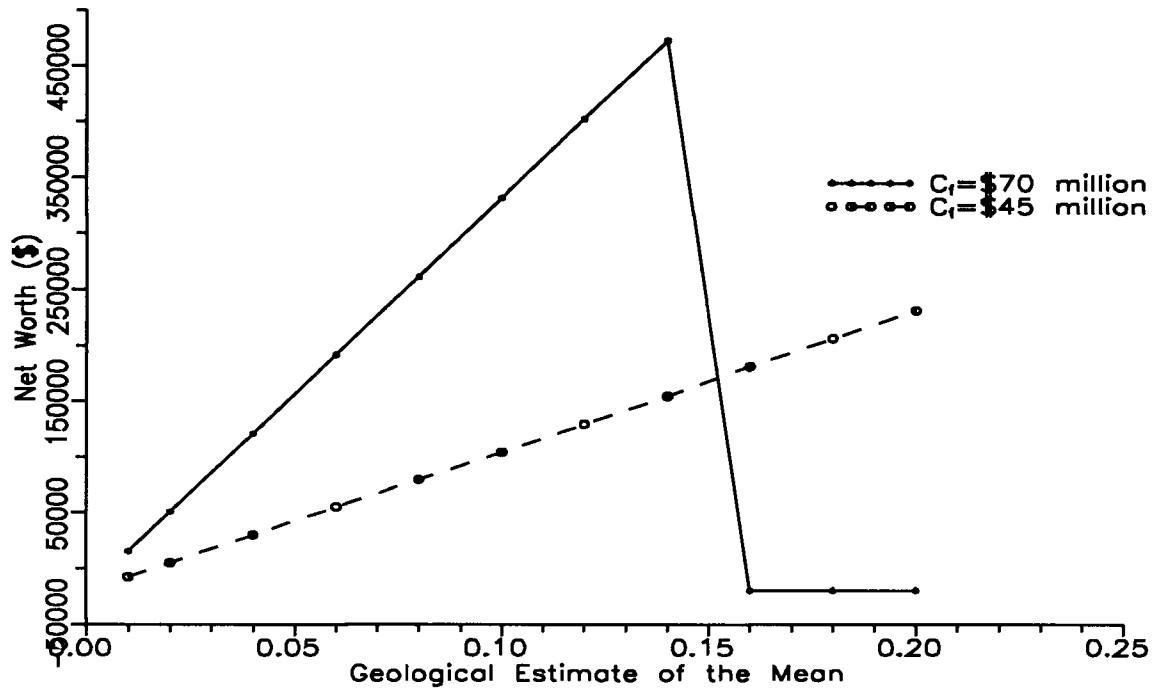


Figure 8-17: Sensitivity of net worth to geological estimate of mean.

The value of W_{net} is relatively insensitive to λ_1 for both costs of failure. $W_{\text{net}} > \$0$, and hence the measurement is cost-effective for $60 \text{ m} < \lambda_1 < 250 \text{ m}$ for C_{f7} and $20 \text{ m} < \lambda_1 < 300 \text{ m}$ for C_{f4} (Fig. 8-18). Correlation lengths greater than 250 m become difficult to study because λ_1 becomes a significant percentage of the domain and the generated realizations do not reproduce the statistical parameters used to generate them. The correlation length for this case study and likely for many others, is difficult to measure because of a lack of information. Nevertheless, it seems to be potentially a less critical parameter than other parameters such as the cost of failure and m_1 . Correlation lengths greater than 60 m are likely for an aquitard formed in a deep marine environment such as the Green Clay.

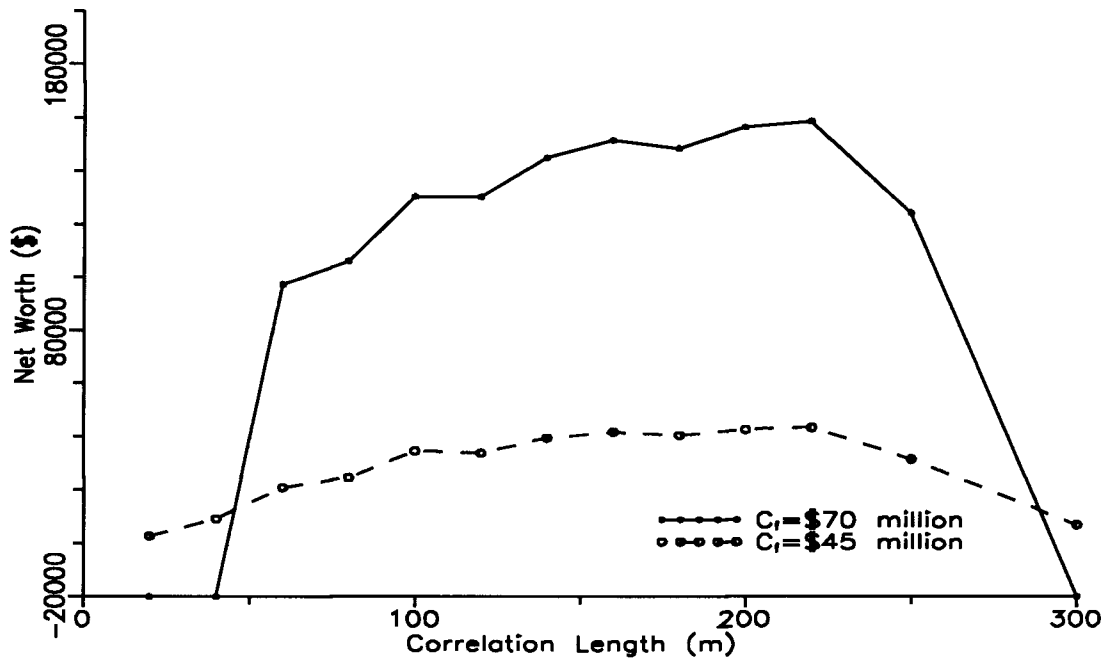


Figure 8-18: Sensitivity of net worth to correlation length.

The sensitivity of W_{net} to the confidence in the geological estimate of the mean is shown in Figure 8-19, for both C_{f7} and C_{f4} . Note that the confidence is quantified in terms of an equivalent number, n_e , of independent hard data. The measurement is cost-effective for $1 < n_e < 29$ for C_{f7} and $1 < n_e < 30$ for C_{f4} . Those bounds correspond to weights of 21.05 and 589.5 for the prior geological mean compared to a weight of 336.2 for the 40 existing hard data. It is extremely unlikely that the weight of the geological mean is greater than that of 40 hard data points, or equal to zero. Therefore, the net worth will be positive, and the datum cost-effective, for all likely values of the prior confidence in the geological estimate of the mean.

Note that at $n_e = 0$, $W_{\text{net}} = \$20,000$. At $n_e = 0$, the estimate of the mean is based completely on the sample data which estimates a mean value of zero. A mean value of zero allows no windows to occur and hence does not allow for failure to occur. If failure cannot occur, $W = \$0$.

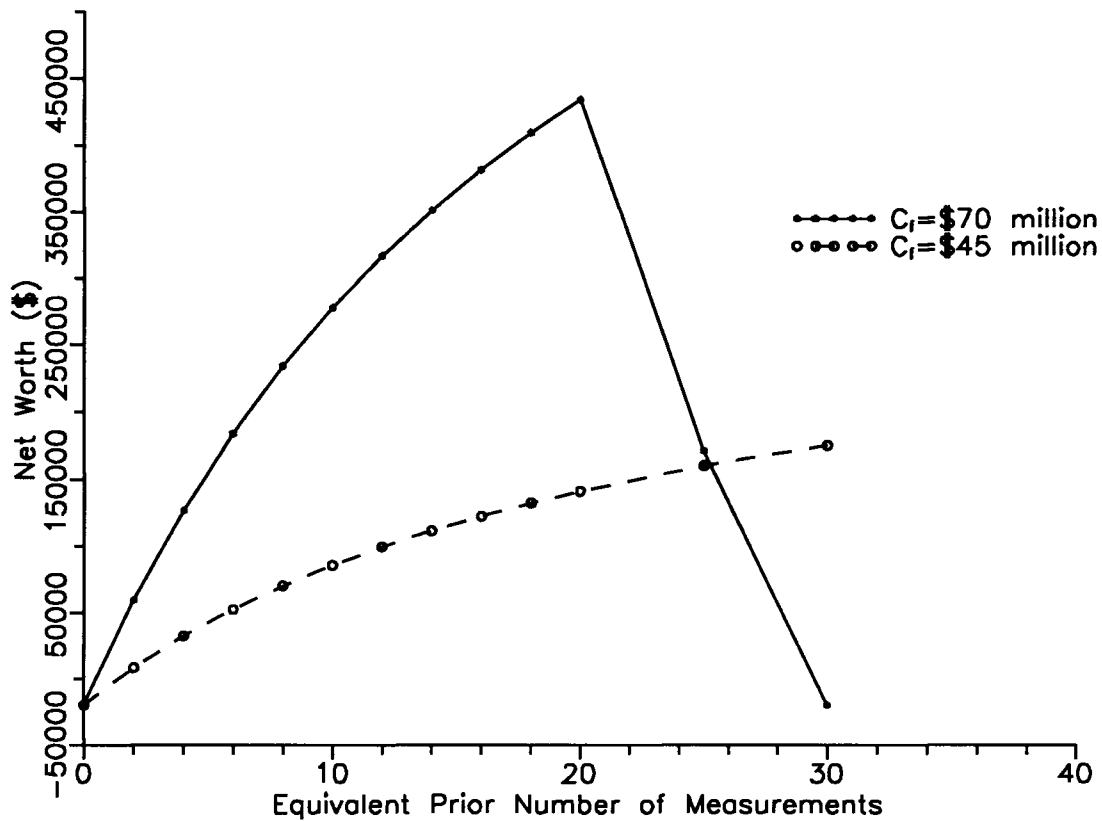


Figure 8-19: Sensitivity of net worth to confidence in prior estimate of mean.

8.4.3 NET WORTH OF SINGLE, HARD MEASUREMENT TAKEN AT DIFFERENT LOCATIONS

In Section 8.4.1 it was determined that a hard measurement taken at point B was cost effective. Section 8.4.2 studied the robustness of this decision. In Section 8.4.3, the framework will be used to make two more realistic and useful data worth decisions. The first is sequentially locating measurement points and the second is determining the maximum size of a grid of measurement points. The former question is more important because sampling programs are much more likely to be carried out in sequential stages of a few measurements at a time, rather than many measurements taken simultaneously on a large grid.

Both of these decisions can be made by estimating W_{net} at a large number of points around the seepage basins and contouring the results. A contour map of W_{net} is shown in Figure 8-20 for C_{f4} . It is assumed

that the cost of taking a hard measurement is constant throughout the region of study. The net worth is a maximum of approximately \$50 000 in the south east corner between the seepage basins and two creeks.

The maximum occurs in this area because it is the most probable location for the contaminant plume.

Refer to Figure 8-5 for the most probable contaminant plume locations.

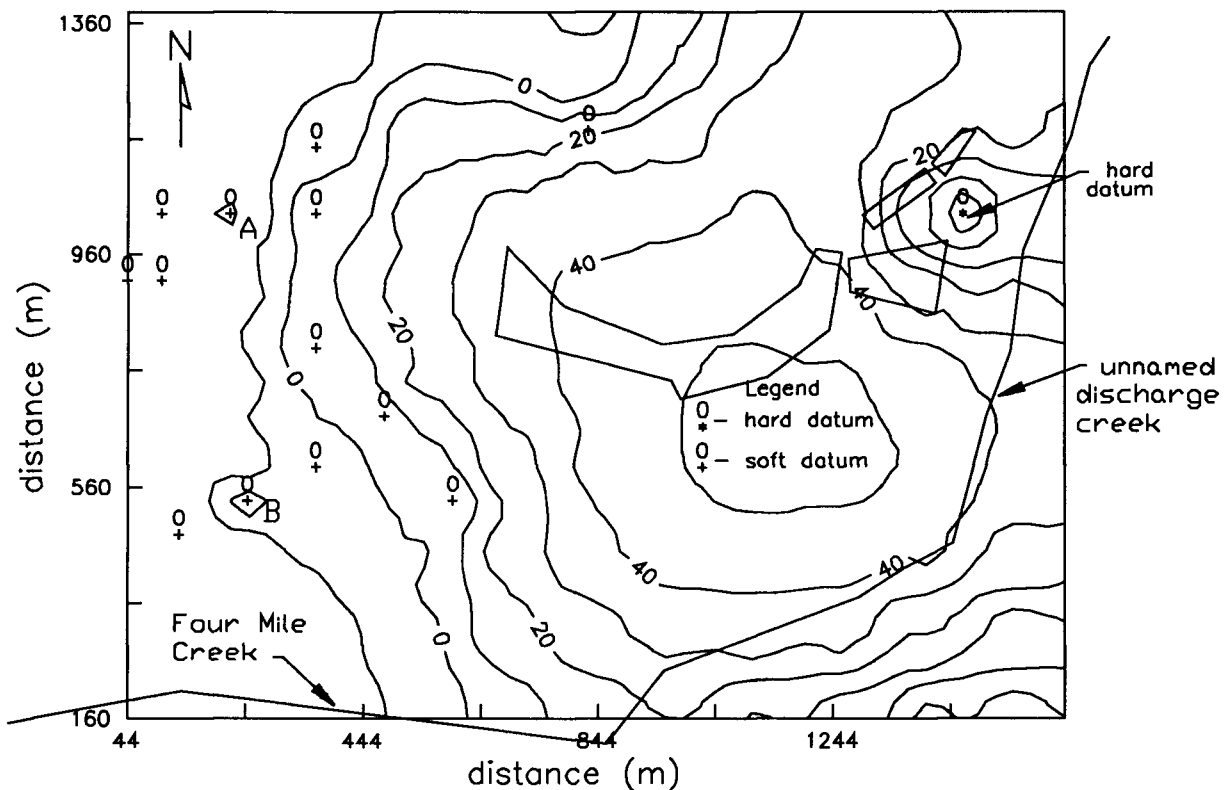


Figure 8-20: Contour map of net worth of a single, hard measurement taken at different locations for cost of failure = \$45 million. (Numbers are in thousands of dollars.)

The value of W_{net} decreases towards the west and north of the seepage basins because of both the conditioning effect of existing soft data and the reduced likelihood of a window causing a failure.

Windows towards the north and west are less likely to cause failure because they are further from the likely path of contaminant plumes.

The strong effect of an existing hard datum on W_{net} is shown by the depression in the north east corner where W_{net} is reduced to -\$20 000. The value of W_{net} decreases as the sampling location approaches the

existing datum because of the correlation effect. The much weaker correlation effect of existing soft data on W_{net} is shown by soft data at points A and B west of the seepage basins.

Note that hard measurements taken on the opposite side of Four Mile Creek and the unnamed creek in the south east corner of the map have a net worth of up to \$40 000, even though the creeks prevent contamination from reaching any window located there. However, because of spatial correlation, a window there may extend across the creeks, allowing failure to occur. Therefore, sampling outside of the zone of where failure can occur can have significant value.

A sequential sampling program could be easily designed as follows. In the first step, a contour map of W_{net} would be created. In the second step, the measurement would be located where W_{net} was a maximum. After the measurement was taken, a new contour map would be produced to locate the next measurement location. Sampling would continue as long as the maximum $W_{\text{net}} > \$0$. The robustness of a decision to take a measurement could be tested by carrying out a sensitivity analysis of measurement's W_{net} to base case parameters.

The contour map can be used as well to determine the maximum limits of a zone over which a grid of measurement points can be taken. For C_{f4} , this zone is bounded by the \$0 W_{net} contour to the west and north-west, Four Mile Creek to the south and the unnamed creek to the east. A small portion of the zone's north end is off the map. However, the exact boundaries of this zone are uncertain. A contour map of W_{net} is shown in Figure 8-20, for C_{f7} . It is very similar to that for C_{f4} , except that W_{net} has increased in value and the area where measurements are cost-effective has increased. Note that a hard measurement now is cost-effective at every location in the region of study, except at the existing hard datum. Therefore, the zone in which hard measurements are cost-effective is variable and depends on the base case parameters, such as the cost of failure. Note, however, that the location of the maximum W_{net} , and hence the highest priority measurement location, has not changed.

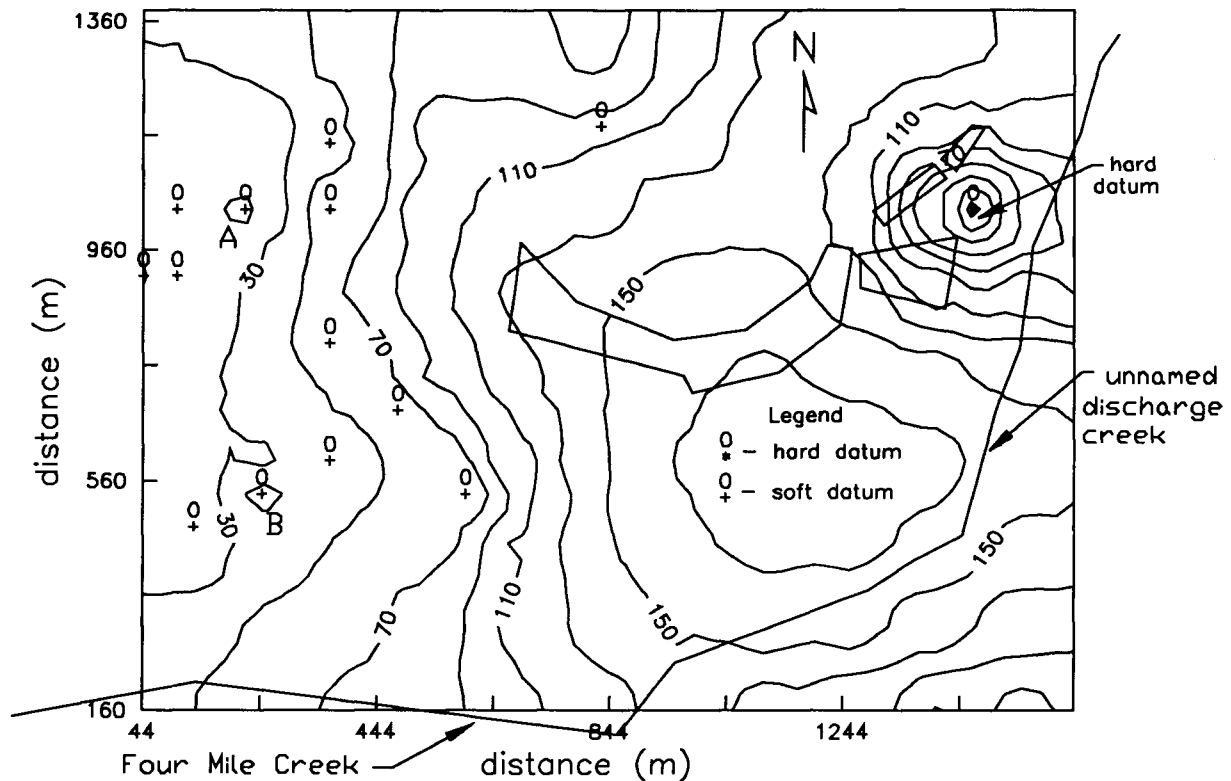


Figure 8-21: Contour map of net worth of a single, hard measurement taken at different locations for cost of failure = \$70 million. (Numbers are in thousands of dollars.)

8.4.4 PATTERNS OF MULTIPLE, HARD MEASUREMENTS

Section 8.4.4 evaluates the worth of patterns of multiple hard measurements. Three patterns of 1,2,3,4, and 5 measurements taken on 29, 145, and 290 m spacing are used. These patterns are shown in Figures 8-22 to 8-24. The data are collected in the order of the numbers marking the measurement points. Note that point 1 is the same for all three patterns. The patterns were picked where W_{net} at the individual measurement points was reasonably constant.

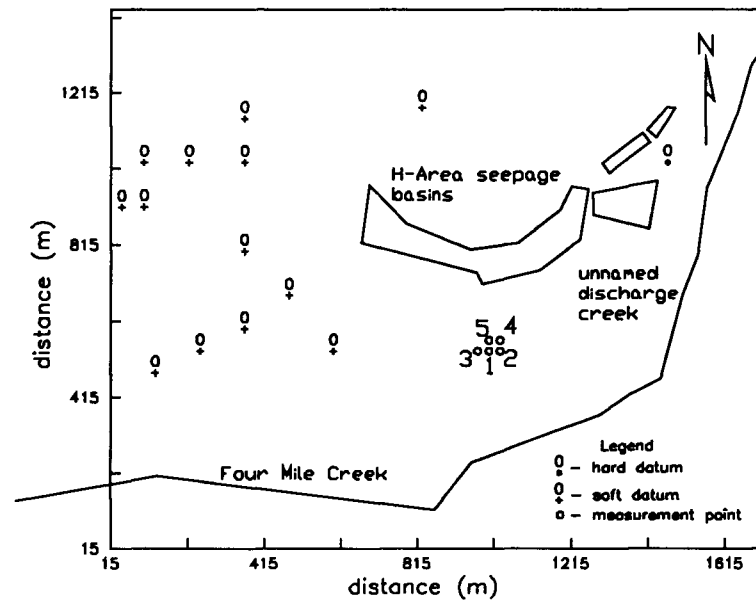


Figure 8-22: Pattern of hard measurement taken on a 29 m spacing.

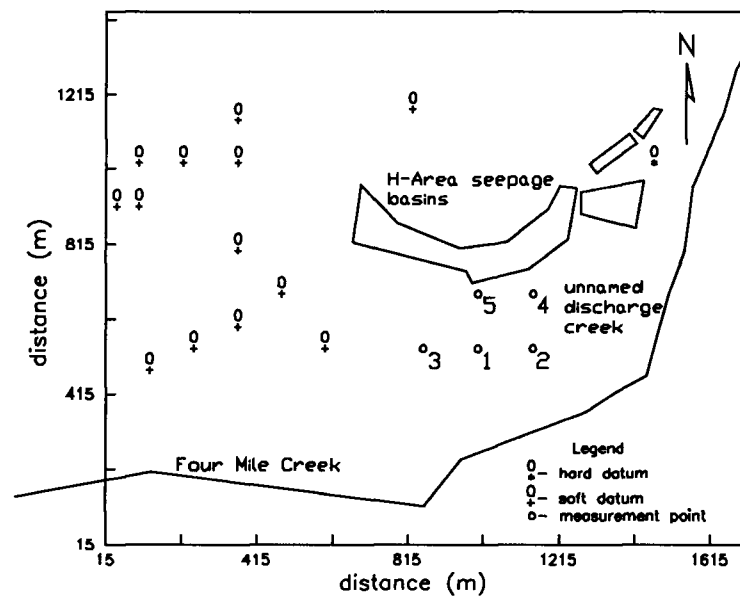


Figure 8-23: Pattern of hard measurement taken on a 145 m spacing.

The patterns were restricted to a maximum of five data because of the CPU time involved in carrying out the data worth analysis. Recall that 100×2^n realizations are needed to estimate the worth of the pattern, where n is the number of measurements in the proposed pattern. Therefore, 3200 realizations are required to evaluate the worth of a pattern of five measurements.

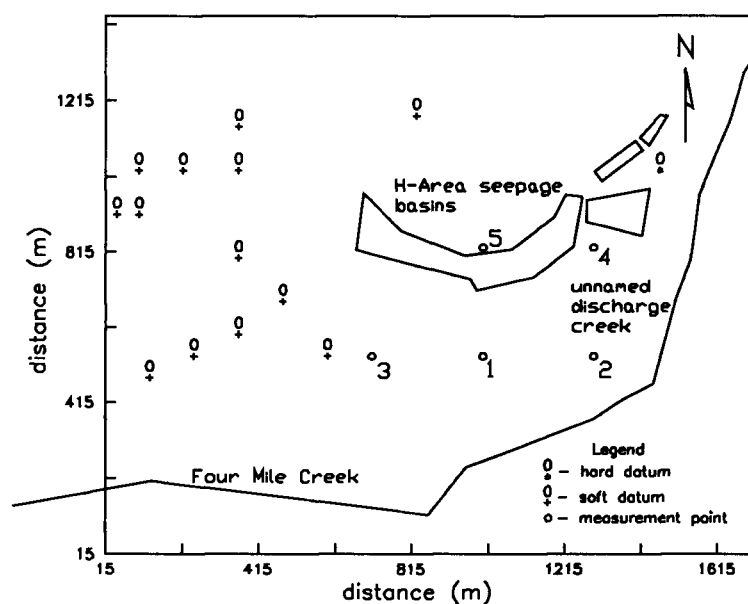


Figure 8-24: Pattern of hard measurement taken on a 290 m spacing.

The value of W_{net} for the patterns are shown in Figure 8-25, for C_{f7} . W_{net} initially increases with the number of measurements in the pattern. The greater the separation distance between the adjacent measurement, the greater the initial increase. This behavior is because the more independent the data, the greater their W_{net} . However, for the 29 m spacing pattern, W_{net} reaches a maximum at 3 measurements and then starts to decline. A similar behavior is shown for the 145 m spacing pattern where a maximum is being approached at five measurements. This maximum is at a greater number of measurement than the 29 m spacing pattern because of the greater separation distance and independence of the measurements. The value of W_{net} continually increases over the five measurements for the 290 m spacing. Note that all patterns are cost-effective.

The net worth for the patterns are shown in Figure 8-26, for C_{f4} . Note that W_{net} for all patterns has been reduced below that for C_{f7} . The value of W_{net} for the pattern on a 29 m spacing continually decreases as the number of measurements increases and becomes negative for greater than five measurements. For the patterns on the 145 m spacing, W_{net} initially increases and reaches a maximum at four measurement and

then starts to decrease. The measurements on the 290 m spacing are almost independent; therefore, W_{net} increases continuously between one and five measurements. Note, that all patterns except five measurement on the 29 m spacing are cost-effective.

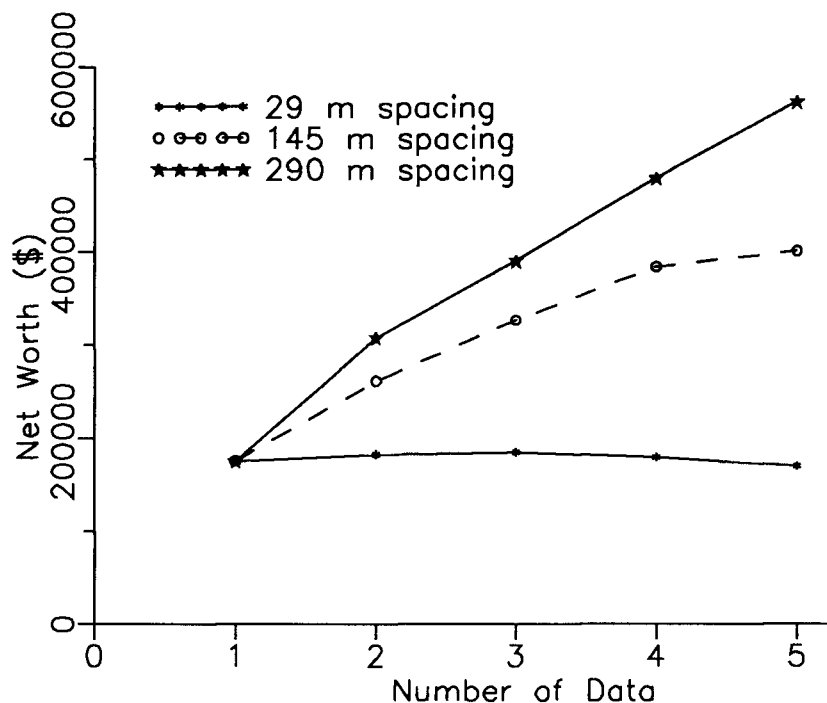


Figure 8-25: Net worth of multiple hard measurements taken at spacings of 29, 145, and 290 m versus number of measurements taken, for cost of failure = \$70 million

The most cost effective pattern was the five measurements with the 290 m spacing. With the 290 m spacing, no limit was found for the optimum number of measurements. The measurements are independent enough that their net worth increases with the number of measurements. However at smaller spacing, or with much existing data, spatial dependence will become important. Under these conditions, the net worth will increase with the number of measurements, reach a maximum and then start to decrease. Hence there will be an optimum number of measurements, which may be as small as one.

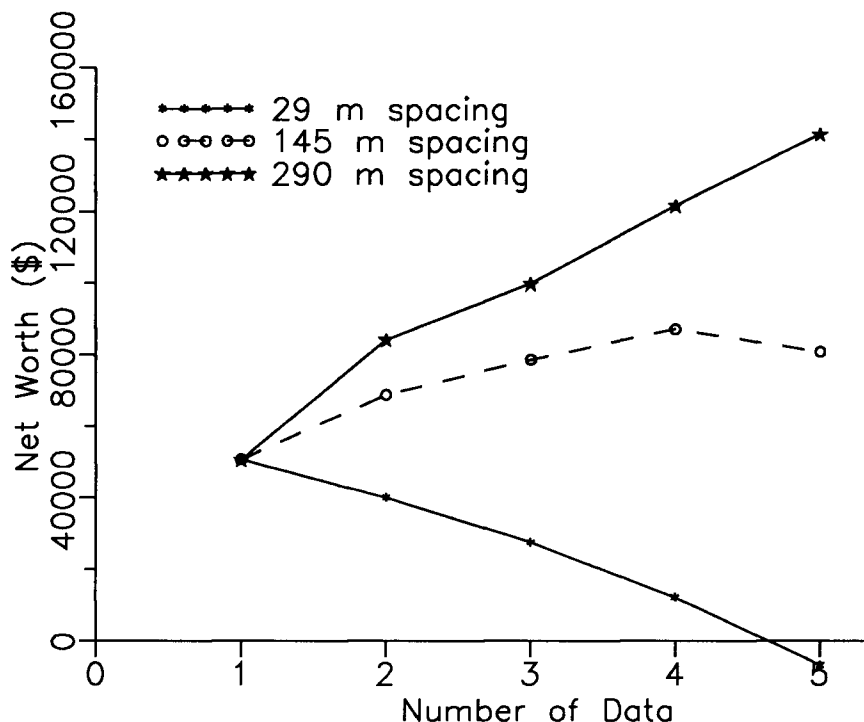


Figure 8-26: Net worth of multiple hard measurements taken at spacings of 29 145 and 290 m versus number of measurements taken, for cost of failure = \$45 million.

The framework could be easily used to design sequential sampling programs involving multiple measurements. In the first step, a contour map of the net worth for a single measurement would be produced and the location of the maximum net worth found. In the second step, the measurements would be located in the region of the maximum net worth. The optimum number and spacing of the measurements would then be determined. Once the measurements were taken, a new contour map would be created to pick out the next measurement locations. Measurements would be taken as long as the maximum net worth was $> \$0$. The robustness of a decision to take a pattern of measurements could be tested by carrying out a sensitivity analysis of the measurements' W_{net} to base case parameters.

8.5 PREPOSTERIOR ANALYSIS OF SOFT, AREAL SURVEY

Section 8.5 evaluates the worth of a soft, areal survey. The assumptions behind the methodology used here are discussed in Section 6.5. It will be assumed that a reflection seismic survey will be carried out.

Based on cost alone, a radar survey would likely be the measurement of choice for delineating shallow stratigraphy. However, a radar survey would unlikely be feasible because it would probably not be able to map the stratigraphy down to the 30 m depth of the Green Clay. Groundwater, the Tan Clay, and clay lenses in the Barnwell and McBean Formations would likely attenuate the radar too much (Knoll, 1992).

It is assumed that the smallest discontinuity will represent a 29 m square. An absolute minimum of two measurements, or geophones, on a line across a window would be required to sample it (Cross, 1992). To be conservative, it is assumed that geophones will be placed on a square grid every five meters to ensure that an adequate number of sampling points fall within any potential window. The analysis will be carried out here for a cost of failure of \$45 million.

Recall that the survey covers the entire area where windows can result in a failure which causes a change in A_D . This area is marked by the \$1 000 contour of the total worth of a single hard measurement and Four Mile Creek and the unnamed discharge creek (Fig. 8-27). (Measurement points to the west of the \$1000 contour are actually equal to \$0.) Its exact size is not known because part of it is off the north end of the map; however, it will be estimated here that the entire area is approximately equal to a 1.3 x 1.3 km square. It is assumed that the total cost of carrying out a seismic survey on a square grid with a five meter spacing over this area is on the order of \$200 000. Road access, type of geology, and other factors are ignored in this estimate. A more detailed cost estimate would required for an in depth analysis.

When discounted back to 1985 at the rate of inflation, the cost of the survey is approximately \$163 000.

Note from Section 8.4, that the area of the survey, and hence total cost, is a function of the cost of failure.

The following likelihood functions for the survey are assumed:

$$P(S_{W_{fd}} | W_{fd}) = 0.2 \quad (8.7)$$

$$P(S_{W_{fd}} | NW_{fd}) = 0.$$

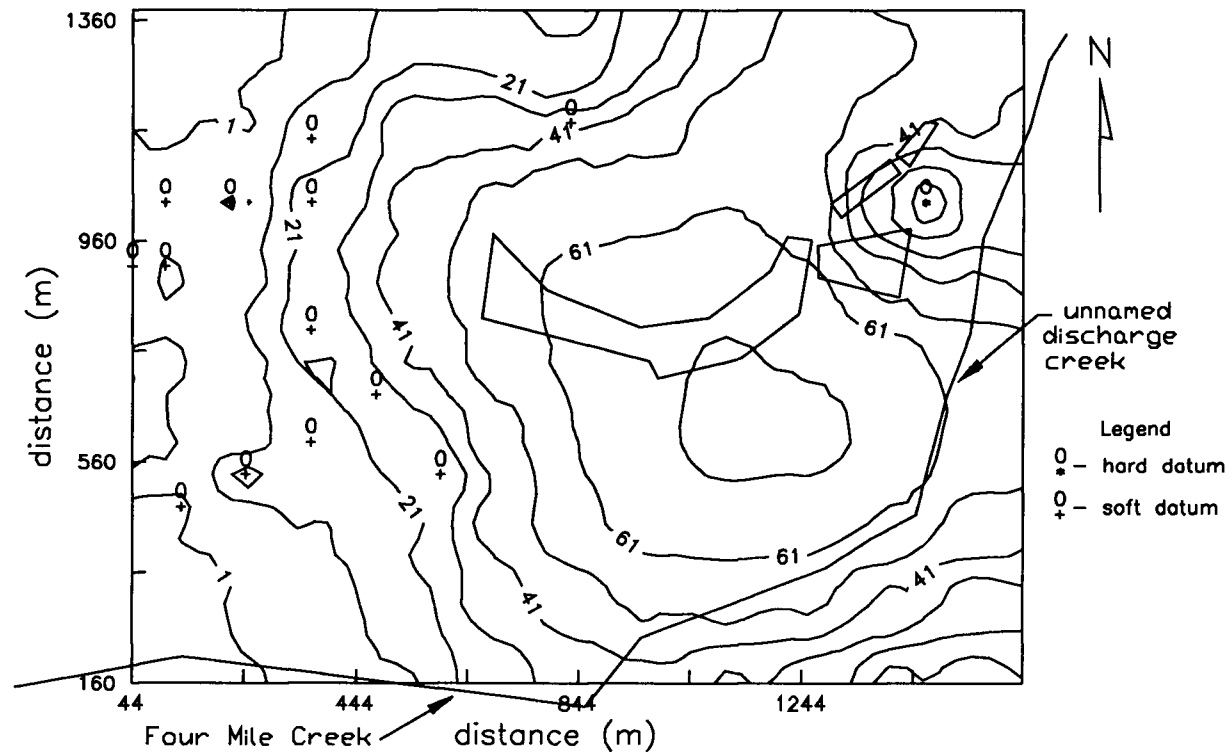


Figure 8-27: Contour plot of total worth for single, hard, point measurements taken throughout the region of study, for cost of failure = \$45 million. (All numbers are in thousands of dollars.)

where W_{fd} represents a window is present which will cause a failure which will alter the prior best design and NW_{fd} represents no window is present which will alter the prior best design. In other words,

$$P(S_F|F) = 0.2 \quad (8.8)$$

$$P(S_F|NF) = 0.$$

where F denotes failure and NF , no failure.

The decision tree used in the prior and the preposterior analysis is shown in Figure 8-28. Note that the decision tree now resembles the decision tree used for the univariate case presented in Chapter 2.

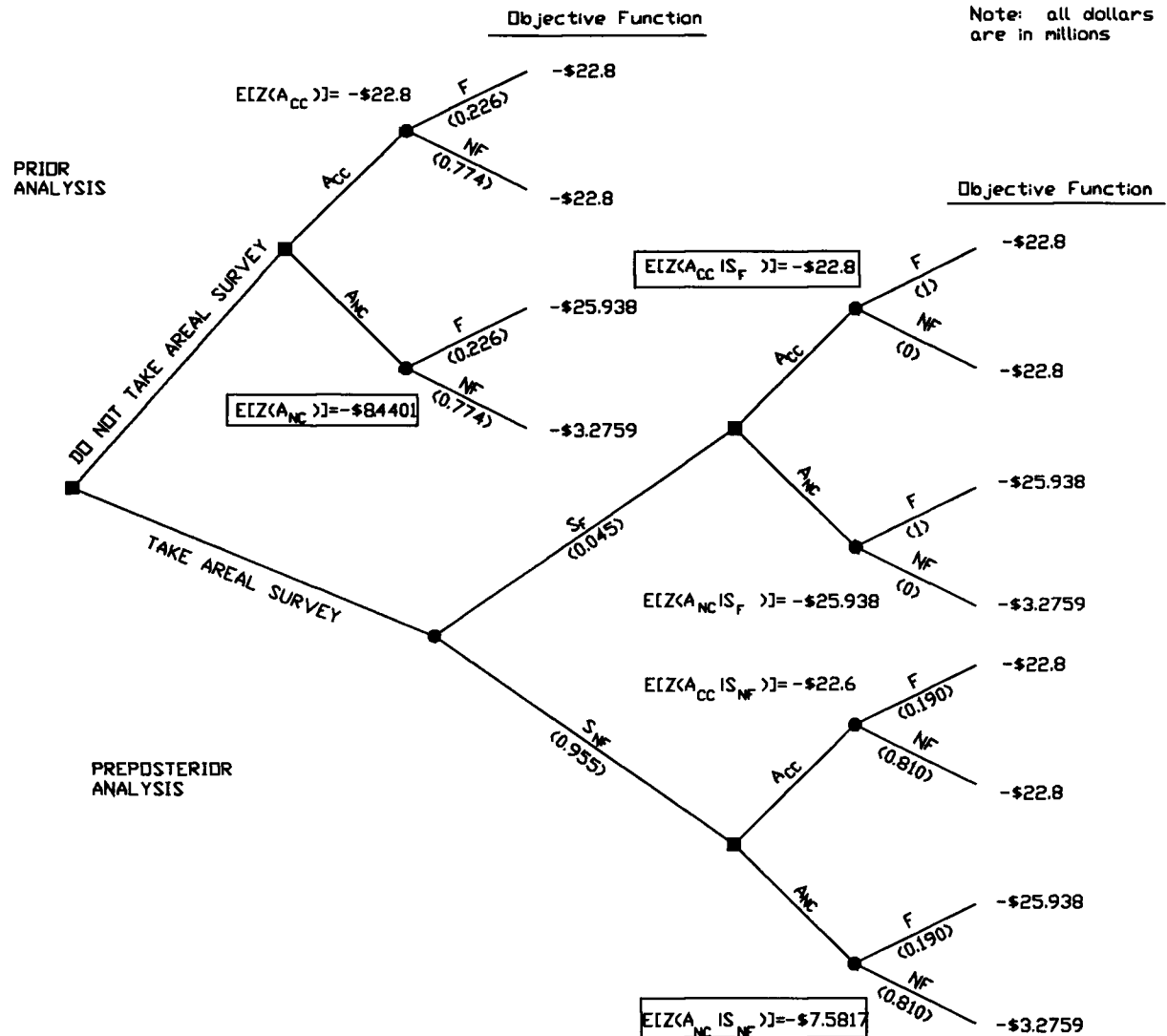


Figure 8-28: Decision tree used in preposterior analysis of soft geophysical survey.

From the prior analysis, the prior probability of failure, $P(F)$, is 0.266 and the expected objective functions for the two alternatives are

$$\begin{aligned}
 E(Z(A_{CC} | \text{Failure})) &= -\$22.8 \text{ million} \\
 E(Z(A_{CC} | \text{No Failure})) &= -\$22.8 \text{ million} \\
 E(Z(A_{NC} | \text{Failure})) &= -\$25.938 \text{ million} \\
 E(Z(A_{NC} | \text{No Failure})) &= -\$3.2759 \text{ million.}
 \end{aligned}$$

The prior best design alternative is A_{NC} with an expected objective function of -\$8.4401 million
 $((0.226)(-\$25.938 \text{ million}) + (0.774)(-\$3.2759 \text{ million})).$

The updated probability of failure, $P(F|S_F)$, from Bayes' equation, given that a window/failure is sampled, is

$$P(F|S_F) = \frac{P(S_F|F)P(F)}{P(S_F)} \quad (8.9)$$

where

$$\begin{aligned} P(S_F) &= P(S_F|F)P(F) + (P(S_{NF}|NF)P(NF)) \\ &= (0.2)(0.226) + (0)(1 - 0.226) \\ &= 0.045 \end{aligned} \quad (8.10)$$

Therefore,

$$P(F|S_F) = \frac{(0.2)(0.226)}{0.045} = 1$$

and

$$\begin{aligned} P(F|S_{NF}) &= \frac{P(S_{NF}|F)P(F)}{P(S_{NF})} \\ &= \frac{(0.8)(0.226)}{(1 - 0.045)} = 0.190 \end{aligned} \quad (8.11)$$

The expected expected objective function for the best posterior design is

$$\begin{aligned} E[E(Z(A_D'))] &= E(Z(A_D'|S_F))P(S_F) + E(Z(A_D'|S_{NF}))P(S_{NF}) \\ &= (-\$22\,800\,000)(0.045) + (-\$7\,581\,700)(0.955) \end{aligned} \quad (8.12)$$

$$= -\$8\,266\,524$$

Therefore, the worth of the soft, areal survey is

$$\begin{aligned} W &= E[E(Z(A_D'))] - E(Z(A_D)) & (8.13) \\ &= -\$8\,266\,524 - (-\$8\,440\,100) \\ &= \$0.173 \text{ million} \end{aligned}$$

Therefore, W_{net} is \$13 000 (\$173 000 - \$163 000) and the geophysical survey is cost-effective. However, as noted in Section 6.5, W_{net} for the survey is highly uncertain; therefore, our major concern is not estimating W_{net} , but calculating the break even, or minimum precision, $P(S_F|F)$, needed to make the survey cost-effective. It is assumed that $P(S_F|NF)$ will remain equal to zero. To calculate the break even precision, the above calculations were repeated for $P(S_F|F)$ between zero and one (Fig. 8-29). The break even $P(S_F|F)$ is approximately, 0.14. The seismic survey will be cost-effective if $P(S_F|F) > 0.14$. This estimate could be potentially very valuable, because while it may be difficult to estimate the exact precision of survey, it will be much simpler to estimate if the precision is above some minimum bound, particular the one in this case which is so low.

Besides evaluating the cost-effectiveness of a seismic survey or a pattern of hard, point measurements, one is concerned with which is the more cost effective measurement program. For example, should a soft, areal geophysical survey be carried out, or should a pattern of five hard, point measurements be taken? This question is tackled below where the W_{net} values of patterns of hard, point measurements taken on the 290 m spacing are compared to the W_{net} value of the seismic survey (Fig. 8-30). W_{net} for the survey equals W_{net} for one hard measurement at approximately $P(S_F|F) = 0.19$. Therefore, if $P(S_F|F) > 0.19$, the survey is the best option and if $P(S_F|F) < 0.19$, the single, hard measurement is the best option. Similarly for five hard measurements, if $P(S_F|F) > 0.23$, the survey is the best option and if $P(S_F|F) < 0.23$, the five hard measurements are the best option.

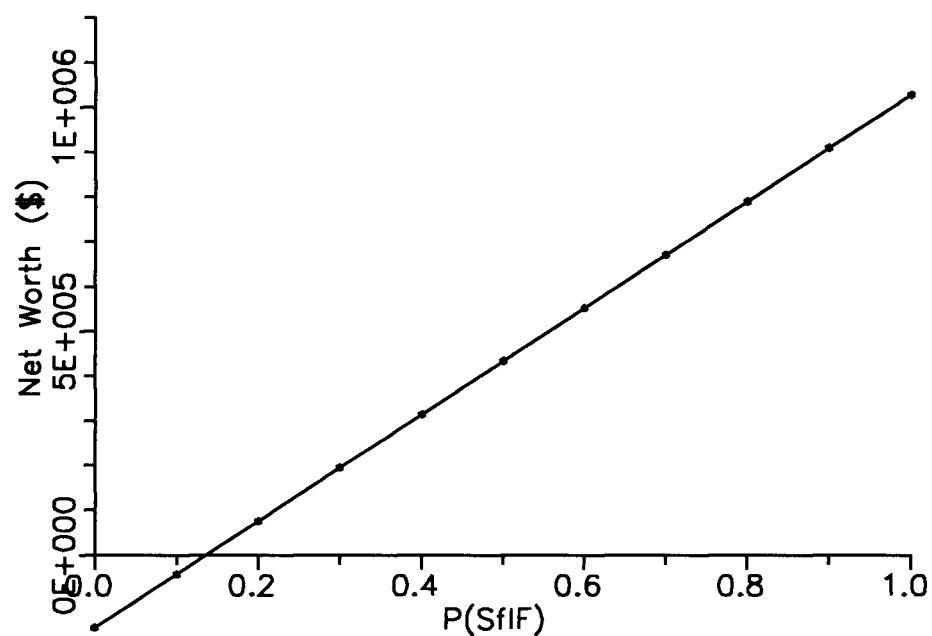


Figure 8-29: Net worth of the geophysical survey vs the probability of sampling a window that will cause failure, given that a window that will cause failure exists.

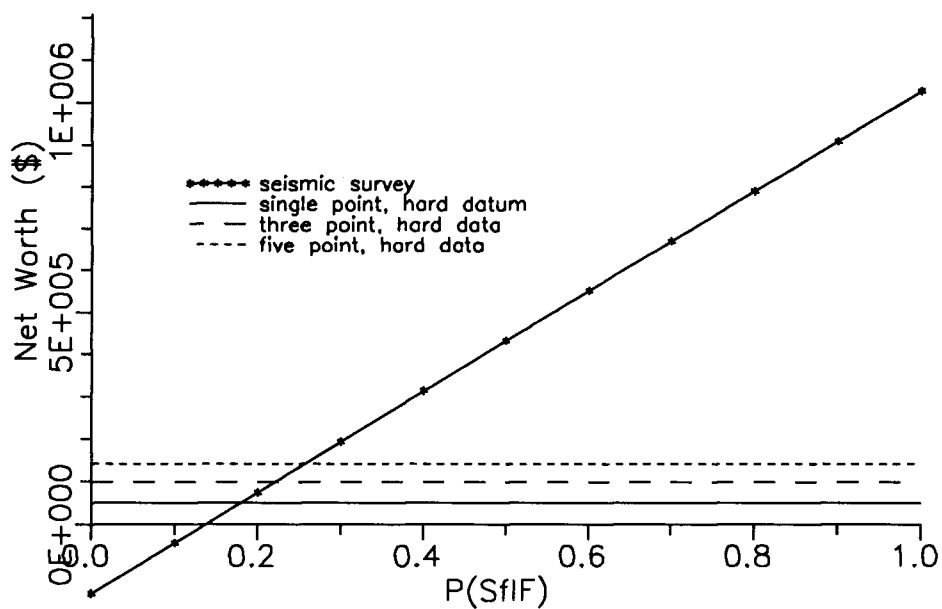


Figure 8-30: Net worth of the seismic survey compared to net worth of patterns of hard, point measurements taken on a 290 m spacing.

8.6 SUMMARY OF CHAPTER 8

The closure design of the H-Area seepage basins located at the Savannah River Site was used as a case study for the framework. The two alternative closure designs considered were to either (a) put a clay cap on the basins or (b) put no clay cap on the basins. The clay cap alternative is assumed to be 100% effective in preventing any contamination from leaving the seepage basins, while the no clay cap alternative is assumed to result in the seepage basins being an active source of contamination. Therefore, failure can only result for the no clay cap alternative. The cost of failure for the no clay cap alternative is not known; therefore, the data worth analyses are carried out with two assumed costs of failure of \$45 million and \$70 million. These costs of failure were arbitrarily selected to force measurements to have a positive worth. The cost of failure of \$45 million results in a more unstable prior best design alternative.

The framework was first used to evaluate the net worth of a single, hard, point measurement. It was found to be cost effective for both costs of failure. A sensitivity analysis was carried out to determine the robustness of this decision. The sensitivity analyses included numerical parameters, economic parameters, geostatistical parameters, and numerical artifacts of the SIS algorithm. In general, none of the parameters tested had a serious effect on the cost effectiveness of the measurement. At lower costs of failure, when the prior best design alternative becomes more unstable, the effect of these parameters on W_{net} increases.

The net worth of patterns of up to five hard, point measurements at sample spacings of 29, 145, and 290 m were studied. The most cost effective pattern was the five measurements with the 290 m spacing. With the 290 m spacing, no limit was found for the optimum number of measurements. The measurements are independent enough that their net worth increases with the number of measurements. However at small spacings, or with much existing data, spatial dependence becomes important. Under these conditions, the net worth will increase with the number of measurements, reach a maximum and then start to decrease. Hence there will be an optimum number of measurements, which may be as small as one.

The framework could be easily used to design sequential sampling programs involving single or multiple measurements. In the first step a contour map of the net worth for a single measurement would be produced and the location of the maximum net worth found. In the second step, the measurement(s) would be located in the region of the maximum net worth. In the case of multiple measurements, the optimum number and spacing of the measurements would then be determined. Once the measurement(s) was taken, a new contour map would be created to pick out the next measurement location(s). Measurements would only be taken as long as the maximum net worth was $> \$0$. The robustness of a decision to take a measurement(s) can be tested by carrying out a sensitivity analysis of W_{net} of the measurement(s) to base case parameters.

Contour plots of W_{net} could also be used to map out the maximum area over which a grid of point measurements could be cost effective. However, this area is uncertain because it is a function of the cost of failure and other base case parameters.

The framework was found to be effective in determining the cost effectiveness of a geophysical survey covering a large area because only the break even precisions (p_1 and p_2) had to be estimated, rather than the exact precision. For the example survey used here, it was estimated that the break even precision, $P(S_F|F)$ (i.e. p_1), was only 0.14. Similarly, the framework also is potentially very useful for determining the most cost effective sampling technique. In the case study, the net worth of patterns of hard, point measurements were compared to the net worth of an areal, soft seismic survey. The seismic survey only needed a precision of $P(S_F|F) > 0.23$ for it to be more cost effective than five hard measurements taken 290 m apart.

8.7 NOTATION

A_{CC}	clay cap alternative
A_D	prior best design alternative
A_D'	posterior best design alternative
A_{NC}	no clay cap alternative
C_{cc}	cost of clay cap alternative
C_{nc}	cost of no clay cap alternative
C_f	cost of failure
C_{f4}	cost of failure of \$45 million
C_{f7}	cost of failure of \$70 million
F	failure
H'	weight of prior data
H_s	weight of sample data
K_h	hydraulic conductivity in horizontal direction
K_v	hydraulic conductivity in vertical direction
m_I	estimate of the mean of $I(x)$
m_I'	prior estimate of the mean of $I(x)$
m_I''	updated estimate of the mean of $I(x)$
n_e	equivalent prior number of measurements
NF	no failure
p_1	probability of sampling a window, given that one is present
p_2	probability of sampling a window, given that one is not present
S_F	outcome of sampling failure
S_{NF}	outcome of sampling no failure
S_{NW}	outcome of sampling no window
$S_{NW_{fd}}$	outcome of sampling NW_{fd}
S_W	outcome of sampling a window
$S_{W_{fd}}$	outcome of sampling W_{fd}

W	worth of data
W_{fd}	window exists which causes failure and changes the prior best design alternative
NW_{fd}	no window exists which will cause a failure which will alter the prior best design alternative
W_{net}	net worth of data
λ_I	correlation length of indicator random variable $I(x)$
μ_I	mean of indicator random variable $I(x)$
σ_I^2	variance of indicator random variable $I(x)$
$\sigma_I^{2''}$	updated variance of indicator random variable $I(x)$
σ_{Wnet}^2	variance of net worth
$\sigma_{Wnet_i}^2$	variance of net worth caused by parameter i

CHAPTER 9: SUMMARY AND CONCLUSIONS

The objective of this thesis is to develop a Bayesian decision framework for answering data worth questions pertaining to hydrogeological design in heterogeneous geological environments. Previous Bayesian methods dealt only with homogeneous systems. The framework is developed specifically for aiding hydrogeologists, dealing with groundwater contamination, in the design of exploration programs searching for aquitard discontinuities. The framework can be valuable in carrying out cost effective remediation: It provides the site engineer with a tool not only for spending site exploration resources more efficiently, but also for deciding when enough information has been collected.

The framework consists of two basic modules: a geostatistical indicator (SIS) algorithm for simulating aquitard heterogeneity and a numerical model for simulating contaminant transport. Bayesian decision analysis ties the two modules together. The Bayesian nature of the framework also provides a methodology for incorporating a conceptual understanding of the local geology with quantitative information. Indicator geostatistics allows the handling of (a) hard, point measurements (which are precise, but are probably few and expensive), (b) soft, point measurements (which are imprecise, but are probably cheaper and more numerous), and (c) hydrogeological parameters which behave in space as non-Gaussian random variables.

It is assumed that the SIS algorithm correctly reproduces the essential characteristics of the local geology. If it does not, then the data worth analyses could be affected. Nevertheless, it is felt that the SIS algorithm is the best method available for handling geological heterogeneity. Finding methods of realistically and numerically representing geological heterogeneity is a current research problem. As improved methods are found, they could be incorporated into the framework.

Many parameters which must be estimated to carry out data worth analyses. For hard measurements, these include geostatistical parameters, hydrogeological parameters, economic parameters, and numerical artifacts of the SIS algorithm. The analyses of soft geophysical surveys are also dependent upon the survey's precision. The sensitivity of the worth of a single, hard measurement to these parameters was studied using the Savannah River Site case history and two generic design examples. The worth was found to be most sensitive to the economic parameters, in particular to the discount rate and the cost of failure. For the hydrogeological parameters in general, it is much more important to know whether the value of the parameter is above or below some threshold value, rather than to know its actual value. For the geostatistical parameters, the worth is relatively insensitive to the correlation length and the confidence in the prior estimate of the mean, but is sensitive to the estimate of the mean. The worth is relatively insensitive to the numerical artifacts of the SIS algorithm.

Sensitivity results indicate that the framework can be robust in determining the cost effectiveness of a measurement program. However, data worth analyses can be unstable when the objective function of the prior best design alternative is close in value to that of another prior design alternative.

In addition, the sensitivity analyses indicate that the perspective of the decision maker can have a major impact on the worth of a sampling program. For example, the owner/operator of a waste disposal site interested in making a rate of return on an investment will evaluate a very different measurement worth than an environmentalist interested in the long-term preservation of the environment. The source of this difference will come primarily from the assumed discount rate, and the perceptions of the cost associated with failure.

For the Savannah River case history, the net worth of patterns of up to five hard, point measurements at spacings of 29, 145, and 290 m were studied. The most cost effective pattern was the five measurements with the 290 m spacing. With the 290 m spacing, no limit was found for the optimum number of measurements. The measurements are almost independent; therefore, their net worth increases with the

number of measurements. However at smaller spacing, or with many existing data, spatial dependence can become important. Under these conditions, the net worth will increase with the number of measurements, reach a maximum and then start to decrease. Hence, the analysis predicts an optimum number of measurements, which may be as small as one.

The framework could be easily used to design sequential sampling programs involving single or multiple measurements. In the first step a contour map of the net worth for a single measurement would be produced and the location of the maximum net worth found. In the second step, the measurement(s) would be located in the region of the maximum net worth. In the case of multiple measurements, the optimum number and spacing of the measurements would be determined. Once the measurement(s) was taken, a new contour map would be created to pick out the next measurement location(s). Measurements would be only taken as long as the maximum net worth is $> \$0$. The robustness of a decision to take a measurement(s) can be tested by carrying out a sensitivity analysis of the measurement's net worth to base case parameters. These include geostatistical, economic, and hydrogeological parameters and numerical artifacts of the SIS algorithm.

The framework was found to be effective in determining the cost effectiveness of a geophysical survey covering a large area because only the break even precision needed to be estimated, rather than the exact precision. The break even precision is the precision at which the net worth = $\$0$. In the case study, the geophysical survey was cost effective if the probability of its locating a window in the area sampled, given that one existed, was > 0.14 . For similar reasons, the framework was also found to be effective in comparing the cost effectiveness of geophysical surveys and patterns of hard point measurement. In the case study, the seismic survey needed only a precision of $P(S_F|F) > 0.23$ to be more cost effective than five hard measurements taken 290 m apart.

Consequently, the developed framework was found to be effective in making data worth decisions involving exploration programs searching for aquitard continuity. This accomplishment represents the

major contribution of this thesis. The present applicability of the framework to answering real data worth question should be tested by back analyzing sampling programs at real groundwater contamination sites where many data have been collected.

A second contribution of this thesis lies in combining geological understanding with quantitative data to gain a geostatistical description of sand/shale heterogeneity. This combination is important because the environment of deposition contains much information about the heterogeneity. The case study demonstrated how the inclusion of geological intuition can be critical in correctly carrying out a data worth analysis. Analysis based on existing quantitative data alone is handicapped because if no windows have been previously found, then the probability of a window existing is zero. However, it is known that alluvial action over the last several million years could have created a window; Upper Three Runs Creek is an existing example. Consequently, ignoring the geological information would have resulted in the incorrect conclusion that data have zero worth and may have resulted in a poor design decision. Application is not straightforward at this time because of the lack of a quantitative relationship between heterogeneity and environment of deposition, but research at other centers is apparently progressing in this direction.

A third contribution is the handling of the effect of uncertainty of aquitard continuity on the prediction of contaminant transport. A final contribution lies in the adaptability of the framework to handle other types of data worth questions. The framework provides a foundation for addressing new data worth questions not only in hydrogeology, but also in other disciplines such as mining and petroleum reservoir engineering.

REFERENCES

- Aaland, R., *Personal Communication*, Westinghouse Savannah River Company, Savannah River Laboratory, Aiken, South Carolina, 1989.
- Alabert, F.G., *Stochastic Imaging of Spatial Distributions Using Hard and Soft Information*, Masters thesis, Stanford University, 1987a.
- Alabert, F.G., The practice of fast conditional simulations through the LU decomposition of the covariance matrix, *Mathematical Geology*, 19 (5), 369-386, 1987b.
- Attanasi, E.D., and M.R. Karlinger, Worth of data and natural disaster insurance, *Water Resources Research*, 15 (6), 1763-1766, 1979.
- Barnes, R.J., A partial history of spatial sampling design, *Geostatistics*, Spring, 10-13, 1989.
- Ben-Zvi, M., B. Berkowitz, and S. Kesler, Preposterior analysis as a tool for data evaluation: Application to aquifer contamination, *Water Resources Management*, 2, 11-20, 1988.
- Ben-Zvi, M. and Y. Bachmat, *Management of a Water Resource Under Uncertainty*, technical report, Hydrological Serv., Jerusalem, Israel, 1979.
- Benjamin, J.R. and C.A. Cornell, *Probability, Statistics, and Decision for Civil Engineers*, McGraw-Hill, Toronto, 1970.
- Benjamin, J.R. and C.A. Cornell, *Probability, Statistics, and Decision for Civil Engineers*, McGraw-Hill, 1970.
- Bogardi, I., A. Bardossy, and L. Duckstein, Multicriterion network design using geostatistics, *Water Resources Research*, 21 (2), 199-208, 1985.
- Boyce, W.E. and R.E. DiPrima, *Elementary Differential Equations and Boundary Value Problems*, John Wiley and Sons, 1969.
- Bratley, P. B.L. Fox, and L.E. Schrage, *A Guide to Simulation*, Springer-Verlag, New York, 1987.
- Brownlow, A.H., *Geochemistry*, Prentice Hall, Englewood Cliffs, N.J., 1982.
- Bury, K.V., *Statistical Models in Applied Science*, John Wiley and Sons, 1975.
- Buss, D.R., G.M. Duffield, T.S. Wadsworth, and J.M. Mercer, *Characterization of Groundwater Flow and Transport in the General Separations Areas Savannah River Plant: Evaluation of a Corrective Groundwater Action for the F and H-Area Seepage Basins*, final report prepared for E.I. duPont de Nemours & Company, Environmental Sciences Division, Savannah River Laboratory, Aiken, South Carolina, 29808 by GeoTrans Inc., 1987.
- Cahn, L.S., *Development of Guidelines for Design of Sampling Programs to Predict Groundwater Discharge*, M.S. Thesis, University of British Columbia, Vancouver, B.C., 1987.
- Clark, I., *Practical Geostatistics*, Applied Science Publishers, 1979.

- Clifton P.M. and S.P. Neuman, Effects of kriging and inverse modeling on conditional simulation of the Avra Valley in southern Arizona, *Water Resources Research*, 18 (4), 1215-1234, 1982.
- Cooke, C.W., Geology of the Coastal Plain of South Carolina, *U.S. Geol. Surv. Bull.* 867, 1936.
- Cross, G. *Personal Communication*, Department of Geophysics, University of British Columbia, Vancouver, B.C., 1992.
- Crouch, E.A.C., and R. Wilson, *Risk/Benefit Analysis*, Ballinger, 1982.
- Davis, D.R. and W.M. Dvoranchik, Evaluation of the worth of additional data, *Water Resources Bulletin*, 7 (4), 700-707, 1971.
- Davis, D.R., L. Duckstein, and R. Krzystofowicz, The worth of hydrologic data for nonoptimal decision making, *Water Resources Research*, 15 (6), 1733-1742, 1979.
- Davis, D.R., C.C. Kisiel, and L. Duckstein, Bayesian decision theory applied to design in hydrology, *Water Resources Research*, 8 (1), 33-41, 1972.
- Davis, M.W., Production of conditional simulations via the LU triangular decomposition of the covariance matrix, *Mathematical Geology*, 19 (2), 91-98, 1987.
- Dawdy, D.R., The worth of hydrologic data, *Water Resources Research*, 15 (6), 1726-1732, 1979.
- de Marsily, G. Spatial variability of properties in porous media: A stochastic approach, *Fundamentals of Transport Phenomena in Porous Media*, J. Bear and M.Y. Corapcioglu (eds.), NATO ASI Series, 719-770, 1984.
- de Marsily, G., *Quantitative Hydrogeology*, Academic Press, New York, 1986.
- Delhomme, J.P., Kriging in the hydrosiences, *Flow Through Porous Media-Recent Developments*, G.F. Pinder (ed.), CML Publications, 99-113, 1983.
- Delhomme, K., and Giannesini, F., Reservoir description techniques improve simulation results in Hassi-Messaoud Field Algeria; SPE Paper No. 8435, *54th Annual Technical Conference and Exhibition of the SPE in Las Vegas*, Nevada, Sept 23-25, 1979.
- Desbarats, A.J., Numerical estimation of effective permeability in sand-shale formations, *Water Resources Research*, Vol. 23 (2), 273-286, 1987a.
- Desbarats, A.J., *Stochastic Modeling of Flow in Sand - Shale Sequences*, Ph.D. Dissertation, Stanford University, 1987b.
- Domenico, D.A., and F.W. Schwartz, *Physical and Chemical Hydrogeology*, John Wiley, Toronto, 1990.
- Drever, J.I. *The Geochemistry of Natural Water*, Prentice Hall, Englewood Cliffs, N.J., 1982.
- Drew, L.J., Pattern drilling exploration: optimum pattern types and hole spacings when searching for elliptical targets, *Math. Geology*, 11 (2), 223-254, 1979.
- Duffield, G.M., D.R. Buss, and D.E. Stephenson, Velocity prediction errors related to flow model calibration uncertainty, *ModelCARE 90: Calibration and Reliability in Groundwater Modelling*, IAHS Publ. no. 195, 1990.

- Duffield, G.M., D.R. Buss, D.E. Stephenson, and J.W. Mercer, A grid refinement approach to flow and transport modeling of a proposed ground-water corrective action at the Savannah River Plant, Aiken, South Carolina, *Proceedings of Conference on Solving Ground Water Problems with Models*, NWWA, Denver, Co., 2, 1097-1120, 1987.
- Duffield, G.M., D.E. Stephenson, D.R. Buss, and T.D. Wadsworth, Effects of heterogeneous porous geology on ground-water flow and transport modeling in multiaquifer systems, *Proceedings of the Solving of Ground-Water Problems with Models Conference and Exposition*, NWWA, Indianapolis, IN, 1989.
- Fogg, G.E., Groundwater flow and sand body interconnectedness in a thick multiple-aquifer system, *Water Resources Research*, 22 (5), 679-694, 1986.
- Fogg, G.E., E. Simpson, and S.P. Neuman, *Aquifer Modeling Applied to an Arizona Groundwater Basin*, Tech. Rep. 32., Dept. of Hydrol. and Water Res., Univ. of Arizona, Tucson, 1979.
- Freeze, R.A., et. al. Advances in the assessment of data worth for engineering decision analysis in groundwater contamination problems, *Groundwater Flow and Quality Modelling*, E. Custodio et al. (eds.), Reidel Pub. Co., 665-697, 1988.
- Freeze, R.A. and J.A. Cherry, *Groundwater*, Prentice Hall, Englewood Cliffs, N.J., 1979.
- Frind, E.O., and G.B. Matanga, The dual formulation and flow for contaminant transport modeling 1. Review of theory and accuracy aspects, *Water Resources Research*, 21, (2), 159-169, 1985.
- Fritz, P. and J.C. Fontes eds., *Handbook of Environmental Isotope Geochemistry, V.1., The Terrestrial Environment A*, Elsevier, New York, 1980.
- Gates, J.S. and C.C. Kisiel, Worth of additional data to a digital computer model of a groundwater basin, *Water Resources Research*, 10 (5), 1031-1038, 1974.
- Geehan, G.W., Lawton, T.F., Sakurai, S., Klob, H., Clifton, T.R., Inman, K.F. and Nitzberg, K.E., Geologic prediction of shale continuity Prudhoe Bay Field, *Reservoir Characterization*, Lake, L.W and Carrol, H.B. Jr. (eds.) Academic Press, 1986.
- Ghauri, W.K., A.F. Osborne, and W.L. Magnuson, Changing concepts in carbonate waterflooding--West Texas Denver unit project--an illustrative example, *J. of Petroleum Technology*, June, 595-606, 1974.
- Gomez-Hernandez, J.J, *Personal Communication*, Stanford University, Dept. of Applied Earth Science, 1990.
- Gomez-Hernandez, J.J, and R.M., Srivastava, *Isim3d: A Three Dimensional Multiple Indicator Conditional Simulation Program*, *Computers and Geosciences*, 16 (4), 395-440, 1990.
- Hachich, W. and E.H. Vanmarcke, Probabilistic updating of pore pressure fields, *J. of Geot. Eng.*, 109 (3), 373-387, 1983.
- Haldorsen, H.H., On modeling of vertical permeability barriers in single-well simulations models, *SPE Formation Evaluation*, Sept., 349-358, 1989.

- Haldorsen, H.H. and Chang, D.M., Notes on stochastic shales; from outcrop to simulation model, *Reservoir Characterization*, Lake, L.W and Carrol, H.B. Jr. (eds.) Academic Press, 1986.
- Haldorsen, H.H. and L.W., Lake, A new approach to shale management in field-scale models, *SPEJ*, Aug., 447-457, 1984.
- Hazeu, G.J.A., Krakstad, O.S., Rian, D.T., Skaug, M., The application of new approaches for shale management in a three dimensional simulation study of the Frigg Field, *SPE Form. Eval.*, Sept., 493-502, 1988.
- Hewett, T.A. and R.A. Behrens, Conditional simulation of reservoir heterogeneity with fractals, SPE 18326, *63rd Annual Technical Conference and Exhibition of the Society of Petroleum Engineers*, Houston, TX, Oct. 2-5, 645-660, 1988.
- Isaaks, E.H. and M. Srivastava, Spatial continuity measures for probabilistic and deterministic geostatistics, *MGUS* conference, 1987.
- Jackson, R.E., R.J. Patterson, B.W. Graham, J. Bakr, D Belanger, H Lockwood, and M. Priddle, *Contaminant Hydrogeology of Toxic Organic Chemicals at a Disposal Site, Gloucester, Ontario, 1. Chemical Concepts and Site Assessment*, NHRI paper No. 23, IWD Scientific series No 141, National Hydrology Research Institute Inland Waters Directorate, Ottawa, Canada, 1985.
- Jardine, D., D.P. Andrews, J.W. Wishart, and J.W. Younge, Distribution and continuity of carbonate reservoirs, *J. of Petroleum Technology*, July, 873-885, 1977.
- Journel, A.G., Fundamental of geostatistics in five lessons, *Short Course in Geology: Volume Eight*, American Geophysical Union, 1989.
- Journel, A.G., Nonparametric estimation of spatial distributions, *Mathematical Geology*, 15 (3), 445-468, 1983.
- Journel, A.G. and Ch. J. Huijbreghts, *Mining Geostatistics*, Academic Press, 1978.
- Kennedy, Jenks, and Chilton, *Soil and Groundwater Investigation, Pennwalt Inorganic Chemical Division, Tacoma, WA*, Feb., 1990.
- Killian, T.H., N.L. Kolb, P Corbu, and I.W. Marine, *Environmental Information Document, H-Area Seepage Basins*, E.I. du Pont de Nemours and co., Savannah River Laboratory, DPST-85-706, 1987.
- Kitanidis, P.K., Parameter uncertainty in estimation of spatial functions: Bayesian analysis, *Water Resources Research*, 22 (4), 499-507, 1986.
- Kitanidis, P.K. and E.G. Vomvoris, A geostatistical approach to the inverse problem in groundwater modeling (steady state) and one-dimensional simulations, *Water Resources Research*, 19 (3), 677-690, 1983.
- Kossack, C.A., Prediction of layer lengths from layer heights for reservoir simulation: a statistical analysis of outcrop data, *J. Pet. Tech.*, 81 (8), 867-971, 1989.
- Knoll, M., *Personal Communication*, Department of Geological Sciences, U.B.C., Vancouver, B.C., 1992.

- Le Blanc, R. J. Sr. Distribution and continuity of sandstone reservoir--part 1, *J. of Pet. Tech.*, July, 776-792, 1977a.
- Le Blanc, R. J. Sr. Distribution and continuity of sandstone reservoir--part 2, *J. of Pet. Tech.*, July, 793-805, 1977b.
- Leopold, L.B., and Wolman, M.G., River channel patterns: braided, meandering, and straight; *Professional Paper 282-B*, USGS, Washington, D.C., 39-85, 1957.
- Lewis, C., *Personal Communication*, Westinghouse Savannah River Company, Savannah River Laboratory, Aiken, South Carolina, 1989.
- Maddock III, T. Management model as a tool for studying the worth of data, *Water Resources Research*, 9 (2), 270-280, 1973.
- Mantoglou, A., Digital simulation of multivariate two- and three- dimensional stochastic processes with spectral turning band method, *Mathematical Geology*, 19, 129-150, 1987.
- Marin, C.M. M.A. Medina Jr., and J.B. Butcher, Monte Carlo analysis and Bayesian decision theory for assessing the effects of waste sites on groundwater, I: Theory, *J. of Contaminant Hydrology*, 5, 1-13, 1989a.
- Massmann, R. A Freeze, L. Smith, T. Sperling, and B. James, Hydrogeological decision analysis: 2. Applications to ground-water contamination, *Groundwater*, 29 (4), 536-548, 1991.
- Massmann, J. and R.A. Freeze, Groundwater contamination from waste management sites: The interaction between risk-based engineering design and regulatory policy 1. methodology, *Water Resources Research*, 23 (2), 351-367, 1987a.
- Massmann, J. and R.A. Freeze, Groundwater contamination from waste management sites: The interaction between risk-based engineering design and regulatory policy 2. results, *Water Resources Research*, 23 (2), 368-380, 1987b.
- Massmann, J.W., *Groundwater Contamination from Waste-Management Sites: The Interaction Between Risk-Based Engineering Design and Regulatory Policy*, Ph.D. Thesis, University of British Columbia, Vancouver, B.C., 1987.
- McDonald, M.G. and A.W. Harbaugh, *A Modular Three-Dimensional Finite-Difference Ground-Water Flow Model*, U.S. Geological Survey Open File Report 83-875, 1988.
- Medina M.A. Jr., J.B. Butcher, and M.M. Carlos. , Monte Carlo analysis and Bayesian decision theory for assessing the effects of waste sites on groundwater, II: Applications, *J. of Contaminant Hydrology*, 5, 15-31, 1989b.
- Meyers, D.E. To be or not to be ... stationary? That is the question, *Mathematical Geology*, 21 (3), 347-362, 1989.
- National Research Council, *Ground Water Models: Scientific and Regulatory Applications*, Water Science and Technology Board, 1990.
- Newson, J.M. and J.L. Wilson, Vertical flow in wellbores: short-circuits for contaminants, *Eos*, Transactions, American Geophysical Union, 69 (44), 1215, 1988.

- NUS Corp, *Remedial Investigation, CIBA-GEIGY Site, Toms River, N.J.*, Sept. 1986.
- Nystrom, P.G., Jr. and R.H. Willoughby, eds. Geological investigations related to stratigraphy in the Kaolin mining district, Aiken Co., South Carolina, *Car. Geol. Soc. Field Trip Guide Book*, 1982.
- Parizek, R.R., and R.W. Root Jr., *Development of a Ground-Water Velocity Model for the Radioactive Waste Management Facility Savannah River Plant, South Carolina*, Final Report submitted to E.I. duPont and Co., Savannah River Laboratory, Aiken, South Carolina, 1986.
- Phillips, F.M., and J.L. Wilson, An approach to estimating hydraulic conductivity spatial correlation scales using geological characteristics, *Water Resources Research*, 25 (1), 141-143, 1989.
- Pollack, D.W., *Documentation of Computer Programs to Compute and Display Pathlines Using Results from the U.S. Geological Survey Modular Three-Dimensional Finite-Difference Ground-Water Flow Model*, U.S.G.S., 1989.
- Potter, P.E., Maynard, J.B., and Pryor, W.A., *Sedimentology of Shale*, Springer-Verlag, New York, 1985.
- Press, F. and R. Siever, *Earth*, W.H. Freeman and Co., 1978.
- Price, V., *Personal Communication*, Westinghouse Savannah River Company, Savannah River Laboratory, Aiken, South Carolina, 1989.
- Ravenne, C., R. Eschard, A. Gali, Y. Mathieu, L. Montadert, J.L. Rudkiewicz, Heterogeneities and geometry of sedimentary bodies in a fluvio-deltaic reservoir, *SPE Formation Evaluation*, June, 239-247, 1989.
- Reading, H.G., *Sedimentary Environments and Facies*, Elsevier, New York, 1983.
- Richardson, J.G., D.G. Harris, R.H. Rossen, and G. Van Hee, The effect of small, discontinuous shales on oil recovery, *J. of Petroleum Technology*, Nov. 1531-1537, 1978.
- Riggs, J.L., W.F. Rentz, and A.L. Kahl, *Essentials of Engineering Economics*, McGraw-Hill Ryerson Ltd., 1983.
- Root, R.W. Jr., *A Comparison of Deterministic and Geostatistical Modeling Methods as Applied to Numerical Simulation of Ground-Water Flow at the Savannah River Plant, South Carolina*, Ph. D. Thesis, Pennsylvania University, 1987.
- Rouhani, S. Variance Reduction Analysis, *Water Resources Research*, 21 (6), 837-846, 1985.
- Roux, P.H. and W.F. Althoff, Investigation of organic contamination of groundwater in South Brunswick Township, New Jersey, *Groundwater*, 18 (5), 464-471, 1980.
- Selby, M.J., *Earth's Changing Surface*, Clarendon Press, Oxford, 1985.
- Sinclair, A.J., *Personal Communication*, Dept. of Geological Sc., U.B.C., Vancouver, B.C., Canada, 1991.
- Sinclair, A.J., *Personal Communication*, Dept. of Geological Sc., U.B.C., Vancouver, B.C., Canada, 1990.

- Slichter, L.B., Geophysics applied to prospecting for ores, in Pt. 2 of Bateman, A.M. (ed.), *Economic Geology*, 50th anniversary volume, 1905-1955: Urbana Ill., Econ. Geology Pub. Co., 885-969, 1955.
- Sneider, R.M., Tinker, C.N. and Meckel, L.D., Deltaic environment reservoir types and their characteristics, *J. of Pet. Tech.*, Nov., 1538-1546, 1978.
- Sperling, T. *Personal Communication*, Gartner Lee Ltd., Vancouver, B.C. 1992.
- Sperling, T., R. Allan Freeze, J. Massmann, L. Smith, B. James, Hydrogeological decision analysis: 3. Application to design of a groundwater control system at an open pit mine, *Groundwater*, (in press).
- Sperling, T., *Risk-Cost-Benefit Framework for the Design of Dewatering Systems in Open-Pit Mines*, Ph.D Thesis, University of British Columbia, Vancouver, B.C., 1991.
- Srivastava, M., *Personal Communication*, FSS Canada, Vancouver, B.C., 1990.
- Sullivan, J.A., *Non-Parametric Estimation of Spatial Distributions*, Ph.D. Thesis, Stanford University, Stanford, CA, 1985.
- Wadman, D.H., Lamprecht, D.E. and Mrosovsky, I., Joint geologic/engineering analysis of the Sadlerochit reservoir, Pudhoe Bay Field *J. of Pet. Tech.*, July, 933-940, 1979.
- Walker R.G., *Facies Models*, Geoscience Canada, Reprint Series 1, 1983.
- Weber, K.J., How heterogeneity affects oil recovery, *Reservoir Characterization*, Lake, L.W and Carrol, H.B. Jr. (eds.) Academic Press, 1986.
- Weber, K.J., Influence of common sedimentary structures on fluid flow in reservoir models, *J. of Pet. Tech.*, March, 665-672., 1982.
- Weber, K.J., Klootwijk, P.H., Konieczek, J., van der Vlugt, W.R., Simulation of water injection in a barrier-bar-type, Oil-rim reservoir in Nigeria, *J. Pet. Tech.*, July, 1555-1565, 1978.
- Wu, T.H., Vyas, S.K., and Chang, N.Y., Probabilistic analysis of seepage *J. Soil Mech. and Foundation Division*, ASCE, April, 323-340, 1973.
- Yeh, W.W-G., Review of parameter identification procedures in groundwater hydrology: the inverse problem, *Water Resources Research*, 22 (2), 95-108, 1986.
- Zeito, G.A., Interbedding of shale breaks and reservoir heterogeneities, *J. Pet. Tech.*, Oct, 1223-1228, 1965.

APPENDIX 1: GREEN CLAY DATA BASE

THICK	- thickness of Green Clay (m)
GCTOP	- top elevation of Green Clay (m)
GCBOT	- bottom elevation of Green Clay (m)
GLOG	- G =geophysical log available.
GC	- Y = Green Clay indicated on lithologic logs - N = Green Clay not indicated on lithologic logs
DH	- difference in head across green clay (m)

Borehole	Co-ordinate		THICK (m)	GC	GCTOP (m)	GCBOT (m)	GLOG	DH (m)
	E	N						
BGC-1A	57196	73551	0.9	Y	36.3	35.4		
BGC-2A	55887	74350	2.4	Y	41.3	38.9		
BH-1	64590	76000	3.9	N	47.7	43.7	G	
BH-10	65000	74000	3.3	Y	46.3	43.0	G	
BH-11	65199	74301	1.6	Y	45.9	44.3	G	
BH-12	65998	74001	3.3	Y	48.0	44.7	G	
BH-13	64002	72999	3.3	N	47.0	43.7	G	
BH-14	65018	72993	2.3	N	43.5	41.2	G	
BH-15	66008	72992	1.4	Y	46.5	45.0	G	
BH-159	64380	73866	3.9	N	43.3	39.4	G	
BH-16	64592	72504	3.3	Y	43.5	40.3	G	
BH-160	64438	74365	3.3	Y	45.8	42.6		
BH-18	65165	75035	4.9	Y	48.2	43.4		
BH-2	64000	74999	3.3	N	45.9	42.7	G	
BH-20	65175	75025	1.6	Y	48.2	46.6	G	
BH-22	64880	75115	0.0	N	43.8	43.8		
BH-23	65050	75115	6.6	Y	43.8	37.2		21.3
BH-24	64600	73693	3.0	N	43.3	40.4	G	
BH-25	64675	75035	3.3	Y	46.0	42.7		
BH-29	64880	74940	0.0	N	43.3	43.3		
BH-3	64601	75008	3.3	N	44.8	41.5	G	
BH-31	65050	74940	1.6	Y	49.4	47.8		
BH-32	64520	74840	0.0	N	44.7	44.7		
BH-33	64675	74840	3.3	Y	42.6	39.3		
BH-37	64520	74660	0.0	N	43.4	43.4		
BH-38	64590	74745	0.7	Y	46.6	46.0		
BH-39	64675	74660	0.0	N	46.0	46.0		
BH-4	65305	75106	1.6	Y	47.2	45.6	G	21.3
BH-41	64880	74775	3.3	Y	42.7	39.4		
BH-42	65050	74775	4.9	Y	43.4	38.5		
BH-45	64880	74610	0.0	N	43.5	43.5		
BH-46	62894	73662	2.1	N	44.9	42.8	G	
BH-47	65050	74610	3.6	Y	45.4	41.8	G	
BH-48	65505	74590	3.8	Y	48.6	44.8		17.4
BH-49	65640	74590	3.8	Y	48.5	44.8		
BH-5	66001	75001	3.8	Y	44.3	40.5	G	
BH-50	65790	74590	1.6	Y	45.3	43.7		17.1
BH-54	64188	73869	3.3	N	43.0	39.7	G	
BH-55	64520	74420	1.5	Y	43.4	41.9	G	
BH-56	64675	74465	1.4	Y	46.1	44.8		
BH-57	64880	74440	3.3	Y	46.0	42.7		
BH-58	65050	74440	3.3	Y	42.0	38.7		
BH-6	64586	74500	1.5	Y	46.4	44.9	G	
BH-62	64190	74024	3.0	N	42.6	39.7	G	
BH-63	65640	74459	3.3	Y	48.7	45.4	G	
BH-64	65790	74405	1.6	Y	44.8	43.2		17.4

Borehole	Co-ordinate		THICK (m)	GC	GCTOP (m)	GCBOT (m)	GLOG	DH (m)
	E	N						
BH-66	64378	74025	1.6	Y	45.7	44.1	G	23.3
BH-69	64765	74245	0.0	N	46.2	46.2		
BH-7	63015	73995	2.6	Y	42.9	40.3	G	
BH-72	65502	74332	1.6	Y	44.5	42.8	G	
BH-73	65705	74340	0.0	N	43.0	43.0		
BH-77	64520	74165	0.0	N	44.2	44.2		
BH-78	64771	74088	3.3	Y	45.6	42.3		
BH-8	63995	73994	2.5	N	43.4	40.9	G	
BH-80	64465	73990	0.0	N	44.3	44.3		
BH-81	64765	73955	2.0	N	44.1	42.1	G	
BH-83	64259	74365	2.0	N	43.6	41.6	G	22.3
BH-84	64253	74256	1.6	N	40.8	39.1	G	
BH-85	64440	74256	0.0	N	44.2	44.2		
BH-G6L1	64362	74334	0.0	N	42.8	42.8		
BH-86L2	64367	74292	1.6	N	44.1	42.5	G	
BH-89	64465	73820	3.3	Y	43.9	40.6		
BH-9	64601	74011	0.0	N	43.0	43.0		
BH-90	64591	73851	3.3	Y	44.4	41.1	G	
BH-92	64765	73785	3.3	Y	42.3	39.0		
BH-98	64465	73620	0.0	N	43.3	43.3		
DH-2	62090	71760	0.0	N	39.5	39.5		22.3
DH-3	61520	71629	0.0	N	37.8	37.8		
DH-4	53190	77000	0.0	N	40.0	40.0		
DH-5	52650	77335	0.0	N	40.3	40.3		
F-10	53472	78985	0.0	N	42.7	42.7		
F-11	54200	78400	0.0	N	42.7	42.7		
F-13	53480	78275	2.6	Y	43.9	41.2		
F-14	53480	79270	1.6	Y	45.9	44.2		
F-28	53660	78657	0.0	N	42.7	42.7		
F-6	53549	79843	0.0	N	42.7	42.7		
F-8	53400	78475	1.6	Y	44.1	42.5		22.3
F-9	53400	79480	0.0	N	42.7	42.7		
FC-1A	53115	79665	3.6	Y	48.9	45.3		
FC-2A	55424	79244	3.3	Y	48.6	45.3		
FC-3A	57620	78727	0.7	Y	51.2	50.5		
FC-4A	53897	82243	0.3	Y	42.3	42.0	G	
FC-5A	54672	87988	1.6	N	53.0	51.3	G	
FF-4	52942	76922	0.0	N	42.7	42.7		
FU-1	53475	79121	0.0	N	42.7	42.7		
FU-2	53478	78648	5.7	Y	46.8	41.0		
FU-3	54390	78320	0.0	N	42.7	42.7		24.6
H-35D	58548	71918	3.3	Y	38.1	34.8	G	
HC-1A	61867	71755	0.7	Y	40.4	39.7	G	
HC-10A	61531	75815	1.3	Y	41.3	40.0	G	
HC-11A	62147	74519	1.0	Y	44.6	43.6	G	
HC-13A	63610	73394	1.0	Y	41.1	40.1	G	14.8

Borehole	Co-ordinate		THICK (m)	GC	GCTOP (m)	GCBOT (m)	GLOG	DH (m)
	E	N						
HC-14A	60658	67560	1.6	Y	38.2	36.6	G	19.4
HC-16A	65462	72596	1.8	Y	43.0	41.2	G	
HC-17A	61700	73200	0.7	Y	42.0	41.3		
HC-18A	63409	71560	1.0	Y	37.4	36.4		
HC-2A	61866	71794	2.6	Y	41.6	38.9	G	26.2
HC-3A	62266	74742	3.0	Y	39.2	36.3	G	24.9
HC-7A	66992	74352	0.7	Y	46.6	45.9	G	13.8
HC-8A	59990	77492	1.0	Y	50.2	49.2	G	
HC-9A	64084	75135	1.5	Y	44.0	42.4	G	
PDM-5	54695	74819	0.7	Y	42.7	42.0		
PWAA-17	54826	72978	0.3	Y	40.4	40.0		16.4
PWCC-13	54387	73057	0.7	Y	42.3	41.7		
PWCC-25	55350	72350	2.3	Y	40.7	38.4		
PWEE-9	53941	73132	1.0	Y	40.0	39.0		
PWM--1	54210	75182	1.0	Y	41.7	40.7		
PWM--4	53968	75360	1.0	Y	41.3	40.4		
PWM-1	54370	75063	1.0	Y	41.7	40.7		
PWM-13	55338	74344	2.0	Y	42.3	40.4		
PWM-17	55660	74106	2.0	Y	41.7	39.7		
PWM-5	54695	74819	0.3	Y	41.7	41.3		
PWM-9	55016	74582	0.7	Y	41.0	40.4		
PWQ-3	54300	74614	1.0	Y	40.0	39.0		
PWQ-5	54457	74498	2.3	Y	39.7	37.4		
PWQ-7	54619	74378	1.0	Y	41.3	40.4		
PWQ-9	54779	74260	1.0	Y	41.7	40.7		
PWU-17	55184	73463	0.7	Y	39.7	39.0		
PWU-5P	54219	74176	2.0	Y	41.0	39.0		
PWW-5	54106	74010	0.0	N	39.4	39.4		
PWW-5P	54106	74010	0.0	N	39.4	39.4		
PWY-21	55268	72903	0.3	Y	41.0	40.7		
SDS-12A	66610	77742	3.3	N	50.7	47.4	G	
SDS-7A	67681	76515	1.3	N	44.0	42.7	G	
12H-11	61150	72100	1.3	Y	42.7	41.3		
12H-18	62473	71310	0.0	N	41.0	41.0		
12H-19	62473	71270	0.0	N	41.0	41.0		
12H-20	62498	70975	2.6	Y	40.0	37.4		
12H-21U	62636	70966	1.3	Y	39.8	38.5		
12H-22U	62730	70956	3.3	Y	39.4	36.1		
12H-23	62850	70956	0.0	N	39.4	39.4		
12H-27U	62794	70945	3.3	Y	40.6	37.3		
12H-3	62708	71300	1.0	Y	40.7	39.7		
12H-30	62900	70956	1.2	Y	39.4	38.2		
12H-39	62670	70826	0.0	N	39.4	39.4		
12H-40U	62740	70832	0.0	Y	39.4	39.4		
14F-1	52800	76720	1.6	Y	43.3	41.7		

Borehole	Co-ordinate		THICK (m)	GC	GCTOP (m)	GCBOT (m)	GLOG	DH (m)
	E	N						
14F-2	52786	76814	2.3	Y	44.3	42.0		
14F-3U	52786	76940	1.3	Y	43.3	42.0		
14F-4	52786	77072	1.6	Y	43.6	42.0		
14F-6	52600	76694	1.6	Y	42.7	41.0		
14F-7U	52600	76816	0.0	N	42.7	42.7		
14F-8	52600	76940	1.6	Y	44.3	42.7		
14F-9	52600	77072	1.6	Y	41.7	40.0		
55F-1U	52332	77072	0.0	N	41.0	41.0		
55F-2	52332	76696	1.6	Y	42.0	40.4		
55F-3	52332	76940	1.6	Y	41.7	40.0		
55F-4U	52332	76816	0.3	Y	38.4	38.1		